Nonlinearity and Controller Performance for

Product Property Control in a

Gas-Phase Polyethylene Reactor

by

MaryAnn Alexandra Benda

A thesis submitted to the Department of Chemical Engineering
in conformity with the requirements for the degree
of Master of Science (Engineering)

Queen's University
Kingston, Ontario, Canada
August, 2000.

The author has granted a non-exclusive licence allowing the National Library of Canada to reproduce, loan, distribute or sell copies of this thesis in microform, paper or electronic formats.

The author retains ownership of the copyright in this thesis. Neither the thesis nor substantial extracts from it may be printed or otherwise reproduced without the author's permission.

L'auteur a accordé une licence non exclusive permettant à la Bibliothèque nationale du Canada de reproduire, prêter, distribuer ou vendre des copies de cette thèse sous la forme de microfiche/film, de reproduction sur papier ou sur format électronique.

L'auteur conserve la propriété du droit d'auteur qui protège cette thèse. Ni la thèse ni des extraits substantiels de celle-ci ne doivent être imprimés ou autrement reproduits sans son autorisation.

0-612-52877-4

Canada

Abstract

Most chemical processes are inherently nonlinear in nature. Although a wealth of information on nonlinear processes and control exists, the implementation of nonlinear control techniques is not commonplace in industry. Instead, due to the additional design, implementation and maintenance efforts required for nonlinear control, practitioners often accept the performance and economic losses that result from employing linear controllers. In some cases, the losses are minor; however, in others, they may be significant due to the nonlinearity of the process. It would be advantageous to bridge the gap between the nonlinearity of a process and whether the potential benefits of a nonlinear control scheme outweigh the additional efforts required.

The primary objectives of this thesis are to measure the steady-state nonlinearity of a gas-phase fluidized-bed polyethylene reactor, and to relate those measures of curvature to the performance degradation that results from the use of linear control, relative to nonlinear control.

Recently defined steady-state RMS curvature is used to examine the product property behaviour of a published polyethylene reactor model. Illustrative examples detail the calculation and interpretation of the elements of curvature.

A comprehensive study is undertaken to examine the nonlinearity of regions of product property grades of polyethylene, including grade transition regions, and operation about a steady-state point. Curvature values for the regions examined ranged from insignificant ($c_{RMS} \approx 0$) to severe ($c_{RMS} = 117$). A comparison is made between two forms of the model, one being the nominal form, and the other, the transformed version in which the melt index property is logarithmically transformed. In all cases considered, the transformed model displays less curvature than the nominal model; significant reduction in nonlinearity is seen in all cases.

The curvature values obtained for the selected grade regimes are compared to the performance of linear controllers, relative to nonlinear controllers. The expectation was that as the curvature of a region increased, the degradation of linear control performance would intensify. An input/output linearizing feedback controller was designed for use with simulation studies. Scaled performance measures adapted from IAE were used to compare the performance of linear controllers, relative to nonlinear control schemes. The outcome of comparative studies was that no trend between RMS curvature and the chosen performance measure was found.

Several possible reasons were given for the lack of correlation between linear control performance and RMS curvature. The most promising explanation is that RMS curvature is a steady-state measure, which is insufficient in determining the nonlinearity of the dynamic polyethylene model. Consequently, an important recommendation for future work is the assessment of dynamic nonlinearity of the model.

i

Acknowledgements

Contents

List of Tables

List of Figures

Nomenclature

$\mathbf{a}_i$ $p \times p$ Hessian matrix of state i

$\mathbf{a}_{cat}$ Active site concentration in the catalyst

$\mathbf{A}$ $n \times p(p+1)/2$ matrix of non-redundant acceleration vectors in the transformed orthonormal basis

$\mathbf{A}_r$ Rearranged acceleration array: n-dimensional array of $p \times p$ faces

b   Molar flow rate of bleed stream from polyethylene reactor

Bw   Polyethylene reactor bed weight

c   Root mean squared curvature. Also denoted c_{RMS}.

c_e Curvature experienced along the steady-state locus, in direction $\mathbf{e}$ in input space

c_{ijk} i^{th} face, j^{th} row, k^{th} element of the relative curvature array, $\mathbf{C}_r$

C_t Total gas concentration in polyethylene reactor

$\mathbf{C}_r$ Rearranged relative curvature array for the region defined by $\mathbf{S}$

e   Error between output and set-point

$\mathbf{e}$ An arbitrary direction in the input space

f   Vector field describing inertial state dynamics on the state space, or

       Vector field describing dynamics on the state space

F_{cat} Inlet molar flow rate of catalyst

F_{H2} Inlet molar flow rate of hydrogen gas

F_{M2} Inlet molar flow rate of butene gas

g   Vector field describing input dynamics on the state space

gl   Mismatch factor in the polyethylene gas mass-balance model

h   State-output map

[H_2]   Concentration of hydrogen gas in polyethylene reactor

[I]   Reactive impurity concentration in polyethylene reactor

$k_0...k_7$ Parameters in the polyethylene melt index model

k_d Rate constant for deactivation of active sites

k_H Consumption rate constant for hydrogen reacting with polyethylene

k_{p1} Propagation rate constant for ethylene

k_{p2} Propagation rate constant for butene

$K(\bullet)$ Tracking error function

L_f, L_g Lie derivatives in the direction of f and g, respectively

m Dimension of output vector

mw_1 Molecular weight of ethylene

mw_2 Molecular weight of butene

M_1 Ethylene monomer

M_2 Butene comonomer

M_3 Higher alpha-order olefin (e.g. hexene)

MI   Melt Index of polymer

n Dimension of state vector

Op   Polymer outflow rate

$p_0...p_4$ Parameters in the polyethylene density model

p Dimension of input vector

p^n Dimension of the space normal to the tangent space, but spanned by the

         acceleration vectors

PR	Production rate of polyethylene
q	Orthogonal basis vectors obtained from the $\mathbf{Q}$ matrix
$\mathbf{Q}$	$n \times n$ matrix of orthonormal basis vectors resulting from QR decomposition
[R]	Cocatalyst concentration in polyethylene reactor
$\mathbf{R_l}$	$p \times p$ upper triangular matrix of velocities in the transformed orthonormal basis
s	Laplace variable
S	Solubility of butene in polyethylene
S	$n \times n$ invertible scaling matrix (may have superscripts ^{in} or ^{out})
t	Time
T	Temperature
u	p-dimensional vector of input values
v	Derivative vectors of states
V	Matrix of $n \times p$ state velocity vectors
Vg	Volume of gas in the polyethylene reactor
Vs	Equivalent gas volume of butene dissolved in polyethylene
W	Matrix of $n \times p(p+1)/2$ non-redundant state acceleration vectors
x	n-dimensional vector of state variables
y	m-dimensional vector of output variables
y_{sp}	Set-point trajectory
Y	Number of moles of active sites in the polyethylene reactor
z	Variable of integration
z	Vector of scaled state coordinates

Greek Letters

α Relative order of a process

β Matrix of proportional mode tuning parameters for the error-trajectory control

formulation

γ Matrix of integral mode tuning parameters for the error-trajectory control

formulation

λ Relative gain

ρ Density of polyethylene

Φ p-dimensional vector of inputs in the transformed orthogonal basis

Ξ Steady-state locus: nonlinear mapping of inputs to the state or output space.

Abbreviations

CV   Controlled variable

GMC   Generic Model Control

IAD   Integral of the absolute deviation

IAE   Integral of the absolute error

MIMO   Multiple-input, multiple-output

MV   Manipulated variable

ODE   Ordinary Differential Equation

RGA   Relative gain array

RMS   Root-mean-squared

SISO   Single-input, single-output

SP   Set-point

Superscripts

eq   Indicates an equivalent linear approximation of scaling in the output space after input-prescribed scaling was specified

in   Indicates that scaling is taken with respect to the input space

out   Indicates that scaling is taken with respect to the output space

t   Indicates the first p columns of the matrix $\mathbf{Q}$

ϕ Indicates properties defined from scaled, orthogonal inputs

'   Indicates the transpose of a matrix or vector

Subscripts

o   Indicates a steady-state value

RMS   Root mean squared value

Overstrikes

.   First derivative of the specified quantity

..   Second derivative of the specified quantity

~   Indicates a scaled quantity

Chapter 1

Introduction

Most processes in chemical engineering industry are inherently nonlinear in nature. This, combined with increasing pressures to conserve energy, reduce capital cost, and provide tighter control of highly integrated processes (Lee and Sullivan, 1988), motivates the practitioner to implement a control law commensurate with such objectives. To further actuate this end, a wealth of research and results are available on nonlinear processes and control.

Although the implementation of nonlinear control provides important benefits, the use of linear control strategies still dominates industry. Presumably, linear techniques often provide adequate control of processes displaying mild to moderate nonlinearity. However, processes displaying a high degree of nonlinearity may require nonlinear control strategies. Nonetheless, practitioners tend to be reluctant to implement such controllers due to the considerable amount of developmental effort required, and disregard the economic and performance losses associated with the inadequacies of linear control. In this vein, it would be of practical importance to be able to assess the degree of nonlinearity of a process or a region of interest within a process, in order to ascertain whether nonlinear control is merited.

The topic of nonlinearity assessment has been an active area of research in recent years. Ogunnaike et al. (1993), Nikolaou (1993), and Allgöwer (1995) have proposed operator-based techniques for measuring nonlinearity. However, these approaches

1

provide little insight into the process structure and do not describe the specific elements that account for curvature (Guay et al., 1995). Koung and MacGregor (1991, 1992) examine the influence of nonlinearity on the singular-value decomposition of local steady-state gain information. Stack and Doyle III (1995, 1997 a,b) advocate using an optimal-control structure as a tool to assess control-relevant nonlinearity. Once the optimal-control structure is designed, an open-loop measure can be used to examine nonlinearity. Haber (1985) presented various methods of detecting nonlinearity within a process from input-output records.

An intriguing result is presented by Guay et al. (1995), which quantifies the magnitude and nature of the nonlinearity. This technique defines the nonlinearity of a process as its departure from a first-order Taylor series approximation. The curvature is estimated by comparing the magnitude and direction of the second-order terms to the first-order terms. Moreover, this technique allows for the appropriate representation of the size and orientation of the operating region by a carefully selected scaling. Guay (1996) further extended his work on steady-state measures of curvature to include a measure of dynamic nonlinearity.

The primary objectives of this thesis are to illustrate and exemplify Guay et al.'s steady-state open-loop measure of curvature, to put it to practical use by assessing the nonlinearity of regions within a gas-phase fluidized-bed polyethylene reactor model, and to determine if these measures are helpful in predicting control performance. Background information is given, practical implementation issues are raised, and some recommendations for future work are given.

Guay et al.'s measures of nonlinearity are applied to and assessed using the gas-

2

phase polyethylene reactor model developed by McAuley et al. (1990), and McAuley and MacGregor (1991, 1993). Background on the gas-phase production of polyethylene is given in Chapter 2, in addition to the model used to describe the process. This chapter also provides the prerequisite material for Guay et al.'s steady-state measure of curvature. The key points of Guay et al.'s work are: the decomposition of second-order derivative information into tangential and normal constituents, and the development of a scale-independent measure of curvature. The effects of interaction and of various components of nonlinearity (specifically tangential and normal elements) on the geometry of the steady-state locus are discussed. Additionally in Chapter 2, the error-trajectory approach to nonlinear controller design is presented, as this control scheme is used later in the thesis.

In Chapter 3, we examine 2×2 portions of the polyethylene reactor model to visualize interaction and curvature on the steady-state locus. Examples are also provided detailing the calculation of steady-state RMS curvatures and the interpretation and illustration of the components of curvature.

In Chapter 4, nonlinearity assessment of the polyethylene reactor model is performed. Regions of operation in the model are chosen based on realistic grade settings, which include film resins, and injection and rotational molded polyethylene. To properly define a region of operation about the selected grades, and to provide a generic, scale-independent measure of curvature, the regions around the grades are scaled. The nonlinearity of numerous regions within the polyethylene model is calculated, yielding a wide range of curvature values. Two forms of the polyethylene model are investigated; because practitioners often opt to control the logarithm transform of melt index (rather

3

than melt index directly) on the theory that this transform reduces the nonlinearity of the model, we assess the curvature of regions within each form of the model. The curvature results of each form of the model are compared.

The objective of Chapter 5 is to determine whether operating regions with high curvatures suffer larger linear control performance losses than regions with lower curvatures. Closed-loop simulations were performed to assess this relationship. First in Chapter 5, the control law is developed, which is based on an error-trajectory nonlinear controller design. This control scheme is an input-output linearizing controller with state feedback, and is tuned such that the error-trajectory response specification reflects the natural dynamic behaviour of the system. A normalized measure of performance is defined and utilized to quantify control performance. This measure quantifies the normalized difference between the integral absolute error (or deviation) of nonlinear and linear controllers. It is our expectation that the performance measure for linearly controlled processes should increase with increasing curvature. The specific results obtained for the investigation of the relationship between RMS curvature and control performance are discussed. In addition, Chapter 5 includes a discussion of possible explanations for unexpected results, as well as recommendations for future considerations.

A summary and conclusions to the work investigated in this thesis are given in Chapter 6. Contributions presented by the author, as well as recommendations for future consideration are also imparted in this final chapter.

Chapter 2

Background

2.1 Production of Polyethylene

Polyethylene has become one of the most widely produced polymers in the world, with a production of over 55 million tons expected for 1999 (Modern Plastics, p.114, July 1999). Improvements in process understanding and control stand to benefit this large business. Such improved understanding can evolve from the ability to assess the degree of nonlinearity inherent in the process. This knowledge may aid control practitioners in control scheme design and implementation. In this investigation, recently developed measures of curvature (Guay et al., 1995) are used to assess the steady-state nonlinearity of a gas-phase polyethylene reactor model. In what follows, the polyethylene production process is briefly outlined. Moreover, the model developed by McAuley et al. (1990) and McAuley and MacGregor (1991, 1993), to describe this process is introduced.

2.1.1 Process Description

The process being studied here is one that makes use of a fluidized-bed reactor for gas-phase polyethylene production, which is of the same type as Union Carbide's UNIPOL process (Miller, 1977), or BP's fluidized bed polyethylene production process (Chinh and Dumain, 1990). The polymerization involves the reaction of ethylene, an alpha-olefin comonomer such as 1-butene, and hydrogen, using a Ziegler-Natta or metallocene catalyst. A schematic of the process is shown in Figure 2.1.
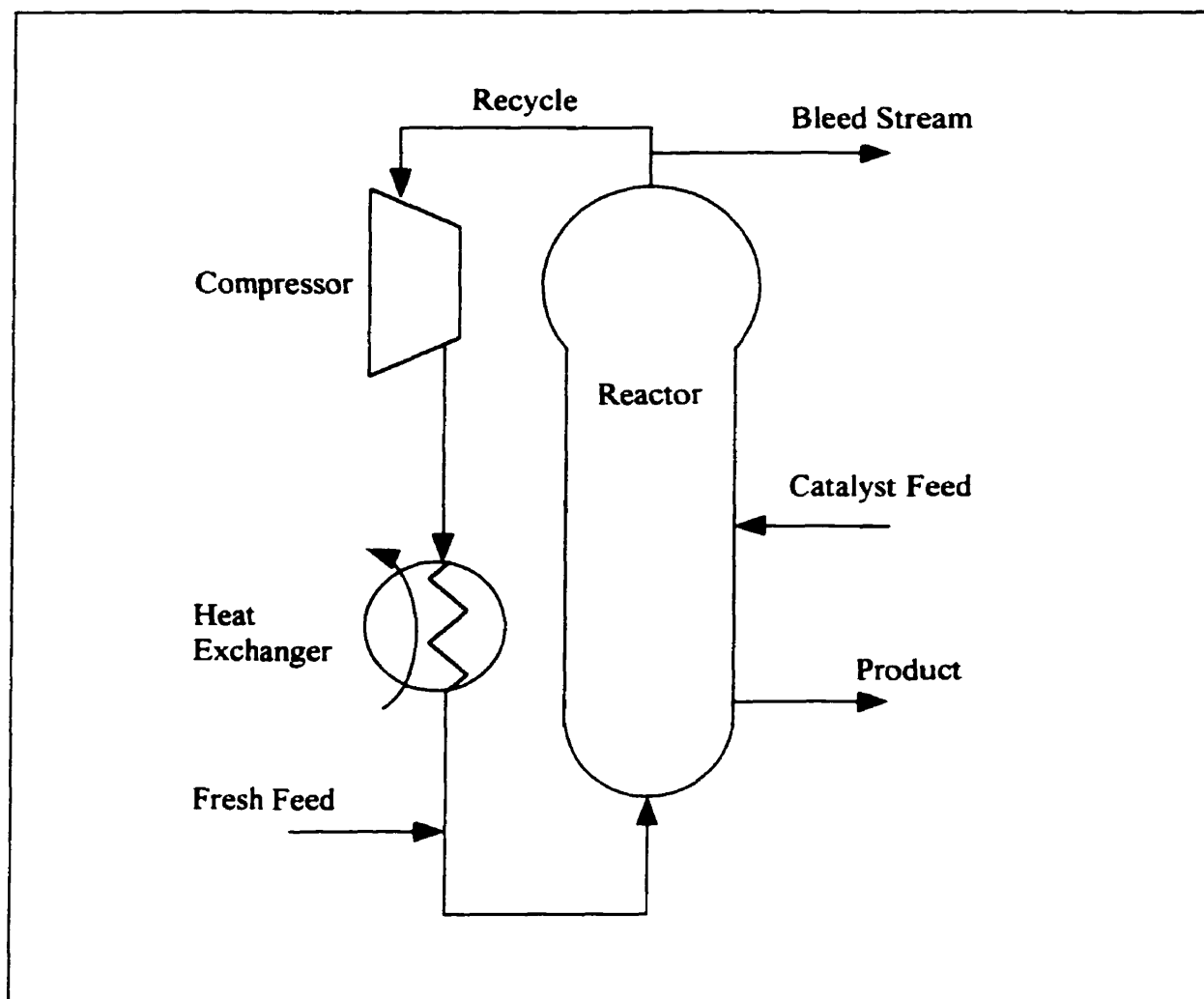
Figure 2.1. Schematic of a fluidized-bed polyethylene reactor.

The feed to the column is comprised of hydrogen, nitrogen, ethylene, and comonomer. The role of these gases is to supply reactants to growing polymer chains, and to act as fluidization and heat transfer media. Catalyst and co-catalyst are fed to the reactor continuously. A valve near the bottom of the reactor opens periodically, allowing polymer product to be removed. Unreacted gases are recovered from the product, and recycled back into the reactor. The discharged polyethylene is degassed and sent for additive incorporation, and pelletization. The enlarged upper section of the reactor

allows the polymer particles to disengage from the fluidizing gas. A bleed stream, located at the top of the reactor, prevents the accumulation of inerts and impurities. The recycle stream is rather large compared to the size of the feed stream, typically a ratio of 20 or 40:1. This large ratio is due to the relatively low single-pass conversion experienced within the reactor. The recycle stream is fed through a cooler to remove heat generated by the exothermic polymerization reaction. The reactor system is outfitted with several sensors, including pressure sensors, that indicate the mass of material in the bed, temperature sensors, and a gas chromatograph, which determines gas composition on-line (McAuley et al., 1990, and McAuley and MacGregor, 1991).

2.1.2 The Polyethylene Reactor Model

The polyethylene reactor model used in this work is that of McAuley and MacGregor (1991, 1993). It is a two-tiered nonlinear model comprised of a static algebraic component (McAuley and MacGregor, 1991), and a dynamic gas mass-balance component (McAuley and MacGregor, 1993).

The algebraic model equations predict instantaneous melt index and density from reactor temperature and gas compositions: (2.1)

$$\ln(MI) = k_7\left(\frac{1}{T} - \frac{1}{T_0}\right) + 3.5\ln\left(k_6 + k_1\frac{[M_2]}{[M_1]} + k_2\frac{[M_3]}{[M_1]} + k_3\frac{[H_2]}{[M_1]} + k_4\frac{[R]}{[M_1]} + k_5\frac{[I]}{[M_1]}\right)$$

where T and T_0 are the current temperature and a reference temperature, $[M_i]$ are gas-phase monomer concentrations (i = 1, 2, 3 indicates ethylene, butene, and a higher alpha-olefin, respectively). Polyethylene is usually produced using a single alpha-olefin comonomer, but two different comonomers can be present in the reactor during grade

7

changeovers. [H_2], [R], and [I] are each the hydrogen, cocatalyst, and reactive impurity concentrations in the reactor. Appropriate values for parameters k_1 to k_7 depend on the specific type of catalyst used in the reactor.

Polyethylene density depends on the number and type of short-chain branches. The incorporation of butene and higher alpha-order olefins result in short branches protruding from the polymer backbone. These branches inhibit crystalinity, thereby reducing density. To relate the density of the polymer being produced to gas-phase reactant concentrations, McAuley and MacGregor (1991) developed the following model:

$$\rho = p_0 + p_1 \ln(MI) - \left(p_2 \frac{[M_2]}{[M_1]} + p_3 \frac{[M_3]}{[M_1]} \right)^{p_4} \qquad (2.2)$$

The comonomer to monomer ratio terms in equation (2.2) reflect the fact that the relative rates of comonomer and ethylene incorporation into the polymer depend on their gas-phase concentrations. Parameters p_2 and p_3 reflect the kinetic rate constants for propagation reactions, and the ability of short-chain branches of different lengths to reduce density. For complete derivations of the models in equations (2.1) and (2.2), see McAuley et al. (1990), and McAuley and MacGregor (1991).

The models presented above are instantaneous property models, in that the model predicts the properties of polymer being produced at a given instant in time. The instantaneous properties may be quite different from the bulk or cumulative properties of the polymer in the reactor if reactor operating conditions have changed with time. In what follows in this research, the instantaneous properties are of interest for control. Alternatively, the cumulative properties could be controlled. In such case, the above models would need to be integrated over time, using an appropriate mixing model (McAuley and MacGregor, 1991). McAuley and MacGregor (1993) recommend

controlling the instantaneous product properties, shown in McAuley and MacGregor (1991), rather than cumulative properties.

In addition to the above nonlinear static portion of the reactor model, a dynamic portion exists. This dynamic portion is based on mass balances made on reactive species in the gas phase. The gas mass-balance model was presented by McAuley and MacGregor (1993):

$$\frac{d[H_2]}{dt} = \frac{1}{Vg}\left(F_{H2} - k_H \cdot Y \cdot [H_2] - \frac{[H_2]\cdot b}{C_t} - gl \cdot [H_2]\right)$$

$$\frac{d[M_2]}{dt} = \frac{1}{Vg + Vs}\left(F_{M2} - k_{p2} \cdot Y \cdot [M_2] - \frac{[M_2]b}{C_t} - S[M_2]Op\right)$$

$$\frac{dY}{dt} = F_{cat} \cdot a_{cat} - \frac{Y \cdot Op}{Bw} - k_d Y$$

$$\frac{dBw}{dt} = Y\left(k_{p1}[M_1]mw_1 + k_{p2}[M_2]mw_2\right) - Op$$

(2.3)

Y is the number of moles of active sites in the reactor. Bw is the mass of polymer in the fluidized bed. F_{H2}, F_{M2}, and F_{cat} are each the inlet molar flow rates of hydrogen, butene, and catalyst, respectively. Vg is the volume of the gas-phase. Vs represents the gas volume equivalent of butene dissolved in the polymer (hydrogen is negligibly soluble in polymer.) The parameter a_{cat} is the concentration of active sites in the entering catalyst. C_t denotes the total gas concentration in the reactor, b is the molar flow rate of the bleed stream, S is the solubility of butene in the polymer, and Op is the polymer outflow rate. The molecular weights of ethylene and butene are mw_1 and mw_2, respectively. The parameters k_{p1}, k_{p2}, and k_H are kinetic rate constants for ethylene, butene and hydrogen consumption reactions, whereas k_d is the rate-constant for deactivation of active catalyst sites. The parameter gl is a mismatch factor to account for some model imperfections; it is often updated recursively.

Notice that the dynamic material balance equations (2.3) do not contain an ordinary differential equation to predict the ethylene concentration. This is because fast and accurate measurements for ethylene concentration are available on-line. Also, the ethylene concentration, or partial pressure, in the reactor can be tightly controlled around a set-point. Changes between different polyethylene grades are typically made by adjusting the hydrogen and butene concentrations in the reactor, while holding the ethylene partial pressure relatively constant. Also, note that this set of model equations does not include balances on other comonomers. For simplicity, only polyethylene grades with butene as the comonomer will be considered in this thesis. However, extension of the results to other comonomers would be straightforward.

As it stands, the complete model ((2.1), (2.2), and (2.3)) depends on a number of assumptions. The reaction zone has been modelled as a well-mixed gas, interacting with a well-mixed solid phase (i.e., modelled as a CSTR). The assumption of a well-mixed gas phase holds (McAuley, Talbot, and Harris, 1994) by virtue of the high recycle to fresh feed ratio, and negligible axial and radial temperature and concentration gradients. Additionally, the total molar concentration in the gas-phase, C_t, which is proportional to the reactor pressure, and the ethylene concentration, $[M_1]$, are assumed to be held constant by controllers that adjust the flow of ethylene and nitrogen. Similarly, the bleed flow rate is kept steady by a flow controller, unless an operator adjusts the flow rate set point. Finally, the reactor is assumed to be operating under perfect bed-weight control, and perfect temperature control about a set-point temperature, T_0.

2.1.3 Simplifications of the Model Equations

The state equations of (2.3) can be simplified slightly. Based on the assumption that bed weight is maintained at a constant mass, the quantity dBw/dt becomes zero. Substituting and rearranging yields the final state model: (2.4)

$$\frac{d[H_2]}{dt} = \frac{1}{Vg}\left(F_{H2} - k_H \cdot Y \cdot [H_2] - \frac{[H_2]\cdot b}{C_t} - gl \cdot [H_2]\right)$$

$$\frac{d[M_2]}{dt} = \frac{1}{Vg+Vs}\left(F_{M2} - k_{p2} \cdot Y \cdot [M_2] - \frac{[M_2]b}{C_t} - S[M_2]Y\left(k_{p1}[M_1]mw_1 + k_{p2}[M_2]mw_2\right)\right)$$

$$\frac{dY}{dt} = F_{cat} \cdot a_{cat} - \frac{Y^2\left(k_{p1}[M_1]mw_1 + k_{p2}[M_2]mw_2\right)}{Bw} - k_d Y$$

A table of parameter values that will be used in the simplified output and state models is given in Table 2.1:

k_H (L/mol h)	= 1008	b (kg/h)	= 520	k_0 (g/(10 min))$^{1/3.5}$	=0.40
g_l (L/h)	= 3.6e-9	C_t (mol/L)	= 0.711	k_1 (g/(10 min))$^{1/3.5}$	=1.50
Vg (L)	= 423747	S (L/g)	= 0.002159	k_3 (g/(10 min))$^{1/3.5}$	=2.20
Vs (L)	= 151122	mw_1 (g/mol)	= 28.05	p_0 (g/cm^3)	=0.96
k_{p1} (L/mol h)	= 302400	mw_2 (g/mol)	= 56.12	p_1 ((g/cm^3)/ln(g/10min))	=0.0025
k_{p2} (L/mol h)	= 38448	a_{cat} (mol/kg)	= 1.0944	p_2 ((g/cm^3)$^{1/p4}$)	=0.0070
k_d (1/h)	= 0.36	Bw (tonnes)	= 70	p_4	=0.50

Table 2.1. Parameter values used in the simplified output and state models.

Note that appropriate values for the parameters depend on the particular catalyst being used in the reactor.

This work focuses on a system employing only one comonomer: butene. Higher alpha-order olefin comonomers are neglected. The final outputs that are of control interest in this thesis consist of melt index, density, and production rate, and therefore, the

final output model takes the form:

$$\ln(MI) = 3.5 \ln\left(k_0 + k_1 \frac{[M_2]}{[M_1]} + k_3 \frac{[H_2]}{[M_1]} \right)$$

$$\rho = p_0 + p_1 \ln(MI) - \left(p_2 \frac{[M_2]}{[M_1]} \right)^{p_4} \tag{2.5}$$

$$PR = Y\left(k_{p1}[M_1]mw_1 + k_{p2}[M_2]mw_2 \right)$$

Following McAuley and MacGregor (1991), the impurity and cocatalyst terms in the instantaneous melt index model have been condensed into a single paramter, k_0, because measurements of all of the different impurities that can affect melt index are typically not available on-line. McAuley and MacGregor (1991) developed a technique to update parameters k_0 and p_0 using off-line laboratory data, so that melt index and density could be monitored between off-line product property measurements. Subsequently, McAuley and MacGregor (1993) developed and simulated a nonlinear melt index and density control scheme using the models in Equations (2.1), (2.2), and (2.3). Since melt index and density measurements are not available on-line, implementation of the proposed nonlinear control scheme requires estimates of melt index and density from the product property monitoring scheme (McAuley and MacGregor, 1991). In addition, an Extended Kalman Filter was required as part of the nonlinear control scheme to update parameters k_{p2} and k_d and to obtain a reasonable estimate of polymer outflow rate. This parameter updating would ensure that the nonlinear ODE model would match plant behaviour. To make such a complex nonlinear control scheme work well, the designer must make certain that all of the nonlinear mathematical models used give good predictions, and that the monitoring scheme, Extended Kalman Filter, and the nonlinear control algorithm all work well together. An important question that arises is whether the potential benefits

that could be achieved using a nonlinear product property control scheme, compared to the traditional linear control scheme, merit the extra effort involved in implementation and maintenance.

In this thesis, the assessment of nonlinearity is performed on the simplified form of the model. Techniques used for nonlinearity assessment are reviewed in the next section, and the theory behind the curvature assessment employed throughout this work is described.

2.2   Nonlinearity Assessment

Most chemical processes exhibit some degree of nonlinearity. The severity of nonlinearity can greatly affect the stability and performance of the controller being implemented. Although much research has been done in the area of nonlinear process control (see reviews: Bequette (1991), Kravaris and Kantor (1990a,b), and McLellan et al. (1990)), reluctance exists among many practitioners to employ nonlinear control schemes due to the extra design, implementation, and maintenance efforts required and because the benefits of employing a nonlinear control scheme are often hard to quantify at the design stage. However, some processes, or parts thereof, exhibit such a severe degree of nonlinearity that linear techniques compromise control performance. Both the degree of nonlinearity of the process at a given operating point, and the intended range and direction of operation (Guay et al., 1995) are of particular importance. This being so, it is of great value to be able to assess the degree of nonlinearity of a process, in order to gain insight into whether the benefits of a nonlinear controller would warrant the additional efforts required.

In recent years, a few authors have developed methods for assessing nonlinearity. Operator-based approaches have been proposed by Nikoloau (1993), Ogunnaike et al. (1993), and Allgöwer (1995). Nikoloau measures dynamic nonlinearity by calculating the 2-norm of the best linear approximation of a nonlinear operator, where the 2-norm is based on a newly constructed inner product. Degree of nonlinearity is measured by Ogunnaike et al. by first determining the linear approximation of the nonlinear operator and then calculating the norm of the difference between the linear approximations of adjacent regions on a domain of process operation. A short-coming of this technique is that it is designed for SISO systems only, and that extension to dynamic nonlinearity measurement is difficult. Allgöwer describes degree of nonlinearity as the norm of the largest difference between the output of a nonlinear system and the output of its best linear approximation, considered for the worst-case input sequence. This measure of nonlinearity is computationally involved and depends on the choice of input signals considered. Each of these operator-based approaches suffers from limited insight into process structure, and does not describe the specific causes of curvature (Guay et al., 1995).

Koung and MacGregor (1991, 1992) define deterministic nonlinearities as a structured model mismatch seen in the singular-value decomposition of steady-state gain matrices. The extent of mismatch is measured by the relative degree of input or output rotation of the steady-state gain information, as well as a change in the magnitude of the singular values of the decomposed gain matrix.

Haber (1985) presented various computationally simple methods of determining the presence of nonlinearity within a system from input-output records. However, these

methods only detect nonlinearity, but don't quantify it.

Stack and Doyle III (1995, 1997a,b) describe using an optimal-control structure to analyze nonlinearity, since it includes controller performance specifications in addition to the control-law dynamics of a given process, which they claim is important in measuring control-relevant nonlinearity. (Control-relevant nonlinearity is defined as the influence that nonlinearities have in a closed-loop, taking into consideration specific performance goals.) The optimal-control structure can be designed analytically using Lagrangian methods. Control-relevant nonlinearity is then assessed using any open-loop nonlinearity measure that incorporates the effects of scaling. The nonlinearity measure is applied to the optimal control law. The value of this approach is that it assesses the nonlinearity that is eliminated to achieve optimal control performance rather than complete process nonlinearity.

In what follows, the curvature measure of Guay et al. (1995) is outlined. Guay et al.'s steady-state measure of curvature is an extension of earlier work measuring curvature in nonlinear least squares regression by Bates and Watts (1980, 1988). Key points of Guay et al.'s work are the decomposition of second-order derivative information into tangential and normal constituents, and the development of a scale-independent measure of curvature. Although not considered in this thesis, Guay's steady-state measure was extended to provide a measure of dynamic nonlinearity. The fundamental theory behind this dynamic measure is an extension of the steady-state nonlinearity case. Guay (1996) describes measuring dynamic nonlinearity of a process by considering first- and second-order derivative information in an operator setting, treating the dynamic process as an input-output operator. Provisions are made for scaling strategies.

Leung (1998) investigated the relationship between steady-state RMS and controller performance degradation for several simple examples, using the progression of IAE as a function of set point change as an indication of degradation. Leung also investigated curvature of the set point - IAE relationship. This work assessed controller performance changes over a range of varying set points about a fixed operating point. The distinction between Leung's work and the work presented here is as follows: the work in this thesis focuses on a multi-input multi-output industrial process example, and provides an in-depth investigation of steady-state curvature behaviour, including interpretations of the diagnostics in terms of input contours on the steady-state locus. Additionally, this work provides a detailed investigation of the relationship between RMS curvature and controller performance degradation over major changes in operation and for disturbance rejection.

2.2.1 The Steady-State Locus

The technique presented here is Guay et al.'s (1995) open-loop steady-state measure of curvature. Guay et al. (1995) also developed extensions of this steady-state work to process dynamics. Although dynamic measures of nonlinearity are not examined in this thesis, it is recommended that the assessment of dynamic nonlinearity of the polyethylene reactor model be done in the future.

Guay et al.'s steady-state measure of nonlinearity is performed by first analyzing the local geometry of the input-state map, and then applying corresponding output mappings to assess the nonlinearity of the input-output map. In applying measures of nonlinearity, either the input-state map or its inverse could be considered, however, the

work in this thesis focuses only on input-state and input-output maps, and not their inverses.

Consider the input-state relationship of the following asymptotically stable nonlinear system:

$$\dot{x} = f(x, u) \tag{2.6}$$

where x is an n-dimensional vector of states, and u is a p-dimensional vector of inputs. In the polyethylene reactor model, the corresponding input-state relationship is: (2.7)

$$
\begin{bmatrix} \dfrac{d[H_2]}{dt} \\[2mm] \dfrac{d[M_2]}{dt} \\[2mm] \dfrac{dY}{dt} \end{bmatrix} = \begin{bmatrix} \dfrac{1}{Vg}\left(F_{H2} - k_H \cdot Y \cdot [H_2] - \dfrac{[H_2]\cdot b}{C_t} - gl \cdot [H_2]\right) \\[3mm] \dfrac{1}{Vg + Vs}\left(F_{M2} - k_{p2} \cdot Y \cdot [M_2] - \dfrac{[M_2]b}{C_t} - S[M_2]Y\left(k_{p1}[M_1]mw_1 + k_{p2}[M_2]mw_2\right)\right) \\[3mm] F_{cat} \cdot a_{cat} - \dfrac{Y^2\left(k_{p1}[M_1]mw_1 + k_{p2}[M_2]mw_2\right)}{Bw} - k_d Y \end{bmatrix}
$$

$$
\text{with } u = \begin{bmatrix} F_{H2} \\ F_{M2} \\ F_{cat} \end{bmatrix}
$$

The *steady-state* input-state map is termed the steady-state locus, $\Xi(u)$, a construct used to describe static input-state behaviour. The steady-state locus, $\Xi(u)$, can be considered a hyper-surface, parameterized by p inputs, residing in n-dimensional state space (for the polyethylene reactor model above, $p=n=3$). More simply, $\Xi(u)$ is the plot of the final values of the model states, after one or more inputs have been adjusted, generated by setting the state time-derivatives to zero and solving for the values of states, given a set of input values.

The measure of nonlinearity used by Guay et al. is one that employs a second-order Taylor series approximation of the process, and compares it to the linear approximation of the locus at a given point. The degree to which the second order

17

approximation deviates from the linear approximation provides an estimate of the nonlinearity of the process at that point. A schematic of these concepts for a 2-state system, for changes in a particular input is shown in Figure 2.2.
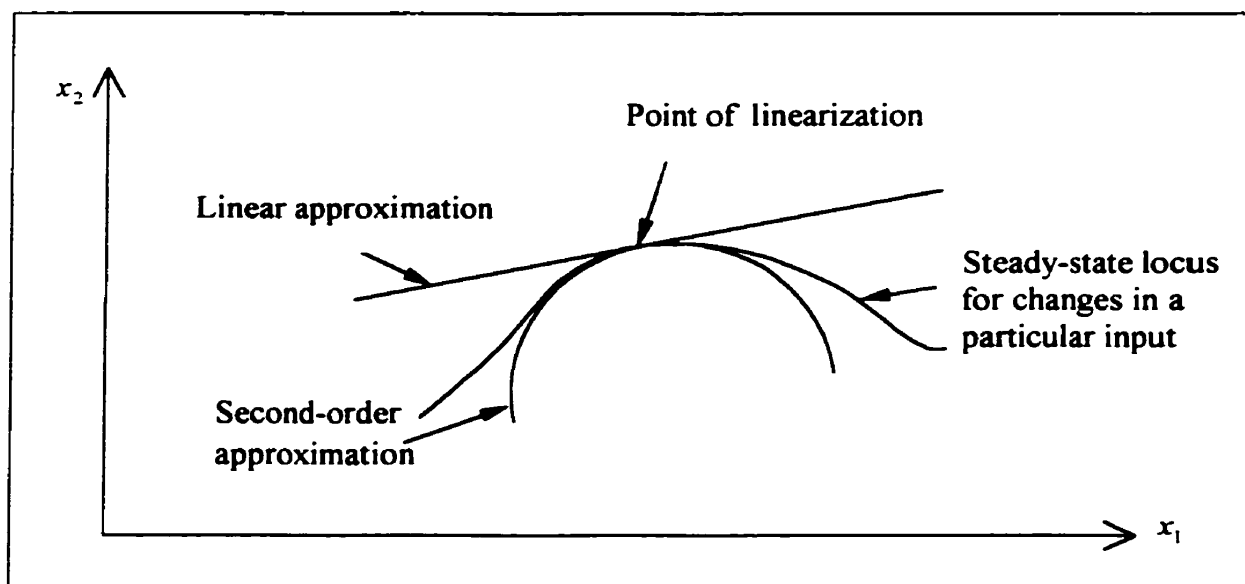
Figure 2.2 The steady-state locus, and its first- and second-order approximations.

2.2.2 Towards a Measure of Curvature

A model is said to be nonlinear when any second-derivative of the states with respect to the input parameters is nonzero; thus, nonlinearity is assessed by investigating the second derivatives of the states with respect to the inputs. A set of locally defined velocity and acceleration vectors are calculated at the steady-state operating point of interest:

$$\dot{v}_i = \frac{\partial \Xi(\mathbf{u})}{\partial u_i}, 1 \le i \le p \tag{2.8}$$

$$\ddot{\mathbf{v}}_{ij} = \frac{\partial^2 \Xi(\mathbf{u})}{\partial u_i \partial u_j}, 1 \le \{i, j\} \le p$$
(2.9)

where $\dot{\mathbf{v}}_i$ is the first derivative of the state vector with respect to input i, and $\ddot{\mathbf{v}}_{ij}$ is the state vector twice-differentiated: once with respect to input i and again with respect to input j. These velocity and acceleration vectors are important elements in assessing nonlinearity. The first-order, or velocity, vectors help define the tangential approximation of the steady-state locus. The second-order information, obtained from the acceleration vectors, describes both the degree of nonlinearity, and its causes. This information is of importance because the components of acceleration which lie along the tangential approximation result in curvature which is fundamentally different than the curvature resulting from components which lie normal to the tangential approximation. For this reason, second-order information is resolved into tangential and normal components. The nonlinearity resulting from tangential and normal acceleration components are appropriately called tangential curvature and the normal component of curvature, respectively.

Tangential curvature, also called parameter effects nonlinearity, depends on the parameterization of the model and presents itself as unequally spaced curves of constant input-parameter values on the steady-state locus. This type of nonlinearity is the result of the changing magnitudes and directions of the velocity vector components that lie tangent to the steady-state locus. Tangential acceleration causes linear, orthogonal, uniformly spaced lines in the input-space, when mapped onto the steady-state locus, to become skewed, curved, and unequally spaced, as is shown in Figure 2.3. Often a reparameterization of the model inputs, such as logarithmic or square root transforms, can

reduce the severity of this type of nonlinearity (Bates and Watts, 1988).
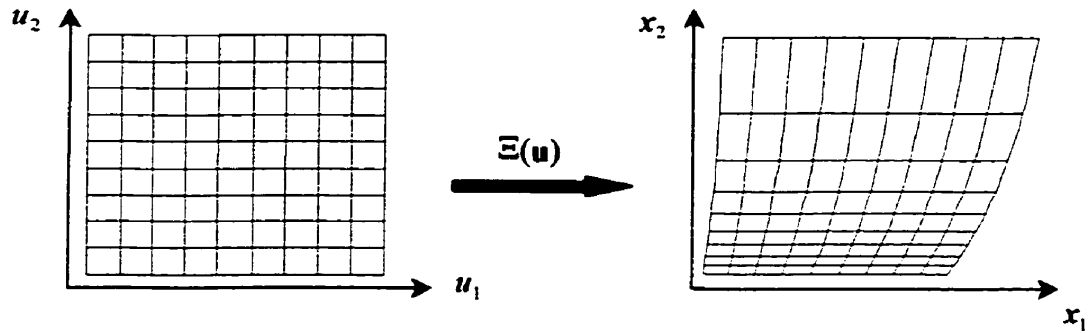
Figure 2.3 Schematic representing the consequences of tangential nonlinearity. Constant input lines are mapped into the state-space, where they may become distorted.

Intrinsic curvature, which is another term for the normal component of curvature, depends on the form of the steady-state map, and presents itself as the curvature of the steady-state locus relative to its surrounding space. It results from the changes in magnitude and direction of velocity vector components that lie normal to the tangent space. Unlike the case for parameter-effects nonlinearity, intrinsic curvature is invariant under a reparameterization of the model (Bates and Watts, 1988).

The acceleration vectors of a model can be decomposed into these two types of curvature by projection onto the space tangent to the steady-state locus, and onto the space orthogonal to the tangent space, respectively. In this thesis, *space* will refer to a general class of hyperplanes (i.e. vectors, planes and hyperplanes). Once the acceleration vectors have been resolved in this way, one can determine how the nonlinearity is distributed in the model.

To separate the acceleration vectors into their tangential and normal components, one must define an orthogonal basis for the state-space. p basis vectors will span the

20

tangent space, and p^n basis vectors span the space normal to the tangent space (the normal space that is spanned by the acceleration vectors). Note that it is possible to have additional normal dimensions that are not spanned by the acceleration vectors, and thus, p^n is not necessarily equal to n-p. The orthogonal basis is defined by first taking the velocity and nonredundant acceleration vectors, and arranging them in an $n \times p(p+3)/2$ matrix, $[V, W]$, given by:

$$[\mathbf{V}, \mathbf{W}] = (\dot{\mathbf{v}}_1 \dot{\mathbf{v}}_2 \cdots \dot{\mathbf{v}}_p \ddot{\mathbf{v}}_{1,1} \ddot{\mathbf{v}}_{1,2} \ddot{\mathbf{v}}_{2,2} \cdots \ddot{\mathbf{v}}_{1,p} \cdots \ddot{\mathbf{v}}_{p,p})$$ (2.10)

Taking the QR decomposition of the above matrix yields an orthonormal basis, $\mathbf{Q}$, for the tangent space and the space normal to the tangent space, but that is spanned by the acceleration vectors. Pre-multiplication of the velocity, and acceleration matrices, $\mathbf{V}$ and $\mathbf{W}$, by $\mathbf{Q}'$ yields the equivalent matrices in the new transformed basis. In keeping with Guay et al.'s nomenclature:

$$\mathbf{A} = \mathbf{Q}'\mathbf{W}$$ (2.11)

$$\mathbf{R}_1 = \mathbf{Q}'\mathbf{V}$$ (2.12)

where $\mathbf{R}_1$ is a $p \times p$ upper triangular matrix of velocities in the transformed basis. $\mathbf{A}$ is an $n \times p(p+1)/2$ matrix, where the first p rows comprise the tangential components, and the next p^n rows yield the normal components.

Curvature measures can now be presented in this transformed basis. The curvature of the steady-state locus, measured at a given point, along a direction, $\mathbf{e}$, in the input space, is given as the ratio of the norm of the resulting acceleration vector to the squared norm of the corresponding velocity vector:

$$c_e = \frac{\|\mathbf{e}'\mathbf{A}_r\mathbf{e}\|}{\|\mathbf{R}_1\mathbf{e}\|^2}$$ (2.13)

where A_r is a 3-dimensional array of n matrices, a_i, obtained from rearranging A. Each a_i is the $p \times p$ Hessian of transformed state i (see Guay et al., 1995):

$$A_r = \left[a_1, a_2, \cdots, a_n \right]'$$

(2.17)

To aid in the visualization of A_r, it may alternatively be represented as a three-dimensional block consisting of $p \times p$ Hessians of the transformed states, x'_i:
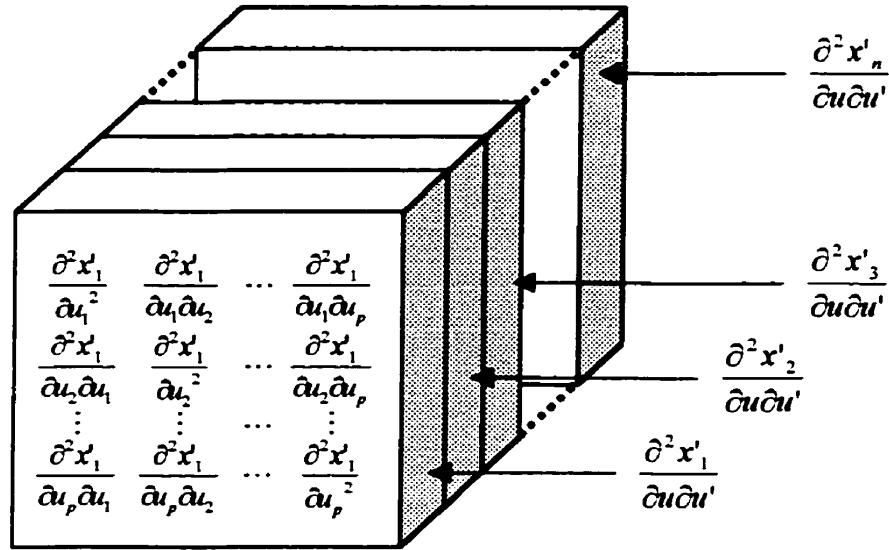
Figure 2.4 Another representation of the structure of A_r. Each slab (Hessian) of the three-dimensional block represents a face.

The subscript r, denotes some redundancy in the acceleration values as a result of rearranging the matrix A (e.g., both $\partial^2 x'/\partial u_1 \partial u_2$ and $\partial^2 x'/\partial u_2 \partial u_1$ are shown in the array, though they represent the same quantity. A_r can be used to decompose the tangential and normal curvature contributions by evaluating either the first p, or the last p^n faces, respectively.

The curvature measure developed above displays a high dependence on the scaling of the problem. Because the identical problem with different scaling of the states

and input parameters can produce very different curvature results, it can be difficult to obtain an appreciation of the degree of nonlinearity. A more useful approach would be one which is capable of producing a unique measure of curvature; one that is scale-independent.

2.2.3 Scaling

In addition to removing the unit-dependency of curvature on state variables, scaling is performed to reflect the intended region of operation on the steady-state locus. A larger operating region often results in a greater deviation of the process from its linear approximation such that the nonlinearity effects are more severe than when operating the same process in a smaller operating region. Appropriate scaling can account for this.

Assume that the operating region can be approximated, around a given point, by an ellipse of the form:

$$\Delta x'(S^{out'}S^{out})\Delta x = 1 \tag{2.15}$$

where S^{out} is an invertible scaling matrix that takes into account the size of the region of interest in the state space, and $\Delta x = x - x_0$ is the deviation of the state variables from the steady-state point of interest. S^{out} can be chosen as a diagonal matrix, whose elements reflect the expected range of operation for the states. This is termed output-prescribed (or more accurately, in this case, state-prescribed) scaling (Guay et al., 1995).

Alternatively, one could specify an elliptical region of interest in the input space, which corresponds to a region in the state space that, due to nonlinearity, might not be elliptical. Note that these two regions are related by the process map, and cannot be specified independently. The elements of an input-prescribed scaling matrix, S^{in}, are

chosen to reflect the intended region of operation within the input space. The equation of the ellipse in the input space is:

$$\Delta u' S^{in'} S^{in} \Delta u = 1 \qquad (2.16)$$

This elliptical region is then mapped into the state space, where it may become non-elliptical due to nonlinearity. However, the scaling procedure described by Guay et al. (1995) is defined for an elliptical region in the state space. Thus, a linear mapping of the input ellipse into the state space results in an elliptical approximation of the input prescribed region in the state space:

$$\Delta x = V \Delta u \qquad (2.17)$$

where V is the steady-state gain matrix. The corresponding elliptical approximation in the state space of the region defined in the input space is:

$$\Delta x' \left[\left(V^{-1} \right)' S^{in'} S^{in} \left(V^{-1} \right) \right] \Delta x = 1 \qquad (2.18)$$

The equivalent scaling matrix, S_{eq}^{out}, in the state space would take the form:

$$S_{eq}^{out} = S^{in} V^{-1} \qquad (2.19)$$

where S_{eq}^{out} typically becomes non-diagonal. This alternative procedure is termed input-prescribed scaling (Guay et al., 1995).

For simplicity, let S represent either the output prescribed scaling matrix, S^{out}, or the equivalent output scaling matrix, S_{eq}^{out}. Once S is chosen, the resulting ellipse in the state space, (2.15) or (2.18), can be transformed into a unit circle, by a linear change of coordinates $z = S\Delta x$ such that:

$$z'z = 1 \qquad (2.20)$$

The velocity and acceleration arrays may be scaled using the S matrix, by pre-multiplication by S prior to performing the QR decomposition. In z-coordinates:

$$\tilde{V} = SV \tag{2.21}$$

$$\tilde{W} = SW \tag{2.22}$$

where the tilde indicates a scaled quantity.

In addition to the selection of the orthogonal basis vectors in the state space, u can be transformed into orthogonal inputs, Φ, such that the denominator on the right-hand side of (2.13) is unity for a perturbation of unit length in any direction in Φ. The transformation is given by a linear change of coordinates as follows:

$$\Phi = R_1 \Delta u \tag{2.23}$$

In this form, the perturbation of each individual input will affect a change of the state variables along the direction of only one of the new basis vectors defined for the state space. Therefore, this transformation removes first-order interaction effects. The velocity vectors due to these new properly scaled orthogonal inputs are simply the tangential basis vectors defined for the state space. The velocity and acceleration vectors become:

$$\dot{v}^{\bullet} = \dot{v}^{u} R_1^{-1} = Q^{t} \tag{2.24}$$

$$\ddot{v}_r^{\bullet} = \left(R_1^{-1}\right)' \tilde{A}_r \left(R_1^{-1}\right) = \tilde{C}_r \tag{2.25}$$

Q^{t} is the matrix defined by the first p columns of Q, and $\tilde{C}_r$ is the rearranged relative curvature array for the region defined by S. $\tilde{C}_r$ is similar in structure to A_r in that it is a 3-dimensional array of $p \times p$ Hessian matrices, and contains n faces.

2.2.4 Root Mean Squared Curvature

Recall, the procedure for quantifying nonlinearity described in 2.2.2 measures the curvature of a process perturbed in a specific input direction. However, it is desirable to acquire a mean measure of curvature, averaged over all possible input directions. Such a curvature measure is called the root mean squared (RMS) curvature, c (or c_{RMS}, as it will be denoted in later chapters). It is calculated as follows (Guay et al., 1995, Bates and Watts, 1988):

$$c^2 = \frac{1}{p(p+2)} \sum_{i=1}^{n} \left[2 \sum_{j=1}^{p} \sum_{k=1}^{p} c_{ijk}^2 + \left(\sum_{j=1}^{p} c_{ijj} \right)^2 \right] \qquad (2.26)$$

where c_{ijk} is the ith face, j^{th} row, k^{th} element of the relative curvature array $\tilde{C}_r$.

The curvature measure of Guay et al. (previously illustrated in Figure 2.2), is the RMS curvature. As shown in Figure 2.5, it quantifies the degree of deviation between a second-order approximation of the properly scaled model and a linear approximation,
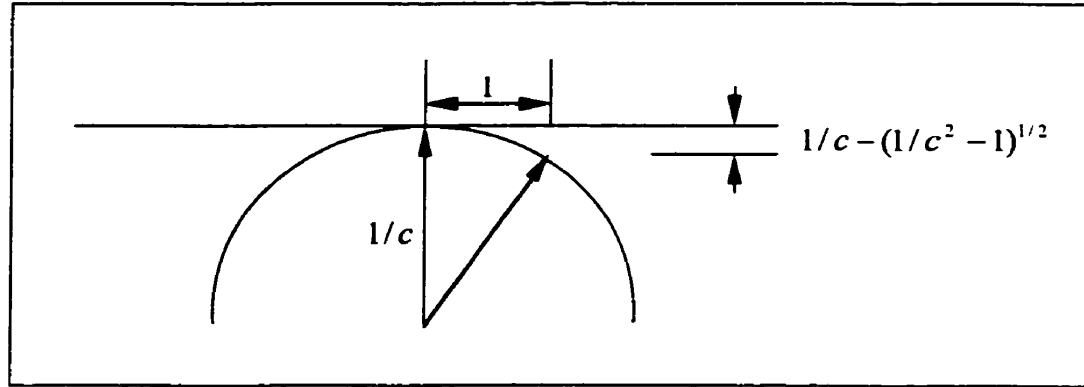
Figure 2.5 Schematic illustrating the relationship between RMS curvature, and percent deviation (following Guay et al., 1995).

where the nonlinear steady-state locus is locally approximated by a sphere of radius $1/c$. The magnitude of the deviation from the tangent plane approximation can be measured at

the boundary of the region of interest to be

$$|\text{deviation}| = \left(\frac{1}{c} - \left(\frac{1}{c^2} - 1\right)^{0.5}\right) \times 100\%$$ (2.27)

As a benchmark value, Guay et al. suggest that an RMS curvature value of 0.3 or greater indicates considerable nonlinearity. This RMS curvature value of 0.3 corresponds to a 15% deviation between the second-order approximation and the linear approximation, measured at a unit distance in z-coordinates, from the point of linearization. This measure of deviation can be conveniently compared to the size of the region of interest, which has been scaled to unity. Guay et al. also provide an outline of various other values of c and their corresponding percent deviations.

2.2.5 Extension to the Input-Output Map

What is presented above allows for the measurement of nonlinearity of the input-state map. An extension to the input-output relationship, developed by Guay et al., is now presented. Consider the following output function:

$$y = h(x)$$ (2.28)

where y is an m-dimensional vector of output variables. In the polyethylene reactor model, the outputs are related to the states in the following way:

$$\begin{bmatrix} \ln(MI) \\ \rho \\ PR \end{bmatrix} = \begin{bmatrix} 3.5\ln\left(k_0 + k_1\frac{[M_2]}{[M_1]} + k_3\frac{[H_2]}{[M_1]}\right) \\ p_0 + p_1\ln(MI) - \left(p_2\frac{[M_2]}{[M_1]}\right)^{p_4} \\ Y\left(k_{p1}[M_1]mw_1 + k_{p2}[M_2]mw_2\right) \end{bmatrix}$$ (2.29)

and the input-state relation was given in equation (2.7). In an open region surrounding a

27

point of interest, if $\partial h/\partial x$ and the differentiated input-state map, $\partial \Xi/\partial u$, both have full ranks of m and p, respectively, and if the input-output gain matrix, $\partial h/\partial x \cdot \partial \Xi/\partial u$, has full rank p everywhere on the operating region, then the first- and second-derivative information is determined by:

$$\frac{dy}{du} = \frac{\partial h}{\partial x}\frac{\partial \Xi}{\partial u} \quad and \quad \frac{d^2 y}{du^2} = \frac{\partial^2 h}{\partial x^2}\left(\frac{\partial \Xi}{\partial u}\right)^2 + \frac{\partial h}{\partial x}\frac{\partial^2 \Xi}{\partial u^2} \quad (2.30)$$

The above rank conditions hold for the polyethylene model, so that input-output nonlinearity can be assessed by employing equation (2.30). The remainder of the procedure for calculating RMS curvature, now between inputs and outputs rather than inputs and states, is as before.

2.2.6 Effects of Curvature and Interaction on the Geometry of the Steady-State Locus

The presence and severity of both interaction and curvature can significantly hinder the performance of a controller; thus, the detection and measurement of these characteristics can be of assistance in the design of a control scheme. Although the main goal of this thesis is to compare the performance of linear and nonlinear controllers operating at various RMS curvatures and to examine the control performance improvement that results from implementing a nonlinear controller, background on interaction is also presented because it will aid in the visualization and understanding of the steady-state locus. The purpose of this section is to illustrate the effects of curvature and interaction on the geometry of the steady-state locus. Piette et al. (1995) have presented a graphical interpretation of interaction measures to analyze multivariable

processes. Geometric descriptions of nonlinearity have been presented by Bates and Watts (1988) and Guay et al. (1995).

Consider a 2-input-parameterized steady-state locus residing in 2-dimensional state space. That is, a 2-dimensional surface comprised of 2 'sets' of constant input contours, 1 'set' for each input variable. The orientation with respect to the coordinate axes and the bending and spacing of the constant input lines demonstrates the presence and degree of interaction and nonlinearity in the steady-state model.

Linear interaction presents itself in two forms: one-way and transmission interaction. One-way interaction occurs as the result of one state variable being dependent on both manipulated variables, and the other state variable being affected by only one of the input variables. This is illustrated in Figure 2.6. A change in u_2 affects only x_2, whereas a change in u_1 results in changes in both states.
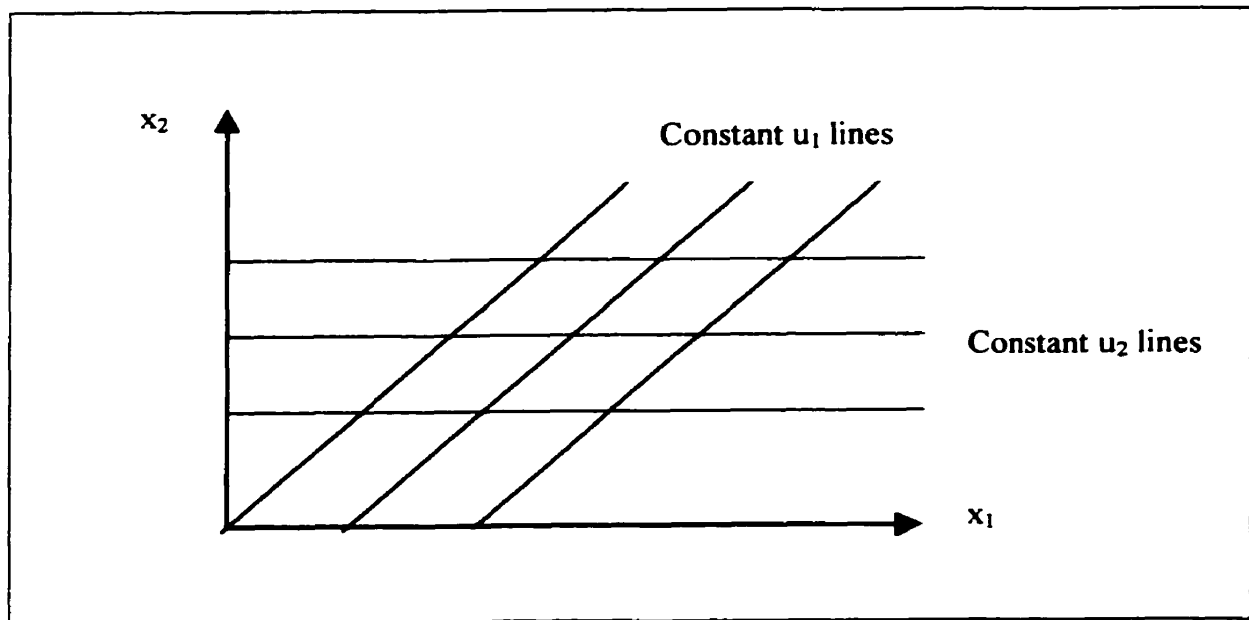
Figure 2.6 A graphical illustration of one-way interaction.

Transmission interaction, which causes the most serious control problems (Marlin, 1995) is also called figure-8 interaction, and occurs due to the existence of paths from both inputs to both outputs. Transmission interaction occurs when a change in the set point of one controller affects its output via a path through another controller. Visually, transmission interaction presents itself as shown in Figure 2.7. Now a change in either u_1 or u_2 will effect a change in both state variables. Transmission interaction is indicated by the rotation of both sets of constant input contours, relative to the coordinate axes, regardless of whether the contours are orthogonal to one another (Piette et al, 1995).
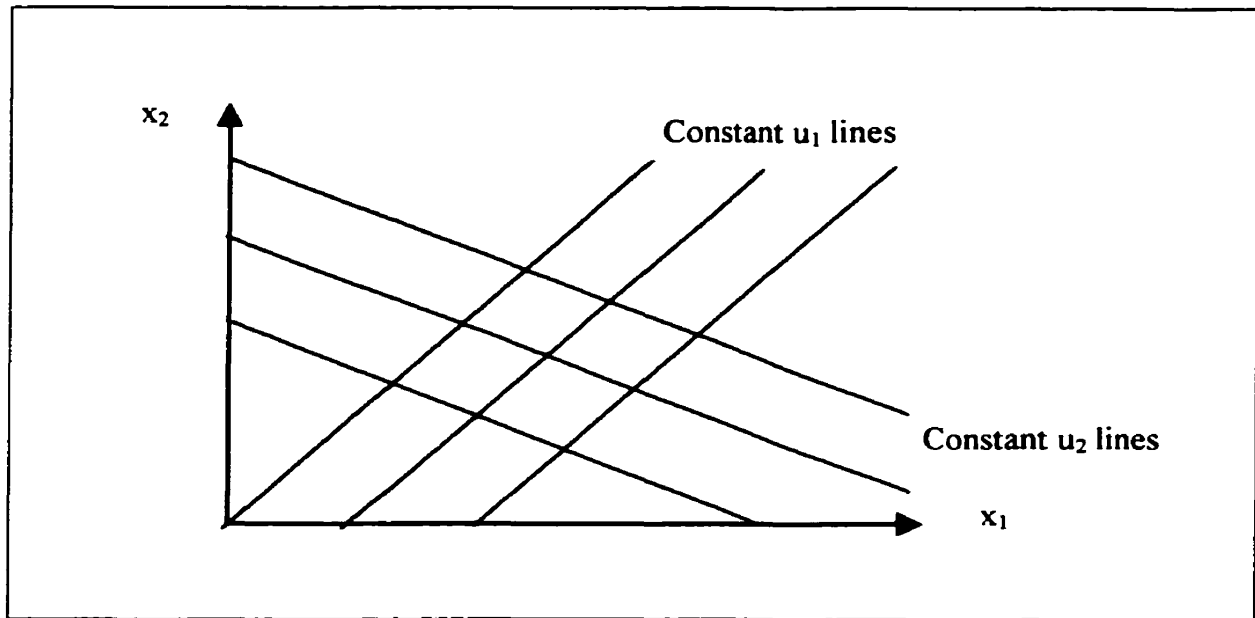
Figure 2.7 Graphical representation of a process displaying transmission interaction.

A tool for detecting and quantifying transmission interaction is the relative gain. The relative gain is calculated as (Marlin, 1995):

$$\lambda_{ij} = \frac{\left(\dfrac{\partial y_i}{\partial u_j}\right) u_k = \text{const}, k \neq j}{\left(\dfrac{\partial y_i}{\partial u_j}\right) y_k = \text{const}, k \neq i} = \frac{\left(\dfrac{\partial y_i}{\partial u_j}\right) \text{all other loops open}}{\left(\dfrac{\partial y_i}{\partial u_j}\right) \text{all other loops closed}}$$ (2.31)

λ_{ij} depicts the degree to which the effective gain $\partial y_i / \partial u_j$ is amplified or attenuated as a result of the other loops being closed.

The relative gains can be placed into a square matrix or calculated directly in matrix form to yield the relative gain array (e.g., Marlin, 1995):

$$RGA = V \cdot {}^{*} V^{-T}$$ (2.32)

V is the gain matrix, and .* denotes the Hadamard product (element-wise multiplication).

Although the relative gain array measures linear transmission interaction, a change in interaction structure along the steady-state locus indicates nonlinearity. In addition to a change in interaction structure, nonlinearity is also detected by the bending of the steady-state locus relative to surrounding state space, and to the curving and non-uniformity of spacing of the constant input contours on the locus itself.

Bending of the steady-state locus relative to surrounding state space is a result of the changing magnitude and direction of acceleration vectors that lie in the space normal to the tangent space. As mentioned earlier, this type of curvature is called intrinsic curvature, or the normal component of nonlinearity. A necessary, but not sufficient, condition for this type of nonlinearity to exist is that the state space must be of larger dimension than the input space. If input and state spaces are of the same size, the steady-state locus will completely "fill up" the state space, leaving no extra dimension relative to which the locus can bend. In this case, only the tangential component of nonlinearity may be present.

31

The consequence of the tangential component of nonlinearity is that evenly spaced, linear, orthogonal, constant input contours in the input space are mapped into the output space where they may become rotated, bent, non-uniformly spaced, and non-orthogonal. Tangential curvature itself can be assessed either by calculation of the RMS curvature over the first p faces of the relative curvature array $\tilde{C}_r$, or by examining the individual components of $\tilde{C}_r$.

Consider Figure 2.8, where the orthogonal basis vectors, q_1, q_2, obtained from the Q matrix, span the tangent space. Notice the absence of normal components, since $n=p=2$. Bates and Watts (1988) explain how to interpret the elements c_{ijk} of the relative curvature array. $\tilde{C}_r$ is similar in structure to A_r in that it is a 3-dimensional array consisting of n faces of $p \times p$ Hessian matrices; however, $\tilde{C}_r$ is defined for the scaling region prescribed by S, and for the transformed states and input coordinates. For the 2×2 system, the relative curvature array structure is as follows:

$$\tilde{C}_r = \left[\begin{pmatrix} c_{111} & c_{112} \\ c_{121} & c_{122} \end{pmatrix}, \begin{pmatrix} c_{211} & c_{212} \\ c_{221} & c_{222} \end{pmatrix} \right]$$

(2.33)

The c_{iii} elements are the *compansion*, or self-acceleration, terms. These elements of tangential nonlinearity cause compression or expansion of the constant input contours. Compansion results from the change in length of the velocity vector $\dot{v}_i$ (associated with ϕ_i) along the q_i direction as ϕ_i undergoes a unit change. Another characteristic of tangential acceleration is *arcing*, which results from the arcing terms, c_{jii}, $i \neq j$. These terms reflect bending of the constant input contours, and are a consequence of the change in the velocity vector $\dot{v}_i$ along the direction q_j, as ϕ_i changes. Another feature seen in

Figure 2.8 is the fanning out of the constant input lines. The *fanning* terms, c_{jji} are the result of a change in the q_j direction of the $\dot{v}_j$ velocity vector as ϕ_i is changed. Because of symmetry, $c_{jji}=c_{jij}$ are also considered fanning terms.
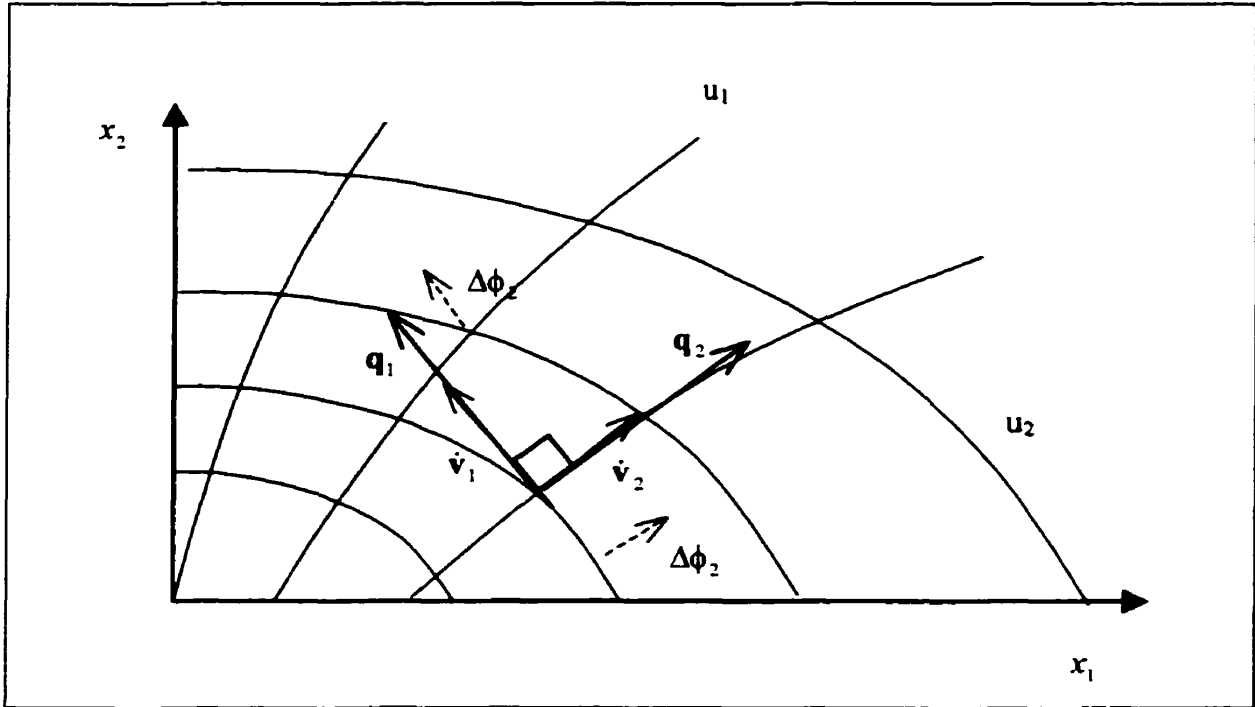
Figure 2.8 A steady-state locus displaying tangential nonlinearity.

To summarize the key aspects of the preceding work, nonlinearity can be *qualified* in terms of its effect on the geometry of the steady-state locus. Changing interaction structure, and tangential and normal components of nonlinearity all impact on the graphical representation of the steady-state locus. The degree of curvature is *quantified* by examining the magnitude of the second-order derivative information in a Taylor series approximation, relative to the first-order information. To permit comparison of curvature results with a benchmark value, appropriate scaling is applied. Scaling is chosen to properly reflect the region of operation, and remove the unit-

dependency of the RMS curvature measure on state variables. These measures were performed on the input-state map. Extension to the output space is easily accomplished by an output mapping.

2.3   Generic Model Control - An Error Trajectory Approach

The nonlinear controllers implemented in this work were all developed using the error-trajectory approach, resulting in controllers with the Generic Model Control (GMC) structure of Lee and Sullivan (1988). The error-trajectory approach is one that enables the direct implementation of the nonlinear process model, which is an appropriate choice bearing in mind that most chemical processes are inherently nonlinear in nature. The error-trajectory technique for controller design incorporates the process model, from which the explicit nonlinear control law is solved. Effectively, GMC is an example of input-output linearization using state feedback, with subsequent pole placement. Feedback linearization of nonlinear systems is described in further detail by Isidori (1989).

The polyethylene reactor model is a nonlinear model that can be written in the control affine form given below:

$$\dot{x} = f(x) + g(x)u$$
$$y = h(x)$$
(2.34)

where, in keeping with the earlier convention, x is an n-dimensional vector of states, u is a p-dimensional vector of inputs, and y is an output vector of dimension m. The error-trajectory approach can allow for the incorporation of known disturbances within the process model, thereby providing a feedforward element to the control law. Modelled

disturbances pertaining to the polyethylene model can include changes in bleed valve position, changes in pressure, and hence, C_t, changes in ethylene partial pressure, and therefore [M_1], and changes in B_w due to changing bed level set point. From (2.34), it follows that:

$$\dot{\mathbf{y}} = \frac{\partial \mathbf{h}}{\partial \mathbf{x}} \dot{\mathbf{x}}$$ (2.35)

The goal of the error-trajectory control law is to return the true process back to its desired set point by reducing the output tracking error. The output tracking error is defined to be:

$$e(t) = y_{sp}(t) - y(t)$$ (2.36)

where $y_{sp}(t)$ is the output set point. The controller is designed and tuned by specifying a desired tracking error-trajectory, which is a suitably well-behaved function $K(\cdot)$ of the tracking error and its higher-order derivatives (McLellan et al., 1990). Suitably well-behaved means that the control action will evolve directly from the error-trajectory description of the process. The tracking-error function is a linear function of the form:

$$K[e^{(\alpha)}(t), e^{(\alpha-1)}(t), \ldots, \dot{e}(t), e(t), t] = 0$$ (2.37)

where α is the relative order of the process. Relative order (also referred to as relative degree or difference order) is the number of times the output must be differentiated before the control will appear explicitly in the output function (Isidori, 1989) and represents the inherent integration of a process between the input and the output variables (Kravaris and Kantor, 1990).

In order to be able to solve for a control law expression, the error-trajectory function specified must be a function of at least the αth-order derivative of the tracking

35

error (McLellan et al., 1990). For a process model that has relative order one, the appropriate tracking-error function is:

$$\dot{e}(t) + \beta e(t) = 0 \qquad (2.38)$$

where β is a diagonal matrix of tuning parameters. Equation (2.38) defines an error trajectory controller with proportional action, that, in an ideal world would ensure that the process returns to steady state. However, if unmodelled nonstationary disturbances result in plant/model mismatch, there will be offset (unless appropriate steps are taken to adapt model parameters to eliminate the mismatch). For this reason, integral action must be added to the error-trajectory specification:

$$\dot{e}(t) + \beta e(t) + \gamma \int_{t_0}^{t} e(z)dz = 0 \qquad (2.39)$$

The motivation for including integral action in the controller is two-fold. Not only does it eliminate offset, thereby enhancing disturbance rejection and improving robustness, but it also serves as an approximate model inverse for unmeasured output/input or state/input disturbances (McLellan et al. 1990). This feature is necessarily applied to the present work, as many of the disturbances entering the polyethylene reactor are unmeasured and unmodelled.

Equation (2.39) is the GMC design equation. Lee and Sullivan (1988) chose the GMC parameter set such that (for the SISO case):

$$\beta = \frac{2\zeta}{\tau} \quad \text{and} \quad \gamma = \frac{1}{\tau^2} \qquad (2.40)$$

where τ and ζ are tuning parameters chosen from generalized GMC profile specification plots (see Lee and Sullivan, 1988) to give the desired shape and timing of response. For the MIMO error-trajectory specification given in equation (2.39), the coefficient matrices

β and γ are typically diagonal for decoupled performance. Equation (2.39) effectively specifies a pole placement for the error trajectory to asymptotically approach perfect tracking. The result is feedback linearization with pole placement.

Harris and McLellan (1990) proposed a set of necessary conditions that must be met for the implementation of the GMC algorithm:

i)   The process relative order must be one.

ii)   The process must have invertible dynamics.

iii)   The inverse of $g(x)$ must exist and be non-singular everywhere on the operating region.

iv)   The control actions extracted from the GMC formulation must be feasible.

v)   All of the states are measured or observable.

All of these conditions are met by the polyethylene reactor. Although Y, the number of moles of active sites in the reactor, cannot be measured, it can be observed using an Extended Kalman Filter (McAuley and MacGregor, 1991, 1993).

The final steps in the development of the control law are now presented. Given the GMC expression, the approximate or known process model is substituted into equation (2.39). Due to the control affine nature of the model, the control action, $u(t)$, appears explicitly in the error-trajectory equation. For simplicity, the control algorithm for a SISO process is exemplified below. Recall that the output model once differentiated is:

$$\dot{y} = \frac{\partial h}{\partial x}\dot{x} \quad \text{or} \quad \dot{y} = L_f h(x) + u(t) L_g h(x) \tag{2.41}$$

Substituting the above into the GMC expression, and rearranging, yields the control law:

$$u(t) = \frac{\dot{y}_{sp} + \beta(y_{sp} - y) + \gamma \int_{t_0}^{t} (y_{sp} - y)dz - L_f h(\mathbf{x})}{L_g h(\mathbf{x})} \qquad (2.42)$$

In the above, L_f and L_g are the Lie derivatives of the output map, $h(x)$. Lie derivatives are directional derivatives of $h(x)$, in the direction of the specified vector field; for example, $L_f h(x) = \frac{\partial h(x)}{\partial x} f(x)$.

For the case of multiple inputs and outputs, equation (2.42) becomes:

$$\mathbf{u}(t) = \left(L_g \mathbf{h}(\mathbf{x})\right)^{-1} \left[\dot{\mathbf{y}}_{sp} + \beta(\mathbf{y}_{sp} - \mathbf{y}) + \gamma \int_{t_0}^{t} (\mathbf{y}_{sp} - \mathbf{y})dz - L_f \mathbf{h}(\mathbf{x}) \right] \qquad (2.43)$$

where β and γ are each a diagonal matrix of error-trajectory tuning parameters. $L_f \mathbf{h}$ can be computed as the matrix multiplication of the Jacobian of $\mathbf{h}(\mathbf{x})$ with respect to $\mathbf{x}$, and $f(x)$. Similarly, $L_g \mathbf{h}$ can be computed as the matrix multiplication of the Jacobian $\frac{\partial \mathbf{h}}{\partial \mathbf{x}}$, and $g(x)$. It is clear that $L_g \mathbf{h}(\mathbf{x})$ must be non-singular to yield a solution, which implies that the relative order of the MIMO process must be one. In the MIMO case, if the dimensions m and p are the same, and if at least one element of u appears in each of the m equations, the problem reduces to solving m equations in m unknowns. This is the case with the polyethylene model of interest, where $m = 3$. Simultaneous solution of these m equations results in a full multivariable control law. If, however, each of the m equations is solved independently for each of the elements of u, a multi-loop control law results, with m SISO controllers. In this thesis, only multivariable control laws are employed. The issue of constraints on manipulated variables can be readily addressed by clamping; if a manipulated variable value is calculated such that it exceeds its upper or lower limit, the limiting value shall be implemented in its stead.

Dadebo et al. (1997) and Lee and Sullivan (1988) proposed similar approaches for selecting the tuning parameters of β and γ for an individual loop. Dadebo et al. treated the issue as a pole-placement problem, whereby β and γ were chosen to reflect a specified desired closed-loop dynamic response. They chose an over-damped closed-loop response with all poles placed at the same location. Lee and Sullivan propose a tuning metric, also based on a pole-placement solution. The desired shape and timing of the response is chosen from a correlational figure from which the individual elements of β and γ can be selected. Using Lee and Sullivan's tuning, the closed-loop response of the controller is a decaying second-order type, possibly oscillatory trajectory with initial overshoot in the controlled variable. Focussing on the linear error trajectory, the corresponding relationship between a single output and set point is a second-order closed-loop transfer function:

$$\frac{y(s)}{y_{sp}(s)} = \frac{\beta s + \gamma}{s^2 + \beta s + \gamma} \tag{2.44}$$

Note the presence of the process zero, which is the cause of controlled variable overshoot. Clearly, the presence of oscillations and the size of the overshoot are dependent on the choice of parameter values. It is important to note that these parameters must be chosen to reflect realistic process behaviour; a tuning trade-off exists between performance and manipulated variable action.

2.4 Summary

This chapter provides the necessary background information for the work considered in the rest of this thesis. In Section 2.1, the process for the production of

polyethylene was described, with the introduction of the model equations developed by McAuley et al. (1990), and McAuley and MacGregor (1991, 1993). The polyethylene reactor model is a nonlinear two-tiered model consisting of dynamic and static components. Simplifications to the original model were made, resulting in a three-input, three-output nonlinear dynamic model. This model is used in later chapters to assess the nonlinearity of the polyethylene reactor process.

In addition to providing a literature review of alternative work done in nonlinearity assessment, Section 2.2 also details the development of Guay et al.'s (1995) measure of curvature. Guay et al. estimate curvature by examining the local geometry of the steady-state locus. Second-order derivative information is decomposed into scaled tangential and normal components, which can then be manipulated to yield a local averaged measure of curvature.

To summarize the controller formulation in Section 2.3, an error-trajectory approach was taken in designing a nonlinear control scheme. After recognizing the need for integral action, a GMC controller resulted. A set of necessary conditions for the implementation of this GMC algorithm was described, of which all conditions are met by the polyethylene model, and finally, tuning suggestions were discussed.

Chapter 3

The Geometry of the Steady-State Locus:

Visualizing Curvature and Interaction

3.1 Introduction

The objective of this chapter is to provide an understanding of the physical relationships within the polyethylene reactor, and to relate those to the geometry of the steady-state locus. The characteristics of the geometry of the steady-state locus are illustrated graphically to demonstrate the effects of curvature and interaction, which were introduced in Chapter 2.

In what follows, the full polyethylene model presented by McAuley and MacGregor (1993), shown in Chapter 2, is simplified to a 3-state, 3-input (3×3) model, but to a different form than that shown in equation (2.4). Then, 2×2 portions of that model are explored. The simplified model form examined in this chapter consists of the following states: hydrogen and butene gas concentrations within the reactor and the production rate of polyethylene:

$$\mathbf{x} = \begin{bmatrix} [H_2] \\ [M_2] \\ PR \end{bmatrix} \tag{3.1}$$

The choice of these states was motivated by the fact that they are measurable states that represent important variables within the reactor. Other states could have been selected.

41

The number of moles of active sites, although directly related to the production rate, is not a measured quantity, whereas gas concentrations and production rate are. The input variables are as before:

$$\mathbf{u} = \begin{bmatrix} F_{H2} \\ F_{M2} \\ F_{cat} \end{bmatrix}$$ (3.2)

Because visualization of the interaction and curvature structure of the full 3×3 model is diffucult, the steady-state loci of the 2×2 portions of the model are presented and employed to illustrate these effects. The relevant measures, RMS curvature and RGA, are calculated and discussed.

3.2   Scaling Region

The region of interest in this chapter was arbitrarily chosen to encompass most of the steady-state locus. The region of interest in the input space is approximated by the ellipsoid:

$$\frac{\Delta F_{H2}^{\ 2}}{900^2} + \frac{\Delta F_{M2}^{\ 2}}{27000^2} + \frac{\Delta F_{cat}}{3.6^2} = 1$$ (3.3)

The choice for input-prescribed scaling was done for illustrative purposes, although it has a potential benefit over output-prescribed scaling in that it does tend to capture the inherent orientation of the steady-state process (Guay et al., 1995).

It is important to note that for practical purposes, a scaling region should be chosen to reflect the true process deviations. If we examine the scaling region defined by the ellipsoid in equation (3.3), we see that it would have little significance around the input [500 10000 2]'. This would imply that the manipulated variable ranges are:

$$\begin{bmatrix} -400 \\ -17000 \\ -1.6 \end{bmatrix} \leq \begin{bmatrix} F_{H2} \\ F_{M2} \\ F_{cat} \end{bmatrix} \leq \begin{bmatrix} 1400 \\ 37000 \\ 5.6 \end{bmatrix} \qquad (3.4)$$

Clearly, the lower bounds on the input flow rates are nonsensical. Consider the ellipse defined for the first two manipulated variables, shown in Figure 3.1:
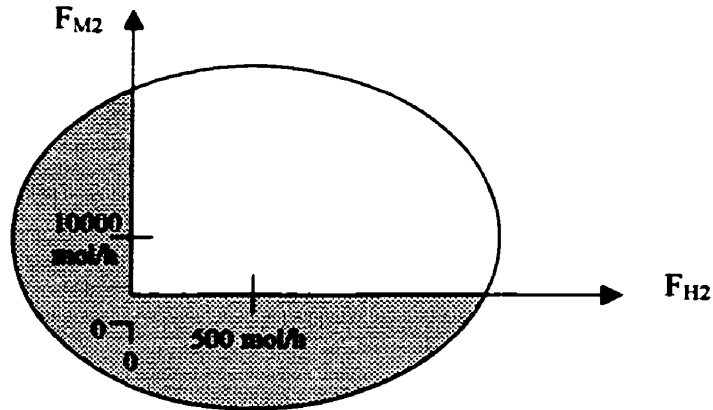
Figure 3.1. A schematic of the scaling region in the input space. A large portion of the scaled region is unattainable (shaded). An artificially large RMS curvature value may result.

This scaling implies a much larger operating region than is achievable, and may result in an artificially inflated curvature value. Therefore, a practitioner should take care to select an appropriate scaling. RMS curvatures can also be computed over non-elliptical regions; however, in this instance numerical integration of the curvatures over the region would likely be required. The curvature assessment in what follows in this chapter ignores this shortcoming of the scaling chosen. Rather, this choice provides an illustrative, not practically realizable view. This scaling is preserved for each point on the steady-state locus.

3.3 The Gas Mass-Balance Steady-State Loci

Because the states of interest in this evaluation are slightly different from those given in the final simplified model in Chapter 2, the full state model of (2.3) must be re-simplified to represent the proper states. At steady-state, equation (2.3) becomes:

$$\frac{d[H_2]}{dt} = 0 = \frac{1}{Vg}\left(F_{H2} - k_H \cdot Y \cdot [H_2] - \frac{[H_2] \cdot b}{C_t} - gl \cdot [H_2]\right) \qquad (3.5)$$

$$\frac{d[M_2]}{dt} = 0 = \frac{1}{Vg + Vs}\left(F_{M2} - k_{p2} \cdot Y \cdot [M_2] - \frac{[M_2] \cdot b}{C_t} - S[M_2]Op\right)$$

$$\frac{dY}{dt} = 0 = F_{cat} \cdot a_{cat} - \frac{Y \cdot Op}{Bw} - k_d Y$$

$$\frac{dBw}{dt} = 0 = Y\left(k_{p1}[M_1]mw_1 + k_{p2}[M_2]mw_2\right) - Op$$

Note that the differential bed weight equation contains the production rate equation:

$$PR = Y\left(k_{p1}[M_1]mw_1 + k_{p2}[M_2]mw_2\right) \qquad (3.6)$$

Therefore, PR=Op. Now we have four steady-state equations describing the relationship among four states, [H2], [M2], Y, and PR. To reduce this to a 3×3 problem, relation $\frac{dY}{dt} = 0$ is solved for Y in terms of F_{cat}, a_{cat}, k_d, PR, and Bw and substituted into the

remaining equations: $\qquad\qquad\qquad\qquad\qquad\qquad\qquad\qquad\qquad\qquad\qquad$ (3.7)

$$\frac{d[H_2]}{dt} = 0 = \frac{1}{Vg}\left(F_{H2} - \frac{k_h \cdot F_{cat} \cdot a_{cat} \cdot [H_2]}{\frac{PR}{Bw} + k_d} - \frac{[H_2] \cdot b}{C_t} - gl \cdot [H_2]\right)$$

$$\frac{d[M_2]}{dt} = 0 = \frac{1}{Vg + Vs}\left(F_{M2} - \frac{k_{p2} \cdot F_{cat} \cdot a_{cat} \cdot [M_2]}{\frac{PR}{Bw} + k_d} - \frac{[M_2] \cdot b}{C_t} - S[M_2]PR\right)$$

$$\frac{dBw}{dt} = 0 = F_{cat}a_{cat}\frac{\left(k_{p1}[M_1]mw_1 + k_{p2}[M_2]mw_2\right)}{\frac{PR}{Bw} + k_d} - PR$$

Curvature and interaction effects for this form of the model will be examined. The parameter values and constants are as presented in Chapter 2.

The effect of a pair of input variables on a pair of state variables is assessed in the following sections. The simplified gas mass-balance model shown in (3.7) is a three state, three input model; since the examination involves all possible combinations of states and inputs on the 2×2 level, nine views of the steady state locus result. The assessment will be divided into three parts, each of which will focus on the effects of two input variable combinations on a specific set of states. The steady-state loci were generated by varying hydrogen gas flowrate from 500 to 2300 mol/h, butene gas flowrate from 10000 to 64000 mol/h, and catalyst flowrate from 2.0 to 9.2 kg/h. The spacing between constant input contours corresponds to input increments as follows: 200 mol/h hydrogen flow, 6000 mol/h butene flow, and 0.8 kg/h catalyst flow. Recall that a single input is held constant while the other two are varied. The constant nominal value for hydrogen flow is 1500 mol/h, for butene flow it is 40000 mol/h, and 5.6 kg/h for catalyst flow rate.

To demonstrate the calculation of RMS curvature and the interpretation of the entries of the relative curvature array, $\tilde{C}_r$, two examples are given in 3.3.1.1.

3.3.1 Effect on Hydrogen and Butene Concentration

This section presents the effects of two input variables at a time on the concentration of butene and hydrogen gases in the reactor.

3.3.1.1 Effects of Butene and Catalyst Flow Rate

In this portion of the overall steady-state model, the effects of varying F_{M2} and F_{cat} on [H_2] and [M_2] are assessed. F_{H2} is held constant at 1500 mol/h.

Example 3.1

These calculations show how the curvature around point 1, shown in Figure 3.2, was determined. Point 1 is centered at:

$$\mathbf{u} = \begin{bmatrix} F_{H2} \\ F_{M2} \\ F_{cat} \end{bmatrix} = \begin{bmatrix} 1500 \ mol \, / \, h \\ 16000 \ mol \, / \, h \\ 2.0 \ kg \, / \, h \end{bmatrix} \tag{3.8}$$

The expected manipulated variable range is 54000 mol/h for butene flow and 7.2 kg/h for catalyst flow. Hydrogen flowrate is held constant. This choice of input range suggests the use of input prescribed scaling. The velocities are found by differentiating equation set (3.7) with respect to each input and solving for $\dot{v}_1$, and $\dot{v}_2$, where $\dot{v}_i$ is dx/du_i. The corresponding velocity matrix, $\mathbf{V}$, is:

$$\mathbf{V} = \begin{bmatrix} 7.560 \cdot 10^{-9} & -0.002766 \\ 5.282 \cdot 10^{-6} & -0.02831 \end{bmatrix} \tag{3.9}$$

Differentiating the velocity expressions with respect to inputs again, the acceleration array, $\mathbf{W_r}$, results:

$$\mathbf{W}_r = \left[\begin{bmatrix} -1.271 \cdot 10^{-14} & 1.273 \cdot 10^{-9} \\ 1.273 \cdot 10^{-9} & 0.0007704 \end{bmatrix}, \begin{bmatrix} 9.661 \cdot 10^{-12} & -1.800 \cdot 10^{-6} \\ -1.800 \cdot 10^{-6} & 0.02395 \end{bmatrix} \right]' \tag{3.10}$$

The input-prescribed elliptical scaling region is represented by:

$$S^{in} = \begin{bmatrix} \dfrac{1}{27000} & 0 \\ 0 & \dfrac{1}{3.6} \end{bmatrix}$$

(3.11)

Its elliptical approximation in state-space is:

$$S_{eq}^{out} = S^{in} V^{-1} = \begin{bmatrix} -72.83 & 7.1159 \\ -101.9 & 0.1459 \end{bmatrix}$$

(3.12)

The scaled matrix of velocity and non-redundant acceleration vectors is: (3.13)

$$[\tilde{V}, \tilde{W}] = S_{eq}^{out} [V, W] = \begin{bmatrix} 3.703 \cdot 10^{-5} & 0 & 6.967 \cdot 10^{-11} & 1.290 \cdot 10^{-5} & 0.1143 \\ -2 \cdot 10^{-16} & 0.2778 & 2.705 \cdot 10^{-12} & -3.923 \cdot 10^{-7} & -0.07503 \end{bmatrix}$$

Similarly, $\tilde{A}_r$ would be calculated as $\tilde{A}_r = S_{eq}^{out} A_r$. Taking the QR decomposition of

$[\tilde{V}, \tilde{W}]$ yields: (3.14)

$$Q = \begin{bmatrix} -1 & 0 \\ 0 & -1 \end{bmatrix} \quad R = \begin{bmatrix} -3.703 \cdot 10^{-5} & 0 & -6.967 \cdot 10^{-11} & -1.290 \cdot 10^{-5} & -0.1143 \\ 2 \cdot 10^{-16} & -0.2778 & -2.705 \cdot 10^{-12} & 3.923 \cdot 10^{-7} & 0.07503 \end{bmatrix}$$

R is the matrix of velocity and acceleration values for the new orthogonal basis obtained from Q. The first $p=2$ columns of R comprise the submatrix R_1. The columns of R_1 are the $p=2$ velocity vectors in the basis defined by Q. The last $p(p+1)/2$ columns of R comprise the A matrix, which consists of the non-redundant acceleration vectors defined in the Q basis. A_r is constructed from rearranging the entries in A, with some redundancy. The relative curvature array, $\tilde{C}_r$, is calculated from velocity matrix R_1 and the (scaled) acceleration array, A_r. From equation (2.25):

$$\tilde{C}_r = \left(R_1^{-1}\right)' \tilde{A}_r \left(R_1^{-1}\right) = \left[\begin{bmatrix} -0.05079 & 1.254 \\ 1.254 & -1.481 \end{bmatrix}, \begin{bmatrix} -0.001972 & 0.03813 \\ 0.03813 & 0.9723 \end{bmatrix} \right]'$$

(3.15)

From equation (2.26): $RMS = 1.409$ *End of example.*

Figure 3.2 shows the corresponding steady-state locus for the effects of varying F_{M2} and F_{cat} on $[H_2]$ and $[M_2]$. Consider a change in F_{M2}. F_{M2} affects $[M_2]$ considerably and has a very small effect on $[H_2]$. This small effect on $[H_2]$ is due to the following: by increasing monomer concentration, production rate is increased. Because the assumption that bed weight is held constant by a controller was imposed on this model, an increase in production rate implies an increase in polymer outflow rate. This in turn means that the residence time of the polymer decreases, thereby decreasing the concentration of active sites. Since there are fewer active sites, less chain transfer occurs and the hydrogen concentration goes up. F_{cat} also affects both $[H_2]$ and $[M_2]$. An increase in F_{cat} provides more sites with which H_2 and M_2 can react, and thereby both $[H_2]$ and $[M_2]$ decrease. Since both manipulated variables affect both controlled variables, transmission interaction must be present. This transmission interaction is seen in Figure 3.2, as both sets of constant input lines are rotated relative to the coordinate axis. Since the constant F_{cat} contours are rotated only slightly, a low degree of transmission interaction results, as seen by the relative gains given in Table 3.1.

Notice the small change in interaction structure in Table 3.1. Although the individual relative gain values indicate nothing about curvature, the change in relative gains over the steady-state locus hints at nonlinearity (in this case, however, the change in relative gains is almost negligible).

A large degree of curvature is immediately apparent, especially at high concentrations. Point 2 displays the lowest degree of curvature as verified by the RMS curvature value shown in Table 3.1. (Recall that Guay et al. (1995) concluded that an RMS curvature value less than 0.3 indicates negligible curvature.)

Point	F_{M2} value (mol/h)	F_{cat} value (kg/h)	RMS curvature value	$\lambda_{11}=\lambda_{22}$	$\lambda_{12}=\lambda_{21}$
1	16000	2.0	1.409	-0.015	1.015
2	16000	8.4	0.300	-0.0101	1.0101
3	64000	2.8	1.978	-0.054	1.054
4	58000	8.4	0.328	-0.036	1.036

Table 3.1 Locations and corresponding RMS curvature measures of specific points of interest for the steady-state locus of Figure 3.2.

Figure 3.2. Steady-state locus of hydrogen and butene concentration, parameterized by inputs butene flow and catalyst flow.

Very little fanning, arcing, or compansion effects are seen at point 2. The area surrounding point 1 displays some degree of all of fanning and arcing (of constant F_{M2} contours) as well as compansion effects (of constant F_{cat} contours). Some of these effects

become much more pronounced at point 3. Example 3.2 examines these tangential effects in more detail. For the following example, the matrix $\mathbf{R}_1$ is virtually diagonal, as seen in Example 1. Therefore, although the interpretation of elements c_{ijk} relate to changes in gains due to changes in ϕ_i, we discuss them in terms of u_i because both of these input bases lie along the same direction.

Example 3.2

The relative curvature arrays calculated for the four specified points in Table 3.1 and Figure 3.2 are shown here: (3.16)

$$
\text{Point 1}: \quad \tilde{\mathbf{C}}_r = \left(\begin{bmatrix} -0.0508 & 1.25 \\ 1.25 & -1.48 \end{bmatrix} \atop \begin{bmatrix} -0.00197 & 0.0381 \\ 0.0381 & 0.972 \end{bmatrix} \right)
\qquad
\text{Point 2}: \quad \tilde{\mathbf{C}}_r = \left(\begin{bmatrix} -0.0343 & 0.273 \\ 0.273 & -0.0569 \end{bmatrix} \atop \begin{bmatrix} -0.00308 & 0.0126 \\ 0.0126 & 0.369 \end{bmatrix} \right)
$$

$$
\text{Point 3}: \quad \tilde{\mathbf{C}}_r = \left(\begin{bmatrix} -0.0476 & 0.953 \\ 0.953 & -2.94 \end{bmatrix} \atop \begin{bmatrix} -0.00220 & 0.0330 \\ 0.0330 & 0.707 \end{bmatrix} \right)
\qquad
\text{Point 4}: \quad \tilde{\mathbf{C}}_r = \left(\begin{bmatrix} -0.0344 & 0.287 \\ 0.287 & -0.215 \end{bmatrix} \atop \begin{bmatrix} -0.00303 & 0.0137 \\ 0.0137 & 0.355 \end{bmatrix} \right)
$$

Compansion elements are the c_{111} and c_{222} elements. They represent the degree of compression or expansion experienced by constant input contours. Consider points 1 and 2. Constant F_{cat} contours experience expansion as one moves along the steady-state locus from point 2 to point 1. This is a result of the changing magnitude of the gain associated with F_{cat} (u_2), along the q_2 basis vector, as F_{cat} is varied. Recall, the vector q_i is a vector in the transformed basis, and is orthogonal to q_j. Correspondingly, we see that the c_{222} =0.97 term at point 1 is greater that at point 2, where the value is 0.37. In contrast, the spacing of constant F_{M2} contours is equally uniform at points 1 and 2.

Therefore, it follows that c_{111} entries for point 1, $c_{111} = -0.051$, and point 2, $c_{111} = -0.034$, are similar.

Consider arcing effects next, which are reflected by the c_{122} and c_{211} elements of the relative curvature array. Considering points 1 and 2 again, a greater degree of arcing is seen in constant F_{M2} contours at point 1 than at point 2. This is the result of a change in the q_1 direction of the velocity vector associated with F_{cat} (u_2) as F_{cat} is varied. The degree of arcing in the F_{M2} contours relates to the c_{122} element, which is $c_{122} = -1.48$ at point 1 and $c_{122} = -0.057$ at point 2. Similarly, the degree of arcing of the F_{M2} contours at point 1 is less than at point 3, leading to a smaller c_{122} entry for point 1 than for point 3, where $c_{122} = -2.94$. The arcing of constant F_{cat} contours is negligible at all four points. The corresponding values are the c_{211} elements of $\widetilde{C}_r$. For points 1 through 4, the c_{211} entries are -0.0020, -0.0031, -0.0022, -0.0030, respectively.

Finally consider the effect of fanning, corresponding to the c_{112} (or c_{121}) and c_{221} (or c_{212}) entries. Comparing points 1 and 2 again, it is clear that the constant F_{M2} contours fan out as one moves along the steady-state locus from point 2 to point 1. This fanning result is due to a change in the q_1 direction of the gain associated with F_{cat} (u_2) as F_{M2} (u_1) is varied, or alternatively, to a change in the q_1 direction of the gain associated with F_{M2} (u_1) as F_{cat} (u_2) is varied. Thus, the $c_{112} = 1.25$ entry at point 1 is larger than the corresponding entry at point 2, which is $c_{112} = 0.27$. Because the constant F_{cat} contours experience no obvious fanning, the c_{221} elements for each point are negligible, ranging from 0.013 to 0.038.

End of Example

3.3.1.2 Effects of Hydrogen and Butene Flow Rates

This section deals with the result of varying F_{H2} and F_{M2} on $[H_2]$ and $[M_2]$, while F_{cat} is held constant at 5.6 kg/h. The physical effects on the steady-state locus of changing inflow rates are illustrated in Figure 3.3.
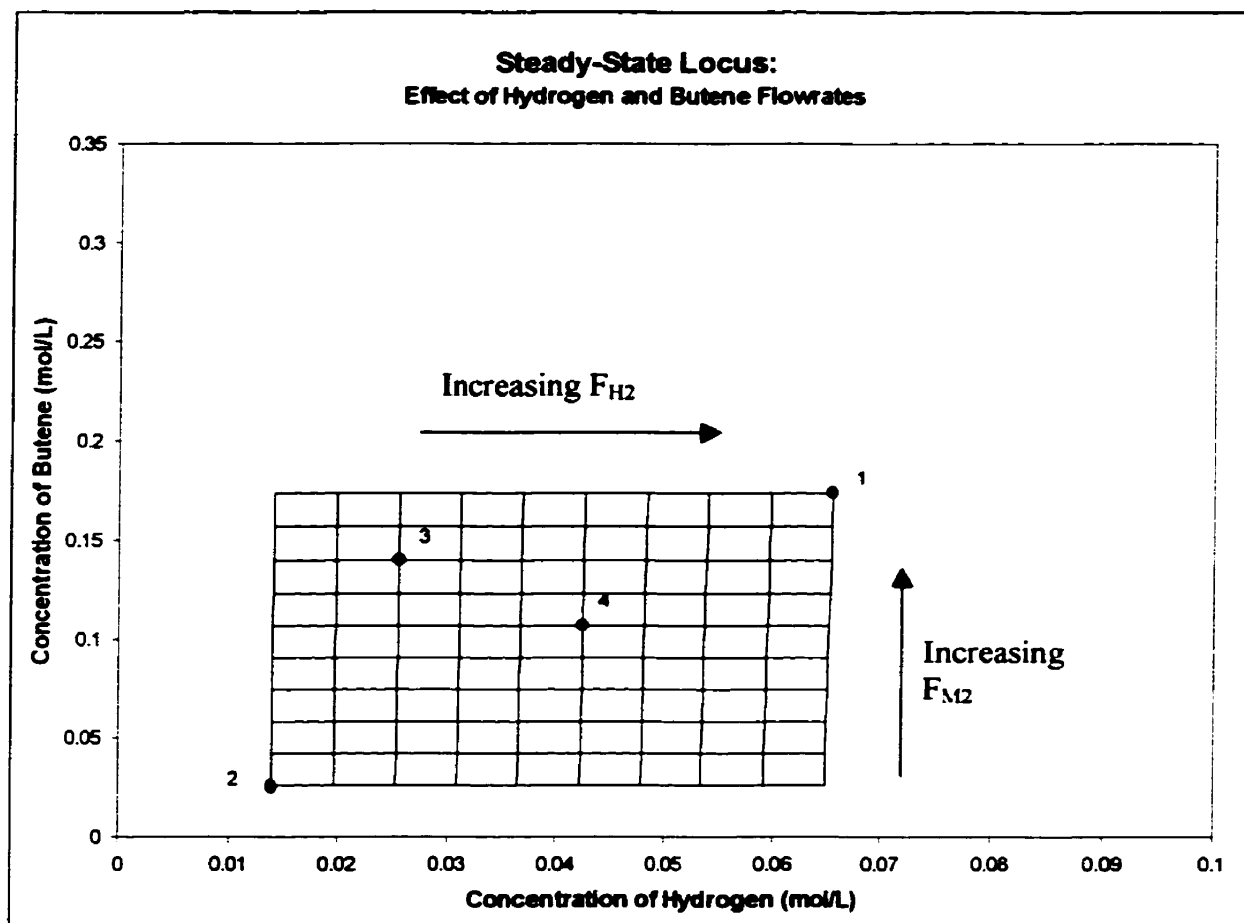
Figure 3.3 Steady-state locus of hydrogen and butene concentration, parameterized by inputs hydrogen and butene flow.

An increase in each reactant effects an increase in the concentration of the corresponding component. The plot displays no transmission interaction, which would be indicated by both sets of constant input contours being rotated relative to the state-

space axes; however, a very low degree of one-way interaction is present. This is demonstrated by the slight deviation of the constant F_{H2} contours from the vertical. The physical interpretation is that while a change in F_{H2} bears no consequence on [M_2], a change in F_{M2} causes a change in both [M_2] and, a much smaller change in [H_2]. The dual effect of F_{M2} on [M_2] and [H_2] was explained in 3.3.1.1. This one-way interaction is not reflected by the relative gains calculated in Table 3.2 for this locus, as relative gains measure two-way, or transmission interaction information.

By inspection, it appears that there is a very low degree of curvature associated with this steady-state locus. This is confirmed by the RMS curvature measures given in Table 3.2, all of which are well below the benchmark value of 0.3. This is of little surprise considering the appearance of the locus; the spacing of the constant input contours is uniform, and no arcing or fanning is apparent.

Point	F_{H2} value (mol/h)	F_{M2} value (mol/h)	RMS curvature value	$\lambda_{11}=\lambda_{22}$	$\lambda_{12}=\lambda_{21}$
1	2300	64000	0.0230	1	0
2	500	10000	0.0243	1	0
3	900	52000	0.0233	1	0
4	1500	40000	0.0236	1	0

Table 3.2 Locations and corresponding curvature and relative gain measures for specific points of interest on the steady-state locus in Figure 3.3.

3.3.1.3 Effects of Hydrogen and Catalyst Flow Rates

In the following investigation on state variables [H_2] and [M_2], F_{H2}, and F_{cat} are manipulated. It is observed from Figure 3.4 that increasing F_{H2} serves only to increase [H_2], while manipulating F_{cat} affects both [H_2] and [M_2] for reasons already described. This would indicate one-way interaction and result in a $\lambda_{11}=1$, which is verified by Table 3.3.

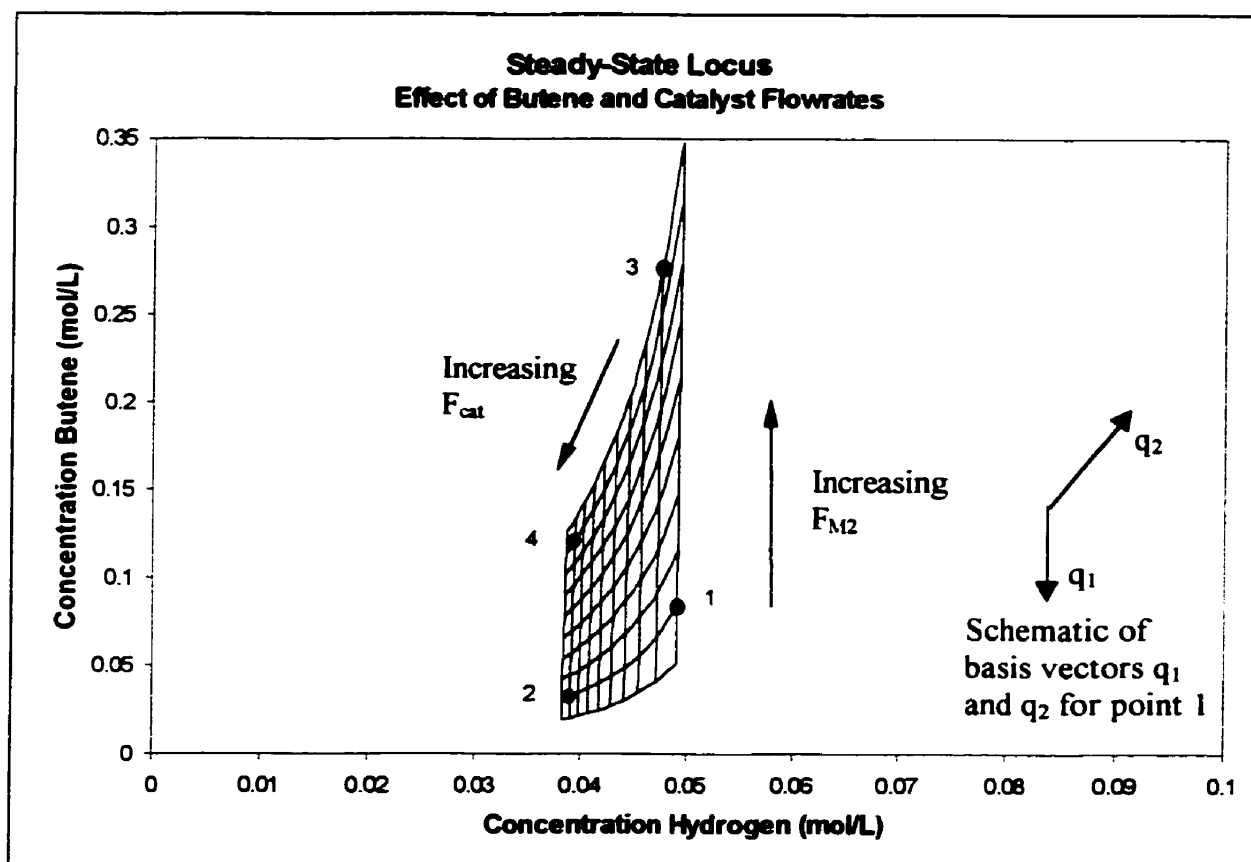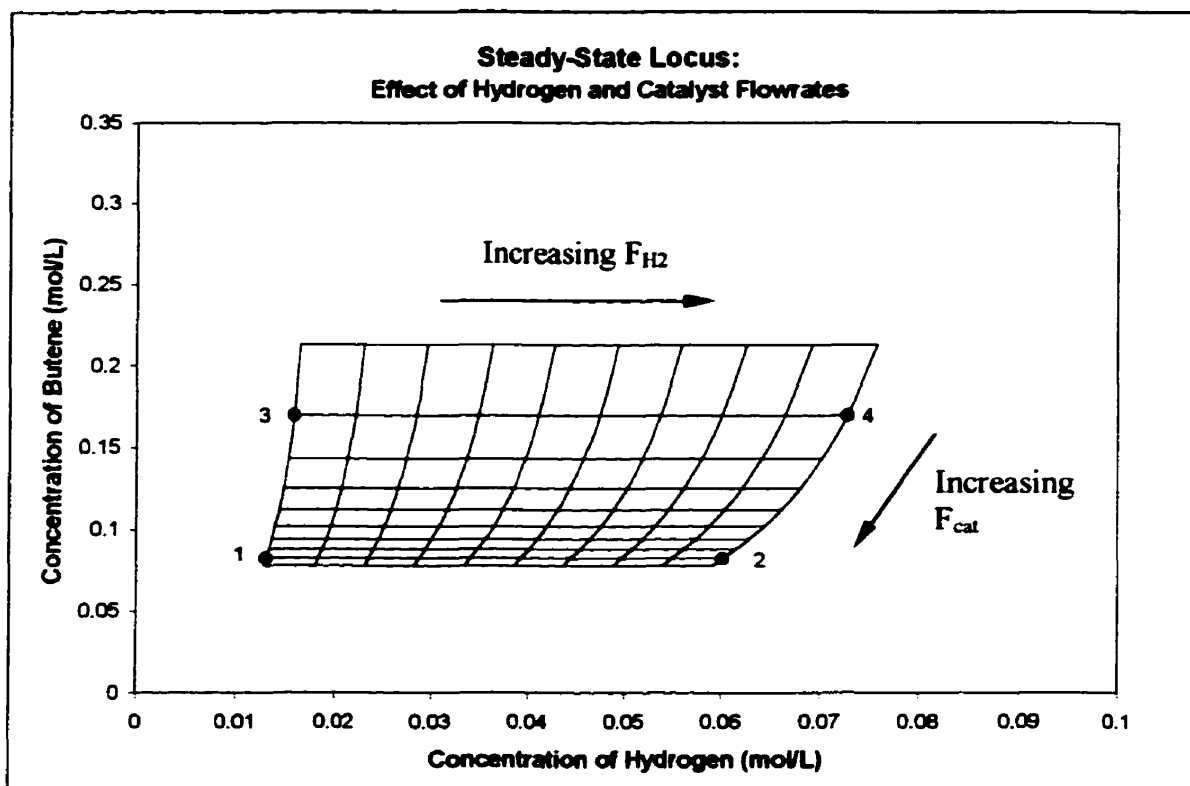**Figure 3.4** Steady-state locus of hydrogen and butene concentration, parameterized by inputs hydrogen and catalyst flow.

Examining the nonlinearity of this plot, curvature is expected to be smallest at point 1. This point represents an area that shows a small degree of arcing and fanning in constant F_{H2} contours, but none in F_{cat} contours. As well, this point exhibits the most uniformity of spacing of both F_{H2} and F_{cat} contours. Although the degree of compansion remains relatively unchanged along the locus to point 2, the degree of arcing of constant F_{H2} contours increases, indicating higher inherent nonlinearity. Point 3 displays significantly higher consequences of compansion among constant Fcat curves than at points 1 and 2. Point 4 marks an area of greatest combination of fanning, arcing, and compansion properties, suggesting the highest degree of curvature. This assessment is supported by the calculated RMS curvature values in Table 3.3.

Point	F_{H2} value (mol/h)	F_{cat} value (kg/h)	RMS curvature value	$\lambda_{11}=\lambda_{22}$	$\lambda_{12}=\lambda_{21}$
1	500	8.4	0.453	1	0
2	2300	8.4	0.456	1	0
3	500	2.8	1.356	1	0
4	2300	2.8	1.404	1	0

Table 3.3 Locations and corresponding curvature and relative gain measures for specific points of interest on the steady-state locus in Figure 3.4.

3.3.2 Effect on Hydrogen Concentration and Production Rate

This section is similar in spirit to the previous one in that the effects of input variables, two at a time, on a given set of states are investigated.

3.3.2.1 Effects of Hydrogen and Butene Flow Rates

The steady-state locus given in Figure 3.5 is generated by varying F_{H2} and F_{M2}, and observing [H₂] and PR. As before, F_{M2} affects PR and [H₂]. F_{H2} has no effect on PR, but serves to influence [H₂]. Therefore, a small degree of one-way interaction is present.

By inspection, it appears that the curvature structure is similarly small at all points. No obvious bending of the constant input contours is visible, and they appear to be equally spaced. Little or no curvature over all points is observed in Table 3.4, as RMS curvature values are very small and almost indistinguishable.

Point	F_{H2} value (mol/h)	F_{M2} value (mol/h)	RMS curvature value	$\lambda_{11}=\lambda_{22}$	$\lambda_{12}=\lambda_{21}$
1	500	16000	0.00727	1	0
2	2300	16000	0.00727	1	0
3	500	58000	0.00675	1	0
4	2300	58000	0.00675	1	0

Table 3.4 Locations and corresponding curvature and relative gain measures for specific points of interest on the steady-state locus in Figure 3.5.
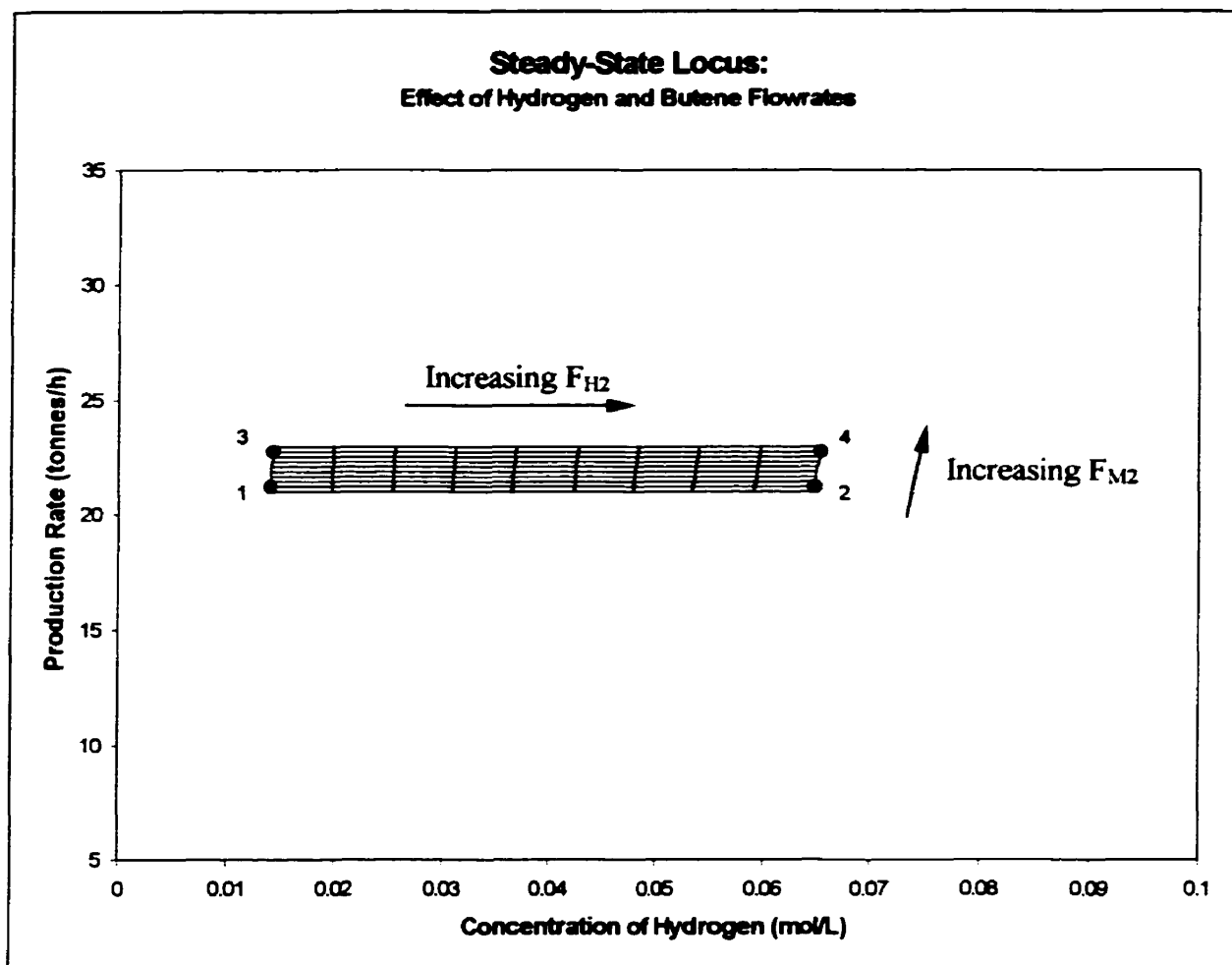
Figure 3.5 Steady-state locus of hydrogen concentration and production rate, parameterized by inputs hydrogen and butene flow.

3.3.2.2 Effects of Hydrogen and Catalyst Flow Rates

Next, the combined effects of F_{H2} and F_{cat} on PR and $[H_2]$ are presented in Figure 3.6. As discussed previously, F_{H2} affects only $[H_2]$; however, F_{cat} causes changes in both $[H_2]$ and PR. As F_{cat} increases, the number of active sites in the reactor increases thereby stimulating production rate, and providing more sites on which hydrogen can react. The result is a one-way interaction structure. As is seen in Figure 3.6, the interaction structure changes over the area of the steady-state locus, implying the presence of nonlinearity.

Point	F_{H2} value (mol/h)	F_{cat} value (kg/h)	RMS curvature value	$\lambda_{11}=\lambda_{22}$	$\lambda_{12}=\lambda_{21}$
1	500	2.8	0.324	1	0
2	2300	2.8	0.334	1	0
3	500	8.4	0.134	1	0
4	2300	8.4	0.136	1	0

Table 3.5 Locations and corresponding curvature and relative gain measures for specific points of interest on the steady-state locus in Figure 3.6.
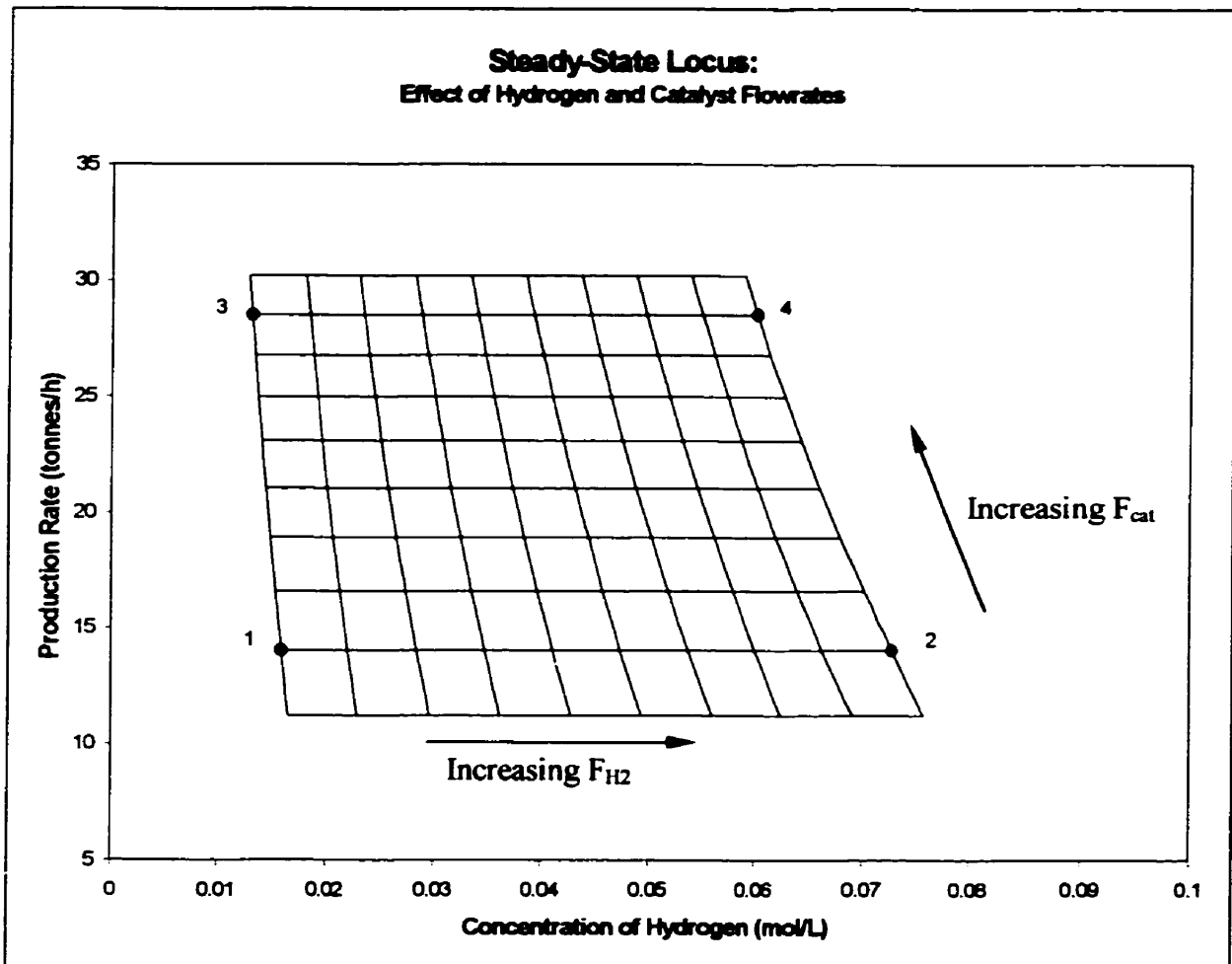
Figure 3.6. Steady-state locus of hydrogen concentration and production rate, parameterized by inputs hydrogen and catalyst flow.

Nonlinearity is assessed at the given points in Table 3.5. Point 3 displays the least amount of curvature in that the constant input lines are straight and most uniformly

57

spaced. Fanning does not appear to be present. Moving along the constant F_{H2} contour from point 3, it is clear that expansion in the spacing between F_{cat} contours develops. Point 4 is similar to 3 except that fanning becomes evident as one-way interaction becomes more pronounced, resulting in an increase in RMS curvature. Point 2 displays the greatest degree of curvature; the constant F_{H2} contours are bent, and fanning becomes more visible. These observations are confirmed by calculation of RMS curvature values in Table 3.5.

3.3.2.3 Effects of Butene and Catalyst Flow Rates

The steady-state locus in Figure 3.7 portrays the effects of F_{M2} and F_{cat} on [H_2] and PR. (The scales of this plot are inconsistent with the other plots because when viewed in the original coordinate range, the constant input contours are too closely spaced to be distinguishable.) The presence of transmission interaction is seen as follows: a shift in F_{cat} affects change in both [H_2] and PR, as does the manipulation of F_{M2}. The relative gains are shown in Table 3.6, indicating a fair amount of transmission interaction.

Point	F_{M2} value (mol/h)	F_{cat} value (kg/h)	RMS curvature value	$\lambda_{11}=\lambda_{22}$	$\lambda_{12}=\lambda_{21}$
1	16000	2.0	2.47	0.213	0.787
2	58000	2.0	1.95	0.204	0.796
3	16000	8.4	0.620	0.337	0.663
4	58000	8.4	0.607	0.326	0.674

Table 3.6 Locations and corresponding curvature and relative gain measures for specific points of interest on the steady-state locus in Figure 3.7.

It is difficult to discern the nonlinearity structure in the plot in Figure 3.7, however, a compansion effect in constant F_{cat} contours becomes pronounced at low F_{cat}

values. In addition, it appears that some degree of fanning is present in the area of points 1 and 2, since the constant F_{M2} lines spread out very slightly at the higher [H_2] end. These characteristics indicate that curvature is most prominent at the higher [H_2] end of the locus; this is found to be so by calculation of RMS curvatures in Table 3.6.
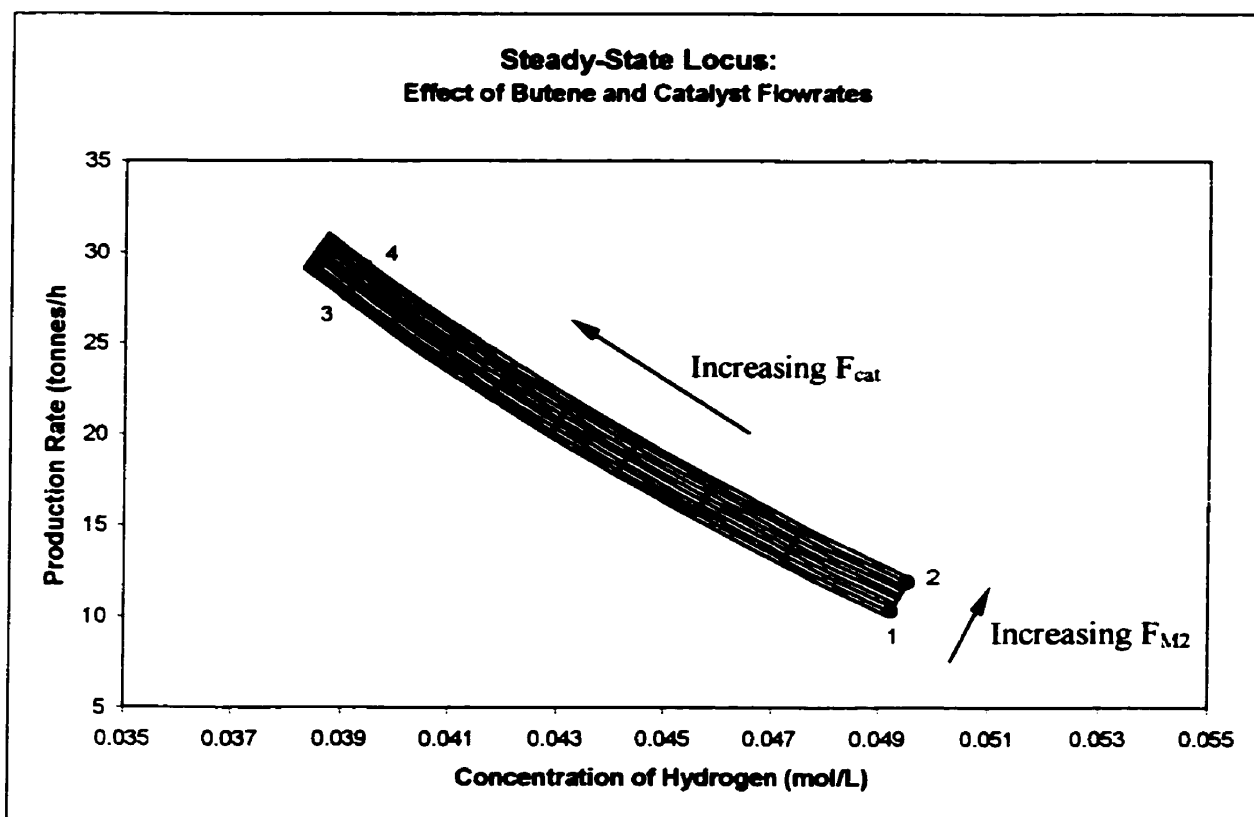
Figure 3.7. Steady-state locus of hydrogen concentration and production rate, parameterized by inputs butene and catalyst flow.

3.3.3 Effect on Butene Concentration and Production Rate

This final section of 2×2 plots deals with the assessment of curvature in the [M_2]-PR state space.

3.3.3.1 Effects of Butene and Catalyst Flow Rates

The steady-state locus of interest, shown in Figure 3.8, is generated by varying F_{M2} and F_{cat}. Once again, transmission interaction is evident. Recall that an increase in F_{M2} results in a corresponding increase in $[M_2]$ and also in propagation rate, and thus, in PR. F_{cat} increases the amount of active sites in the reactor, stimulating PR and a higher consumption of butene. Although Table 3.7 does not show much interaction, it does indicate changes in the relative RGA structure, which further indicate the presence of nonlinearity.

Figure 3.8 Steady-state locus of butene concentration and production rate, parameterized by inputs butene and catalyst flow.

Point	F_{M2} value (mol/h)	F_{cat} value (kg/h)	RMS curvature value	$\lambda_{11}=\lambda_{22}$	$\lambda_{12}=\lambda_{21}$
1	16000	2.8	0.760	0.959	0.041
2	64000	2.8	1.899	0.855	0.145
3	16000	8.4	0.230	0.981	0.019
4	64000	8.4	0.308	0.926	0.074

**Table 3.7** Locations and corresponding curvature and relative gain measures for specific points of interest on the steady-state locus in Figure 3.8.

Consider the points of interest in Figure 3.8. Point 3 displays the straightest and most uniformly spaced constant input lines, and therefore, has the lowest corresponding RMS curvature, as seen in Table 3.7. Point 4 hints at mild bending of constant F_{M2} lines, which explains the slightly elevated RMS curvature value. Point 1 lies in an area of bent F_{M2} lines and expanding spacing between F_{cat} contours. Point 2 displays more of the same, except of a stronger nature, justifying the highest calculated RMS curvature.

The following two sections are special cases. Because both steady-state loci examine state variables PR and [M_2] and the effects of F_{H2}, the 2×2 structure reduces to a 2×1 structure which occurs due to the complete independence of PR and [M_2] from F_{H2}. In other words, F_{H2} can be considered constant. Therefore, the resulting steady-state loci are effectively parameterized by one input, F_{cat} in the locus in 3.3.3.2, and F_{M2} in 3.3.3.3.

The interesting consequence is that since the curvature assessment is performed on a one-dimensional locus in a two-dimensional state space, the state space becomes of higher dimension than the input space, allowing for the presence of intrinsic nonlinearity. Therefore, the RMS curvature can be broken into tangential and normal components.

3.3.3.2 Effects of Catalyst Flow Rate Only

The steady-state locus in Figure 3.9 was generated by varying F_{H2} and F_{cat}, and

observing PR and [M_2]. As mentioned above, F_{H2} has no effect on either [M_2] or PR, while increasing F_{cat} has the effect of raising PR and decreasing [M_2] for reasons already discussed in previous sections.

Note the nonlinearity structure in Figure 3.9. Point 3 shows little bending of the steady-state locus relative to [M_2]-PR space. In addition, the spacing of points along the locus is most uniform here. This would indicate the least degree of both tangential and normal curvature. Moving across the locus to point 1, it is observed that the bending of the locus and the non-uniformity of spacing of points becomes more pronounced, explaining the trend of increasing components of nonlinearity, and thus in overall RMS curvature, as seen in Table 3.8.

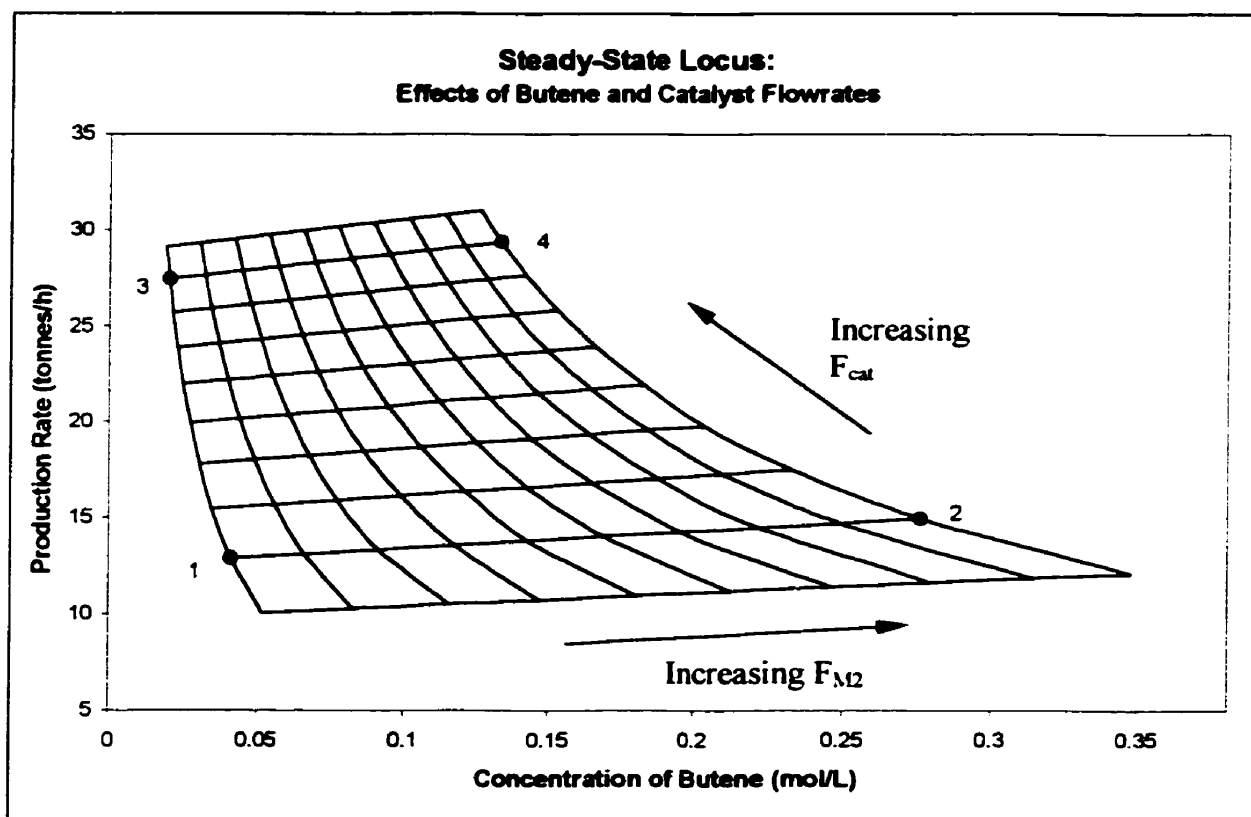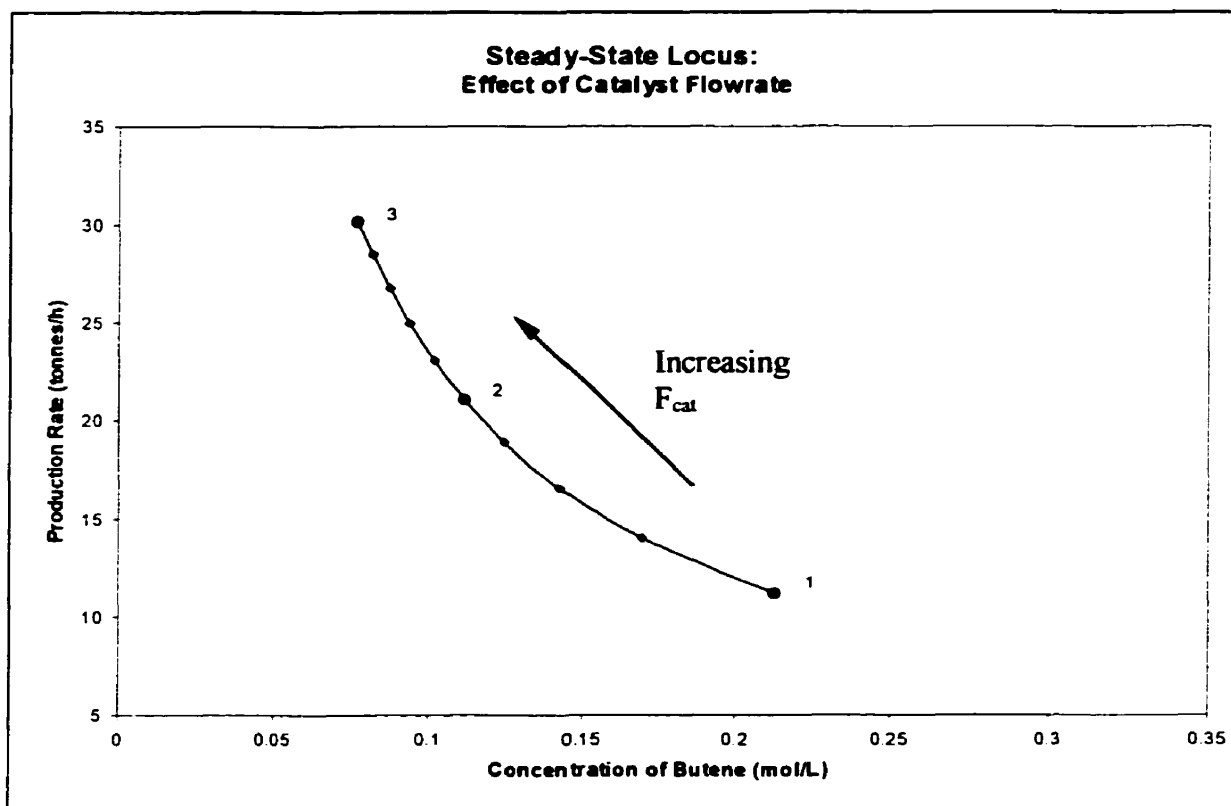**Figure 3.9.** Steady-state locus of butene concentration and production rate, parameterized by input catalyst flow.

Point	Fcat (kg/h)	overall RMS curvature	tangential RMS curvature	normal RMS curvature
1	2.0	1.551	1.301	0.844
2	5.6	0.570	0.488	0.295
3	9.2	0.345	0.298	0.174

Table 3.8 Locations and corresponding RMS curvature measures of specific points of interest for the steady-state locus in Figure 3.9.

Notice that for the 2×1 case, overall RMS curvature is the mean square value of tangential and normal RMS curvature, in accordance with the definition of root mean square curvature given in Chapter 2.

3.3.3.3 Effects of Butene Flow Rate Only

The final steady-state locus of the simplified model is presented in Figure 3.10. Again, this locus is 1-dimensional, and resides in 2-dimensional state space as a consequence of PR and [M2] independence of F_{H2}.

By inspection, it appears that the locus is essentially linear in the intrinsic sense. Indeed, the normal RMS curvature values in Table 3.9 support this claim, being that they are so small.

Point	Fcat (kg/h)	overall RMS curvature	tangential RMS curvature	normal RMS curvature
1	10000	0.0203	0.0174	0.0103
2	40000	0.0196	0.0168	0.0101
3	64000	0.0191	0.0163	0.0099

Table 3.9 Locations and corresponding RMS curvature measures of specific points of interest for the steady-state locus in Figure 3.10.

Additionally, the tangential component of nonlinearity appears to be negligible, as the spacing of points along the steady-state locus appears to be uniform. The tangential RMS value of approximately 0.02 over the entire locus supports this. Resultantly, the overall

RMS curvature value, and therefore the overall nonlinearity displayed by this locus is negligible.
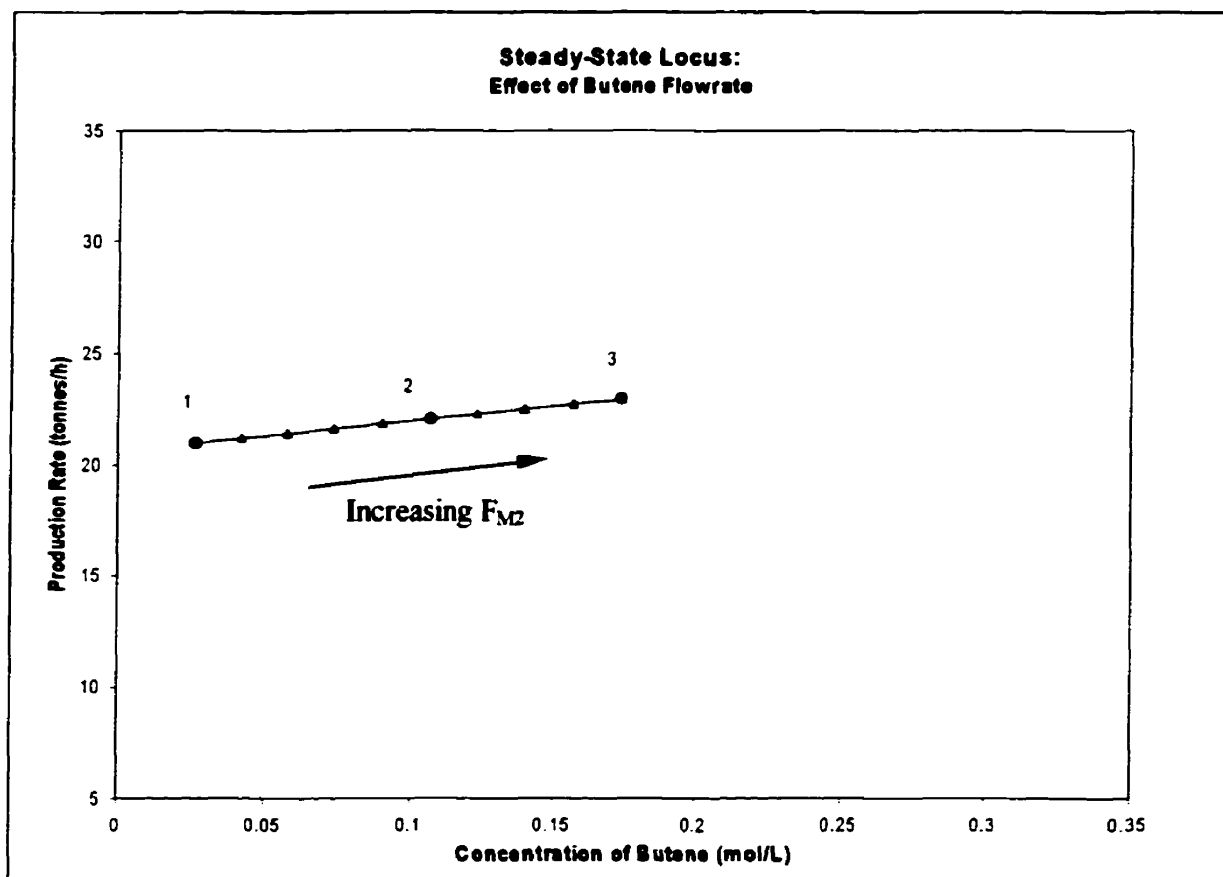
Figure 3.10 Steady-state locus of butene concentration and production rate, parameterized by input butene flow.

3.4 Conclusions

The main objective of this chapter is to offer a visual interpretation and graphical description of interaction and curvature as they are represented on a steady-state locus for the polyethylene reactor. A constant scaling was defined over most of the operating region, not so much to reflect realistic operating conditions, but to afford a consistent

basis in which RMS curvature measures could be compared. Changing interaction structure over the steady-state locus is also an indication of the presence of nonlinearity, and examples of this were presented.

Several 2×2 portions of the simplified 3×3 model display varying degrees of tangential nonlinearity, including arcing, fanning, and compansion effects. Tangential curvature ranged from negligible (c=0.00675) to moderate (2.47). Additionally, special cases in which the 2×2 portions reduced to 2×1 portions introduced the appearance and assessment of intrinsic curvature. In one case, the normal component of nonlinearity over the whole steady-state locus was concluded to be negligible (normal RMS of 0.01). In another view, the degree of intrinsic curvature ranged from small (c=0.174) to moderate (c=0.844) across the locus.

Ideally, this type of information, specifically the calculation of RMS curvature values, can be used to make an informed decision regarding the choice of best control scheme to be implemented. Alternatively, curvature assessment can be employed to draw comparisons of calculated RMS curvature values and control performance based on both linear and nonlinear controllers. This subject will examined in Chapters 4 and 5.

Chapter 4

Nonlinearity Assessment

4.1 Introduction

This chapter is concerned with the nonlinearity assessment of the full polyethylene reactor model, and the theory that predicts control performance based on the root-mean-square measure of curvature. To investigate the nonlinearity of the model, certain issues such as scaling, grade setting, output transformations, and the presence of disturbances must be addressed. The structure of this chapter proceeds by discussing result expectations based on theory, selecting appropriate grade transitions and disturbances, and calculating their corresponding RMS curvature values. In Chapter 5 we examine control performance results and relate them to calculated RMS curvature values.

The model examined in this chapter and in Chapter 5 is the form shown in equations (2.4) and (2.5). This form of the model is transformed in that the first output is the logarithm of melt index. The nominal model is one in which melt index appears directly, without transformation. We will examine the transformed version in detail, but we also discuss the nominal form.

4.2 Curvature Theory and Results Expectation

In later sections of this chapter, various regions of operation are chosen, defined either by transitions among a series of grades, or by disturbances around steady-state

operating points, and the RMS curvature measure associated with these regions is calculated. This type of curvature assessment will enable a technique for comparing anticipated and simulated results. Curvature theory implies that regions of high root-mean-square measures of curvature will exhibit significant nonlinear behaviour. One expectation is that, under linear control, the process will display greater control performance degradation over regions displaying a larger degree of curvature. As curvature increases, the deviation of the linearized-process gain, from the true process gain, would increase; therefore, a linear controller operating over increasingly nonlinear regions would contain increasingly inaccurate gain information. It is this conjecture on which the following expectations of results are based.

Both servo-control performance and regulatory control performance are expected to relate to the RMS curvature measures of the associated operating regions of the polyethylene reactor. On regions of low RMS curvatures, we hypothesize that the departure of the control performance of a linear control scheme from the best possible control, which would be achieved by a nonlinear controller, will be small. Conversely, on regions with high RMS curvature values, much poorer control performance should occur in the linear control case relative to the nonlinear case.

We have made an implicit assumption above; we expect that the best control performance, barring input or output saturation, will be achieved by the nonlinear controller. In fact, due to the nonlinear MIMO nature of this model, we expect that the best control performance will come from the nonlinear multivariable controller. Additionally, the assumption is made that although the process model contains dynamic information, these steady-state RMS measures of curvature will appropriately predict

67

control behaviour of the dynamic system.

In the presence of extreme nonlinearity, it may be advantageous to perform an output transformation, as has been done with melt index. Instead of controlling melt index directly, practitioners usually opt to control the logarithm of this output; that is, $\ln(MI)$. Therefore, by assessing the curvature of the present form of the model, the transformed form, $[\ln(MI), \rho, PR]'$, and another form, the untransformed or nominal form, $[MI, \rho, PR]'$, we shall determine whether in fact the logarithm transformation removes much nonlinearity. If the natural logarithmic transform of melt index does indeed reduce the degree of nonlinearity, it is then reasonable to predict that the degree to which a linear controller would suffer performance loss would be greater in the $[MI, \rho, PR]'$ model than in the associated $[\ln(MI), \rho, PR]'$ model representation.

4.3   Grade Selection for Servo- and Regulatory Control

One of the advantages of gas-phase polyethylene technology, over liquid-phase technology, is its capability to produce a wide range of grades. Gas-phase polyethylene reactors are capable of producing a melt index range of greater than 0.01 g/10 min to 200 g/10 min, and densities between 0.910 g/cm^3 and 0.97 g/cm^3 (James, 1986, Speakman, 1991).

In selecting operating regions over which servo- and regulatory control are simulated and analyzed, our goals were to choose sets of realistic grades, which cover most of the possible grade slate, and which display varying degrees of nonlinearity. With these goals in mind, commercial polyethylene grade information was obtained from the Nova Chemicals website (http://www.novachem.com/OurProducts/pds/indexPE.cfm,

April 8, 1999), from personnel at Imperial Oil (personal communication with Timothy K. Bean, Senior Account Executive, April 7, 1999), and Union Carbide (personal communication with Kimberly Parker, April 8, 1999). A slate of commercial polyethylene grades was identified on which control performance and nonlinearity measures could be assessed. These grades are given in Table 4.1 along with processing and product application information.

Grade	Melt Index g/10 min	Density g/cm^3	Processing	Typical Application
A	1	0.918	Film Resin	Industrial liners, heavy duty bags.
B	2	0.918	Film Resin	Trash bags, bag-on-roll, garment film.
C	0.8	0.921	Film Resin	General-purpose packaging, liners.
D	5.5	0.935	Rotational Molding	Toys, carts, custom molding.
E	12	0.926	Injection Molding	Caps, closures.
F	22	0.925	Injection Molding	Large houseware containers (e.g. trash cans).
G	50	0.926	Injection Molding	Lids, general-purpose housewares (e.g. trash cans).
H	4.5	0.954	Injection Molding	Industrial containers, industrial lids.
I	2	0.942	Rotational Molding	Large agricultural tanks, industrial products.
J	100	0.929	Injection Molding	Carrier resin for colour concentrates.

Table 4.1. Grade slate information obtained from Nova Chemicals, Imperial Oil, and Union Carbide.

The grade transitions that were chosen are changes among grades;

i)   A,B,C (film grades)

ii)   D,H,I (mid-MI molding grades)

iii) J,G (high MI molding grades)

These grades were chosen because much of the grade slate is represented in the transitions. An additional intermediate grade, K, was designed to accompany J and G in a transition study. Grade K was chosen to have a melt index of 75 g/10 min and a density of 0.925 g/cm^3.

Choosing additional grades that provide broader coverage over the grade slate allows for a relatively thorough comparative study among grade transitions. The additional grades chosen for this purpose were selected by simply translating the MI values of Table 4.1 to different numeric values on the grade slate. The newly selected grades are shown in Table 4.2.

Grade	Melt Index g/10 min	Density g/cm^3
L	20	0.918
M	21	0.918
N	19.8	0.921
O	20	0.935
P	5	0.926
Q	19	0.954
R	16.5	0.942
S	55	0.929
T	30	0.925

Table 4.2. Additional grades chosen for comparative study with grade transitions chosen from Table 4.1.

Although melt index and density define a grade, our output model also predicts production rate. Therefore, grade information will include production rate as part of the grade specification. Production rate is given in brackets next to the grade name. For example, A(20) refers to the grade with a melt index of 1 g/10 min, and a density of 0.918 g/cm^3 being produced at a rate of 20 tonnes/h. The complete set of grade transitions is depicted in Figures 4.1 and 4.2. Figure 4.1 shows the grade slate in ρ and MI coordinates, while Figure 4.2 is given in ρ and ln(MI) coordinates.
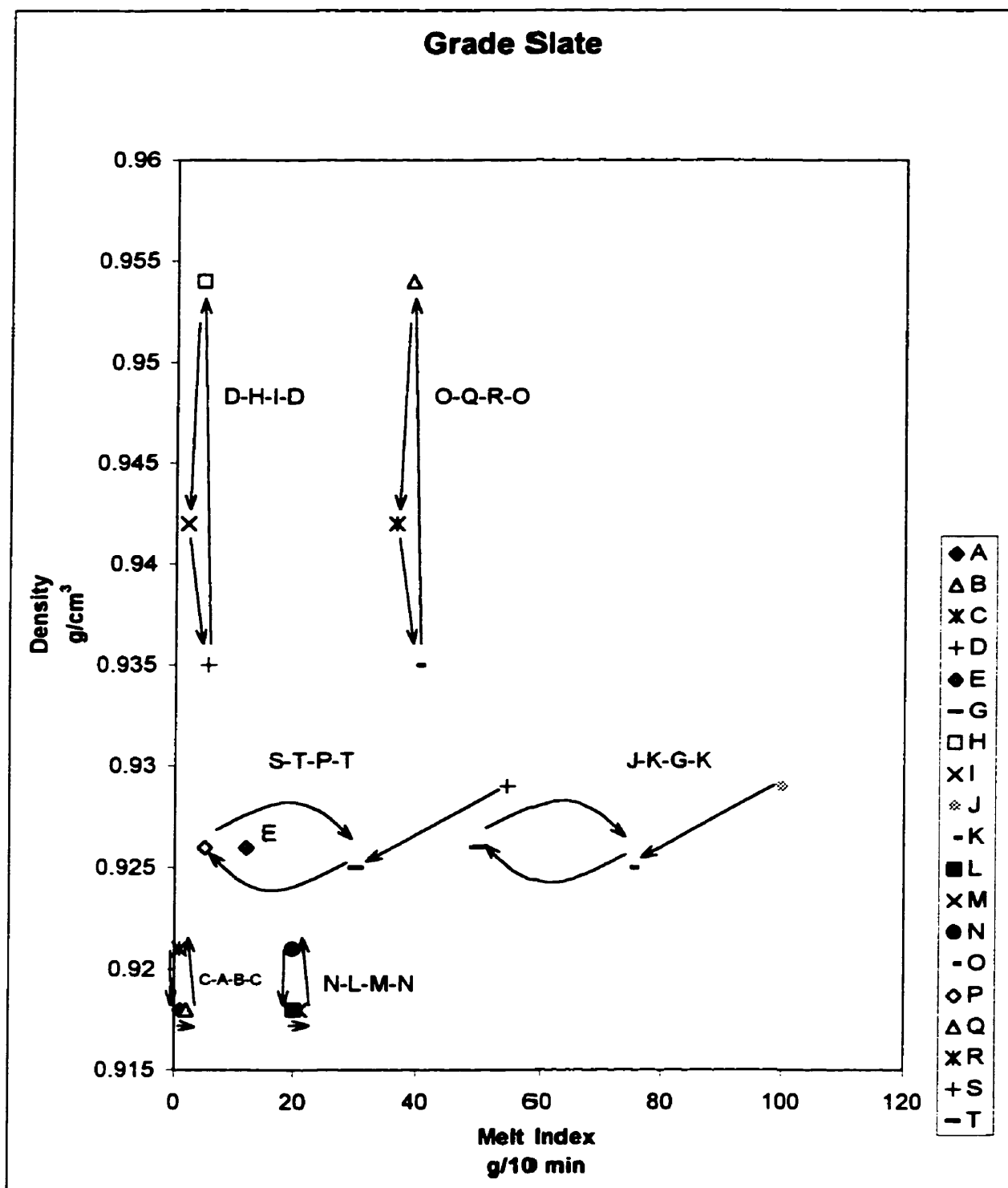
Figure 4.1. Grade slate information in MI-ρ coordinates. Each transition has a production rate sequence of 30-20-30-30 t/h.
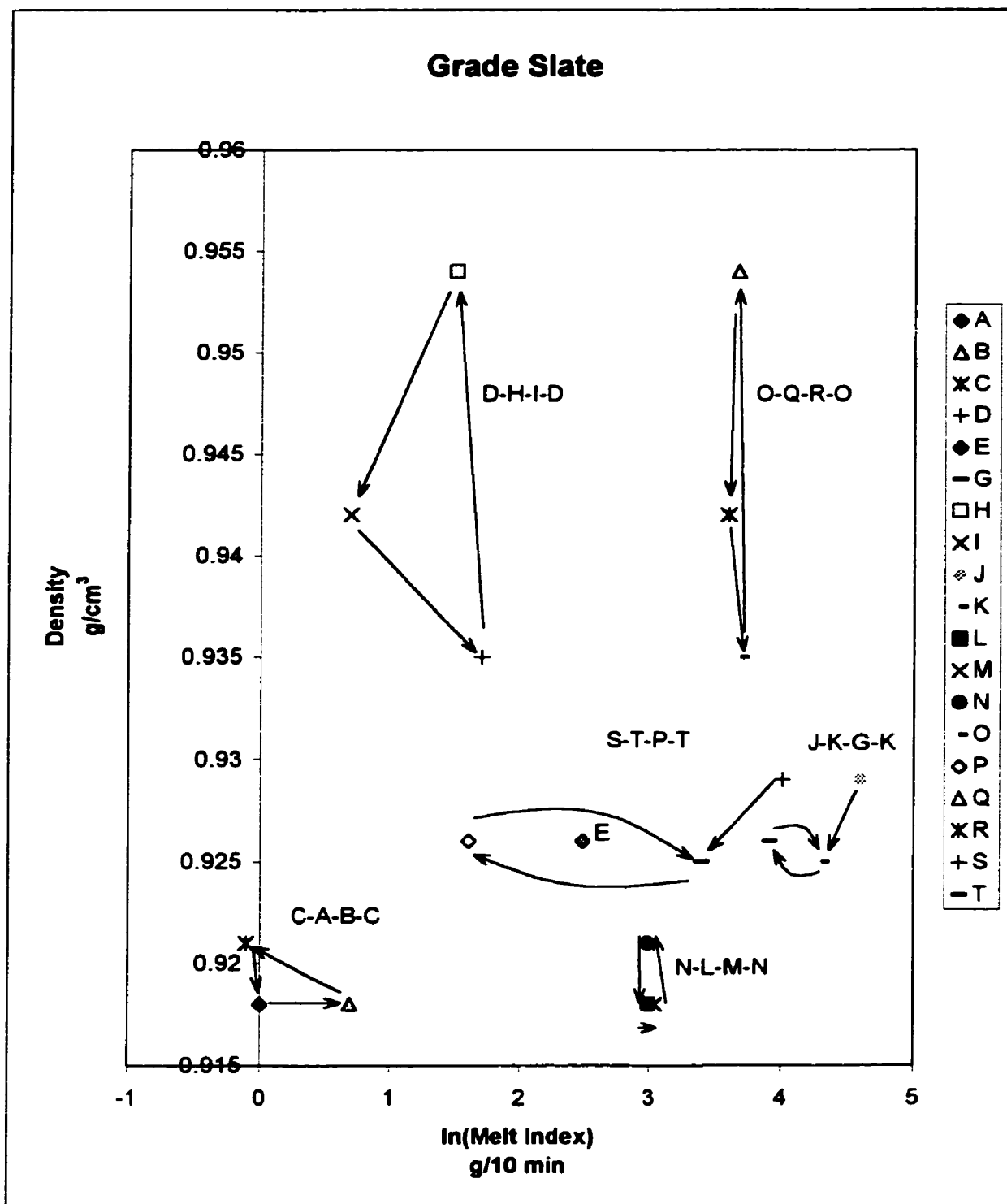
Figure 4.2. Grade slate information in ln(MI)-ρ coordinates. Each transition has a production rate sequence of 30-20-30-30 t/h.

Appropriate grades must also be chosen for disturbance rejection analysis. Because the relationship between control performance and curvature is of interest, we should choose operating regions that provide a wide range of RMS curvature values. After performing a preliminary assessment of RMS curvature values of the candidate grades, the following grades were chosen on which to examine regulatory control:

i)   E at a production rate of 20 tonnes/h

ii)   I at a production rate of 30 tonnes/h

iii)   J at a production rate of 20 tonnes/h

Before the root-mean-square measure of curvature can be computed for the grades proposed for servo- and regulatory control, appropriate operating regions in the output space must first be specified, and those regions scaled to unity.

4.4   Scaling

Grade specifications are given in terms of melt index, and density, and in this thesis, a target production rate is also associated with grade information. Because the grade transitions are defined for outputs, it is reasonable that output-prescribed scaling (rather than input-prescribed scaling) is used to approximate the desired regions of operation.

4.4.1 Scaling for Grade Transitions

The regions of operation for each grade transition set were estimated by the grade set-point ranges for each output. For example, grade transition J(30)-K(20)-G(30)-K(30) is characterized by a total melt index variation of 50 to 100g/10 min, a total density range

of 0.925 to 0.929g/cm^3, and a production rate varying from 20 to 30 tonnes/h. Ellipsoidal regions in the operating space were prescribed using these values. In effect, a hypothetical 'box' is defined by these limits, wherein an ellipsoidal region within this box defines the region of operation.

The ellipsoids specified are aligned with the output coordinate axes, whereas the minimum area ellipsoid for the given grade specifications would, in general, be rotated, as shown in Figure 4.3.
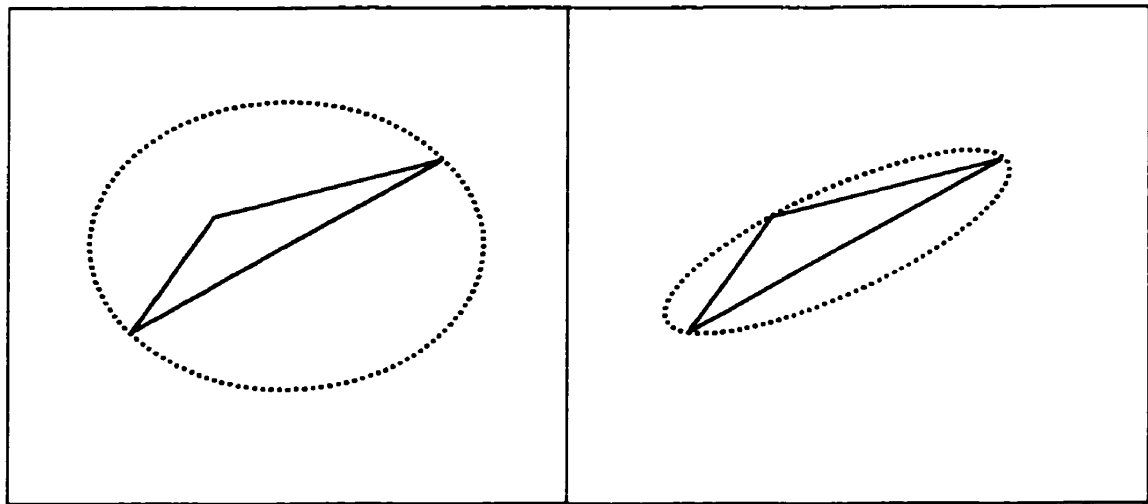
Figure 4.3. Schematic comparing rotated and non-rotated ellipses encompassing the scaling region. The corners of the triangles define arbitrary grade settings. The dashed ellipses represent scaling regions. The rotated ellipse may better define the region of operation. Notice the size difference between ellipses.

However, because the size of the scaling region is an approximate description of the size of the operating region, this non-rotated technique is appropriate. To account for overshoot in the controlled variables, the edges of the specified ellipsoids were extended by 20% from their centres.

In Chapter 2, ellipsoidal scaling regions were defined by scaling matrices such that:

$$\Delta y'(S'S)\Delta y = 1 \qquad\qquad (4.2)$$

where Δy is the deviation of the output variable from steady-state. In the case where the scaling region defines a region of interest for grade transitions, Δy is the deviation of the output variable from its mid-point. S is the diagonal scaling matrix. Each diagonal element of S is the inverse of half of the corresponding output range. By extending that range by 20%, the size of the ellipsoid grows by 20% along each of its axes. For example, the half-ranges of the transition J(30)-K(20)-G(30)-K(30) and S(30)-T(20)-P(30)-T(30) are:

        for melt index: 25 g/10min

        for density: 0.002 g/cm^3

        for production rate: 5 tonnes/h

An increase in these ranges by 20% gives:

        for melt index: 30 g/10min

        for density: 0.0024 g/cm^3

        for production rate: 6 tonnes/h

and the corresponding scaling matrix for grade transitions J(30)-K(20)-G(30)-K(30) and S(30)-T(20)-P(30)-T(30) is given as:

$$S = \begin{bmatrix} 1/30 & 0 & 0 \\ 0 & 1/0.0024 & 0 \\ 0 & 0 & 1/6 \end{bmatrix} \qquad\qquad (4.3)$$

For the grade transitions D(30)-H(20)-I(30)-D(30) and O(30)-Q(20)-R(30)-O(30), the scaling matrix becomes:

$$S = \begin{bmatrix} 1/2.1 & 0 & 0 \\ 0 & 1/0.0114 & 0 \\ 0 & 0 & 1/6 \end{bmatrix} \qquad (4.4)$$

and for the C(30)-A(20)-B(30)-C(30) and N(30)-L(20)-M(30)-N(30) grade transitions, the scaling matrix is given as:

$$S = \begin{bmatrix} 1/0.72 & 0 & 0 \\ 0 & 1/0.0018 & 0 \\ 0 & 0 & 1/6 \end{bmatrix} \qquad (4.5)$$

To illustrate the use of the scaling matrix, Figure 4.4 shows the associated scaling ellipse around grade transition J-K-G-K. Both the original scaling (without the 20% extension in principal axes) and the extended scaling ellipses are shown.
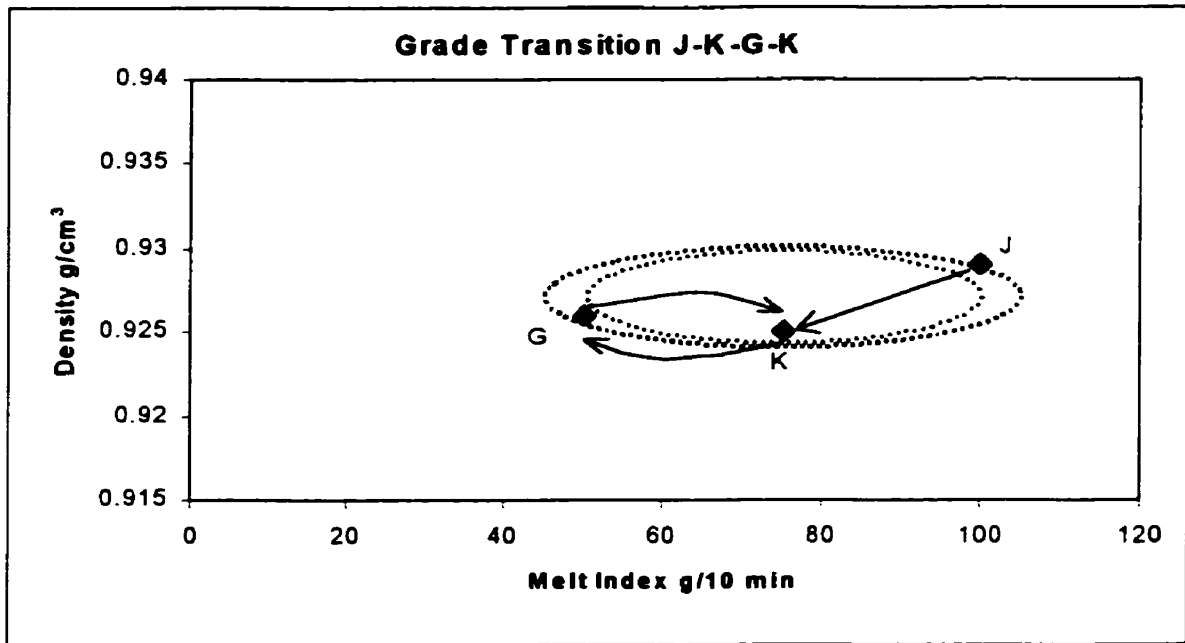
Figure 4.4. Diagram showing how a scaling ellipse is defined for a region of operation. This schematic shows the smaller original scaling ellipse, and the larger ellipse encompassing the 20% increase in principal axes.

Scaling must also be performed for the [ln(MI), ρ, PR]' model. Only the value of the first diagonal element of each scaling matrix will change because the output

transformation is applied only to melt index. Because ln(MI) is a nonlinear transform of melt index, it would not be accurate to calculate ln(half of the range in MI coordinates) for the grade transition sets. Rather, the range should be calculated as half of the range in terms of ln(MI). For example, for C-A-B-C, the half-range of ln(MI) is calculated as:

$$\frac{1}{2}(\ln(2) - \ln(0.8)) = 0.4581 \tag{4.6}$$

For N-L-M-N, the half-range of ln(MI) is:

$$\frac{1}{2}(\ln(21) - \ln(19.8)) = 0.02942 \tag{4.7}$$

Notice the dramatic difference in the size of the ranges for the same size output changes in melt index coordinates. Now the 20% increase to account for overshoot must be included. The increased length of the ellipsoid along the ln(MI) axis is reflected by the following relation for half of the range:

$$120\%\left(\frac{1}{2}\left(\ln MI_{high} - \ln MI_{low}\right)\right) \tag{4.8}$$

The corresponding (1,1) entries in the S matrices for the grade transitions are given in Table 4.3.

Grade transition	Half of the range including the 20% increase	(1,1) entry of S
C-A-B-C	$120\%\left(\frac{1}{2}(\ln(2) - \ln(0.8))\right)$	1 / 0.5498
N-L-M-N	$120\%\left(\frac{1}{2}(\ln(21) - \ln(19.8))\right)$	1 / 0.03530
D-H-I-D	$120\%\left(\frac{1}{2}(\ln(5.5) - \ln(2))\right)$	1 / 0.6070
O-Q-R-O	$120\%\left(\frac{1}{2}(\ln(20) - \ln(16.5))\right)$	1 / 0.1154
J-K-G-K	$120\%\left(\frac{1}{2}(\ln(100) - \ln(50))\right)$	1 / 0.4159
S-T-P-T	$120\%\left(\frac{1}{2}(\ln(55) - \ln(5))\right)$	1 / 1.439

Table 4.3. The half-ranges of the variation of ln(MI) must be calculated differently than those for MI. The calculation technique and the first diagonal entry of S are shown.

4.4.2 Scaling for Disturbance Rejection

The appropriate region of interest for operation around a steady state depends on the nature and size of anticipated disturbances. An approximate region of operation can be estimated either from historical plant data, or from simulating the disturbance under feedback control, and observing typical deviations between output and set point. In this work, the scaling regions were obtained by simulation studies.

The disturbances considered were 25% step increases in both the active site concentration in the catalyst feed, a_{cat}, and in the catalyst deactivation parameter, k_d, occurring at t=50 h and t=150 h, respectively, and a 25% step decrease in the bleed stream flow rate, b, at t=250 h. By observing the responses of the controlled system to these disturbances, appropriate deviations of melt index, density, and production rate, from their corresponding set points, were determined.

In Chapter 5, we assess the curvature of one disturbance rejection point in the nominal model, point J(20), while we look at three points in the transformed model. Therefore, we must determine the scaling for each. The first point considered is that of the nominal model, point J(20).

The expected region of operation at point J(20) was obtained by assigning the half-ranges of [MI, ρ, PR]' to the largest deviations of these outputs from their set points. These 'largest deviations' are actually those largest deviations obtained when the system was subject to either of the control designs given in Appendix A.3, Figure A3.11.a or c. A value of 3.8g/10 min is an appropriate half-range for the MI, while half of the ranges of ρ and PR are 0.001g/cm^3 and 3 tonnes/h, respectively. The resulting scaling matrix for operation around point J(20) is:

$$S = \begin{bmatrix} 1/3.8 & 0 & 0 \\ 0 & 1/0.001 & 0 \\ 0 & 0 & 1/3 \end{bmatrix} \qquad (4.9)$$

Once again, appropriate scaling must be determined to calculate curvature in the transformed model, $[\ln(\text{MI}), \rho, \text{PR}]'$. As before, only the $(1,1)$ element of the S matrix is subject to change. The scaling for the transformed melt index output at a given point is the greater value of:

$$\left(\ln MI_{high} - \ln MI_{midpoint}\right)$$
$$\text{or} \qquad\qquad\qquad\qquad\qquad (4.10)$$
$$\left(\ln MI_{midpoint} - \ln MI_{low}\right)$$

The ln(MI) half-ranges for the three grade regulation points are given in Table 4.4.

Grade	Half of the ln(MI) range	(1,1) element of S
E(20)	$\left(\ln(12.4) - \ln(12)\right)$	1 / 0.0328
I(30)	$\left(\ln(2.055) - \ln(2)\right)$	1 / 0.0271
J(20)	$\left(\ln(106.4) - \ln(100)\right)$	1 / 0.0620

Table 4.4. Table displaying half-ranges of ln(MI) required for the computation of scaling regions for nonlinearity analysis when operating around individual grades.

The scaling matrices for each of the steady-state points, E(20), I(30), J(20), of the transformed model are given below:

$$S_{E(20)} = \begin{bmatrix} \dfrac{1}{0.0328} & 0 & 0 \\ 0 & \dfrac{1}{0.00088} & 0 \\ 0 & 0 & \dfrac{1}{3} \end{bmatrix}$$

$$\mathbf{S}_{I(30)} = \begin{bmatrix} \dfrac{1}{0.0271} & 0 & 0 \\ 0 & \dfrac{1}{0.00075} & 0 \\ 0 & 0 & \dfrac{1}{5} \end{bmatrix}$$

$$\mathbf{S}_{J(20)} = \begin{bmatrix} \dfrac{1}{0.0620} & 0 & 0 \\ 0 & \dfrac{1}{0.001} & 0 \\ 0 & 0 & \dfrac{1}{3} \end{bmatrix}$$

Now that the expected regions of operation have been identified for both servo- and regulatory studies, we may now proceed to calculate the RMS curvature measure for each case.

4.5 Nonlinearity Assessment

The curvatures of each of the forms (transformed and nominal) of the polyethylene reactor model were assessed for both servo- and regulatory control for operation within the regions specified in Section 4.4.

4.5.1 The Nonlinearity of Grade Transitions

The grade transitions defined in Figures 4.1 and 4.2 are the subjects of this nonlinearity assessment. The transformed [ln(MI), ρ ,PR]' form of the polyethylene model is investigated in detail, and the nominal [MI, ρ, PR]' form is examined briefly to determine the effect of the logarithm transform on the curvature measurement.

4.5.1.1 Nonlinearity of the Transformed Model, [ln(MI), ρ, PR]'

Six sets of grade transitions were examined for the transformed model. The RMS curvatures for each grade transition are shown in Table 4.5.

Grade Transition	Scaling	RMS curvature
C(30)-A(20)-B(30)-C(30)	$\dfrac{\Delta \ln MI^2}{0.550^2} + \dfrac{\Delta\rho^2}{0.0018^2} + \dfrac{\Delta PR^2}{6^2} = 1$	2.34
N(30)-L(20)-M(30)-N(30)	$\dfrac{\Delta \ln MI^2}{0.035^2} + \dfrac{\Delta\rho^2}{0.0018^2} + \dfrac{\Delta PR^2}{6^2} = 1$	3.47
D(30)-H(20)-I(30)-D(30)	$\dfrac{\Delta \ln MI^2}{0.607^2} + \dfrac{\Delta\rho^2}{0.0114^2} + \dfrac{\Delta PR^2}{6^2} = 1$	1.63
O(30)-Q(20)-R(30)-O(30)	$\dfrac{\Delta \ln MI^2}{0.115^2} + \dfrac{\Delta\rho^2}{0.0114^2} + \dfrac{\Delta PR^2}{6^2} = 1$	1.03
J(30)-K(20)-G(30)-K(30)	$\dfrac{\Delta \ln MI^2}{0.416^2} + \dfrac{\Delta\rho^2}{0.0024^2} + \dfrac{\Delta PR^2}{6^2} = 1$	0.625
S(30)-T(20)-P(30)-T(30)	$\dfrac{\Delta \ln MI^2}{1.44^2} + \dfrac{\Delta\rho^2}{0.0024^2} + \dfrac{\Delta PR^2}{6^2} = 1$	4.35

Table 4.5. The grade transitions and their associated RMS measures of curvature for the transformed model, [ln(MI), ρ, PR]'.

Please note that for brevity, the nomenclature of the grade transitions shown in Table 4.5 will be shortened to omit the production rate information.

From Table 4.5, we see a diversity of RMS curvature measures, ranging form 0.625 to 4.35, indicating moderate nonlinearity. From the curvature values in Table 4.5, a conjecture is made; it is expected that the grade transition J-K-G-K will result in the best linear control performance because this transition has the smallest curvature value. Notice that no grade transition displays mild nonlinearity, in that the RMS curvature values obtained all lie above the suggested cut-off value of 0.3 (Guay et al., 1995). Arbitrarily comparing the grade transitions J-K-G-K and S-T-P-T, we anticipate that J-K-G-K will display a much lower error from set-point than S-T-P-T when linear controllers are used because the estimated degree of curvature for S-T-P-T is much higher.

4.5.1.2 Nonlinearity of the Nominal Model,[MI, ρ, PR]'

The purpose of this section is to show that, indeed, the logarithm transform of melt index does reduce the degree of nonlinearity of the model. In Table 4.6, the RMS curvature values have been calculated for each of the six grade transitions in the [MI, ρ, PR]' model and compared to those of the transformed model.

In all cases, the transformed model results in lower nonlinearity measures; therefore, we see that the practitioners' choice of controlling ln(MI) versus MI directly, is justified. The degree of nonlinearity reduction by the logarithm transform varies from transition set to transition set. In comparison to the nonlinearity reduction of most regions on the grade slate, a relatively small decrease in curvature is seen in the C-A-B-C transition, as the nonlinearity is reduced from $c_{RMS}=6.70$ to $c_{RMS}=2.34$. All other transitions display an impressive decrease in curvature due to this logarithmic transformation.

Grade Transition	Model	Scaling	RMS curvature
C(30)-A(20)-B(30)-C(30)	[MI, ρ, PR]'	$$\frac{\Delta MI^2}{0.72^2}+\frac{\Delta\rho^2}{0.0018^2}+\frac{\Delta PR^2}{6^2}=1$$	6.70
	[ln(MI), ρ, PR]'	$$\frac{\Delta\ln MI^2}{0.550^2}+\frac{\Delta\rho^2}{0.0018^2}+\frac{\Delta PR^2}{6^2}=1$$	2.34
N(30)-L(20)-M(30)-N(30)	[MI, ρ, PR]'	$$\frac{\Delta MI^2}{0.72^2}+\frac{\Delta\rho^2}{0.0018^2}+\frac{\Delta PR^2}{6^2}=1$$	72.4
	[ln(MI), ρ, PR]'	$$\frac{\Delta\ln MI^2}{0.035^2}+\frac{\Delta\rho^2}{0.0018^2}+\frac{\Delta PR^2}{6^2}=1$$	3.47
D(30)-H(20)-I(30)-D(30)	[MI, ρ, PR]'	$$\frac{\Delta MI^2}{2.1^2}+\frac{\Delta\rho^2}{0.0114^2}+\frac{\Delta PR^2}{6^2}=1$$	14.0
	[ln(MI), ρ, PR]'	$$\frac{\Delta\ln MI^2}{0.607^2}+\frac{\Delta\rho^2}{0.0114^2}+\frac{\Delta PR^2}{6^2}=1$$	1.63
O(30)-Q(20)-R(30)-O(30)	[MI, ρ, PR]'	$$\frac{\Delta MI^2}{2.1^2}+\frac{\Delta\rho^2}{0.0114^2}+\frac{\Delta PR^2}{6^2}=1$$	20.5
	[ln(MI), ρ, PR]'	$$\frac{\Delta\ln MI^2}{0.115^2}+\frac{\Delta\rho^2}{0.0114^2}+\frac{\Delta PR^2}{6^2}=1$$	1.03
J(30)-K(20)-G(30)-K(30)	[MI, ρ, PR]'	$$\frac{\Delta MI^2}{30^2}+\frac{\Delta\rho^2}{0.0024^2}+\frac{\Delta PR^2}{6^2}=1$$	89.6
	[ln(MI), ρ, PR]'	$$\frac{\Delta\ln MI^2}{0.416^2}+\frac{\Delta\rho^2}{0.0024^2}+\frac{\Delta PR^2}{6^2}=1$$	0.625
S(30)-T(20)-P(30)-T(30)	[MI, ρ, PR]'	$$\frac{\Delta MI^2}{30^2}+\frac{\Delta\rho^2}{0.0024^2}+\frac{\Delta PR^2}{6^2}=1$$	117
	[ln(MI), ρ, PR]'	$$\frac{\Delta\ln MI^2}{1.44^2}+\frac{\Delta\rho^2}{0.0024^2}+\frac{\Delta PR^2}{6^2}=1$$	4.35

Table 4.6. The grade transitions and their associated RMS measures of curvature for the nominal model, [MI, ρ, PR]'. The curvatures of the transformed model are given for comparison.

In Chapter 5, the results of one grade transition example are given, in which a simulation study compares the linear control performance between the grade transition J-K-G-K controlling MI versus the same transition in ln(MI).

4.5.2 Nonlinearity of Operation About a Point

Often, it is not just the nonlinearity associated with large excursions such as grade transitions that is of interest, but also the nonlinearity existing in a small region about a steady-state point of operation. Disturbances will occur, and cause the reactor to deviate from steady state. Because disturbance rejection performance may be a function of nonlinearity, the assessment of curvature around an operating point may aid in the decision of control scheme choice. Three steady-state points are examined in the transformed model; additionally, the transformed model is compared to the nominal model at one point.

4.5.2.1   Nonlinearity of the Transformed Model, [ln(MI), ρ, PR]'

In this investigation, three steady-state points with varying RMS curvatures are the focus. In Chapter 5, the disturbance rejection performance for the transformed-model-based controller around points E(20), I(30), and J(20) is studied.

Using the scaling information given in Table 4.4, the RMS curvature information at each of the three points is calculated and displayed in Table 4.7. The curvatures associated with operation about an individual steady-state point display curvatures in the moderate range (c_{RMS}=0.476 at J(20), to c_{RMS}=4.27 at I(30)).

Grade	Scaling	RMS curvature
E(20)	$\dfrac{\Delta \ln MI^2}{0.0328^2} + \dfrac{\Delta \rho^2}{0.00088^2} + \dfrac{\Delta PR^2}{3^2} = 1$	1.25
I(30)	$\dfrac{\Delta \ln MI^2}{0.0271^2} + \dfrac{\Delta \rho^2}{0.00075^2} + \dfrac{\Delta PR^2}{5^2} = 1$	4.27
J(20)	$\dfrac{\Delta \ln MI^2}{0.0620^2} + \dfrac{\Delta \rho^2}{0.001^2} + \dfrac{\Delta PR^2}{3^2} = 1$	0.476

Table 4.7. The steady state regions of operations and their associated RMS measures of curvature for the [ln(MI), ρ, PR]' model.

From the calculated RMS curvature values, the control performance expectations are that linear controllers will perform better at J(20) than at I(30).

4.5.2.2   Nonlinearity of the Nominal Model [MI, ρ, PR]'

To evaluate the impact of the logarithm transform on the curvature of the polyethylene model in the disturbance rejection case, the nominal model, [MI, ρ, PR]', is compared to the transformed model [ln(MI), ρ, PR]', at one point, J(20). The scaling for operation about J(20) in the MI model is:

$$\frac{\Delta MI^2}{3.8^2} + \frac{\Delta \rho}{0.001^2} + \frac{\Delta PR^2}{3^2} = 1 \tag{4-11}$$

In the [MI, ρ, PR]' model, the curvature around point J(20) is $c_{RMS}=57.8$, which is much larger than the curvature of the same point in the transformed model (which has an estimated RMS measure of nonlinearity of 0.476).

As a result of the large difference in curvatures, it is expected that linear control of ln(MI) will result in lower error than the linear control of MI directly, as compared to the respective nonlinear counterparts.

4.6 Conclusions

In this chapter, the focus has been selecting appropriate grades for servo- and regulatory-control simulation studies to select representative regions of operation for each simulation and to calculate the RMS nonlinearity values for each grade transition and disturbance rejection for the transformed model. Additionally, two examples were chosen for which the nonlinearity was assessed for the nominal model, [MI, ρ, PR]', in which the melt index is controlled directly.

The chosen grades for transition studies were C(30)-A(20)-B(30)-C(30), D(30)-H(20)-I(30)-D(30), J(30)-K(20)-G(30)-K(30), N(30)-L(20)-M(30)-N(30), O(30)-Q(20)-R(30)-O(30), and S(30)-T(20)-P(30)-T(30). For operation about steady state, subject to disturbances, the grades of interest were E(20), I(30), and J(20).

Corresponding scaling regions were chosen for the grade transitions by defining an ellipse within a 'box' defined by the upper and lower specifications of the grade transitions. The dimensions of the ellipse were then extended outward by 20% to account for the controlled variable overshoot. Scaling regions for grades subject to disturbance rejection were determined by controlled variable fluctuations in simulation studies.

Varying degrees of curvature were calculated for both servo- and regulatory control. In servo-control of the transformed model, RMS curvature ranged from 0.625 to 4.35. In the nominal model, [MI, ρ, PR]', c_{RMS} ranged from 6.7 to 117. The curvature of each grade transition in the nominal model was substantially larger than in the transformed model. In disturbance rejection studies, the RMS curvature ranged form 0.476 to 4.27 for the transformed model, indicating the presence of a range of moderate nonlinearity.

For the nominal model, the curvature was calculated for regulation about one grade and found to be much higher (c_{RMS}=57.8) than at the same point in the transformed model. This finding and the comparison of RMS curvature for nominal and transformed models in grade transition studies indicates that the logarithm transformation of the melt index does reduce the degree of nonlinearity.

Chapter 5

Closed-Loop Performance Assessment

5.1   Introduction

In Chapter 4, nonlinearity assessment was performed for various grade transition and disturbance-rejection regimes for both the transformed model, [ln(MI), ρ, PR]', and the nominal model, [MI, ρ, PR]'. The nonlinearity information obtained was calculated so that the expectations regarding the impact of RMS curvature on control performance could be tested.   In this chapter, we determine whether operating regions of the polyethylene model with high RMS curvature values indeed suffer noticeably larger performance losses when subjected to linear control, than regions in the model displaying only mild nonlinearity.   Such a comparison is done in two ways; first, the control performance of linear and nonlinear controllers for the transformed model is examined over a large portion of the grade slate, with both servo- and regulatory control goals, and compared to the corresponding RMS curvatures.   Second, the performance of linear versus nonlinear controllers is assessed for both the transformed and the nominal models at identical regions on the grade slate.   We will determine whether linear control of the nominal model (which displays much higher nonlinearity) is less successful than linear control of the transformed model, and whether a correlation exists between performance degradation and RMS curvature.

This chapter is structured in the following way.   First, the control laws are

developed from the error trajectory approach. The derivation of the linear and nonlinear controllers from the model is demonstrated. Then, a comparative study is performed to determine the relationship between RMS curvature and control performance prediction.

5.2   Control Law Development

The design of the error-trajectory controller (McLellan et al., 1990) begins with the error-trajectory specification, which must be a function of at least the αth order derivative of the tracking error (where α is the relative order of the process). Because the polyethylene reactor model is a relative order one process, the error-trajectory specification, as given in equation 2.39, is:

$$\dot{e}(t) + \beta e(t) + \gamma \int_{t_0}^{t} e(z)dz = 0 \qquad (2.39)$$

where $e(t) = \mathbf{y}_{sp}(t) - \mathbf{y}(t)$, and γ and β are diagonal weighting, or tuning, matrices. To design a nonlinear controller, the nonlinear process model, (2.4) and (2.5):

$$\mathbf{y} = \begin{bmatrix} \ln(MI) \\ \rho \\ PR \end{bmatrix} = \mathbf{h}(\mathbf{x}) = \begin{bmatrix} 3.5\ln\left(k_0 + k_1 \dfrac{[M_2]}{[M_1]} + k_3 \dfrac{[H_2]}{[M_1]} \right) \\ p_0 + p_1 \ln(MI) - \left(p_2 \dfrac{[M_2]}{[M_1]} \right)^{p_4} \\ Y\left(k_{p1}[M_1]mw_1 + k_{p2}[M_2]mw_2 \right) \end{bmatrix}$$

$$\dot{\mathbf{x}} = \begin{bmatrix} \dfrac{d[H_2]}{dt} \\ \dfrac{d[M_2]}{dt} \\ \dfrac{dY}{dt} \end{bmatrix} = \begin{bmatrix} \dfrac{1}{Vg}\left(F_{H2} - k_H \cdot Y \cdot [H_2] - \dfrac{[H_2] \cdot b}{C_t} - gl \cdot [H_2] \right) \\ \dfrac{1}{Vg + Vs}\left(F_{M2} - k_{p2} \cdot Y \cdot [M_2] - \dfrac{[M_2]b}{C_t} - S[M_2]Y\left(k_{p1}[M_1]mw_1 + k_{p2}[M_2]mw_2 \right) \right) \\ F_{cat} \cdot a_{cat} - \dfrac{Y^2\left(k_{p1}[M_1]mw_1 + k_{p2}[M_2]mw_2 \right)}{Bw} - k_d Y \end{bmatrix}$$

is substituted into the error trajectory specification, with $\dot{\mathbf{y}}_{sp}=0$ (set points are a series of steps):

$$\left[\frac{\partial \mathbf{h}}{\partial \mathbf{x}} \cdot \frac{d\mathbf{x}}{dt}\right] = \beta[\mathbf{y}_{sp} - \mathbf{y}] + \gamma \int_{t_0}^{t}[\mathbf{y}_{sp}(z) - \mathbf{y}(z)]dz \qquad (5.1)$$

The formulation in equation 5.1 amounts to pole-placement of an input/output path with added integral action. Substituting the Jacobian $\dfrac{\partial \mathbf{h}}{\partial \mathbf{x}}$, and the state equations $\dfrac{d\mathbf{x}}{dt}$ into equation (5.1),

$$\begin{bmatrix} \dfrac{\partial h_1}{\partial x_1} & \dfrac{\partial h_1}{\partial x_2} & \dfrac{\partial h_1}{\partial x_3} \\[2mm] \dfrac{\partial h_2}{\partial x_1} & \dfrac{\partial h_2}{\partial x_2} & \dfrac{\partial h_2}{\partial x_3} \\[2mm] \dfrac{\partial h_3}{\partial x_1} & \dfrac{\partial h_3}{\partial x_2} & \dfrac{\partial h_3}{\partial x_3} \end{bmatrix} \cdot \begin{bmatrix} \dfrac{d[H_2]}{dt} \\[2mm] \dfrac{d[M_2]}{dt} \\[2mm] \dfrac{dY}{dt} \end{bmatrix} = \begin{bmatrix} \beta_1 & 0 & 0 \\ 0 & \beta_2 & 0 \\ 0 & 0 & \beta_3 \end{bmatrix} \cdot \begin{bmatrix} \ln(MI)_{sp} - \ln(MI) \\ \rho_{sp} - \rho \\ PR_{sp} - PR \end{bmatrix} + \ldots$$

$$\begin{bmatrix} \gamma_1 & 0 & 0 \\ 0 & \gamma_2 & 0 \\ 0 & 0 & \gamma_3 \end{bmatrix} \cdot \begin{bmatrix} \int_{t0}^{t}(\ln(MI)_{sp}(z) - \ln(MI)(z))dz \\ \int_{t0}^{t}(\rho_{sp}(z) - \rho(z))dz \\ \int_{t0}^{t}(PR_{sp}(z) - PR(z))dz \end{bmatrix} \qquad (5.2)$$

$$\frac{\partial h_1}{\partial x_1} = \frac{3.5\dfrac{k_3}{[M_1]}}{\left(k_0 + k_1\dfrac{[M_2]}{[M_1]} + k_3\dfrac{[H_2]}{[M_1]}\right)},$$

$$\frac{\partial h_1}{\partial x_2} = \frac{3.5\dfrac{k_1}{[M_1]}}{\left(k_0 + k_1\dfrac{[M_2]}{[M_1]} + k_3\dfrac{[H_2]}{[M_1]}\right)},$$

$$\frac{\partial h_1}{\partial x_3} = 0,$$

$$\frac{\partial h_2}{\partial x_1} = \frac{3.5 p_1 \dfrac{k_3}{[M_1]}}{\left(k_0 + k_1 \dfrac{[M_2]}{[M_1]} + k_3 \dfrac{[H_2]}{[M_1]}\right)},$$

$$\frac{\partial h_2}{\partial x_2} = \frac{3.5 p_1 \dfrac{k_1}{[M_1]}}{\left(k_0 + k_1 \dfrac{[M_2]}{[M_1]} + k_3 \dfrac{[H_2]}{[M_1]}\right)} - \frac{p_4 \cdot p_2}{[M_1]}\left(p_2 \dfrac{[M_2]}{[M_1]}\right)^{(p_4-1)}$$

$$\frac{\partial h_2}{\partial x_3} = 0,$$

$$\frac{\partial h_3}{\partial x_1} = 0,$$

$$\frac{\partial h_3}{\partial x_2} = \frac{kp_2 \cdot mw_2 \cdot Y}{10^6},$$

$$\frac{\partial h_3}{\partial x_3} = \frac{kp_1 \cdot [M_1] \cdot mw_1 + kp_2 \cdot [M_2] \cdot mw_2}{10^6}$$

The controller equations are obtained by solving equations (2.43) in Chapter 2. Note that the above formulation corresponds to the controllers designed for the transformed model. To design a control scheme where melt index is controlled directly, as in the nominal model, one must substitute instead the corresponding model into equation (5.2), as shown in Appendix A.1.

If one is designing a linear controller, the linearized process model is instead substituted into equation (5.1). The linearized polyethylene reactor process model is of the form:

$$\dot{x} = Ax + Bu$$
$$y = Cx$$
(5.3)

The linearization was obtained by performing a first-order Taylor series approximation

about a nominal steady-state point. Matrix **A** is the Jacobian of the process state equations with respect to the vector **x**, and evaluated at a steady-state point. Similarly, **B** is the Jacobian of the state equations with respect to the input vector, $\mathbf{u}=[F_{H2}, F_{M2}, F_{cal}]'$. **C** is the Jacobian of the output function **h(x)**. The matrices **A**, **B**, and **C** are evaluated at the point of linearization, and the **x**, **u**, and **y** vectors are presented in deviation variables.

Nonlinear equation (5.2), and its linear counterpart, are each a set of three equations in three unknowns. The three equations can be solved simultaneously for each of the inputs. For completeness, the nonlinear control solution of the transformed model is shown in Appendix A.2. It is important to note that, although the linear and nonlinear controllers incorporate different model forms, their error-trajectory specifications are the same.

5.3 Tuning

Tuning the resulting individual controllers is accomplished by selecting appropriate values for the diagonal elements of matrices β and γ. The selection of tuning parameters is akin to selecting the desired closed-loop response of the process. A reasonably conservative choice for β and γ is one in which the response specification matches the dynamic behaviour of the system. By performing open-loop step tests on the process model, a set of tuning parameters for individual input/output channels was chosen for the process: (5.4)

$$\beta = \begin{bmatrix} 1 & 0 & 0 \\ 0 & 1 & 0 \\ 0 & 0 & 1 \end{bmatrix}$$

$$\gamma = \begin{bmatrix} \dfrac{1}{4} & 0 & 0 \\ 0 & \dfrac{1}{4} & 0 \\ 0 & 0 & \dfrac{1}{30} \end{bmatrix}$$

Although the dynamics due to butene flow are faster than those due to hydrogen flow, as seen in Figure 5.1a and b, we have chosen equal error trajectory specifications for melt index (predominantly affected by hydrogen concentration) and density (predominantly affected by butene concentration). Such tuning will ensure more aggressive hydrogen valve movement, as seen in Figure 5.2b, which is desirable because of the inherently slower open-loop hydrogen dynamics of the system. With these tuning parameters, the closed-loop responses for instantaneous ln(melt index) and density also have overshoot (see Figure 5.2a), which beneficially increases the rate of change in cumulative properties. For a set point change in production rate, an overshoot is not desired because it might lead to excessive heat removal requirements. To minimize the size of the overshoot in production rate response, the integral action parameter, γ_3, was reduced relative to γ_1 and γ_2 (those of melt index and density), resulting in the control system responses shown in Figure 5.2. The particular error-trajectory specification defined by equation (2.43) and tuning factors in equation 5.4 were used in all of the control simulations shown in the remainder of this thesis.

Manipulated variable bounds exist, and are defined by the following limits:

$$0 \leq F_{H2} \leq 14000 \; mol / h$$
$$0 \leq F_{M2} \leq 64200 \; mol / h \qquad (5.5)$$
$$0 \leq F_{cat} \leq 10 \; kg / h$$

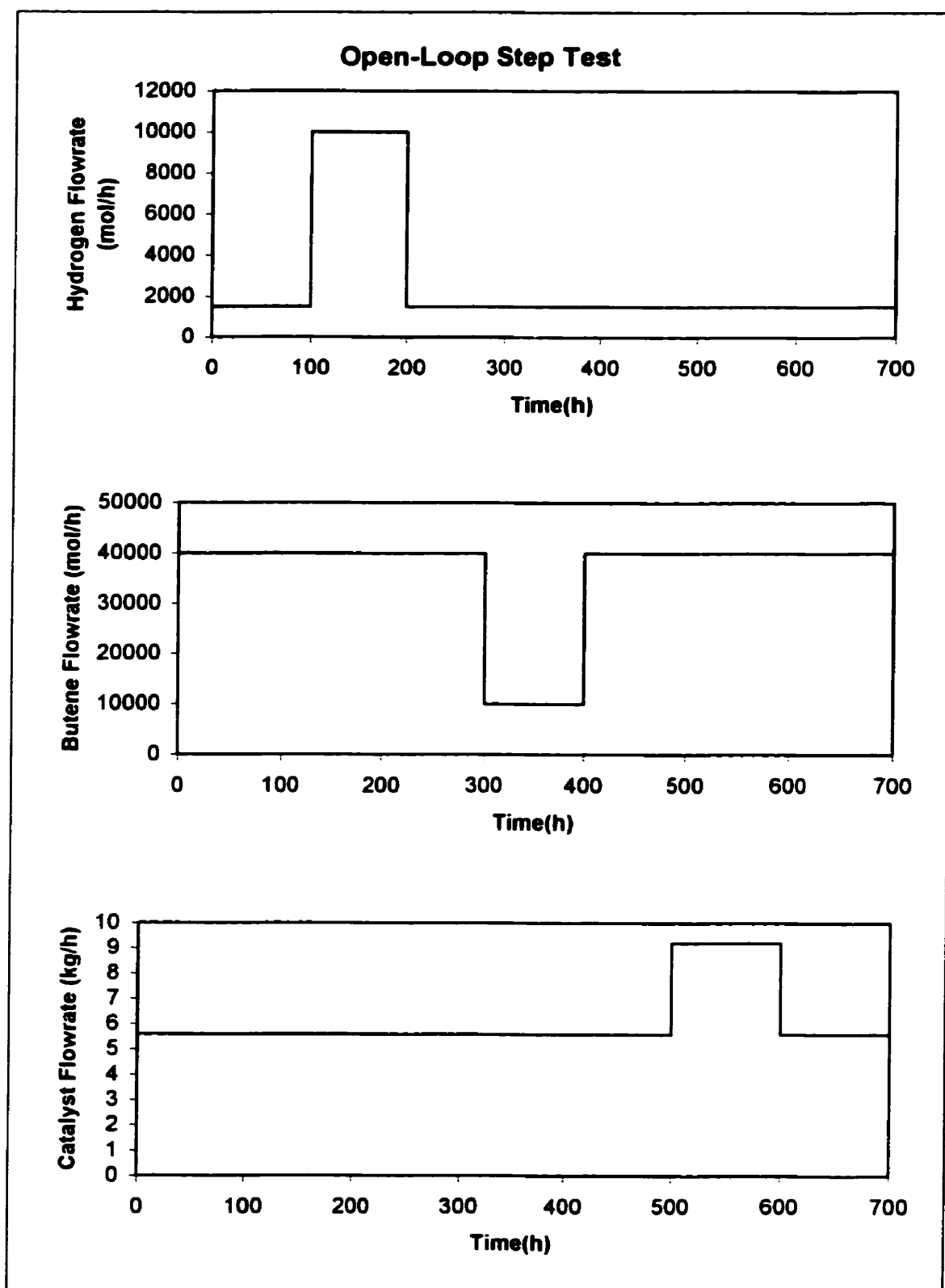These bounds are imposed after the controller has solved an unconstrained solution. If

Figure 5.1a. The transformed model was subjected to step changes in manipulated variables, as shown.
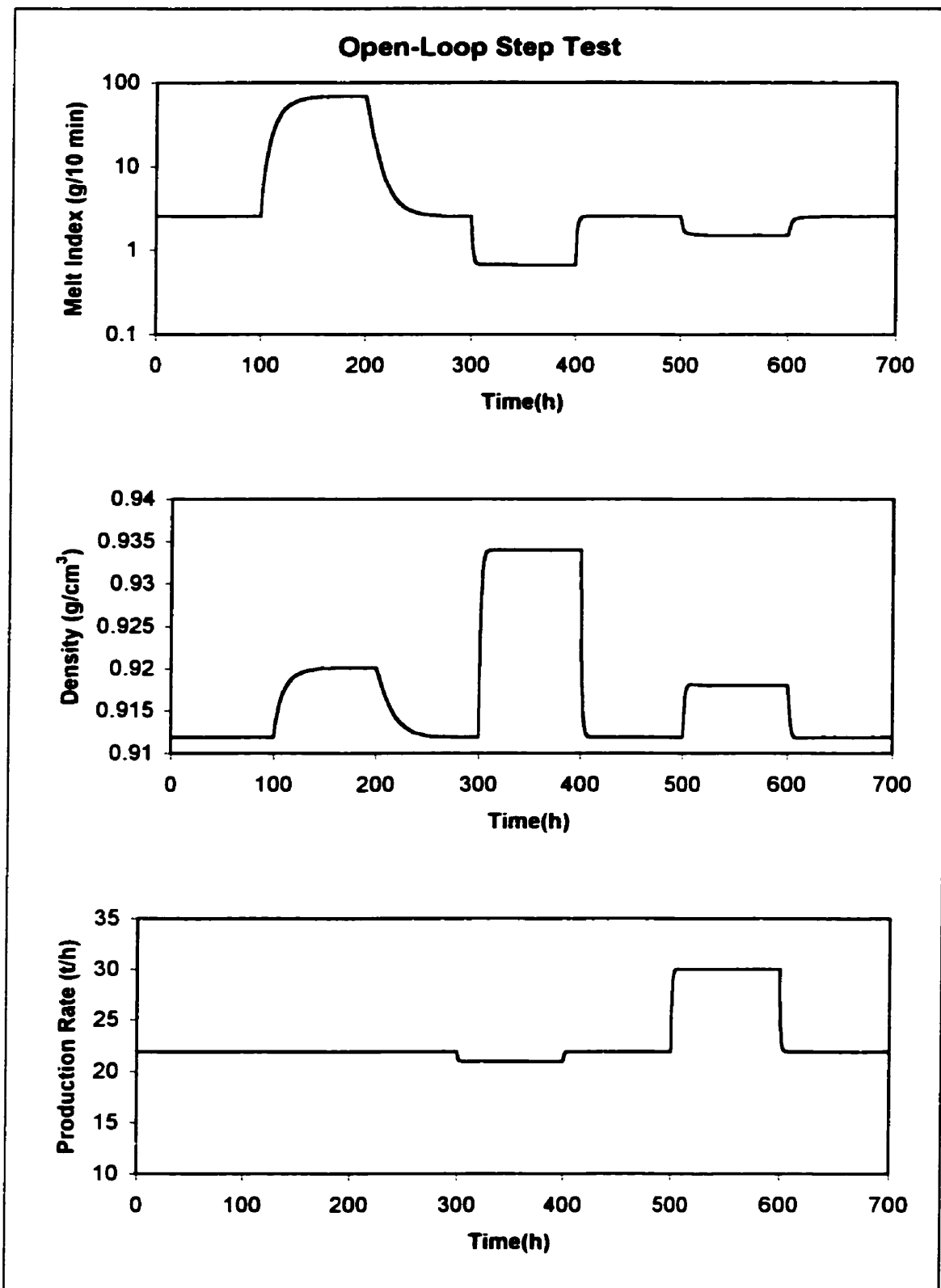
Figure 5.1b. The transformed model was subjected to step changes in manipulated variables, which resulted in the output responses shown above.
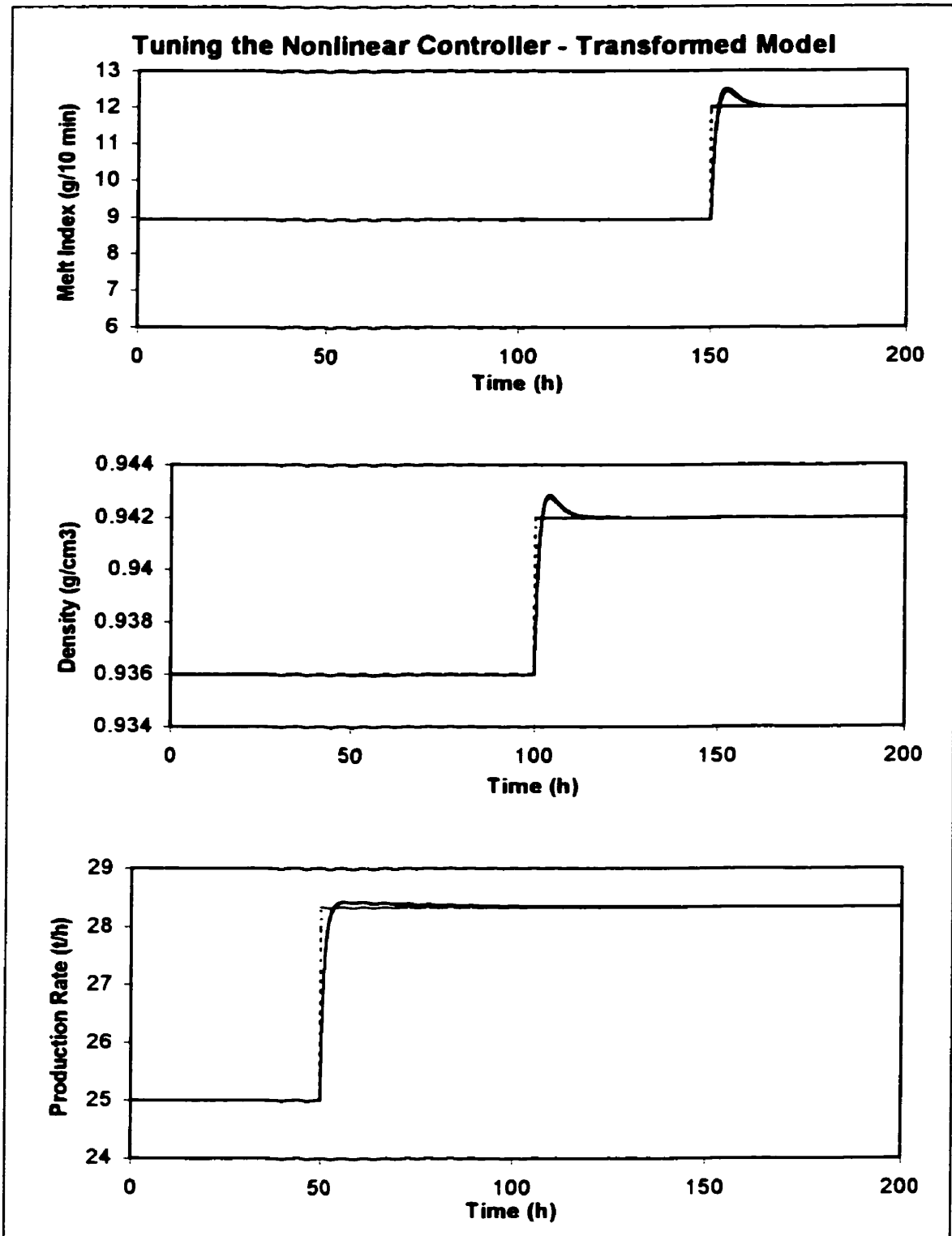
Figure 5.2a. The specified error trajectories and the nonlinear controller results are given above. The tuning parameters for this output response are b1=b2=b3=1, g1=g2=1/4, and g3=1/30. Dashed line: set point. Thick line: Output. Thin line: output specification (output and specification overlap).

Figure 5.2b. The manipulated variable action required to yield the specified error trajectories and the nonlinear controller results in Figure 5.2a. Solid line: manipulated variable. Dashed line: MV bound.

the control law returns any value outside these limits, the manipulated variables are clamped at their specified bounds. Due to manipulated variable clamping, there exists the potential for reset windup, although it didn't appear to pose significant problems in the simulations in this thesis.
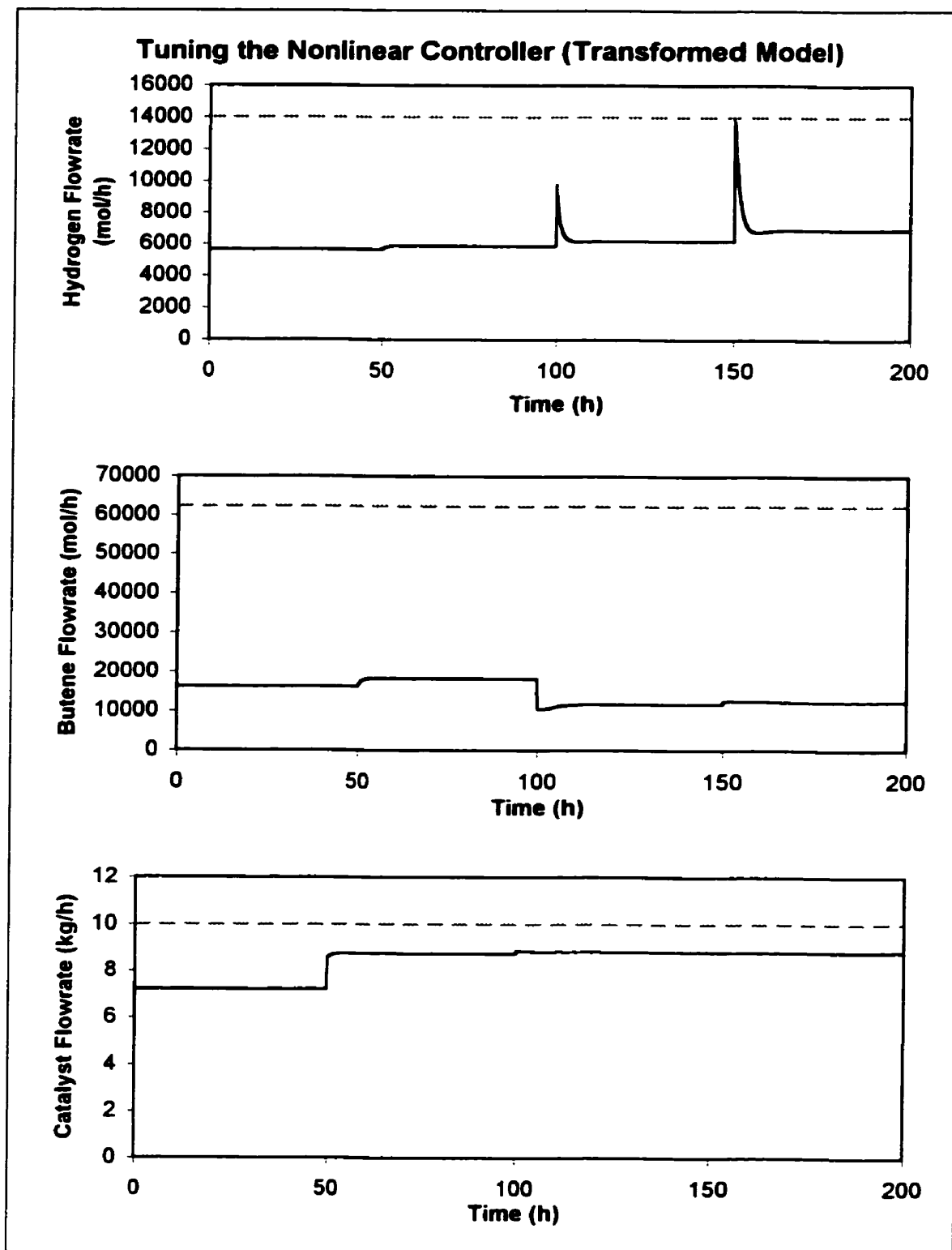
5.4 Performance Assessment

This section examines the control performance for grade transitions and disturbance rejection scenarios previously defined in Chapter 4. First, a performance measure must be defined. The performance of the controllers in this thesis is evaluated using a modified version of the integral of the absolute value of the error (IAE).

The simulation work done in this thesis was accomplished in Matlab™ 5, in which the ODE15s routine was used to solve differential model equations.

5.4.1 Performance Measures

The IAE measure is the accumulation of the absolute value of the deviation of the output from its target. Marlin (1995) defines the integral of the absolute value of the error as:

$$IAE = \int_0^\infty |SP(t) - CV(t)| dt \tag{5.6}$$

where SP is the set point and CV is the current value of the controlled variable. Although the controlled variables in the grade transition work have a set point target, the controllers have been designed such that the controlled variables follow an over-damped second-order-type, with overshoot, error trajectory back to set point, as in equation (2.43).

Therefore, instead of comparing the outputs to the set points, we compare them to the desired output trajectories determined using the error-trajectory specifications. Therefore, for grade transition studies, we define a modified form of the IAE, called the integral of the absolute deviation, or IAD:

$$IAD = \int_0^\infty \left| CV_{spec}(t) - CV(t) \right| dt$$

where CV_{spec} is the desired controlled variable action, defined from the error-trajectory specification. Therefore, IAD is a measure of the deviation of the controlled variable from its specified trajectory. Unless manipulated variable saturation occurs, the IAD value for simulations under nonlinear controller will be approximately zero. For disturbance rejection simulations, the IAE remains the measure of choice because the goal is to return the output values back to the original set point.

The IAE and IAD are further manipulated to yield measures of relative performance; that is, the performance of a linear controller is assessed relative to the performance of the nonlinear controller, which enables a standardized measure of the degree of degradation that occurs as a result of choosing linear, over nonlinear, control. We define normalized IAD (for grade transition studies) as:

$$IAD_{norm} = \frac{IAD_{lin} - IAD_{nonlin}}{IAE_{nominal}}$$

and normalized IAE for (disturbance rejection studies) as:

$$IAE_{norm} = \frac{IAE_{lin} - IAE_{nonlin}}{IAE_{nominal}} \tag{5.7}$$

where $IAE_{nominal} = \int_0^\infty \left| SP(t) - CV_{spec}(t) \right| dt$. Therefore, IAD_{norm} is the difference between the deviation from CV_{spec} incurred by using a linear versus a nonlinear controller,

standardized by the IAE of the difference of the grade set point and the expected controlled variable action. Similarly, IAE_{norm} is the difference in the error incurred as a result of using a linear versus a nonlinear control scheme, normalized by the area between SP and CV_{spec}.

For visual aid, illustrations of IAD and IAE_{nom} are shown in Figure 5.3.
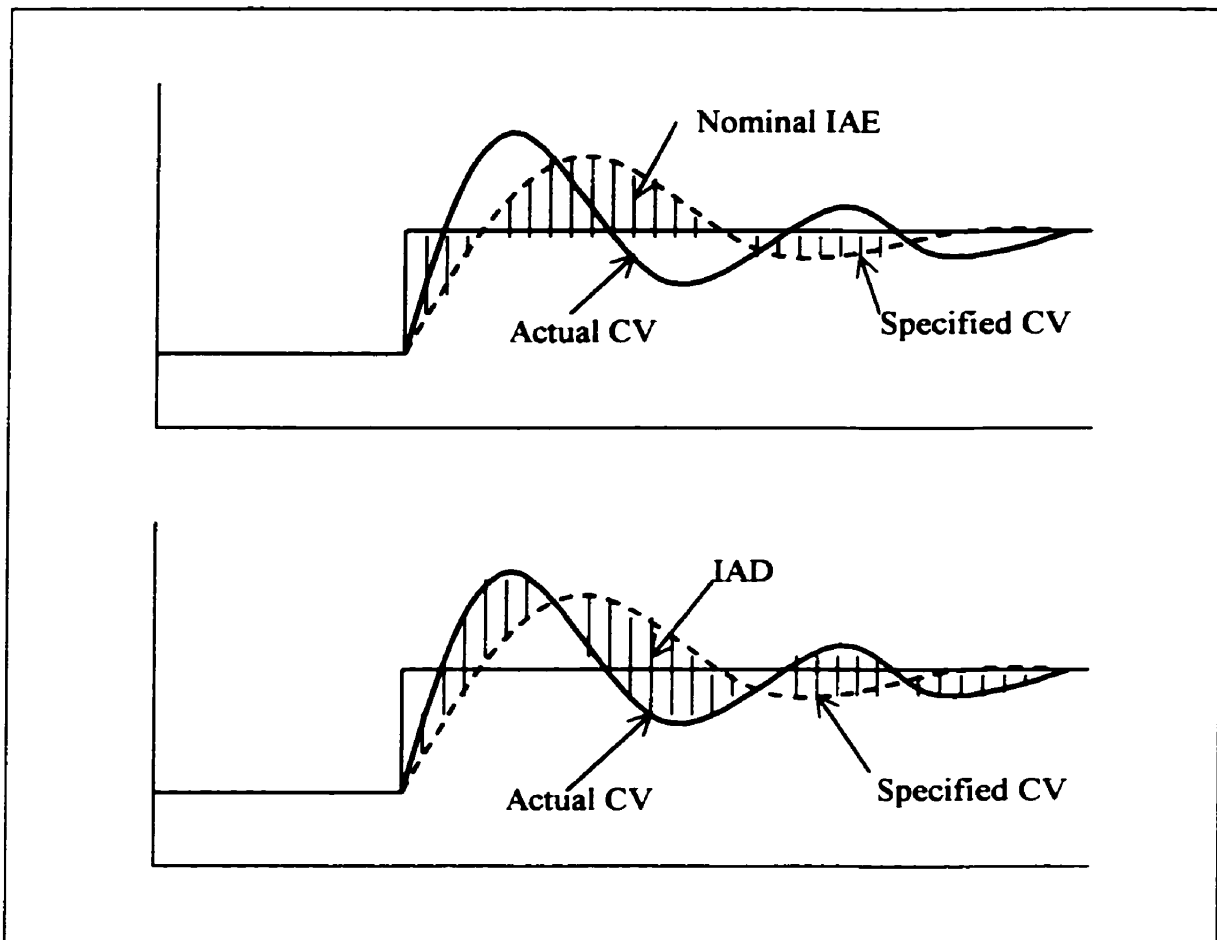

Figure 5.3. Illustration showing how IAD, and IAE_{nom} are measured.

Analogous performance measures could have been defined, such as integral of the product of time and absolute error (ITAE), or integral of the squared error (ISE).

The remainder of this chapter is further broken down into three segments, in which control performance is assessed. In Section 5.4.2, the nonlinearity and control performance of the transformed model subjected to nonlinear and linear multivariable control is examined. In 5.4.3, we look at how the logarithm transform of melt index affects linear performance relative to the linear performance of the nominal model. In Section 5.5 we look at possible causes for some unexpected results, and provide a preliminary investigation into three of these possible causes.

5.4.2 The Transformed Model - Control Performance

Two sets of simulations were investigated: one set in which grade transitions were the focus and one in which the focus was disturbance rejection. One might expect that RMS curvature values predict a larger degradation in linear control performance relative to nonlinear control, as the value of the RMS curvature increases. Therefore, we conjecture that the performance of linear multivariable controllers will suffer greatest losses at high c_{RMS} values, and suffer little loss at RMS curvature values less than 0.3.

5.4.2.1 Grade Transitions

Six grade transition policies of varying curvatures are studied in this section. It is our expectation that, as the value of RMS curvature increases, the success with which linear control is achieved will decrease. The success of control performance is measured as the normalized IAD value for each output. The set of grade transitions studied is shown in Table 5.1, along with the corresponding RMS curvature values. We see from Table 5.1 that these regions in the model display nonlinearities ranging from $c_{RMS}=0.625$

to $c_{RMS}=4.35$, indicating moderate nonlinearity. In all instances, the curvatures are significant relative to the benchmark value of $c_{RMS}=0.3$ proposed by Guay et al. (1995). The simulations of all grade transitions under both linear and nonlinear control are given in Appendix A.3, Figures A3.1 to A3.6. We see from Table 5.1 that all of the outputs at all curvatures, but one (IAD_{norm} of STPT), experience greater performance losses when controlled by linear rather than nonlinear means.

Grade Transition	RMS curvature value	Nomalized IAD ln(MI)	Normalized IAD Density	Normalized IAD Production Rate
S-T-P-T[*]	4.35	-0.0450	3.60	0.289
D-H-I-D	1.63	0.182	0.346	0.312
C-A-B-C	2.34	0.516	4.30	0.220
J-K-G-K[*]	0.625	1.08	6.00	0.381
O-Q-R-O	1.03	0.941	0.340	0.221
N-L-M-N	3.47	11.0	8.95	0.573

Table 5.1. Grade transitions for the transformed model, their corresponding curvatures, and their normalized IAD values that result from choosing linear control, over nonlinear control.
[*] Indicates that the grade transition simulation resulted in manipulated variable saturation.

It was expected that linear control would result in higher IAD values than for the nonlinear controllers, and hence, positive normalized IAD values. The one exception noted above is the one of grade transition S-T-P-T, ironically the region for which the highest degree of curvature was calculated. In this case, the ln(MI) is controlled better by the linear controller than by the nonlinear controller. (However, the improvement is insignificant since the value is close to zero). Although such a result contradicts expectations, it can potentially be explained by addressing the issue of manipulated variable saturation. This unexpected result may be due to the effect of input saturation

rather than nonlinearity compensation since linear control has no capacity to compensate for curvature (other than its integral action, which will return an output to set point). The controllers are not designed to deal with manipulated variable saturation; the linear controller calculated an unconstrained (in terms of MV bounds) solution, which, due to our manipulated variable bounds, happened to be more appropriate than that calculated by the unconstrained nonlinear solution. As seen in Figure A3.1b,d in Appendix A.3, the hydrogen gas flow rate reaches its lower bound of 0 mol/h at t=50h and t=100h, and then reaches its upper bound of 14000 mol/h at t=150h. Therefore, the slight improvement seen in linear control is likely due to imperfect calculation of input values by the linear controller, which by chance, happen to compensate better for the bound saturation.

It is our expectation that the trend between normalized IAD values and RMS curvature values should exhibit a positive correlation. The trend of normalized IAD values with respect to curvature values is shown in Figure 5.4 for each of the three outputs. For each output, a positive correlation is completely lacking. The degree to which nonlinear control resulted in lower normalized IAD values than the linear controller appears to be independent of the curvature experience by the model.

These findings are somewhat unexpected. Possible explanations are that input saturation disrupts the results by artificially favouring the linear controller results, or that directional curvatures may be more adequate for calculating nonlinearity due to the relatively few directions involved in such a limited simulation study. Additionally, because the RMS curvature is an average measure that encompasses all of the outputs, it doesn't describe the effect of curvature on individual inputs.
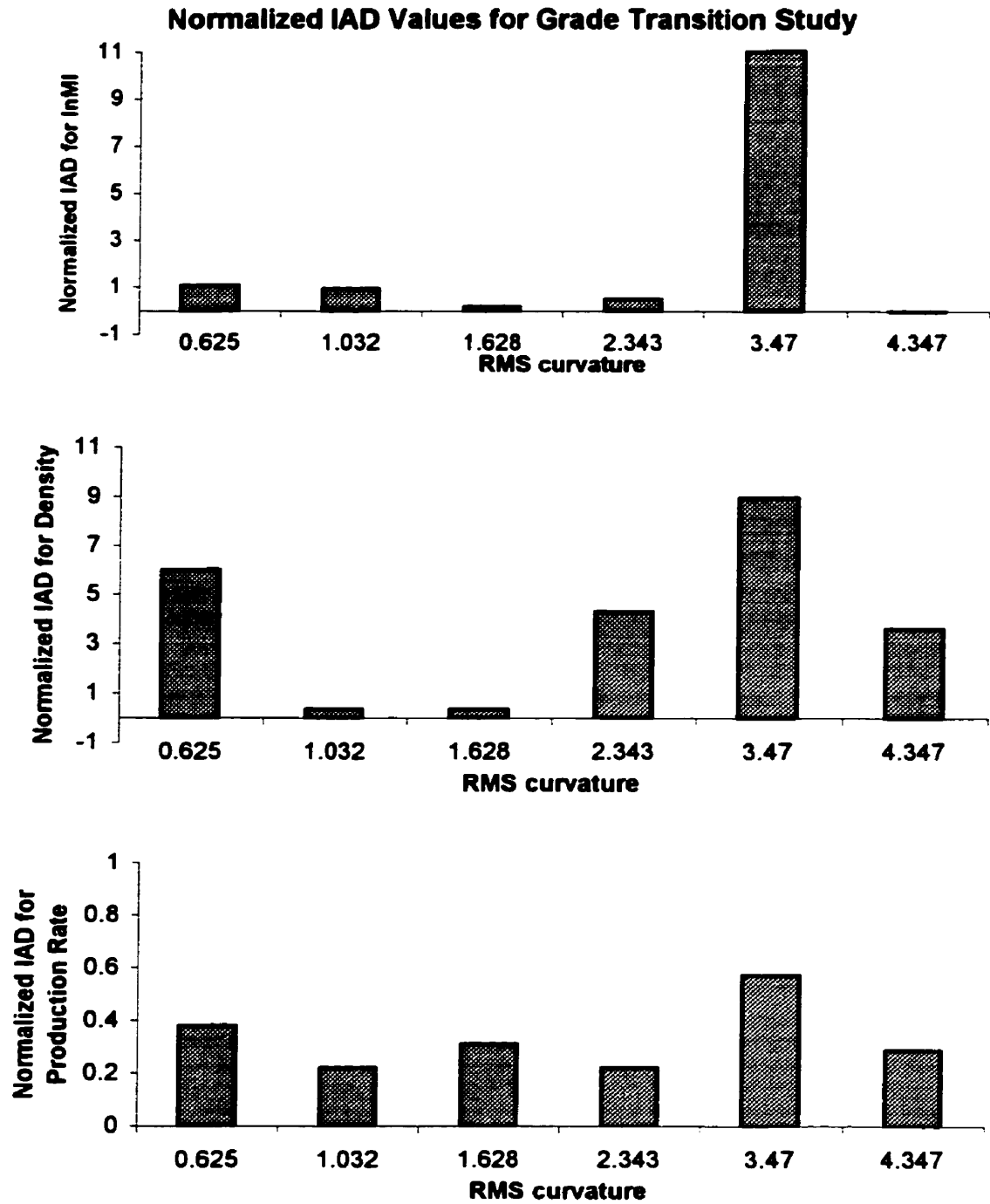
103

Figure 5.4. The relationship between the degree of curvature experienced by a grade transition region within the transformed model and the degree of degradation that occurs as a result of using linear control, as opposed to nonlinear control.

5.4.2.2 Disturbance Rejection

The performance of nonlinear and linear controllers also must be assessed with regard to operation about a point; that is, the disturbance rejection capabilities of each controller must be reviewed. In what follows, the control performance about three points is examined. Operation about these points, J(20), I(30), and E(20), results in moderate RMS curvatures that range from 0.476 to 4.27. The measure of performance for disturbance rejection studies is the normalized IAE, which measures the performance of the system under linear control, relative to the performance under nonlinear control. However, unlike in the grade transition case, the absolute value is calculated as the error between SP and CV, as is typically done.

Each of the grades have been subjected to identical disturbances. The open-loop disturbance effects on grade E(20) are shown in Figure 5.5. After 50 hours of steady-state operation, the system is subjected to a 25% increase in active site concentration in the entering catalyst. Variation in catalyst activity is a common disturbance, especially because of batch-to-batch variation. An increase in catalyst activity affects both production rate and the gas consumption rate, which results in a decrease in hydrogen and butene concentrations. These decreases then cause a lowering of ln(MI) and an increase in density. The increase in density comes about due to the lowering of butene concentration. Despite hydrogen concentration decreasing, which independently would result in a decrease in density, butene concentration has a more dominant effect on density, and therefore, the density increases. After the active site concentration disturbance is resolved, another disturbance is introduced at t=100h. This time the catalyst deactivation constant, k_d, is increased by 25%. This increase in k_d represents a
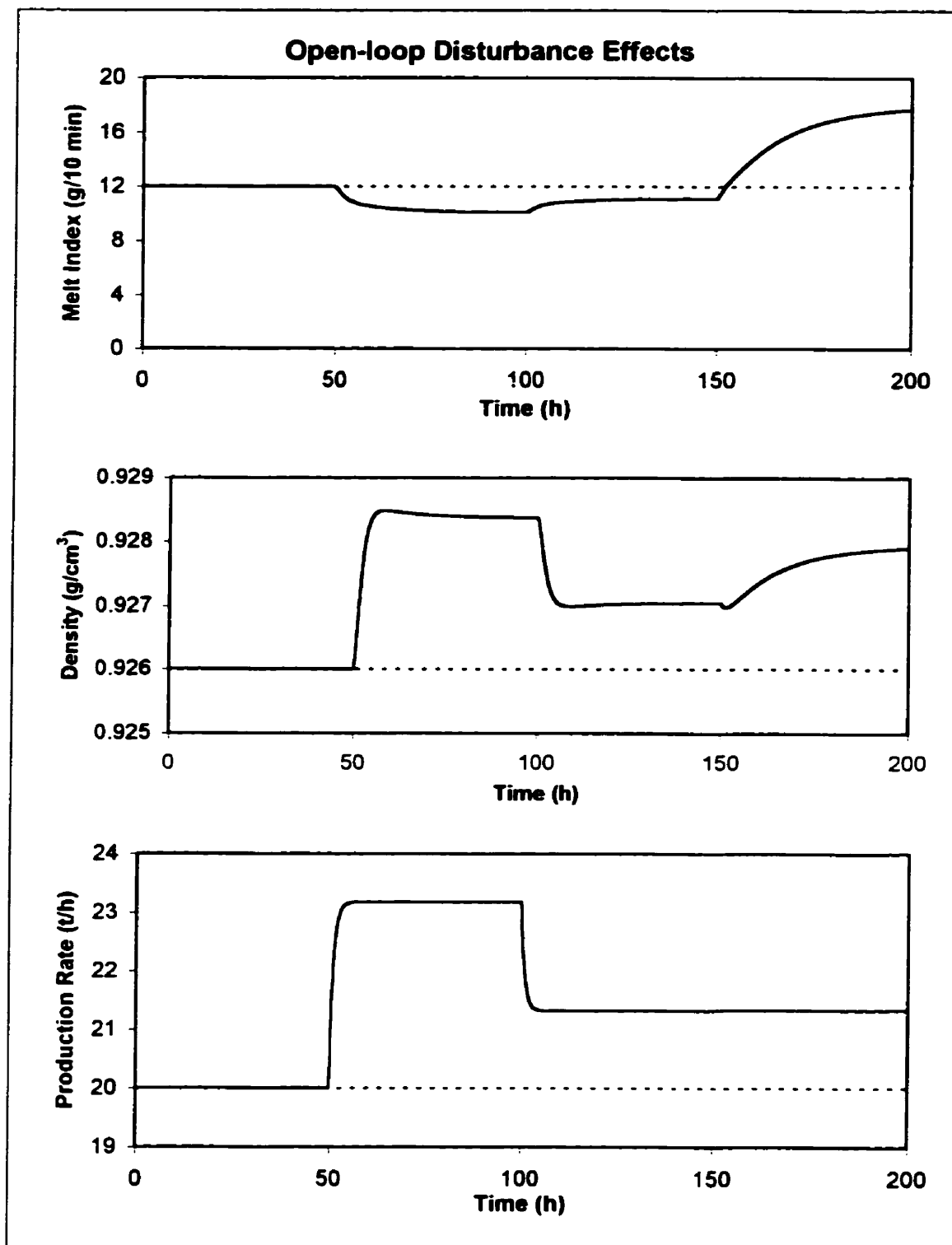
Figure 5.5. The open-loop effect on outputs of increasing a_{cat} at t=50h, increasing k_d at t=100h and decreasing b at t=150h. Solid line: outputs. Dashed line: set point.

deactivation of active sites, which might occur as a result of increased levels of poisons in the reactor. Such impurities react with the polymerization site, thereby rendering the site inactive. This disturbance has an opposite effect on Y compared to the previous disturbance. Finally, the last disturbance enters the system after 150 hours of operation. This disturbance represents a decreased flow rate of the bleed stream. Such a situation might occur if the operator adjusted the bleed valve position, or if the pressure downstream of the bleed valve had changed. This disturbance is simulated as a 25% decrease in b.

Simulation studies were performed on the three above-mentioned steady-state grades. Both linear and nonlinear control schemes were used to return the process to steady state following the introduction of disturbances. The simulation runs are plotted in Figures A3.7 to A3.9 in Appendix A.3.

The curvature of the region of operation about each of the three points defined earlier is shown in Table 5.2.

Grade	RMS curvature	Normalized IAE ln(MI)	Normalized IAE Density	Normalized IAE Production Rate
J(20)	0.476	3.92	21.8	0.0128
E(20)	1.25	1.90	18.4	0.0233
I(30)	4.27	1.61	31.8	-0.0709

Table 5.2. Grades for the transformed model, their corresponding curvatures, and the normalized IAE values that result from choosing linear control, over nonlinear control.

From Table 5.2, we see that for each of the situations, except one (production rate of I(30)), linear control results in poorer control than nonlinear control. For the steady-state operation about point I(30), the linear controller performs marginally better in production
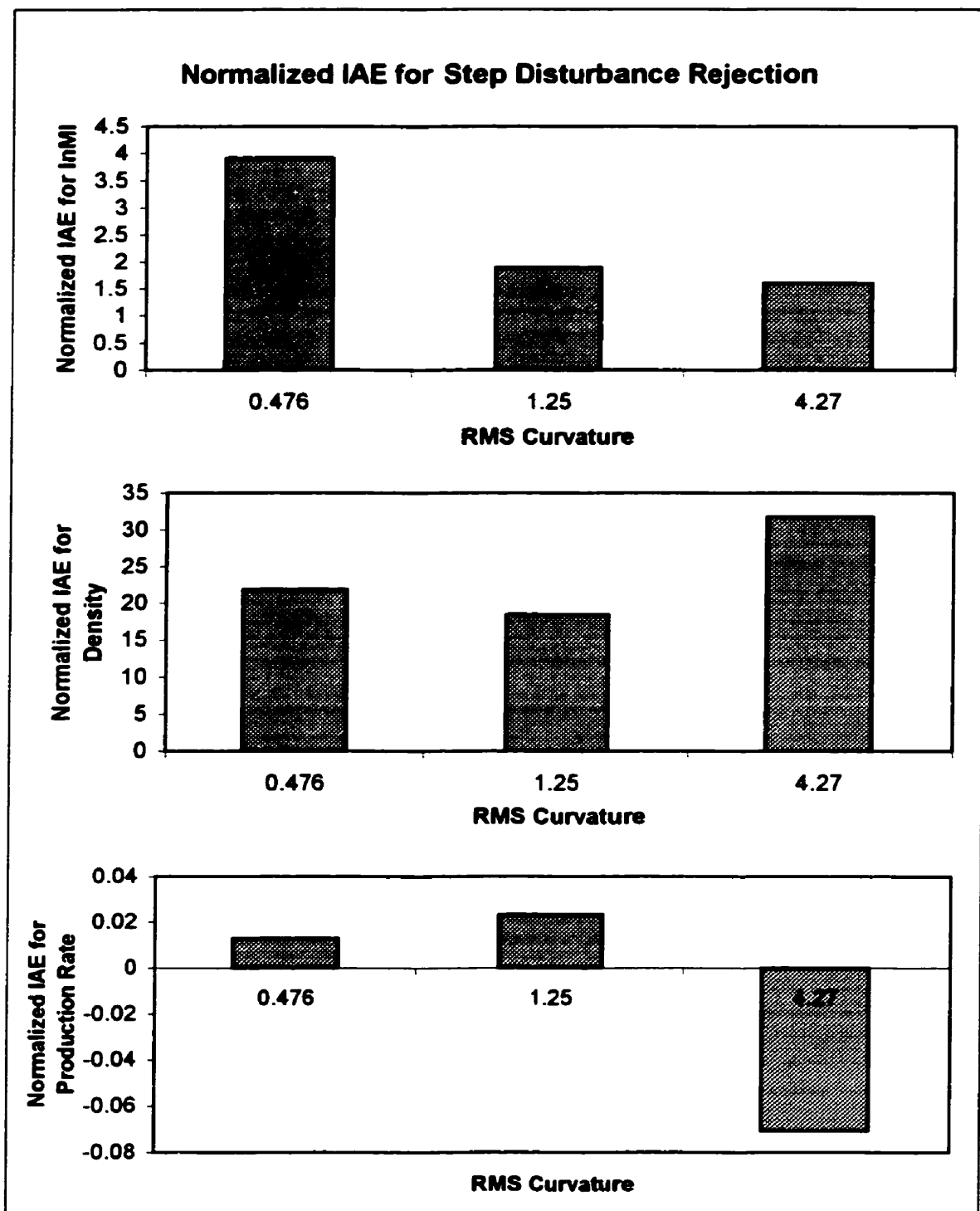
Figure 5.6. The relationship between the degree of curvature experienced by a region under regulatory control within the transformed model and the degree of degradation that occurs as a result of using linear control, as opposed to nonlinear control.

rate than the nonlinear controller; however, the improvement is so negligible, that for all intents and purposes, we can conclude that the linear and nonlinear controllers maintained the production rate equally as well, and for all curvatures.

To examine the performance degradation of linear control (relative to nonlinear control) in relation to the degree of curvature, we look at Figure 5.6. The trend in the normalized IAE values with respect to the RMS curvature is inconclusive. Each of the outputs, ln(MI), density, and production rate, exhibit different trends. The linear melt index controller appears to perform better at higher curvatures, which contradicts the anticipated results. For each of the other two outputs, there is no observable trend that would lead one to conclude that the success with which a process is controlled by linear means has any bearing on the local steady-state nonlinearity of the process.

Although Figure 5.6 shows no definite trends supporting the expectation that higher RMS curvatures result in more degradation of linear control, a relationship between linear control performance and curvature must not be discounted. Rather, perhaps the choice of second-order error-trajectory specification controllers may have been incompatible with the performance assessment measures defined. The IAE_{norm} may be favouring the linear controller because the linear controller may not be providing large enough overshoots to match the desired performance specification. This shortcoming of the linear controller would result in a lowered IAE value as compared to the nonlinear controller, which is performing overshoots as directed. This issue is discussed in Section 5.5. One might suggest comparing the disturbance rejection profiles against the corresponding specified trajectory as is done for grade transitions; a trial of the nonlinear controller without bound saturation would provide a good approximation of the specified

controlled variable trajectory. However, in some instances, due to different gains in the linear control law, the linear controller forced the outputs in a direction opposite to that of the nonlinear controller. Therefore, calculating the corresponding IAD would result in enlarged deviations, which would imply artificially degraded performance. The linear controller may have been following close to a second-order type response but was initially forced in different output directions. Therefore, due to this shortcoming, the alternative has been to assess performance by comparing the output trajectory to the specified set point.

5.4.3 Nominal vs. Transformed Model

Practitioners may often opt to implement the transformed version of the polyethylene model in linear control applications due to the anticipated lower degree of nonlinearity exhibited by the model. As calculated in Chapter 4, the transformed model displays much less nonlinearity than the nominal model, at all of the points considered. A large difference in RMS curvature values might imply that the control performance would differ significantly between models when subjected to linear control. It would be of interest to determine whether any control performance benefit is gained by this transformation. The focus of this section, therefore, is to examine the performance of the linear controller as applied to the transformed model, [ln(MI), ρ, PR]', versus its performance on the much more nonlinear nominal model, [MI, ρ, PR]'.

Two different scenarios are considered in this section. First, we look at the difference in control performance for one grade transition, J-K-G-K, for both nominal and transformed models. In addition, the control performance of disturbance rejection is

also studied, at the point J(20), for both models. The curvatures that were calculated for these two scenarios represent two cases in which the nominal and transformed models differ significantly.

The grade transition study is considered first. The simulations of the process for each controller of the nominal model are shown in Appendix Figures A3.10a-d. Recall that the simulation J-K-G-K for the transformed model was shown earlier, in Figure A3.4a-d. Table 5.3 shows the curvatures and normalized IAE values for both the transformed and nominal model simulations for the grade transition.

Grade and Model	RMS curvature	Normalized IAD ln(MI) or MI	Normalized IAD Density	Normalized IAD Production Rate
J-K-G-K, Transformed	0.625	1.08	6.00	0.381
J-K-G-K, Nominal	89.6	-0.170	9.16	0.381
Grade and Model	RMS curvature	Normalized IAE ln(MI) or MI	Normalized IAE Density	Normalized IAE Production Rate
J(20), Transformed	0.476	3.92	21.8	0.0128
J(20), Nominal	57.8	-0.599	22.9	-0.0210

Table 5.3. Grades for the transformed and nominal models, their corresponding curvatures, and the normalized IAD and IAE values that result from choosing linear control, over nonlinear control.

This table includes a negative normalized IAE value for one output of the nominal model grade transition, once again indicating that the linear controller in some cases serves to control as well as, or better, than the nonlinear controller, even under severe nonlinearity. To attain an appreciation for the difference in control performance between the linear controllers of the transformed and nominal models, we consider Figure 5.7. Figure 5.7 shows the normalized IAD values of each of the outputs at the low and high RMS curvature values of the transformed and nominal models, respectively.

From Figure 5.7, we note that this simulation study fails to support the conjecture that significant steady-state curvatures translate into performance degradation for linear

111

controllers. The normalized IAD values for melt index do not support expectations, by resulting in a lower performance error measure at the much higher RMS curvature of 89.6; density, however, appears to lend support to the theory as the corresponding normalized IAD value is somewhat higher at the higher RMS curvature value. On the other hand, the production rate results in the same normalized IAD value at both the low RMS curvature value, and the high value. These three observations result in another inconclusive result; the conclusion cannot be made that the performance of the linear controllers suffers greater losses as the degree of curvature of the model increases. Additionally, there is no evidence to support any relationship between performance losses of linear controllers and RMS curvature values.
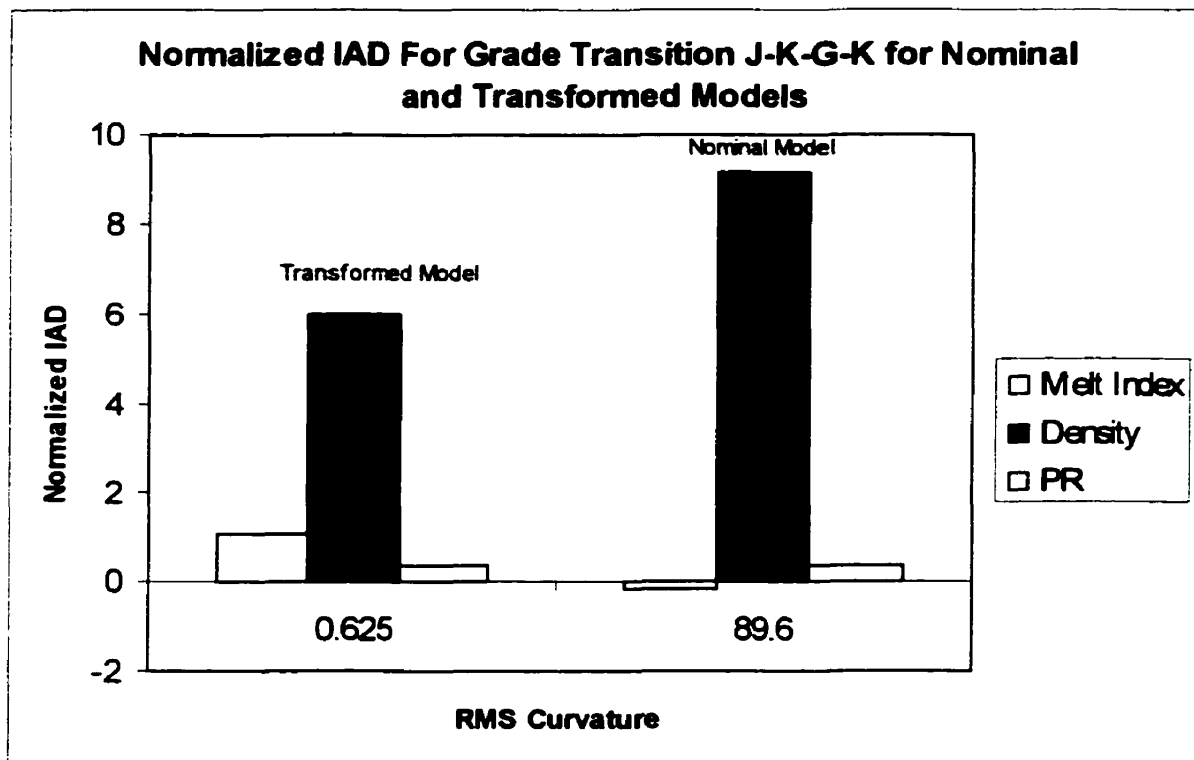

Figure 5.7. The relationship between the degree of curvature experienced by grade transition regions (within the nominal and transformed models) and the degree of degradation that occurs as a result of using linear control, as opposed to nonlinear control.

112

Next, the nominal and transformed models are compared in another control simulation study; the performance of the linear control scheme is examined for each level of curvature in a disturbance rejection study about point $J(20)$. The simulation plots for this study are given in Appendix A.3, Figures A3.7a-d and A3.11a-d. The linear control performance is examined for the transformed model, with a c_{RMS} of 0.476, and for the more nonlinear nominal model at which the curvature is $c_{RMS}=57.8$. These curvature values and their corresponding output results in the form of normalized IAE values are shown in Table 5.3 above. We expect that the linear control scheme will perform better with the transformed model than for the much more nonlinear nominal model. By observing the values in Table 5.3, we see that some negative normalized IAE values are again present. These negative values indicate that the linear control scheme performed with less error than the nonlinear controller, which in itself is unexpected; however, the fact that this result was observed under the very nonlinear model is even more perplexing.

To observe the trend between RMS curvature values and normalized IAE values, consider the plot in Figure 5.8. Figure 5.8 shows the same types of trends for each individual input as does Figure 5.7 above. The normalized IAE for the melt index actually decreases with an increase in c_{RMS}, while the density IAE_{norm} increases, and the production rate IAE_{norm} stays relatively constant. This simulation study also fails to draw a correlation between control performance and RMS curvature.
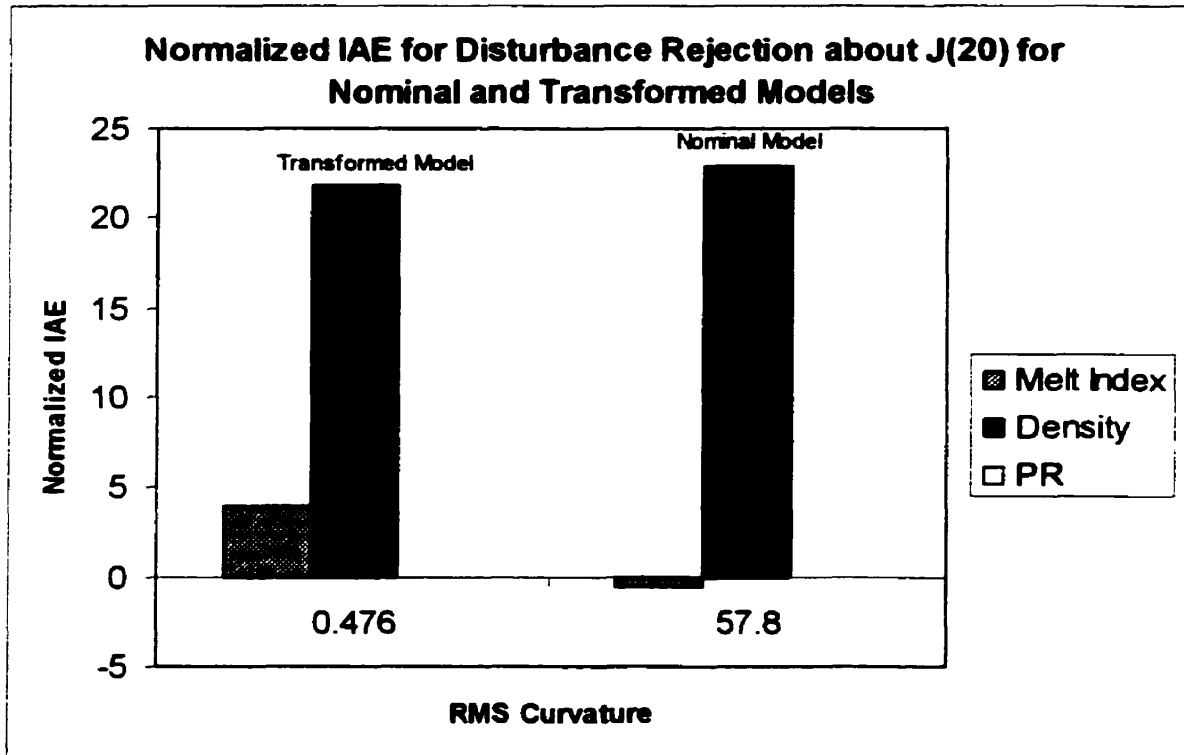
Figure 5.8. The degree of performance degradation that results from linear, versus nonlinear, control as applied to a region of regulatory control for one of each of the transformed model (c_{RMS}=0.476) and the nominal model (c_{RMS}=57.8)

5.5 Looking Ahead - Possible Explanations

Many plausible explanations exist for the unexpected results that were obtained in the performance assessment section above. These factors include control implementation issues, such as manipulated variable bound saturation, feedback linearization issues, and the possible incompatibility of the performance measure and the type of controller implemented, model structure issues, such as the multivariable nature of the problem, and concerns about the RMS curvature measure itself. The matters concerning the RMS measure of curvature include the issue of directionality, the form of the steady-state map, the fact that a steady-state measure is being compared to dynamic performance, and that

114

RMS curvature is a measure averaged over all outputs. A discussion of each of these topics follows. A preliminary investigation of some of these topics is provided.

5.5.1 Manipulated Variable Saturation

One possible explanation for the unexpected results obtained in the grade transition study in Section 5.4.2.1 is that the manipulated-variable bound saturation was obscuring the nonlinearity effects. The control laws used in the simulation studies solved for manipulated variable actions using an unconstrained solution (no MV bounds enforced); however, if the computed values exceeded the MV bounds, they were clamped at their corresponding bound value. In such a scenario, although the nonlinear controller would initially calculate a set of MV moves to provide the specified performance, the implementation of the input bounds might result in degraded performance away from the design specification. It is conceivable that the MV action computed by the linear controller might be more appropriate, purely by chance, when the unforeseen bounds were implemented. Due to this complication, it may be of interest to re-visit the simulation study and either implement a constrained solution, or remove the bounds on the manipulated variable to determine the pure effect of nonlinearities without the confounding factor of saturation.

5.5.2 Potential Incompatibility of Performance Measure and Control Specification

Although the disturbances introduced in our simulations were step disturbances, initial experimentation with pulse disturbances was performed, which resulted in some

noteworthy revelations. Because the control law utilized in this thesis is developed from the error trajectory description, we found that in some cases, the linear controller resulted in artificially improved performance. The term 'artificially' is used because although the error between the set point and the controlled variable was smaller in the linear case, the linear controller failed to provide the specified error trajectory. This performance was particularly evident in the production rate when a pulse disturbance in a_{cat} was introduced. The natural dynamics of the open-loop system result in the production rate returning to set point very quickly. However, when the error trajectory specification is in place in the closed-loop situation, the controller actually slows down the return of the production rate to set point because the tuning for this output is set at a more sluggish response than the open-loop response. For this reason, the nonlinear controller keeps the production rate from returning to set point quickly, whereas the linear controller, having calculated the control moves for following the specified second-order-type error trajectory using an approximate model, fails to follow the proper trace. This failure to conform to the specified trajectory then causes the production rate to fall back to set point quicker in the linear case, and results in a lower IAE than the nonlinear controller, which is actually following its specifications.

Another related concern with implementing second-order-type error-trajectory controllers in disturbance rejection studies is the required overshoot response in the melt index and density outputs. It is conceivable that the linear controller might not return the output to set point with the specified overshoot, which would result in a smaller error from set point to output. Therefore, we are falsely considering the potentially larger error in nonlinear controller overshoots as inferior performance. Perhaps the performance

116

measure chosen is inappropriate for use when assessing second-order error-trajectory controller performance. In future work, one might consider a simpler controller, such as a PID controller, in which overshoots are not required, or one might consider minimizing the overshoot specification in the second-order type error-trajectory controller. Alternatively, one might re-define the performance measure such that controlled variable overshoots do not confuse the issues.

5.5.3 Directionality

RMS curvature is a measure of nonlinearity that is averaged over all possible input directions. In theory, RMS curvature may be a good predictor of control performance if the system is subject to random shocks that drive the process in very many directions, or if the system is subjected to grade changes that include much of the input space. In our grade transition and disturbance rejection simulations, however, very little of the input space was used, and the system was driven in only a few directions by the three selected disturbances, which might mean that the system was only being subjected to certain direction-dependent nonlinearities. For this reason, it may be of interest to single out a grade transition or disturbance rejection, assess the performance in that region, and compare it to the corresponding directional curvature. Presumably, the process will experience different nonlinearities depending on the direction in which a disturbance drives the process, or depending on the input direction taken to bring about a given grade changeover.

5.5.4 The Steady-State Nature of RMS Curvature

The RMS measure of nonlinearity assesses steady-state curvature, and it is being compared to measures of dynamic performance. Steady-state analysis focuses on gain nonlinearity, whereas transient, or dynamic, nonlinearity is likely present as well. Guay (1996) developed a dynamic measure of curvature that quantifies the degree of dynamic nonlinearity experienced by a process model. A future step in related work should be to examine the dynamic nonlinearity of the system.

5.5.5 Multivariate Nature of the Model

The RMS measure of curvature is not only a value averaged over all input directions, but it is also a measure that combines the nonlinearity information of all outputs into one value. Therefore, it provides little information about how each individual output would perform; rather it indicates how all three would behave jointly. Although we assumed that the error measure of each of the outputs would increase with increasing curvature, we found that this did not occur. Therefore, it seems that the multivariable nature of the model may have complicated the interpretation of the curvature measurement with respect to individual output performance. One may choose to step back from such a multi-dimensional problem and re-visit this research with a uni-dimensional model, or examine individual elements in the curvature array.

5.5.6 Choosing the Appropriate Steady-State Map

In Chapter 2, it was discussed that the local geometry of the steady-state input-output map is examined to yield RMS measures of curvature. Recall that the input-

output map is approximated by first- and second-order Taylor series approximations, and that first- and second-derivative information is compared to provide an estimate of curvature. Guay et al. (1995) suggest that the nonlinearity of the steady-state input-output map more directly explains the nonlinearity of open-loop predictions of outputs, given inputs, and that the inverse map more directly applies to control-law nonlinearity, which relates to the nonlinearity of input moves, given outputs. Although the steady-state input-output map and its inverse are related, Guay et al. (1995) feel that control-law nonlinearity is more directly related to the curvature of the inverse map.

The nonlinearity of the process input-output map was studied in this thesis as a starting point, with the intention that more work in this area would follow. This choice of maps may explain some of the discrepancies in the results obtained. Further study in the assessment of nonlinearity of the inverse map is recommended.

5.5.7 Feedback Linearization

Linear error trajectory specifications lead to input-output feedback linearizating controllers, which may not always be the best for controlling nonlinear processes because they can cancel out helpful nonlinear dynamics. Examples of such a phenomenon in this work are seen in the improved performance of the linear controller relative to the nonlinear controller (i.e. IAD_{norm} or IAE_{norm} is negative). Such scenarios are analogous to conclusions reached in linear control theory in which the decoupling of interacting systems does not always benefit control performance.

119

5.6   Further Investigations

As a preliminary investigation into some of the recommendations made, three of these issues are briefly examined. Specifically, the issue of bound saturation raised in Section 5.5.1, the issue of directionality, discussed in Section 5.5.3, and the issue of the multivariable nature of the model, raised in Section 5.5.5, are addressed. The hope is to confirm some of the explanations of the perplexing results obtained.

5.6.1   Manipulated-Variable Saturation

The grade transition studies of the transformed model were revisited, but with the difference that manipulated variable bounds were omitted. Although such simulations would not be realistic because flow bounds would be breached, this type of simulation study might help determine whether input saturation is one factor contributing to the inconclusive results.

For these simulations, the normalized IAD value was once again used to evaluate control performance, and this value was compared to the RMS curvature calculated for the model in the corresponding local region. The RMS curvature values and the normalized IAD values are plotted in Figure 5.9. Comparing Figure 5.9 to Figure 5.4, we see that the trends in normalized IAD are unchanged for the unbounded simulation studies, which leads to the rejection of the factor of manipulated variable saturation as being a possible source of inconsistency between RMS curvature and control performance.
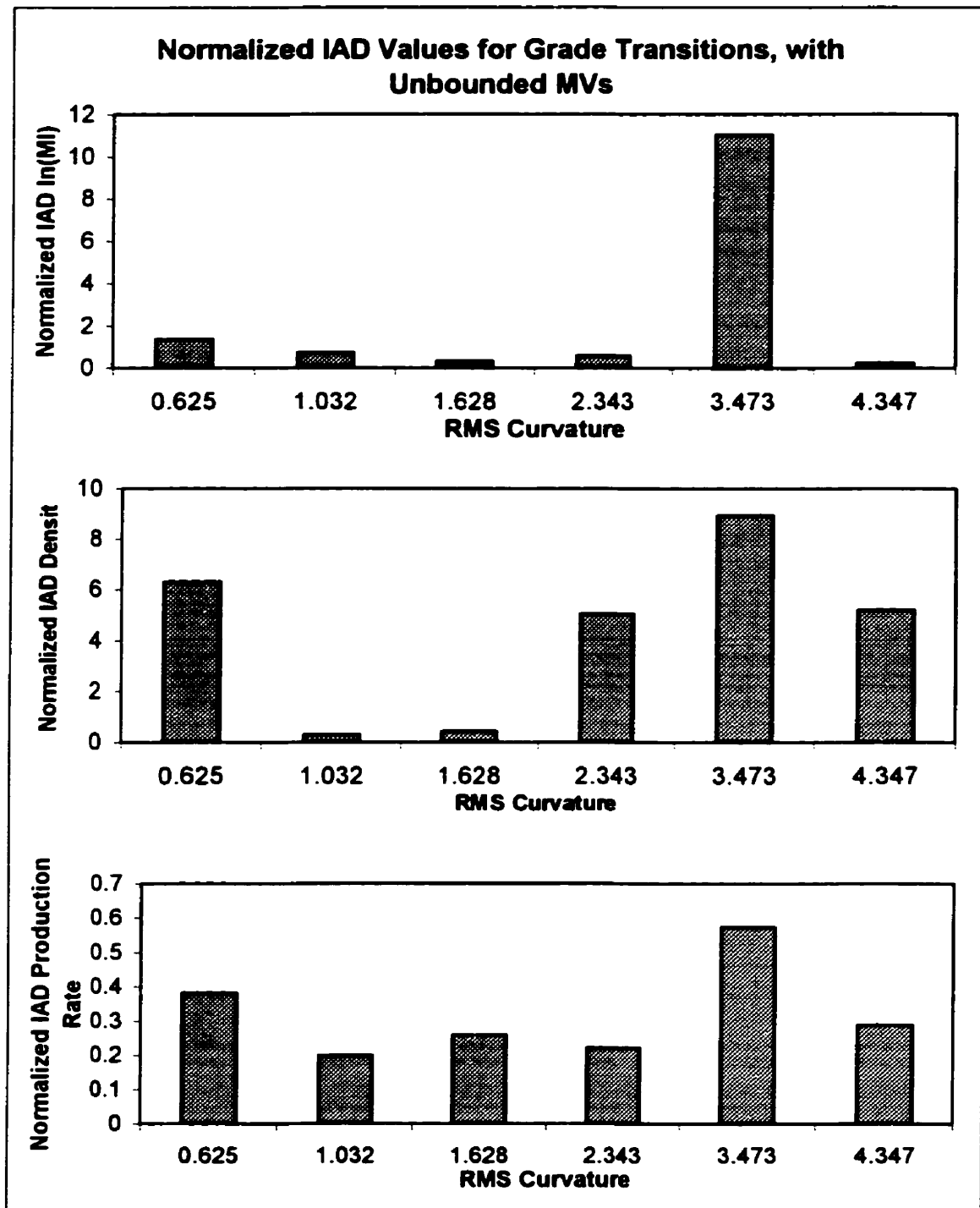
Figure 5.9. The relationship between the degree of curvature experienced by a grade transition region within the transformed model and the RMS curvature during simulations in which the manipulated variable action was not bounded.

5.6.2 Directionality

Directionality can play a major role in affecting control performance. Because RMS curvature is an average measure, the control performance results obtained in this thesis study, which lie in specific directions, may not be correlated to it. In our narrow view of six grade transitions and three disturbances, we have considered only a few input directions. Quite possibly, if one were able to perform a series of experiments in which all input directions were employed, a correlation between RMS curvature and control performance might be found.

One way of addressing directionality is to calculate the curvature of the process input-output map in a specific direction. Nonlinearity can be calculated in directions in which inputs move the process to a new steady state, or return the process to steady state after a disturbance is introduced. First, we determine the steady-state direction in which manipulated variables must move to produce a desired response, such as rejecting a disturbance, or changing the polyethylene grade. The input moves are calculated from the linearized steady-state model of the form (in deviation variables):

$$y = Vu + V_d d$$

Enforcing the set point, y=0, requires:

$$u = -V^{-1} V_d d$$

where V is the steady-state process gain matrix, and V_d is the disturbance gain matrix, both at the steady-state point of linearization. Vector d is the disturbance vector. Next, the local curvature of the model is assessed in the given input direction. Finally, the directional curvature is compared with the normalized IAE value obtained.

For brevity, we have chosen to examine the directional curvature relating to the

disturbance rejection of a change in the parameter values of a_{cat} and b. Each of the two disturbances, a_{cat} and b, are introduced independently.

The directional curvatures of the process model are shown in Table 5.4. Notice the difference in the curvatures for each disturbance.

Grade	Directional Curvature	Normalized IAE lnMI	Normalized IAE Density	Normalized IAE Production Rate
Disturbance: a_{cat}				
J(20)	0.0747	96.3	64.9	-0.0262
E(20)	0.0942	38.8	57.4	-0.0196
I(30)	0.152	45.2	50.7	0.0043
Disturbance: b				
J(20)	0.000648	1.23	0.575	0.754
E(20)	0.000679	0.0793	1.00	0.816
I(30)	0.00632	-0.334	0.409	4.86

Table 5.4. Directional curvatures and control performance for the rejection of disturbances in concentration of active sites in the catalyst, and bleed stream flow rate.

We see that at any one point, the two disturbances affect the process in completely different ways. The a_{cat} disturbance causes the process to experience much more nonlinearity than the disturbance in bleed flow rate, which supports the idea that directionality may play a major role in predicting control performance.

The results from Table 5.4 above are plotted in Figure 5.10 for visual comparison purposes. Unfortunately, the results are no more encouraging than those obtained for the RMS curvature comparisons. For each disturbance, no trend that might support a theory that curvature can be a predictor of control performance is seen. The results look almost randomly assigned.

The directional curvatures were calculated based on the steady-state input solution. However, the dynamic model actually moves the process through many different input directions to return the process to steady state under the error trajectory specification. Perhaps the steady-state approximation of the control moves required is a

poor one, which makes the directional curvature calculated inaccurate. Therefore, another difficulty arises; although an approximate input direction based on a linearized steady-state solution can be calculated, valuable dynamic information is missing, which begs the question, should we be addressing dynamic nonlinearity as opposed to steady-state measures of curvature?
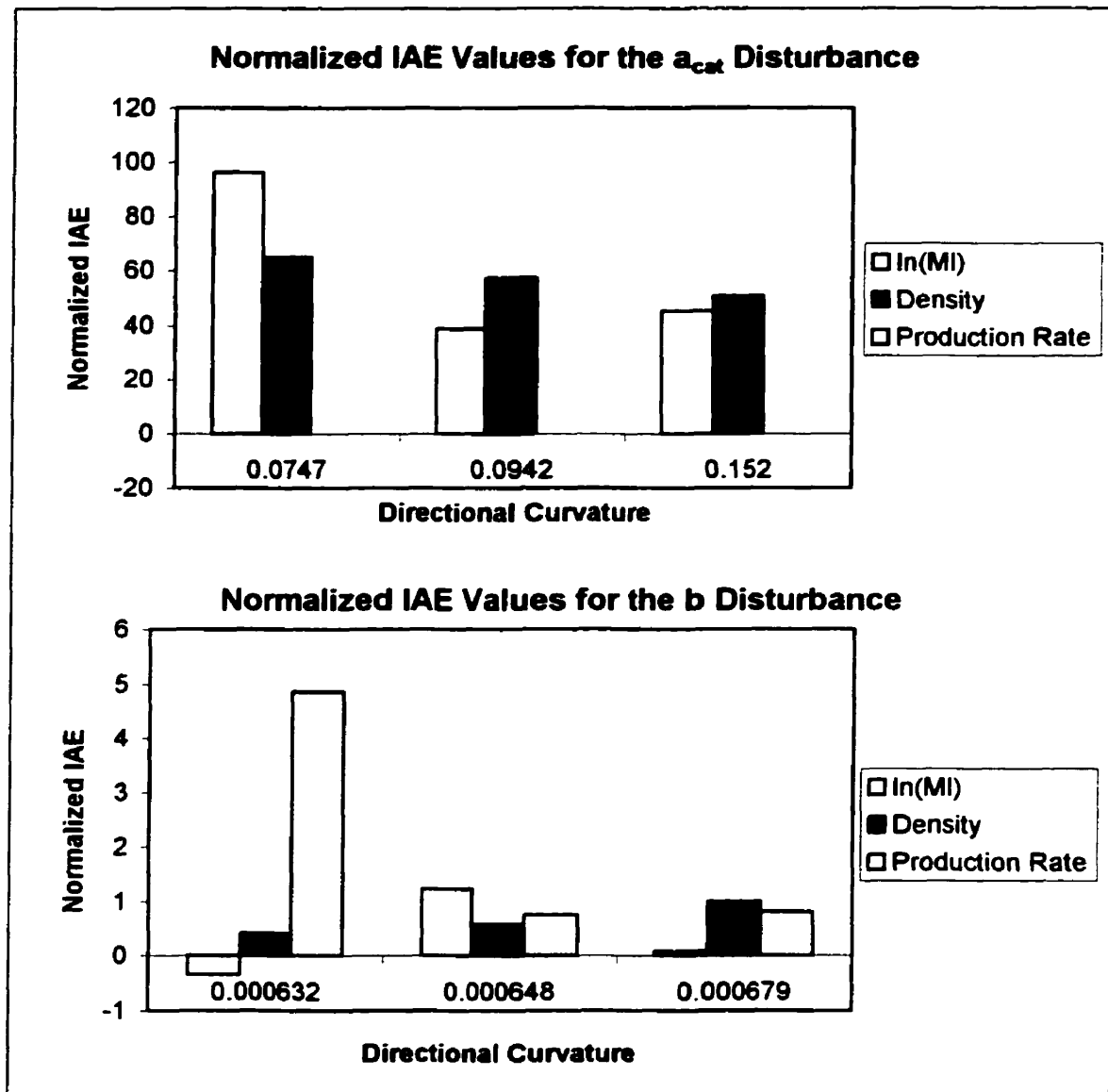

Figure 5.10. The relationship between the directional curvature and the normalized IAE value for independent disturbances in a_{cat} and b.

5.6.3 Multivariable Nature of the Model

A further consideration is to develop a unifying performance index that takes into account all process outputs and their corresponding contributions to the overall size of the grade change. For example, a performance index measured for a grade change in which a large melt index change, and small density and production rate changes occur, will be influenced primarily by the performance of the melt index. To fairly judge all outputs in a performance measure, the scaled values of the outputs are considered cumulatively; each output is scaled relative to the deviation of its nominal trajectory in the grade changeover (as in the scaling matrix S in Chapter 4). This newly developed performance measure is:

$$IAD_{cum} = \frac{IAD_{\ln(MI),scaled} + IAD_{\rho,scaled} + IAD_{PR,scaled}}{IAE_{\ln(MI),nom,scaled} + IAE_{\rho,nom,scaled} + IAE_{PR,nom,scaled}}$$

where
$$IAD_{output,scaled} = \frac{IAD_{output}}{\text{output range during grade change}}$$

$$IAE_{output,scaled} = \frac{IAE_{nom}}{\text{output range during grade change}}$$

The grade transition study of the transformed model is revisited. The grade transitions are listed in Table 5.5.

Grade Transition	RMS curvature value	IAD$_{cum}$
J-K-G-K	0.625	2.36
O-Q-R-O	1.03	0.400
D-H-I-D	1.63	0.335
C-A-B-C	2.34	1.90
N-L-M-N	3.47	6.64
S-T-P-T	4.35	1.64

Table 5.5. Grade transitions for the transformed model, the associated curvatures and cumulative normalized IAD values resulting from choosing linear, over nonlinear control.

125

To prevent confounding the problem with bound saturation issues, the MV bounds were removed in the simulations considered in this section. The simulation results are given in Figure 5.11.
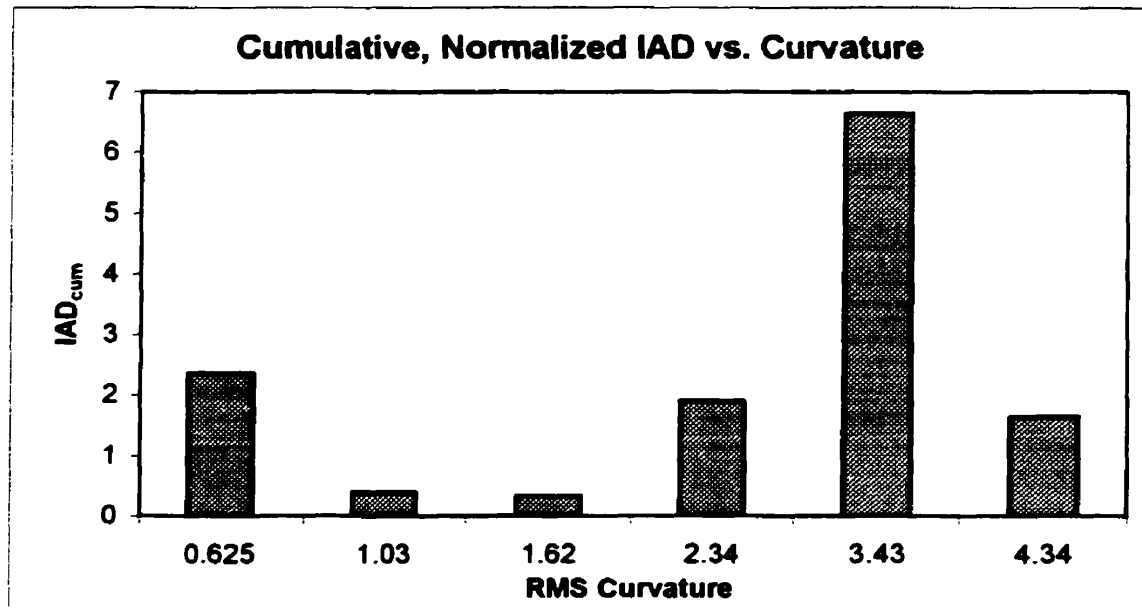

Figure 5.11. The normalized and cumulative performance measure is shown relative to the RMS curvatures. These values are based on simulations in which bound saturation did not occur.

As seen, there is no trend in the IAD_{cum} values with respect to RMS curvature. However, many plausible reasons still exist for the unexpected results.

5.7   Conclusions and Recommendations

In this chapter the development of the control law was presented and the technique used to tune the nonlinear and linear multivariable controllers was illustrated. The control performance was assessed for several situations.

First, the relative controller performance was compared against the curvature of the transformed model. It was determined that no trend exists among RMS curvature and normalized IAD for grade transitions. A possible explanation is that the manipulated variable bound saturation was confounding the model nonlinearity with an imposed system constraint. For disturbance rejection, no evidence was found of a link between RMS curvature and control performance. One explanation of this lack of correlation is that the choice of control scheme (second-order type response specified) and performance measure may not have been suitable to be used concurrently.

The performance of the transformed model was examined relative to the performance of the same controllers on the much more nonlinear nominal model. Once again, there appeared to be no relationship between RMS curvature and control performance.

Some possible explanations for the incongruity between RMS curvature and normalized IAD and IAE values were presented. These explanations included such possible causes as manipulated variable saturation, choice of performance measure and control structure, the multivariable nature of the model, the effect of directionality, the form of the steady-state map, and the steady-state nature of the RMS curvature measure.

Three of these possible causes were investigated briefly. Manipulated variable saturation does not appear to be an issue in this instance, as grade transition simulation results for each case (bounded and unbounded manipulated variables) resulted in similar results. We also performed a preliminary examination of directionality within the model. It was determined that the technique of ascertaining directional curvature yielded no link between it and normalized IAD values. However, it must be noted that the method for

evaluating directional curvatures employed a steady-state linear solution, which may not have been suitable. Finally, a new normalized cumulative performance measure was introduced, where the contribution of each output was weighted depending on the size of the set point change for each output. Analysis of the IAD_{cum} for six grade transition studies (in the absence of manipulated variable saturation) produced inconclusive results in that no trend was detected between the performance and curvature.

Some recommendations for future work include investigating the steady-state curvature of the inverse map, since it more directly predicts the nonlinearity of inputs, given outputs. In addition, the dynamic curvatures should be assessed when dealing with models having dynamic portions. As well, the steady-state and dynamic investigations should perhaps be performed on a SISO system to avoid confusion arising from multivariable issues. Future considerations may include choosing a different control scheme, one that doesn't employ second-order dynamics for use with the given performance measure; alternatively, another choice of performance measure might be more appropriate for this type of control specification.

Chapter 6

Conclusions, Recommendations and

Contributions

With the wealth of research being done in nonlinear control, coupled with the inherent nonlinearity present in most processes, and the potential benefits gained by nonlinear control, one would expect less reluctance among practitioners to implement nonlinear control. However, because of the design, implementation and maintenance demands of such control schemes, a curvature quantification measure would be a useful tool for practitioners to help determine whether the benefits of a nonlinear control scheme outweigh the efforts incurred. Of particular interest is how curvature translates to performance degradation of linear controllers.

Such a measure is the objective of Guay et al.'s (1995) RMS measure of curvature, which has been applied to McAuley et al.'s (1990) and McAuley and MacGregor's (1991, 1993) model of gas-phase fluidized-bed polyethylene production in this thesis. The main objectives of this work are to assess steady-state nonlinearity of polyethylene product property using Guay et al.'s (1995) steady-state curvature measure and the polyethylene model. Furthermore, the expectation is to determine whether the curvature calculated predicts linear control performance degradation, relative to nonlinear control. Additionally, practical implementation issues for the curvature measure are addressed, and recommendations for future considerations in this area are provided.

6.1 Summary and Conclusions

Background for this thesis work is given in Chapter 2. The gas-phase polyethylene reactor model and equipment are detailed. As well, background on the calculation and visualization of the RMS curvature measure of Guay et al. (1995) is given, key points of this work being the examination of the geometry of the steady-state locus. Second-order derivative information is decomposed into tangential and normal components and a technique for scaling is described, enabling a scale-independent measure of nonlinearity. The effects of interaction and nonlinearity of the geometry of the steady-state locus are also discussed. Chapter 2 also provides information on error-trajectory controller design, which is the control choice in this work.

Previous work in the area of nonlinearity assessment (e.g., Guay et al., 1995, Allgöwer, 1995, Stack and Doyle III, 1997b) has been illustrated using small examples. A detailed comparison between steady-state RMS curvature and controller performance degradation for an industrial process has not previously been conducted. In Chapter 3, a comprehensive study is offered by examining major components of an industrial process example, namely state property behaviour of the polyethylene reactor model. Examples detail the calculation of RMS curvature, its effect on the visualization of the steady-state locus, and provide an interpretation of the elements of the relative curvature array. Visualization of curvature (and interaction) is easily achieved by virtually reducing the dimensionality of the model by examining 2×2 portions at a time.

In Chapter 4, the nonlinearity of properly scaled regions within the polyethylene model is assessed.

- *Conclusion i*: The six regions chosen for grade transition studies in the transformed

model display moderate curvatures ranging from $c_{RMS}=0.625$ to $c_{RMS}=4.35$, while the same six transitions within the nominal model result in curvatures in the range $6.70 \leq c_{RMS} \leq 117$.

• *Conclusion ii*: For the steady-state regulation about a point, the curvature of the transformed model is examined for three points, yielding a curvature range of $0.476 \leq c_{RMS} \leq 4.27$. The curvature of the nominal model is compared to that of the transformed model at point J(20), with the nonlinearity of the nominal model being much larger ($c_{RMS}=57.8$) than that of the transformed model ($c_{RMS}=0.476$).

• *Conclusion iii*: For all regions assessed, the nominal model displays a higher degree of curvature than the transformed model, thus supporting the general practice in industry of considering the transformed melt index, rather than melt index directly.

The aim in Chapter 5 is to consider the nonlinearity measures obtained in Chapter 4 and apply control to the corresponding operating regions. The performance of a linear control scheme relative to a nonlinear controller is compared to the earlier computed RMS curvature value. The objective was to find a relationship between RMS curvature and linear performance such that the success or failure of linear control could be predicted by the curvature measure.

Six grade transition studies within the transformed model are examined, and one additional grade transition simulation is studied for the corresponding nominal model. As well, disturbance rejection studies are examined, three using the transformed model, and one using the nominal model. It was expected that the chosen performance index, which quantifies the performance difference between linear and nonlinear controllers, would increase as RMS curvature of the grade regions increased. The performance index

for grade transition studies, the IAD_{norm}, is defined as the difference between the degrees of deviation (from the specified controlled variable trajectory) of linear and nonlinear controllers, normalized by the nominal size of the transition. Similarly, for disturbance rejection studies, the performance is assessed by the IAE_{norm}, which is the difference between the degrees of deviation (of the controlled variable from set point) of linear and nonlinear controllers, standardized by the nominal size of the disturbance effect.

• *Conclusion iv*: No general trend exists between values of the performance index and curvature values. There is no conclusive evidence supporting the theory that RMS curvature is a good predictor of the quality of linear control performance, relative to nonlinear control performance. In most cases, nonlinear control outperformed linear control; however, the degree of improvement with nonlinear control is simply not accounted for by RMS curvature for the polyethylene example.

Several possible reasons are given for the unexpected results obtained. These possible causes include control issues (manipulated variable bound saturation, feedback linearization issues, and controller type, in relation to performance index), model structure issues (its multivariable nature), and questions concerning the RMS curvature measure (directionality, the steady-state nature of the measure, and the form of the steady-state input-output map). As a preliminary investigation, the issues of bound saturation in input variables, the multivariable nature of the model, and directionality were examined. None of the investigations yielded a solution to the question of why the RMS curvature didn't predict linear control performance degradation in our studies.

6.2   Recommendations for Future Work

Some recommendations are given here for consideration in the future. These suggestions result from the investigation into possible reasons for the lack of correlation found between RMS curvature and the specified performance measure.

6.2.1 Dynamic Consideration

One must consider the dynamic nature of the process model and ascertain whether a steady-state measure of curvature is sufficient when considering controller performance degradation. If the process remains in a small operating region, one might expect that perhaps dynamic nonlinearity is of less consequence in that although the nature of the dynamic character could change over an area, it is less likely in small regions. However, in the simulations presented in this thesis, the steady-state measure was not capable of predicting control performance. Therefore, dynamic nonlinearity must also be addressed.

An additional consideration may be to ascertain whether the nonlinearity resides only in the steady-state portion of the model, or if the dynamics are also nonlinear. It is conceivable that if the steady-state portion contains all or most of the nonlinearity, then RMS curvature might be more indicative of linear control performance degradation.

6.2.2 Consider Inverse Map

Guay et al. (1995) suggest assessing the nonlinearity of the steady-state inverse map as opposed to the input-output map. The nonlinearity of a controlled process is more directly related to the ability to predict input, given a desired output, whereas open-loop nonlinearity more directly predicts the nonlinearity of output, given input. Therefore,

further consideration might be given to assessing steady-state nonlinearity of the inverse map.

6.2.3 Directionality

RMS curvature is a measure that is averaged over all input directions. Therefore, perhaps the region in which the curvature was calculated did not accurately reflect the directions in which the process would be perturbed, since only a few directions were actually realized in this narrow assessment of a few simulations. Although additional work was done in assessing the importance of directionality, the curvature was calculated for a steady-state change in inputs required to return the process to set point, given a disturbance. In actuality, the process responded dynamically in many additional input directions to return to steady state, thereby exposing the process to different curvatures than those accounted for by the curvature calculation for the given direction. A resulting recommendation is that a more thorough simulation study in which many more directions are included may reveal a relationship between RMS curvature and linear control performance degradation.

6.2.4 Multivariable Nature of the Model

Due to the multivariable nature of the model, it is difficult to discern the effect of nonlinearity on individual outputs, or on the sum of outputs as a whole because RMS curvature is a measure averaged over all outputs. An attempt was made to define a performance measure, IAD_{cum}, which would allow for a measure of the culminated effect of nonlinearity on all outputs. However, a relationship between IAD_{cum} and RMS

curvature failed to reveal itself. Therefore, to enable a clearer investigation between RMS curvature and performance, perhaps a good starting point might be to assess the curvature of SISO systems. Alternatively, one might develop a different controller performance index.

6.2.5 Scaling

The scaling used in this work was defined by a non-rotated ellipse, defined in the output space. In fact, it is likely that an ellipse that approximates the region of operation in the output space best is rotated relative to the output coordinates axes. Such an ellipse results in different scaling, which may affect in turn the RMS curvature. Because rotated ellipses may have been more appropriate, further investigations in this respect are advisable.

6.2.6 ISE-Based Performance Index

A more appropriate performance index may have been based on the integral of the squared error (ISE). Because the scaling in this work is based on an ellipse, the ISE may have been more consistent with such an underlying quadratic nature.

6.2.7 Anti-reset Windup

A possible complicating factor in this work may have been the existence of reset windup, as the integral term in the controllers accumulated error. Integral windup may result in degraded control performance; therefore, future work in this area should eliminate reset windup, or account for it (e.g. by using a velocity form of a control law)

6.2 Contributions

The following contributions to chemical engineering have been provided by the author.

6.3.1 Application of RMS Curvature Measure

Through this thesis work, it has been discovered that the application of steady-state RMS curvature must not be done blindly. One must not expect that RMS curvature will predict linear control performance, but rather it is only an averaged general measure of gain nonlinearity. It was determined in this study that large values of RMS curvature do not necessarily result in large degradations in linear control performance. Conversely, regions displaying mild curvature can suffer very large performance losses when controlled by linear techniques. Clearly, there exist other factors at work in the assessment of curvature, than simply the implementation of the RMS curvature measure.

6.3.2 Nonlinearity Assessment of the Polyethylene Model

The nonlinearity of several regions of the gas-phase polyethylene model was measured within both the state space and the output space. The assessment focussed on the nonlinear product property behaviour described by the model. Curvature values determined for the regions of interest range in nonlinearity from mild to severe. In addition to quantitative assessment, qualitative assessment explained the effect of nonlinearity on the orientation, spacing and bending of constant input lines on the steady-state locus. A detailed investigation such as this for an industrial example has not previously been reported in the literature.

6.3.3 The Polyethylene Model as a Learning Tool

It was determined that the gas-phase polyethylene model is a rich model in terms of the variety of the degree of inherent nonlinearity present in the model. Regions in the polyethylene model display any of mild, moderate, or severe nonlinearity. As a result, this model is a powerful teaching tool for learning RMS measures of nonlinearity.

6.3.4 Decreased Nonlinearity of the Transformed Model

A contribution that might be of particular interest to practitioners is that quantitative evidence has been found supporting the claim that the logarithm transform of melt index reduces the degree of nonlinearity of the model. In most cases, the nonlinearity of the model was significantly reduced by the transformation. Therefore, practitioners' use of the transformed model, as opposed to the nominal model, is further validated.

6.3.5 Evidence of Robustness of Linear Control

There exists much reluctance in industry to implement nonlinear control techniques, because oftentimes, linear controllers perform with much more robustness than would be expected, even under highly nonlinear conditions. In this thesis, more evidence of this phenomenon was found, in that under highly nonlinear conditions, in some cases the linear controller performed on par with the nonlinear controller.

6.3.5 Insights and Explanations

While a relationship between RMS curvature and linear control performance was

not found, many insights and plausible explanations have been offered, as well as directions and recommendations for future work. The most promising direction of research is likely to be the examination of dynamic nonlinearity assessment.

References

Allgöwer, F. (1995), "Definition and computation of a nonlinearity measure and application to approximate I/O-linearization", Technical Report 95-I, Institut Für Systemdynamik und Regelungstechnik, Universität Stuttgart.

Bates, D. and Watts, D. (1988), *Nonlinear Regression Analysis and Its Applications*, John Wiley and Sons, New York.

Bequette, B. (1991), "Nonlinear Control of Chemical Processes: A Review", *Ind. Eng. Chem. Res.* **30**, 1391-1413.

Chinh, J. C, and Dumain, A. Process and Apparatus for the Gas-Phase Polymerization of Olefins in a Fluidized-Bed Reactor. Eur. Patent Appl. EP351068 A1, Jan 17, 1990.

Dadebo, S. A., Bell, M. L., McLellan, P. J. and McAuley, K. B. (1997) "Temperature control of industrial gas-phase polyethylene reactors", *J. Proc. Cont.* 7(2), 83-95.

Guay, M. (1996), Measurement of Nonlinearity in Chemical Process Control, PhD thesis, Queen's University, Kingston, Canada.

Guay, M., McLellan, P. J., and Bacon, D. W. (1995), "Measurement of Nonlinearity in Chemical Process Control Systems: The Steady-State Map", *The Canadian Journal of Chemical Engineering*, **73**, 868-882.

Haber, R. (1985), "Nonlinearity Tests for Dynamic Processes", *Proceedings of Conference on Identification and System Parameter Estimation*, IFAC.

Harris, T. J. and McLellan, P. J. (1990), "Generic Model Control - A Case Study Revisited", *The Canadian Journal of Chemical Engineering*, **68**, 1066-1070.

Isidori, A. (1989), *Nonlinear Control Systems*, 2nd Edition, Springer-Verlag, Berlin.

Koung, C. and MacGregor, J. (1991), "Geometric Analysis of the Global Stability of Linear Inverse-Based Controlllers for Bivariate Nonlinear Systems", *Ind. Eng. Chem. Res.*, **30**, 1171-1181.

Koung, C. and MacGregor, J. (1992), "Robustness of Multivariable Linear Controllers to Process Nonlinearities", *Ind. Eng. Chem. Res.*, **31**, 1085-1096.

Kravaris, C. and Kantor, J. (1990a), "Geometric Methods for Nonlinear Process Control. 1. Background", *Ind. Eng. Chem. Res.*, **29**, 2295-2310.

Kravaris, C. and Kantor, J. (1990b), "Geometric Methods for Nonlinear Process Control. 2. Controller Synthesis", *Ind. Eng. Chem. Res.*, **29**, 2310-2323.

Lee, P. L. and Sullivan, G. R. (1988), "Generic Model Control (GMC)", *Comput. chem. Engng.*, **12**(6), 573-580.

Leung, J. (1998), Assessing the Impact of Nonlinearity on Process Control, Master's Thesis, Queen's University, Kingston, Canada.

Marlin, T. (1995), *Process Control - Designing Processes and Control Systems for Dynamic Performance*, McGraw-Hill, Inc., New York.

McAuley, K. B. and MacGregor, J. F. (1991), "On-Line Inference of Polymer Properties in an Industrial Polyethylene Reactor", *AIChE Journal*, **37**(6), 825-835
McAuley, K. B. and MacGregor, J. F. (1992), "Optimal Grade Transitions in a Gas-Phase Polyethylene Reactor", *AIChe Journal*, **38**(10), 1564-1576.

McAuley, K. B. and MacGregor, J. F. (1993), "Nonlinear Product Property Control in Industrial Gas-Phase Polyethylene Reactors", *AIChE Journal*, **39**(5), 855-865.

McAuley, K. B., MacGregor, J. F. and Hamielec, A. E. (1990), "A Kinetic Model for Industrial Gas-Phase Ethylene Copolymerization", *AIChE Journal*, **36**(6), 837-850.

McAuley, K. B., Talbot, J. P. and Harris, T. J. (1994), "A Comparison of Two-Phase and Well-Mixed Models for Fluidized-Bed Polyethylene Reactors", *Chemical Engineering Science*, **49**(13), 2035-2045.

McLellan, P. J., Harris, T. J., and Bacon, D. W. (1990), "Error Trajectory Descriptions of Nonlinear Controller Designs", *Chemical Engineering Science*, **45**(10), 3017-3034.

Miller, A. R. Fluidized Bed Reactor. U.S. Patent 4003712, Jan 18, 1977.

Nikolaou, M. (1993), "When is Nonlinear Dynamic Modelling Necessary?", in "Proceedings of the American Control Conference", June, San Francisco, CA, 910-914.

Ogunnaike, B., Pearson, K., and Doyle, III, F. (1993), "Chemical Process Characterization: With Applications in the Rational Selection of Control Strategies", in "Proceedings of the European Control Conference", Groningen, the Netherlands, 1067-1071.

Piette, R., Harris, T. J., and McLellan, P. J. (1995), "Graphical Interpretations of Steady-State Interaction Measures", *Ind. Eng. Chem. Res.* **34**, 4436-4450.

Stack, A. and Doyle, III, F. (1995), "A Measure for Control Relevant Nonlinearity", in "Proceedings of 1995 American Control Conference", June 21-23, Seattle, WA.

Stack, A. and Doyle, III, F. (1997a), "The optimal control structure: an approach to measuring control-law nonlinearity", *Computers chem. Engng* 21(9), 1009-1019.

Stack, A. and Doyle, III, F. (1997b), "Application of a Control-Law Nonlinearity Measure to the Chemical Reactor Analysis", *AIChE Journal*, 43(2), 425-439.

Appendix A

Additional Information

A.1 Error-Trajectory Specification of the Nominal Model in Equation 5.2

$$
\begin{bmatrix}
\dfrac{\partial h_1}{\partial x_1} & \dfrac{\partial h_1}{\partial x_2} & \dfrac{\partial h_1}{\partial x_3} \\
\dfrac{\partial h_2}{\partial x_1} & \dfrac{\partial h_2}{\partial x_2} & \dfrac{\partial h_2}{\partial x_3} \\
\dfrac{\partial h_3}{\partial x_1} & \dfrac{\partial h_3}{\partial x_2} & \dfrac{\partial h_3}{\partial x_3}
\end{bmatrix}
\cdot
\begin{bmatrix}
\dfrac{d[H_2]}{dt} \\
\dfrac{d[M_2]}{dt} \\
\dfrac{dY}{dt}
\end{bmatrix}
=
\begin{bmatrix}
\beta_1 & 0 & 0 \\
0 & \beta_2 & 0 \\
0 & 0 & \beta_3
\end{bmatrix}
\cdot
\begin{bmatrix}
MI_{sp} - MI \\
\rho_{sp} - \rho \\
PR_{sp} - PR
\end{bmatrix}
+ \ldots
$$

$$
\begin{bmatrix}
\gamma_1 & 0 & 0 \\
0 & \gamma_2 & 0 \\
0 & 0 & \gamma_3
\end{bmatrix}
\cdot
\begin{bmatrix}
\int_{t0}^{t} (MI_{sp}(z) - MI(z)) dz \\
\int_{t0}^{t} (\rho_{sp}(z) - \rho(z)) dz \\
\int_{t0}^{t} (PR_{sp}(z) - PR(z)) dz
\end{bmatrix}
$$

$$
\frac{\partial h_1}{\partial x_1} = 3.5 \frac{k_3}{M_1} \left(k_0 + k_1 \frac{[M_2]}{[M_1]} + k_3 \frac{[H_2]}{[M_1]} \right)^{2.5},
$$

$$
\frac{\partial h_1}{\partial x_2} = 3.5 \frac{k_1}{[M_1]} \left(k_0 + k_1 \frac{[M_2]}{[M_1]} + k_3 \frac{[H_2]}{[M_1]} \right)^{2.5},
$$

$$
\frac{\partial h_1}{\partial x_3} = 0,
$$

$$
\frac{\partial h_2}{\partial x_1} = \frac{3.5 p_1 \dfrac{k_3}{[M_1]}}{\left(k_0 + k_1 \dfrac{[M_2]}{[M_1]} + k_3 \dfrac{[H_2]}{[M_1]} \right)},
$$

$$\frac{\partial h_2}{\partial x_2} = \frac{3.5 p_1 \dfrac{k_1}{[M_1]}}{\left(k_0 + k_1 \dfrac{[M_2]}{[M_1]} + k_3 \dfrac{[H_2]}{[M_1]}\right)} - \frac{p_4 \cdot p_2}{[M_1]}\left(p_2 \frac{[M_2]}{[M_1]}\right)^{(p_4-1)}$$

$$\frac{\partial h_2}{\partial x_3} = 0 ,$$

$$\frac{\partial h_3}{\partial x_1} = 0 ,$$

$$\frac{\partial h_3}{\partial x_2} = \frac{kp_2 \cdot mw_2 \cdot Y}{10^6} ,$$

$$\frac{\partial h_3}{\partial x_3} = \frac{kp_1 \cdot [M_1] \cdot mw_1 + kp_2 \cdot [M_2] \cdot mw_2}{10^6}$$

A.2 Nonlinear Control Law Solution for the Multivariable Controller (Nominal Model)

$$F_{H2} = Vg*(-\beta_2 * \rho_{sp} * \frac{dh_2}{dx_2} + \beta_2 * \rho * \frac{dh_1}{dx_2} - \gamma_2 * \int_0^t (\rho_{sp}(t) - \rho(t)) dt \ * \frac{dh_1}{dx_2} - eq1 * \frac{dh_1}{dx_1} * \frac{dh_2}{dx_2} + \ldots$$

$$\frac{dh_2}{dx_1} * eq1 * \frac{dh_1}{dx_2} + \frac{dh_2}{dx_2} * \beta_1 * \ln(MI)_{sp} - \frac{dh_2}{dx_2} * \beta_1 * \ln(MI) + \frac{dh_2}{dx_2} * \gamma_1 * \ldots$$

$$\int_0^t (\ln(MI)_{sp}(t) - \ln(MI)(t)) dt \ ) / (\frac{dh_1}{dx_1} * \frac{dh_2}{dx_2} - \frac{dh_1}{dx_2} * \frac{dh_2}{dx_1})$$

$$F_{M2} = -(Vg+Vs)*(-\frac{dh_1}{dx_1} * \beta_2 * \rho_{sp} + \frac{dh_1}{dx_1} * \beta_2 * \rho - \frac{dh_1}{dx_1} * \gamma_2 * \int_0^t (\rho_{sp}(t) - \rho(t)) dt + \ldots$$

$$\frac{dh_1}{dx_1} * \frac{dh_2}{dx_2} * eq2 + \beta_1 * \ln(MI)_{sp} * \frac{dh_2}{dx_1} - \beta_1 * \ln(MI) * \frac{dh_2}{dx_1} + \gamma_1 * \ldots$$

$$\int_0^t (\ln(MI)_{sp}(t) - \ln(MI)(t)) dt \ * \frac{dh_2}{dx_1} - \frac{dh_1}{dx_1} * eq2 * \frac{dh_2}{dx_1}) / (\frac{dh_1}{dx_1} * \frac{dh_2}{dx_2} - \frac{dh_1}{dx_2} * \frac{dh_2}{dx_1})$$

$$Fcat = 1/a_{cat} * (\beta_3 * PR_{sp} * \frac{dh_1}{dx_1} * \frac{dh_2}{dx_2} - \beta_3 * PR_{sp} * \frac{dh_1}{dx_2} * \frac{dh_2}{dx_1} - \beta_3 * PR * \frac{dh_1}{dx_1} * \frac{dh_2}{dx_2} + \beta_3 * PR * \ldots$$

$$\frac{dh_1}{dx_2} * \frac{dh_2}{dx_1} + \gamma_3 * \int_0^t (PR_{sp}(t) - PR(t)) dt * \frac{dh_1}{dx_1} * \frac{dh_2}{dx_2} - \gamma_3 * \int_0^t (PR_{sp}(t) - PR(t)) dt * \ldots$$

$$\frac{dh_1}{dx_2} * \frac{dh_2}{dx_1} - \frac{dh_3}{dx_2} * \frac{dh_1}{dx_1} * \beta_2 * \rho_{sp} + \frac{dh_3}{dx_2} * \frac{dh_1}{dx_1} * \beta_2 * \rho - \frac{dh_3}{dx_2} * \frac{dh_1}{dx_1} * \gamma_2 * \int_0^t (\rho_{sp}(t) - \rho(t)) dt + \ldots$$

$$\frac{dh_3}{dx_2} * \beta_1 * \ln(MI)_{sp} * \frac{dh_2}{dx_1} - \frac{dh_3}{dx_2} * \beta_1 * \ln(MI) * \frac{dh_2}{dx_1} + \frac{dh_3}{dx_2} * \gamma_1 * \ldots$$

$$\int_0^t (\ln(MI)_{sp}(t) - \ln(MI)(t)) dt * \frac{dh_2}{dx_1} - \frac{dh_3}{dx_3} * eq3 * \frac{dh_1}{dx_1} * \frac{dh_2}{dx_2} + \frac{dh_3}{dx_3} * eq3 * \frac{dh_1}{dx_2} * \frac{dh_2}{dx_1})/ \ldots$$

$$((\frac{dh_1}{dx_1} * \frac{dh_2}{dx_2} - \frac{dh_1}{dx_2} * \frac{dh_2}{dx_1}) * \frac{dh_3}{dx_3});$$

where

eq1 = 1/Vg * (-kh * Y * H$_2$ - H$_2$ * b/Ct - gl * H$_2$)
eq2 = 1/(Vg + Vs) * (-kp2 * Y * M$_2$ - M$_2$ * b/Ct - S * M$_2$ * Y * (kp1 * M1 * mw$_1$ + kp2 * M$_2$ * mw$_2$))
eq3 = -Y^2 * (kp1 * M1 * mw$_1$ + kp2 * M$_2$ * mw$_2$)/Bw/1000000 - kd * Y

and $\frac{\partial h_i}{\partial x_j}$, i,j = 1..3, are as in Appendix A.1

A.3 Simulation Figures

The simulation figures denoted in Chapter 5 are given in this appendix.
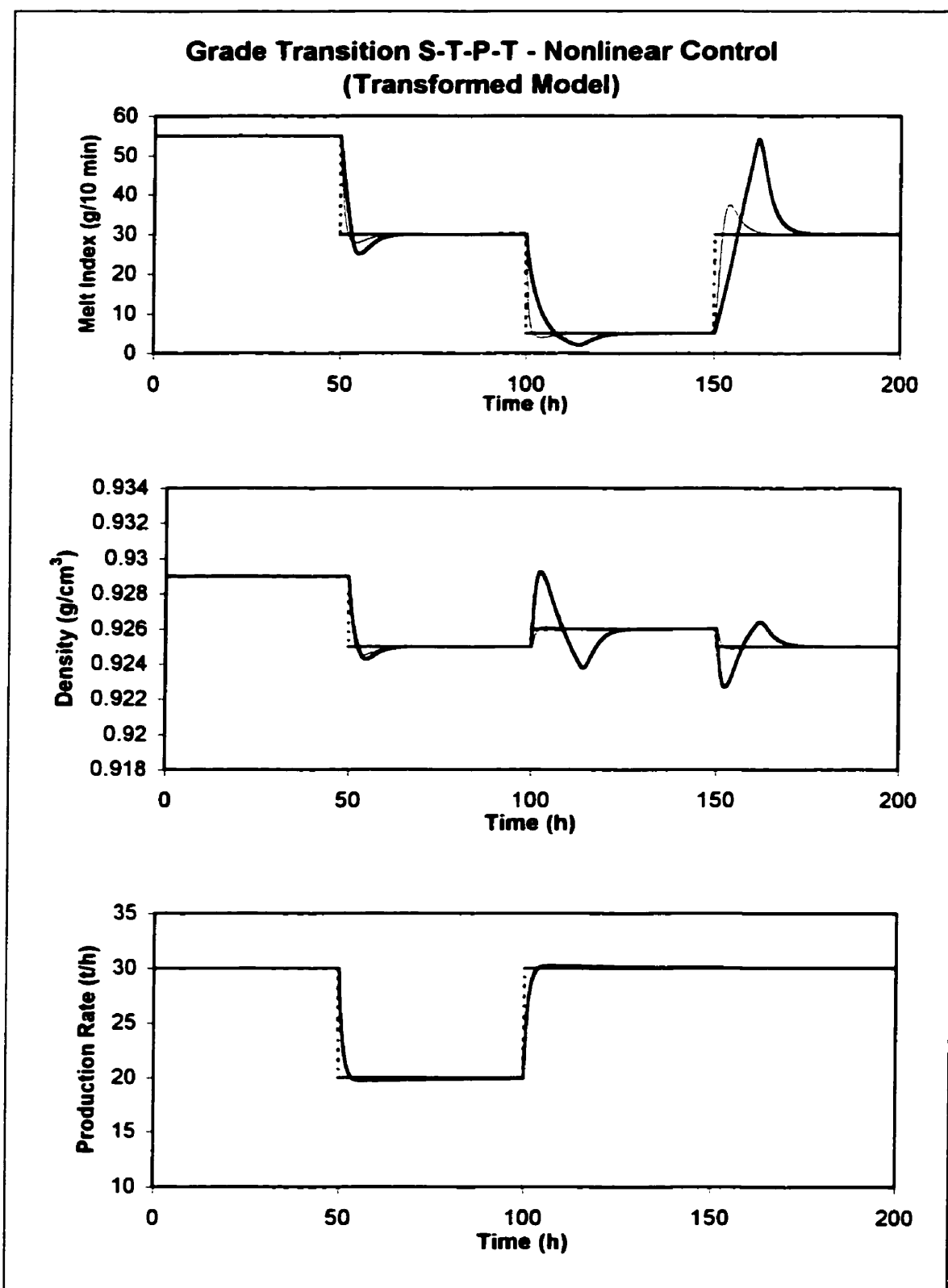
Figure A3.1.a. Simulation of the S-T-P-T grade transition, under nonlinear control of the transformed model. Dashed line: set point. Thick line: output. Thin line: error-trajectory specification.
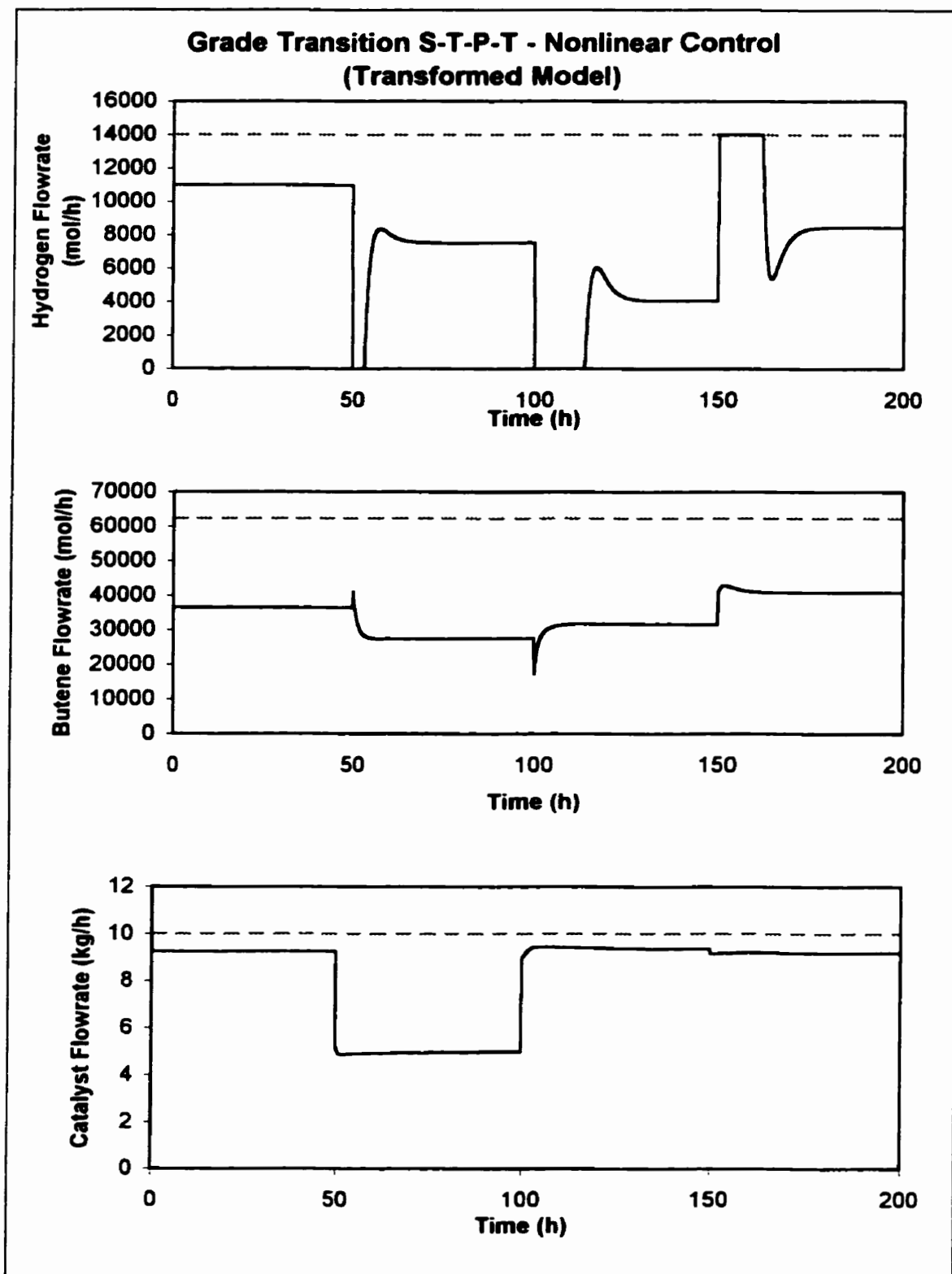
Figure A3.1.b. Simulation of the S-T-P-T grade transition, under nonlinear control of the transformed model. Solid line: manipulated variable. Dashed line: manipulated variable bound.
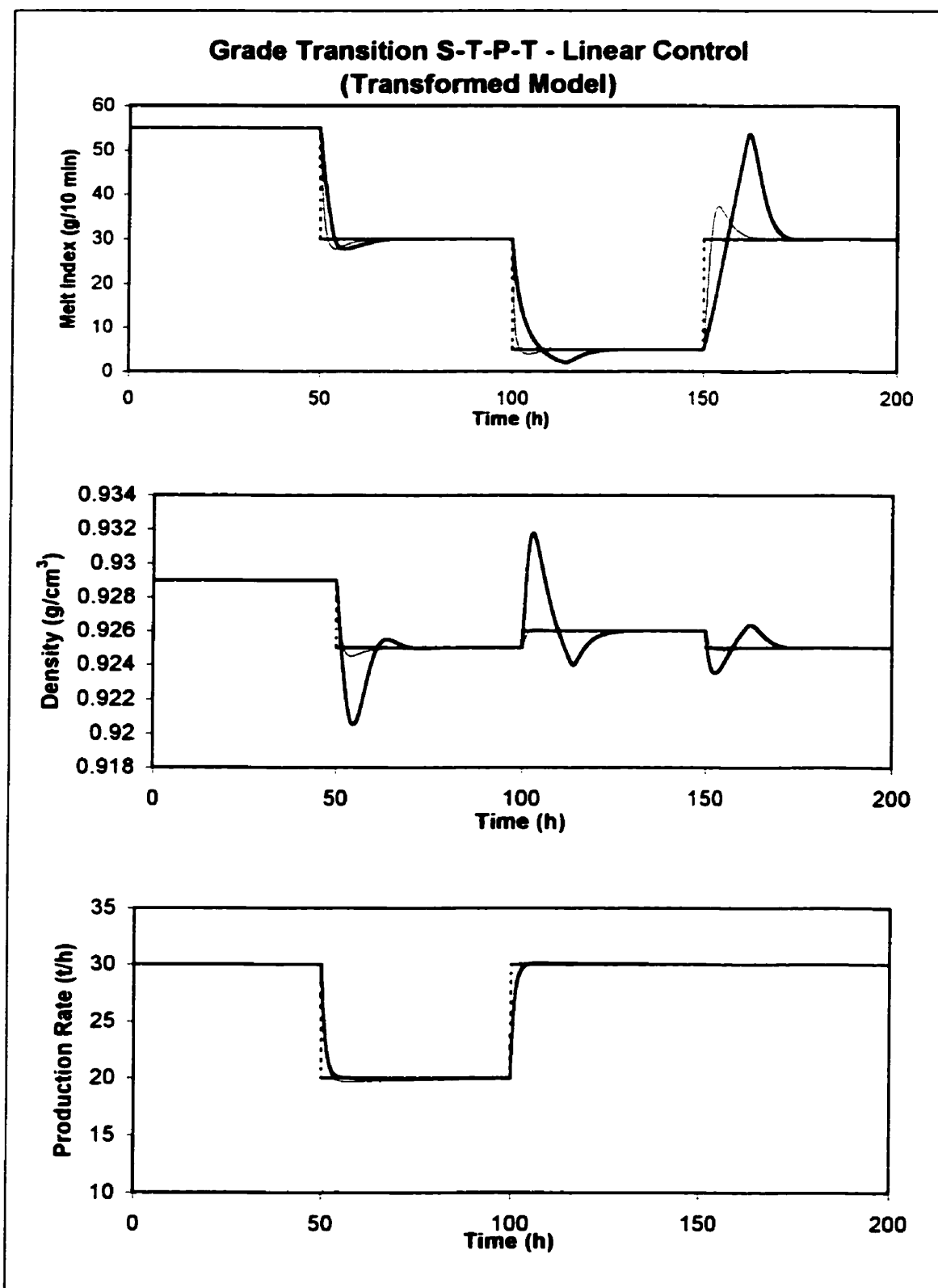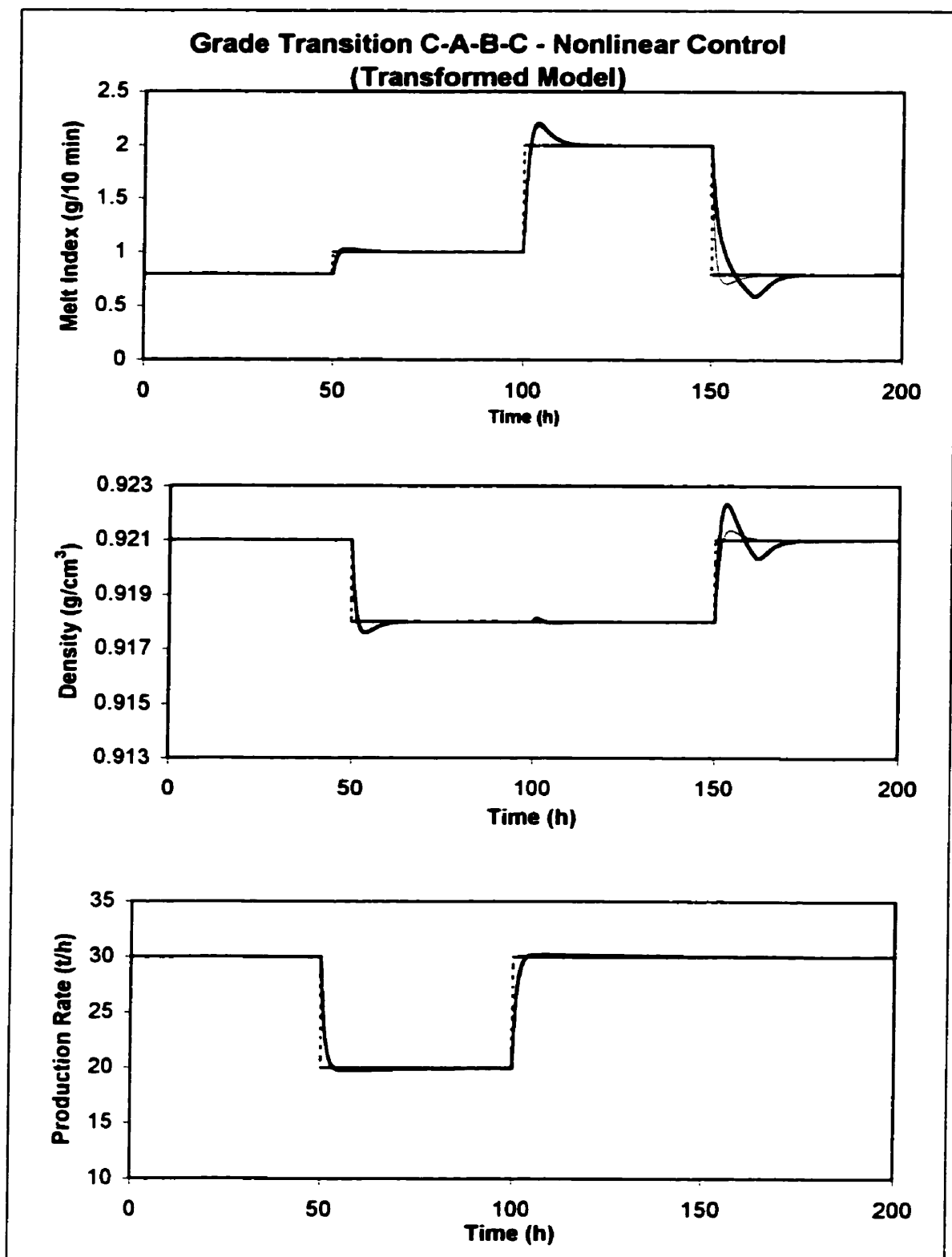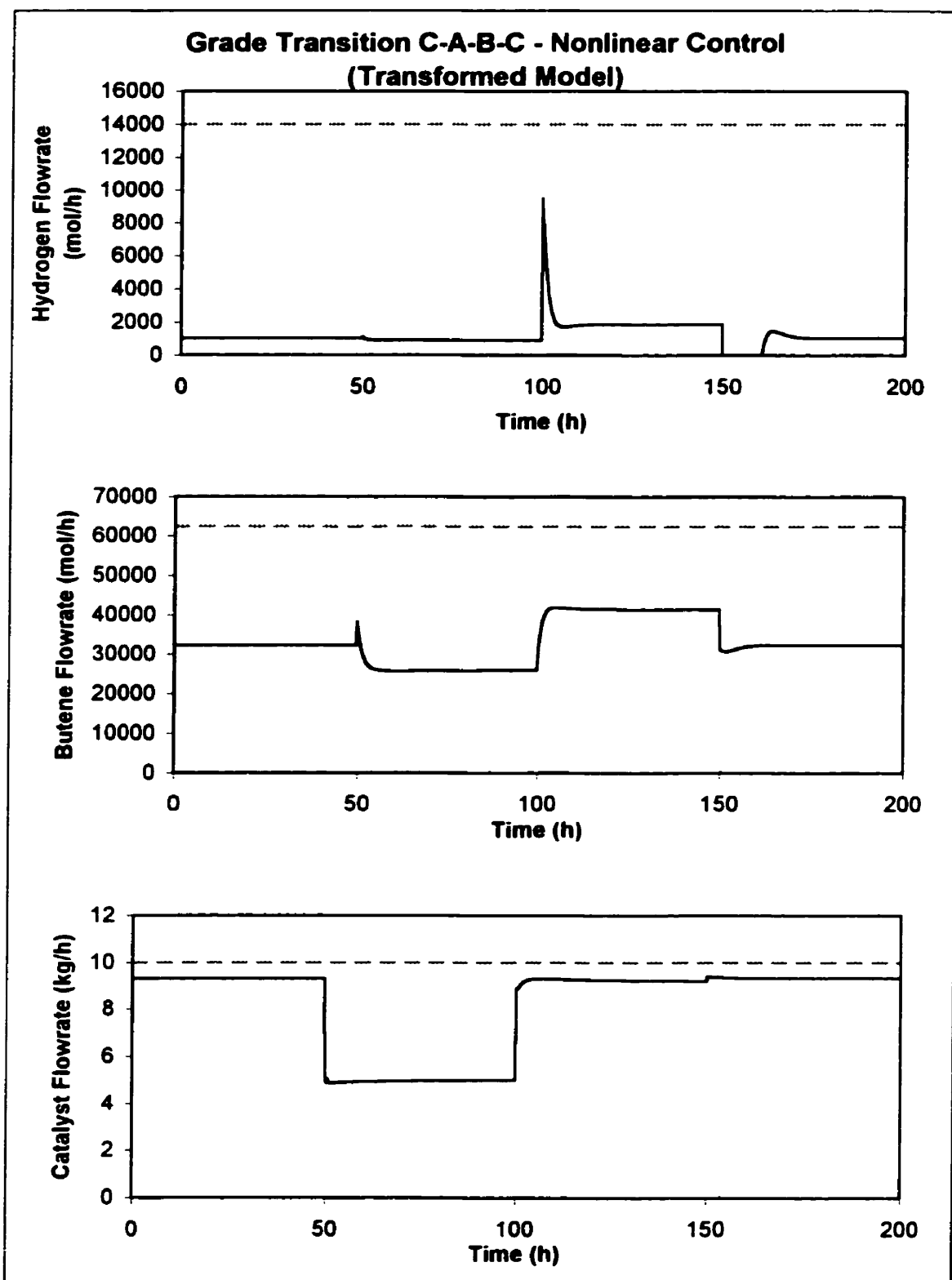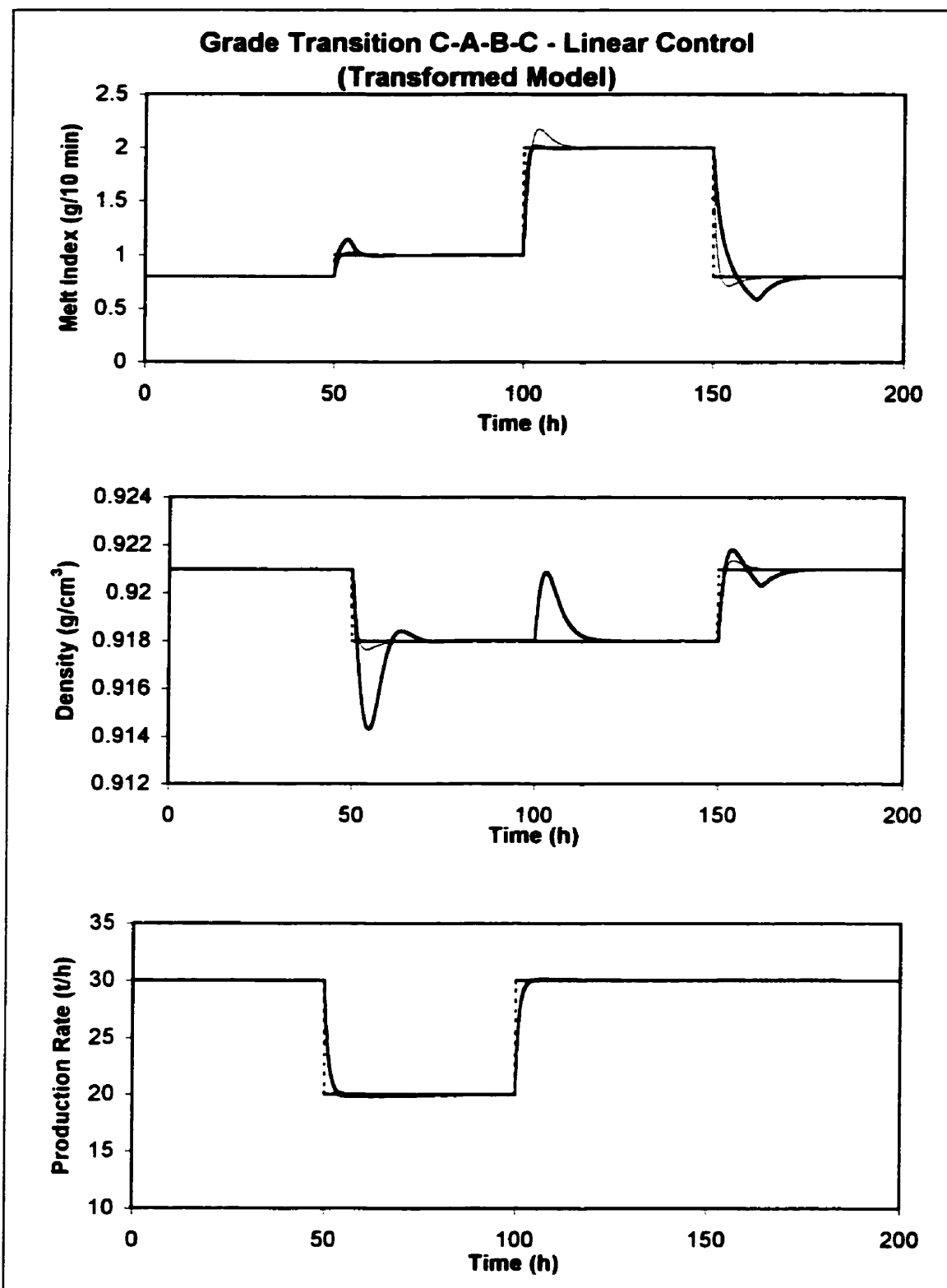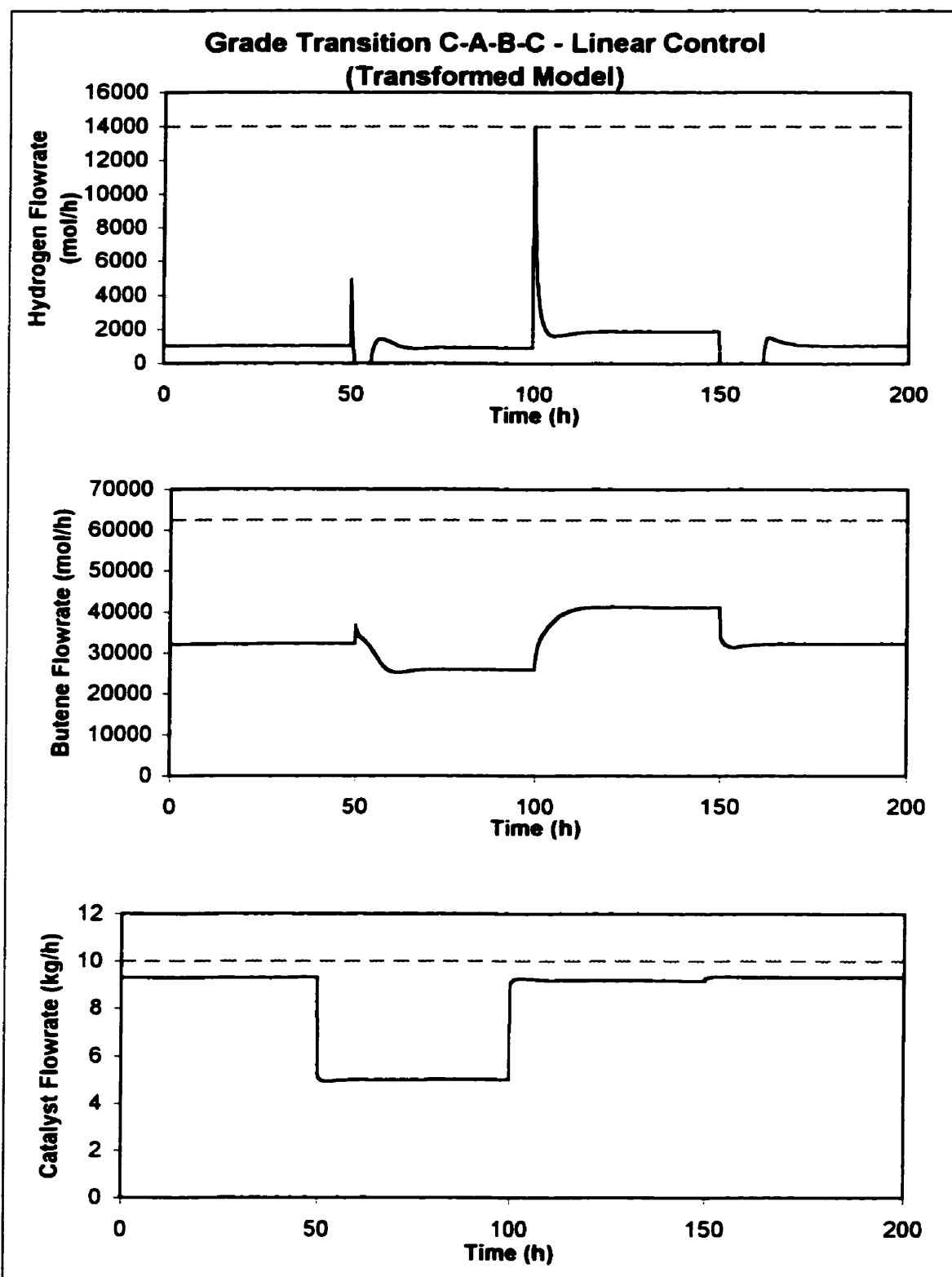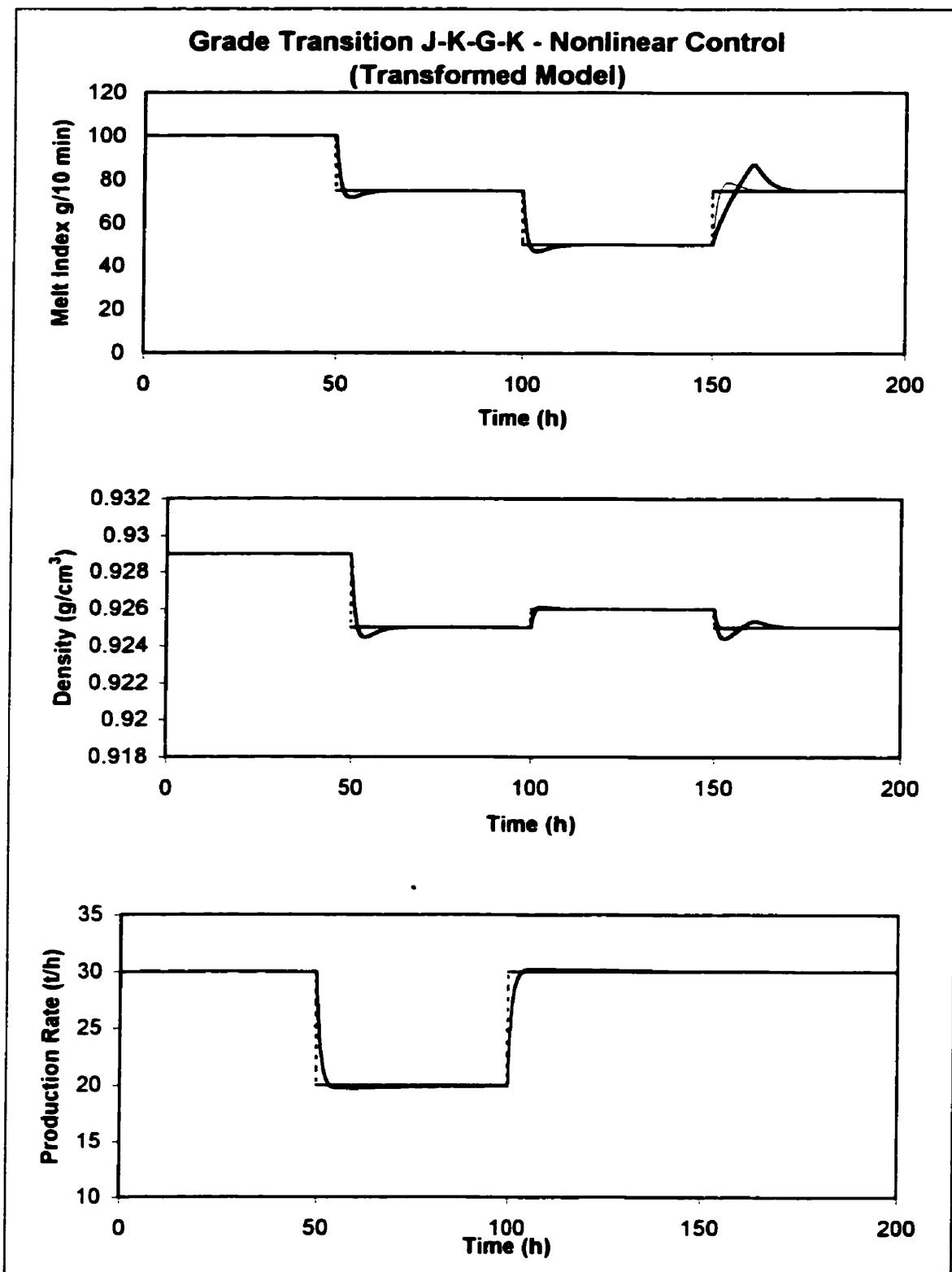
Figure A3.1.c. Simulation of the S-T-P-T grade transition, under linear control of the transformed model. Dashed line: set point. Thick line: output. Thin line: error-trajectory specification.
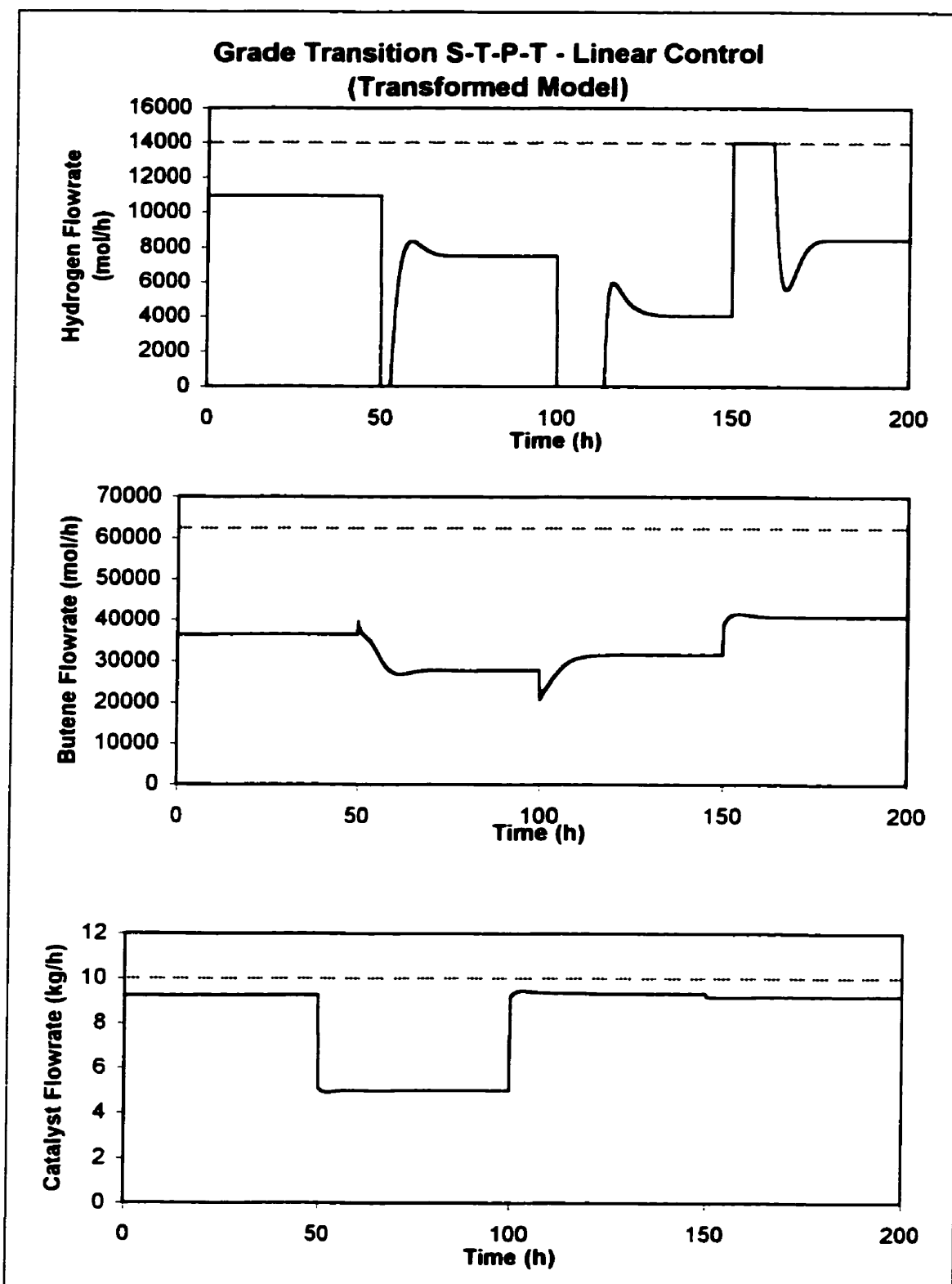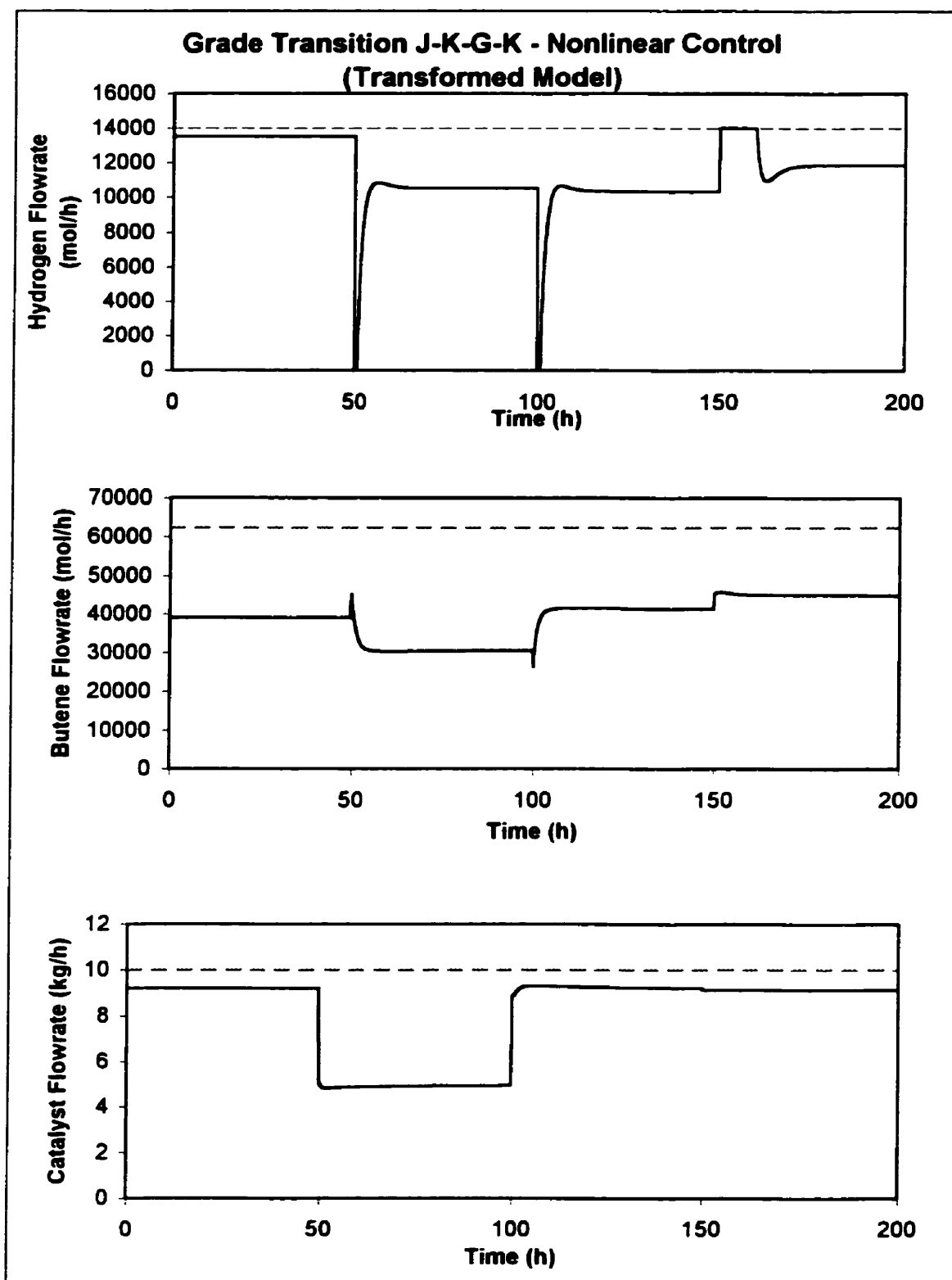
Figure A3.1.d. Simulation of the S-T-P-T grade transition, under linear control of the transformed model. Solid line: manipulated variable. Dashed line: manipulated variable bound.
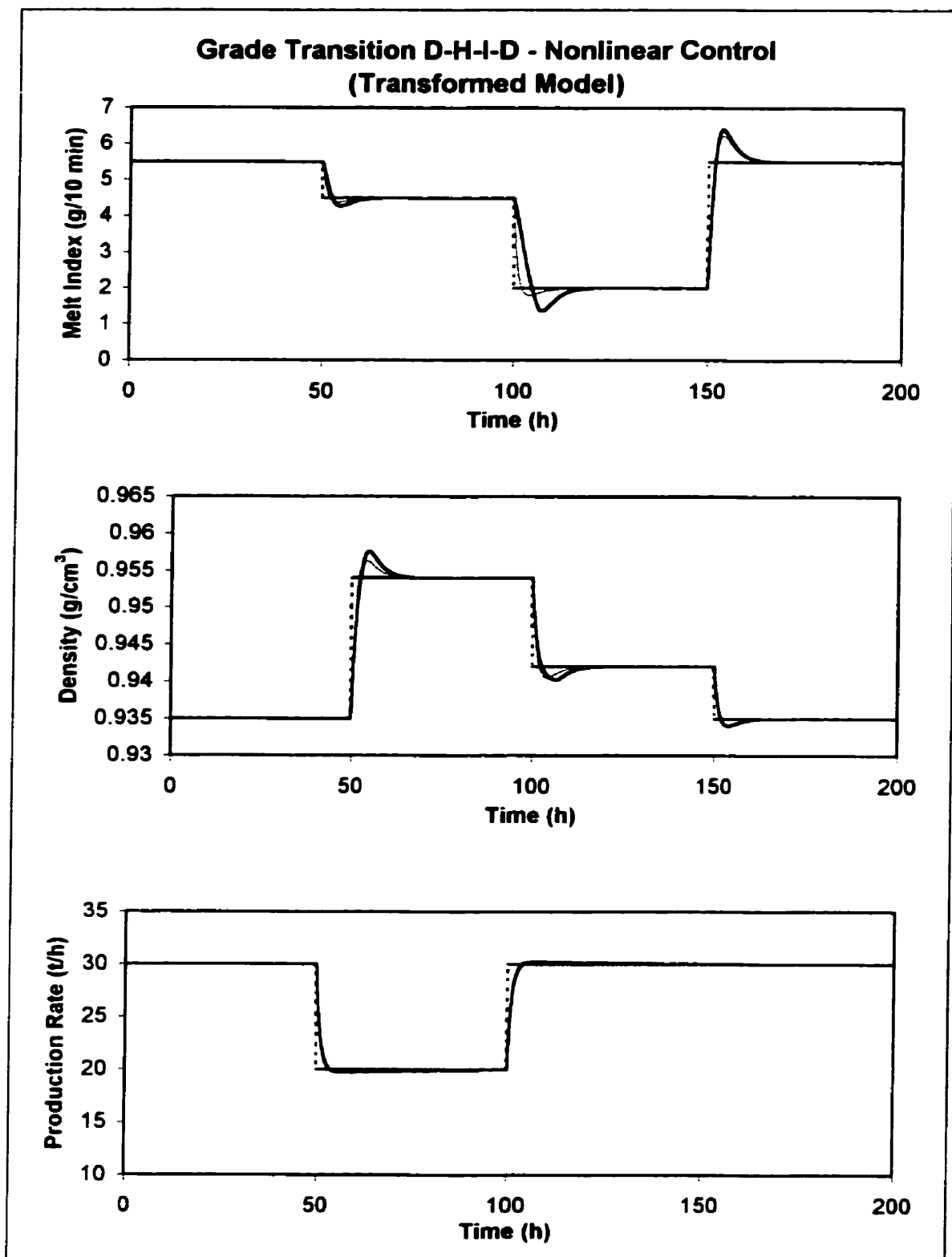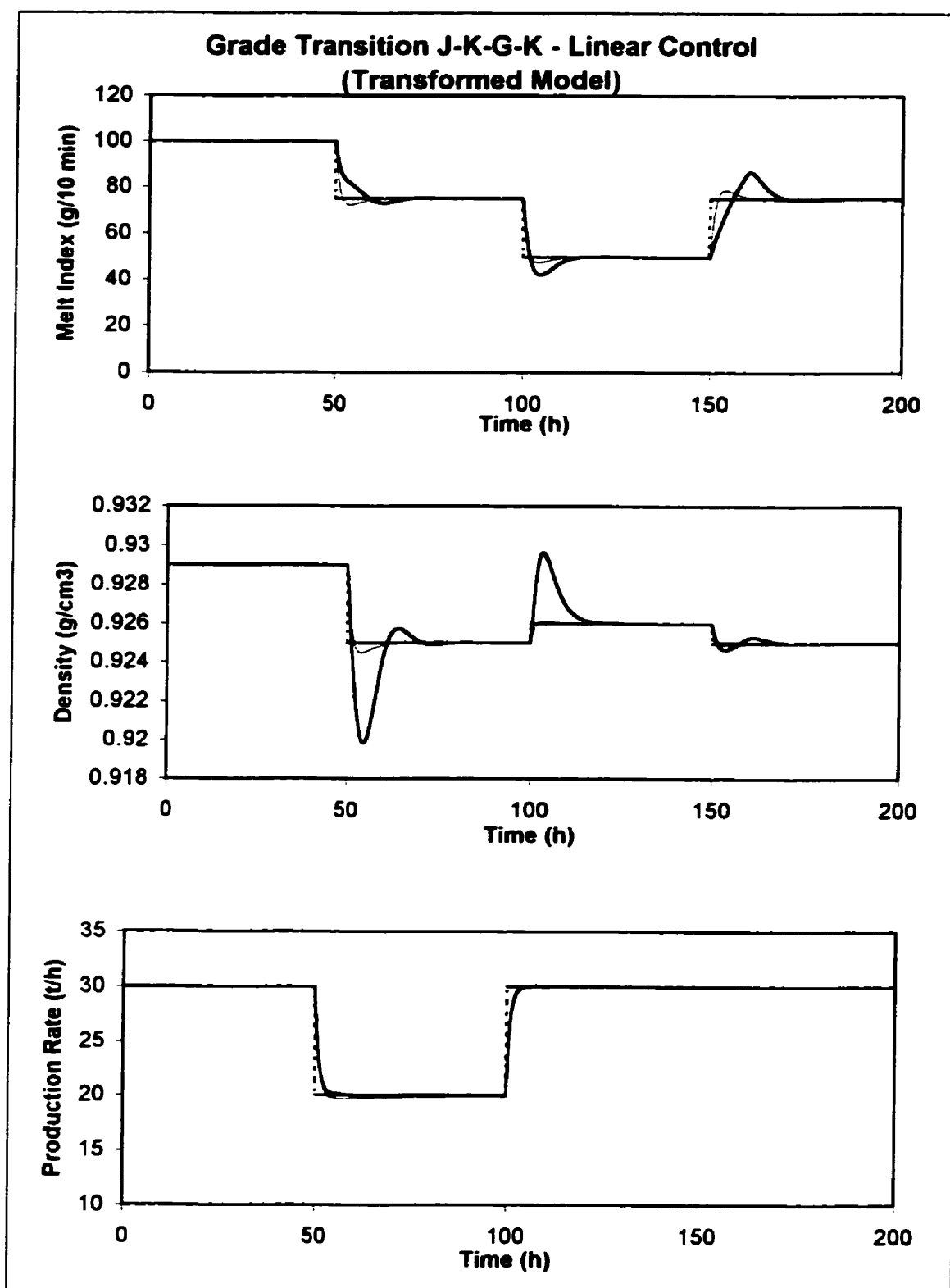
Figure A3.2.a. Simulation of the D-H-I-D grade transition, under nonlinear control of the transformed model. Dashed line: set point. Thick line: output. Thin line: error trajectory specification.
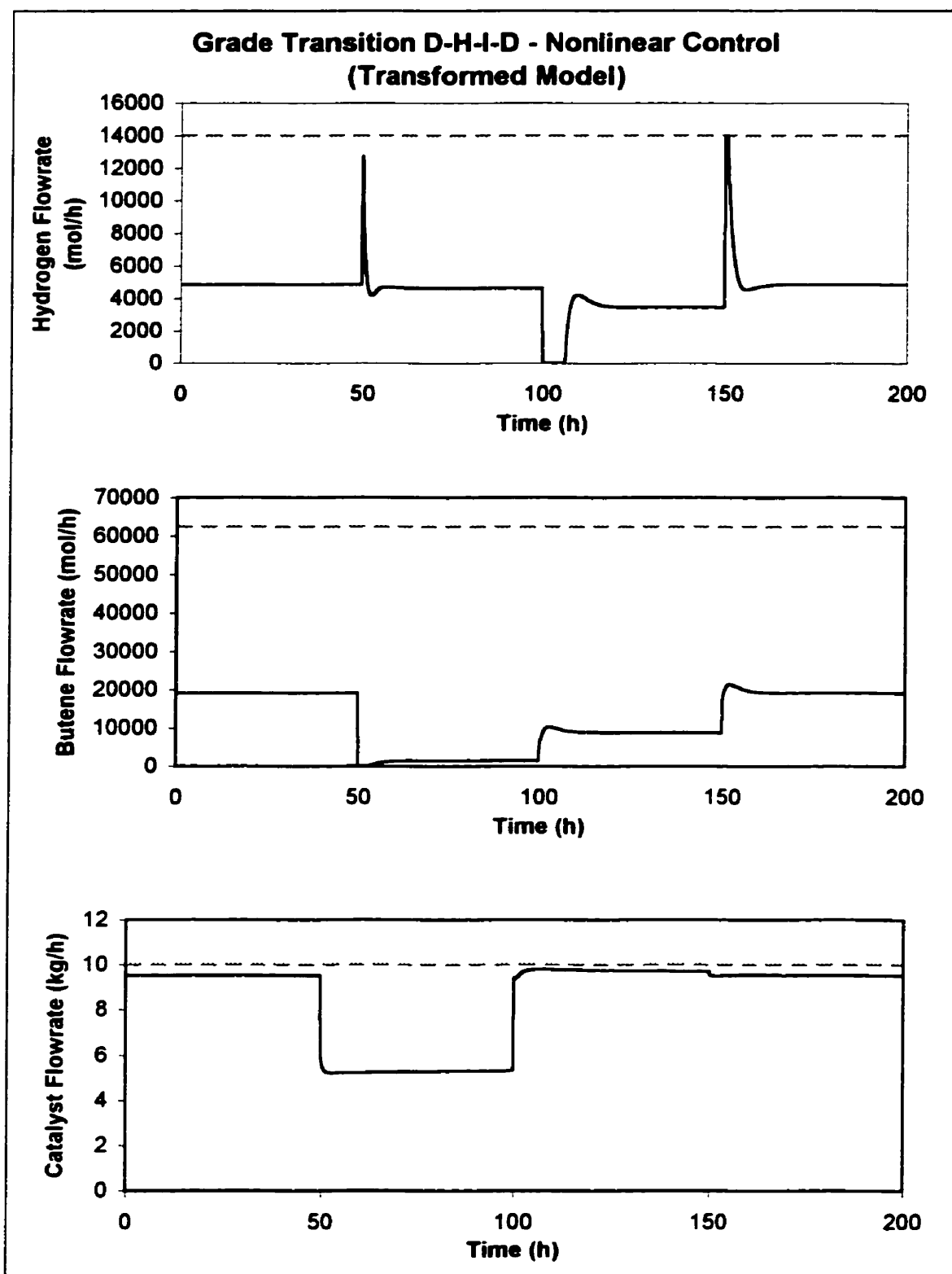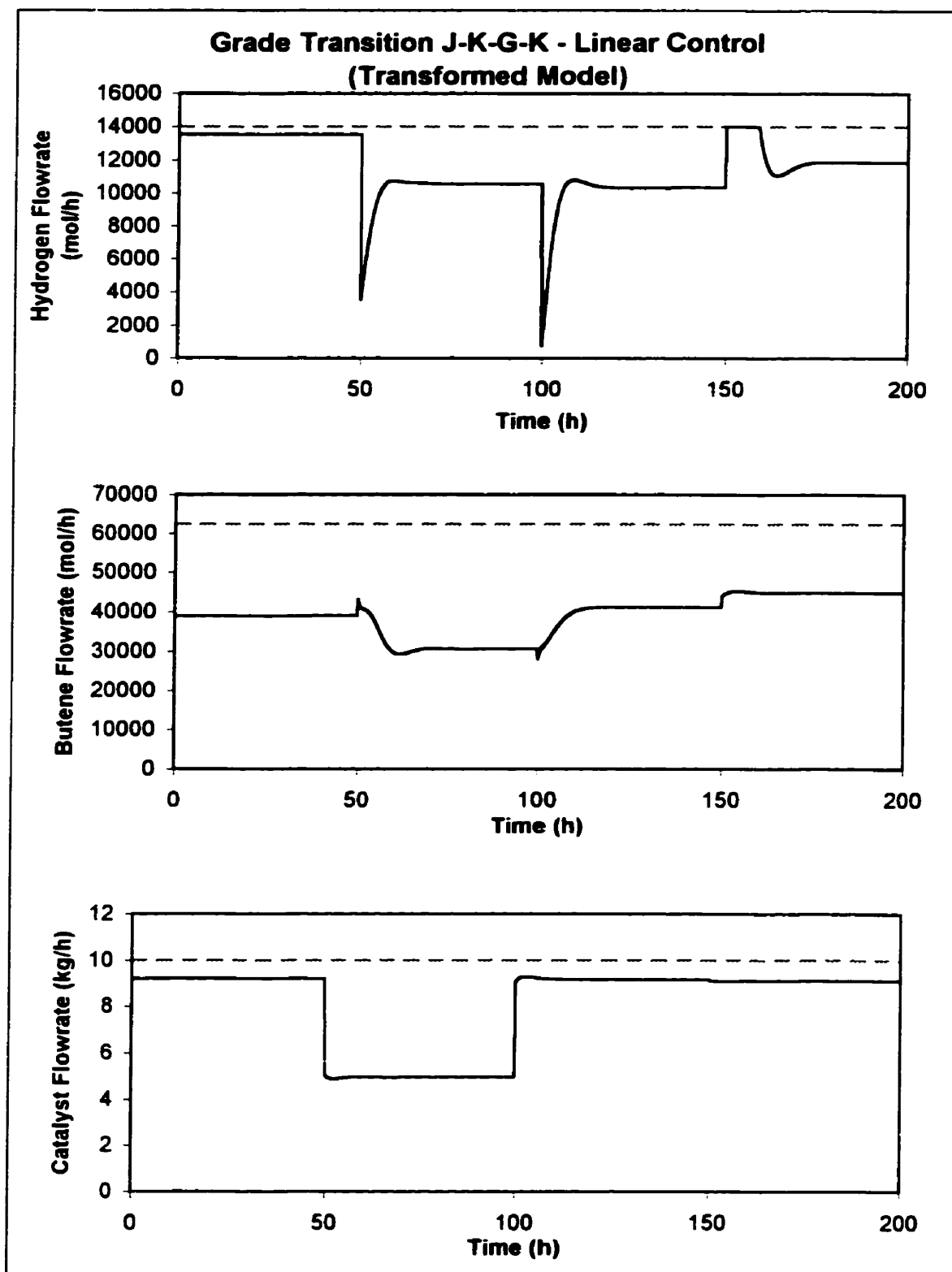
Figure A3.2.b. Simulation of the D-H-I-D grade transition, under nonlinear control of the transformed model. Solid line: manipulated variable. Dashed line: manipulated variable bound.
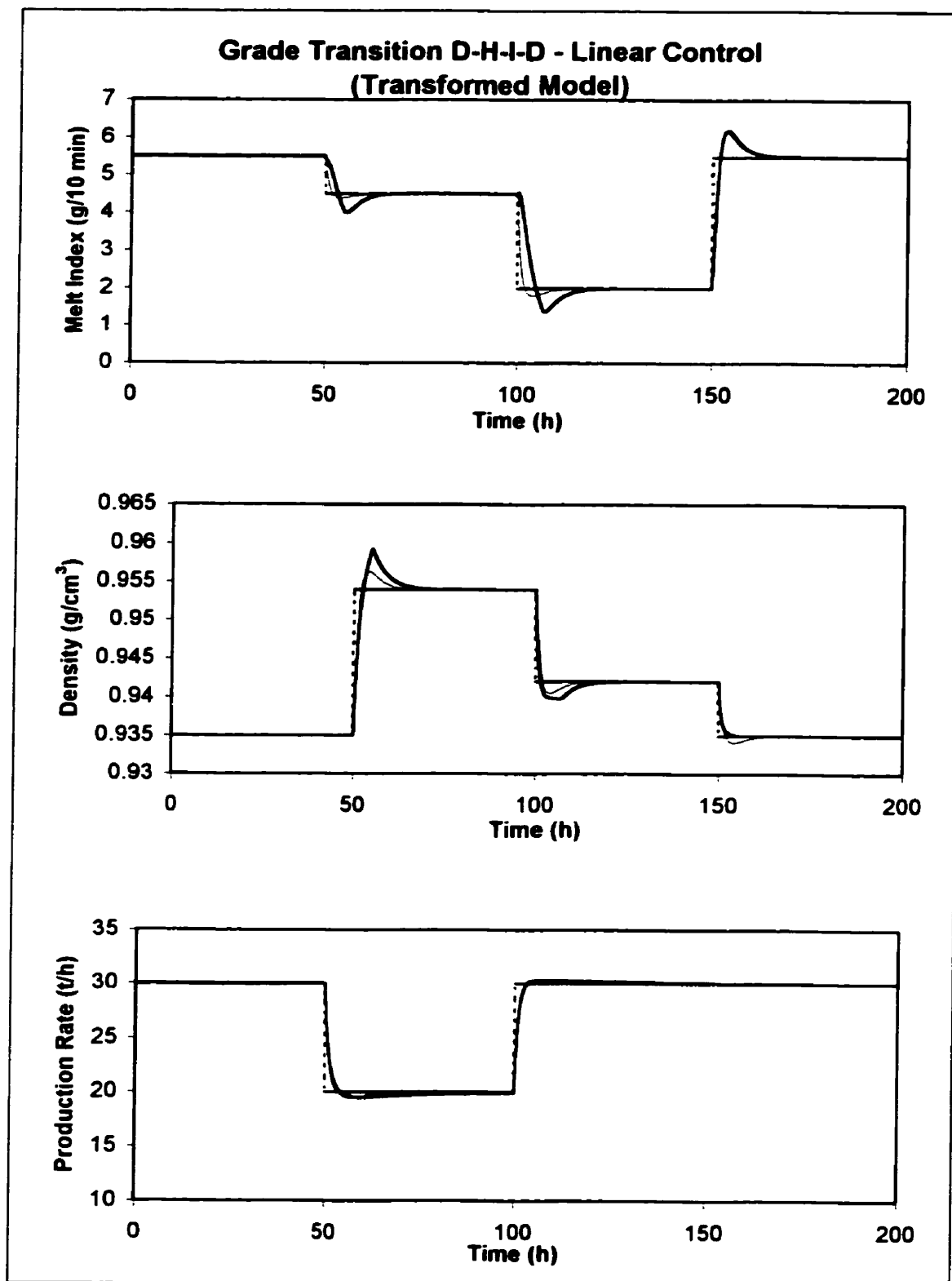
Figure A3.2.c. Simulation of the D-H-I-D grade transition, under linear control of the transformed model. Dashed line: set point. Thick line: output. Thin line: error-trajectory specification.
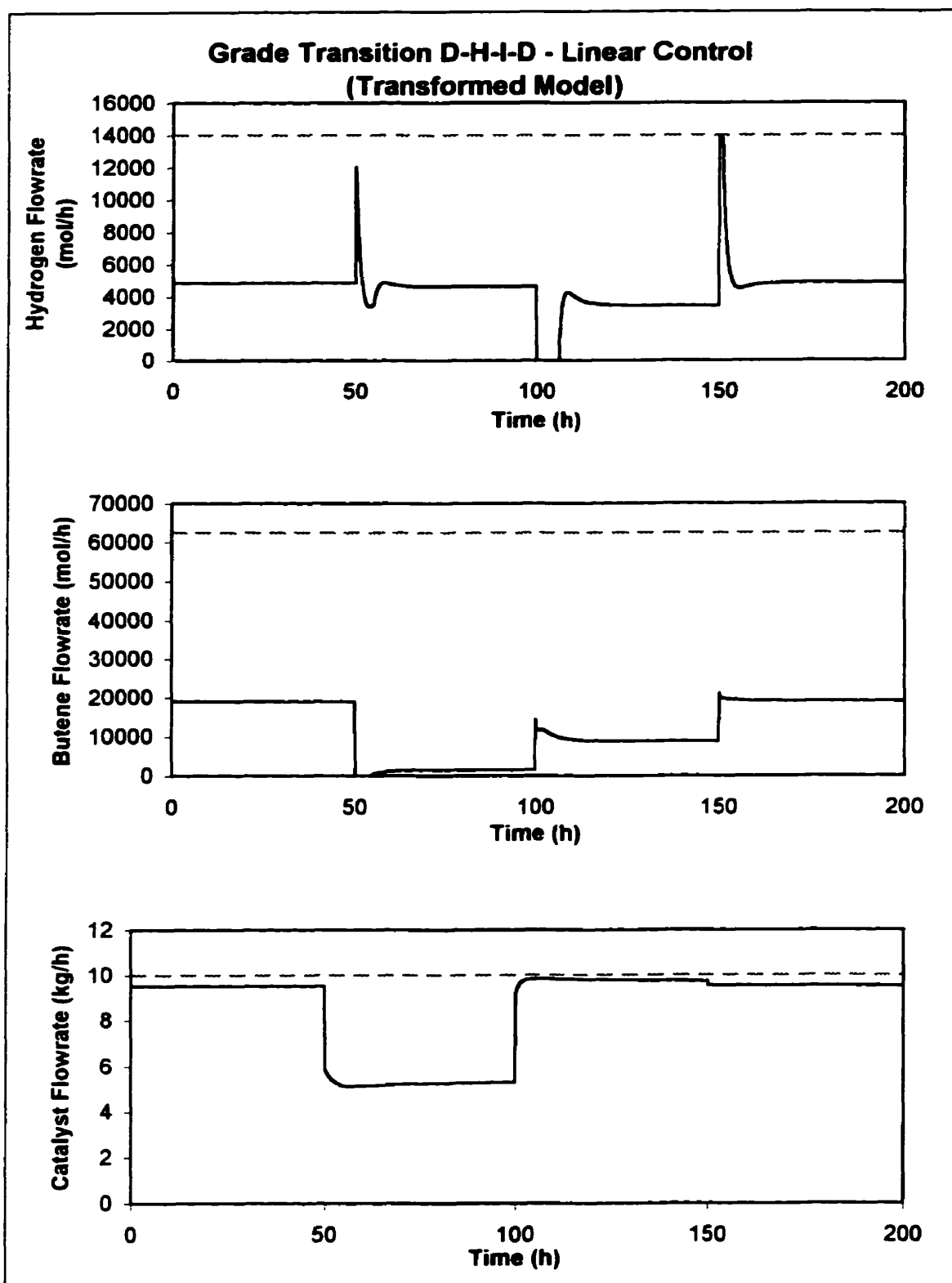
Figure A3.2.d. Simulation of the D-H-I-D grade transition, under linear control of the transformed model. Solid line: manipulated variable. Dashed line: manipulated variable bound.
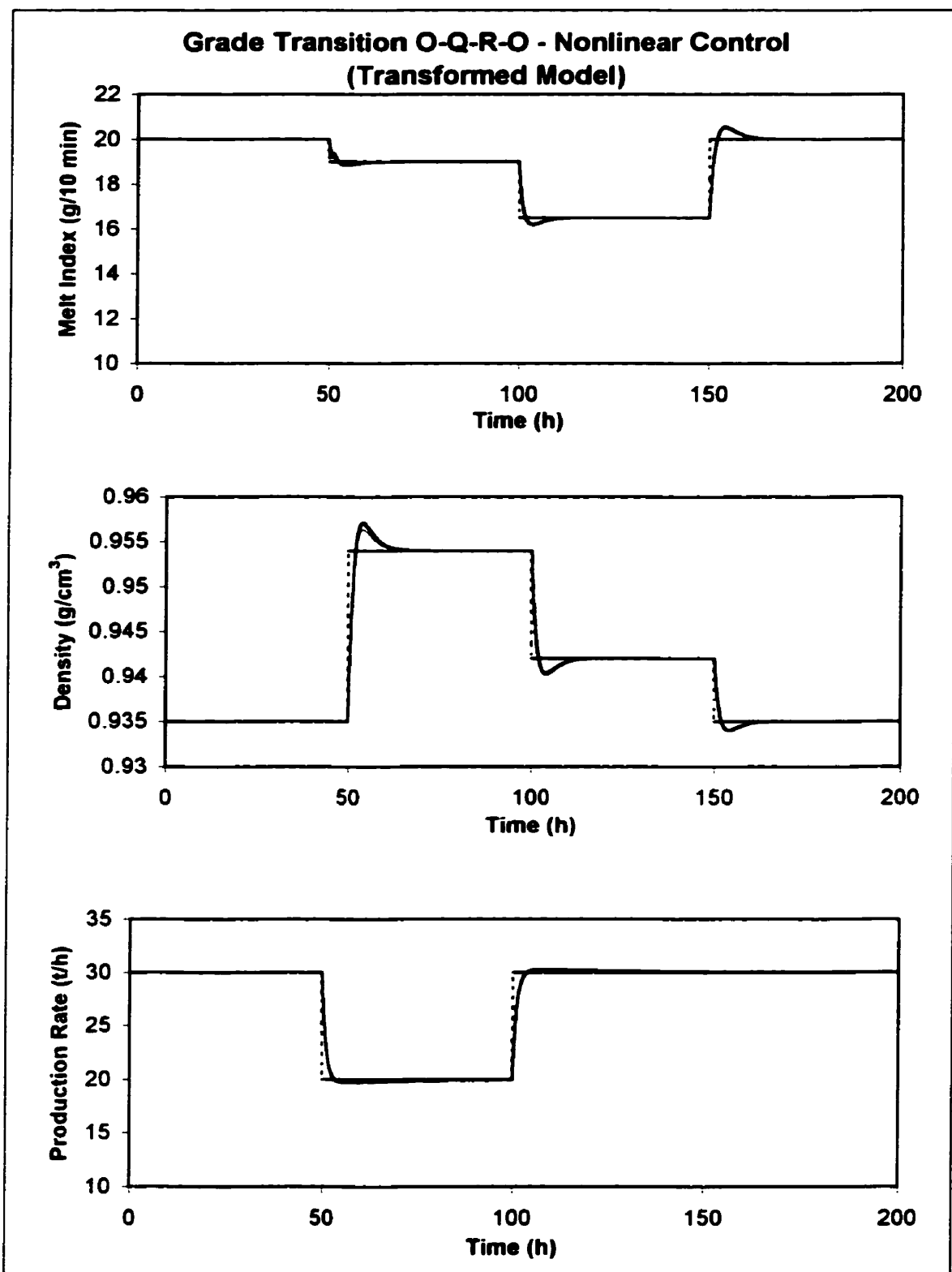
Figure A3.3.a. Simulation of the C-A-B-C grade transition, under nonlinear control of the transformed model. Dashed line: set point. Thick line: output. Thin line: error-trajectory specification.
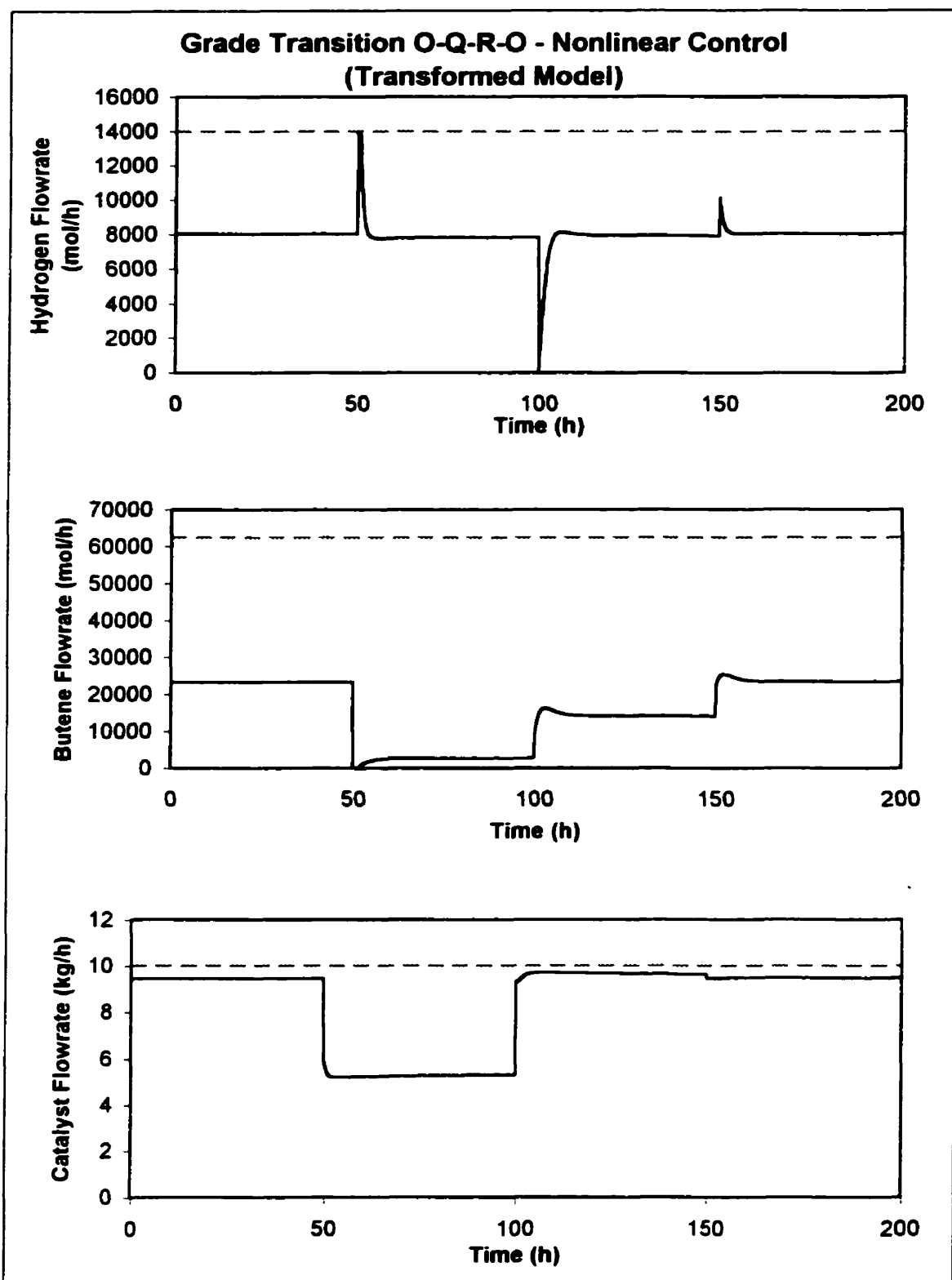
Figure A3.3.b. Simulation of the C-A-B-C grade transition, under nonlinear control of the transformed model. Solid line: manipulated variable. Dashed line: manipulated variable bound.
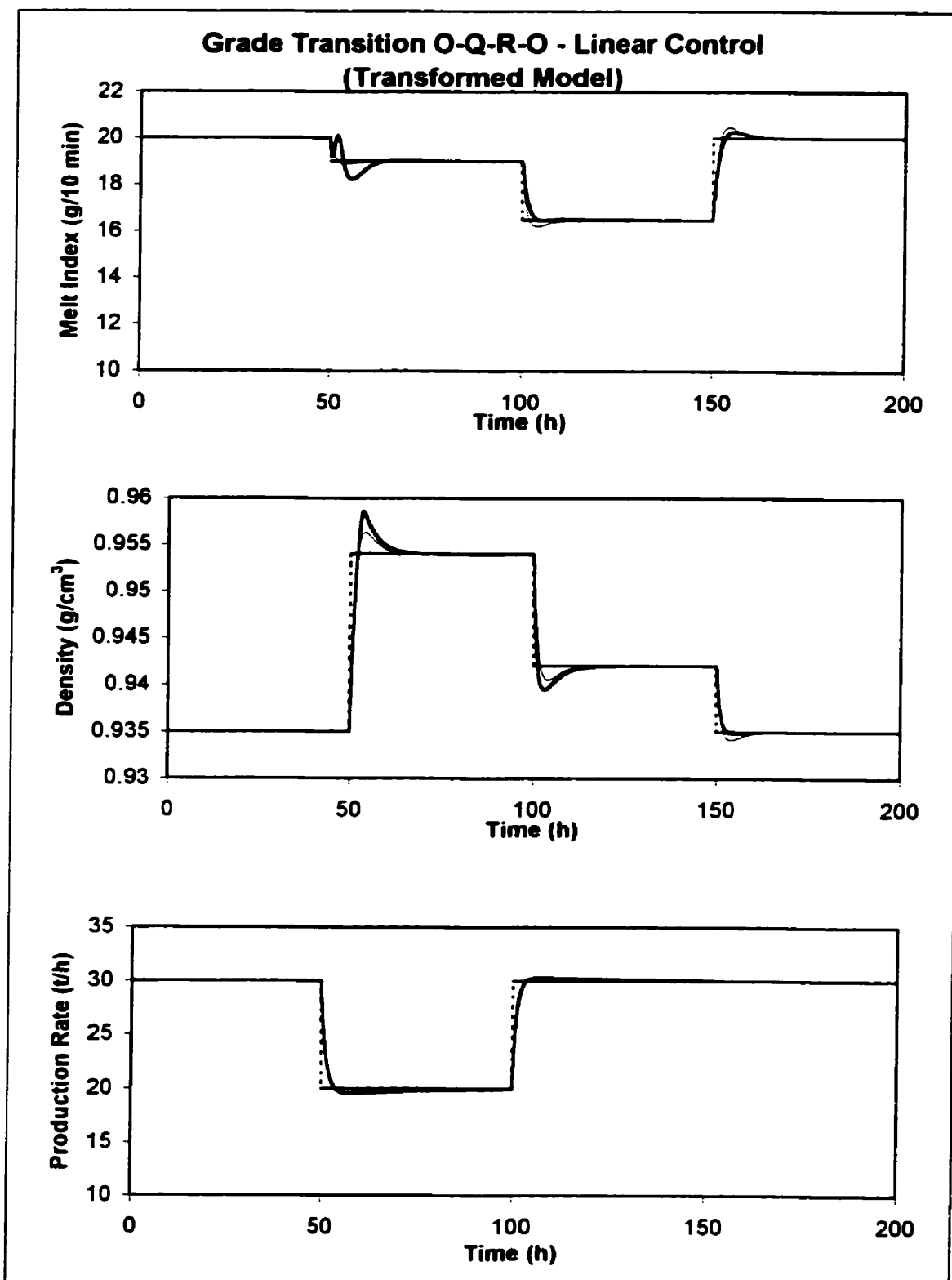
Figure A3.3.c. Simulation of the C-A-B-C grade transition, under linear control of the transformed model. Dashed line: set point. Thick line: output. Thin line: error-trajectory specification.

Figure A3.3.d. Simulation of the C-A-B-C grade transition, under linear control of the transformed model. Solid line: manipulated variable. Dashed line: manipulated variable bound.

156

Figure A3.4.a. Simulation of the J-K-G-K grade transition, under nonlinear control of the transformed model. Dashed line: set point. Thick line: output. Thin line: error-trajectory specification.
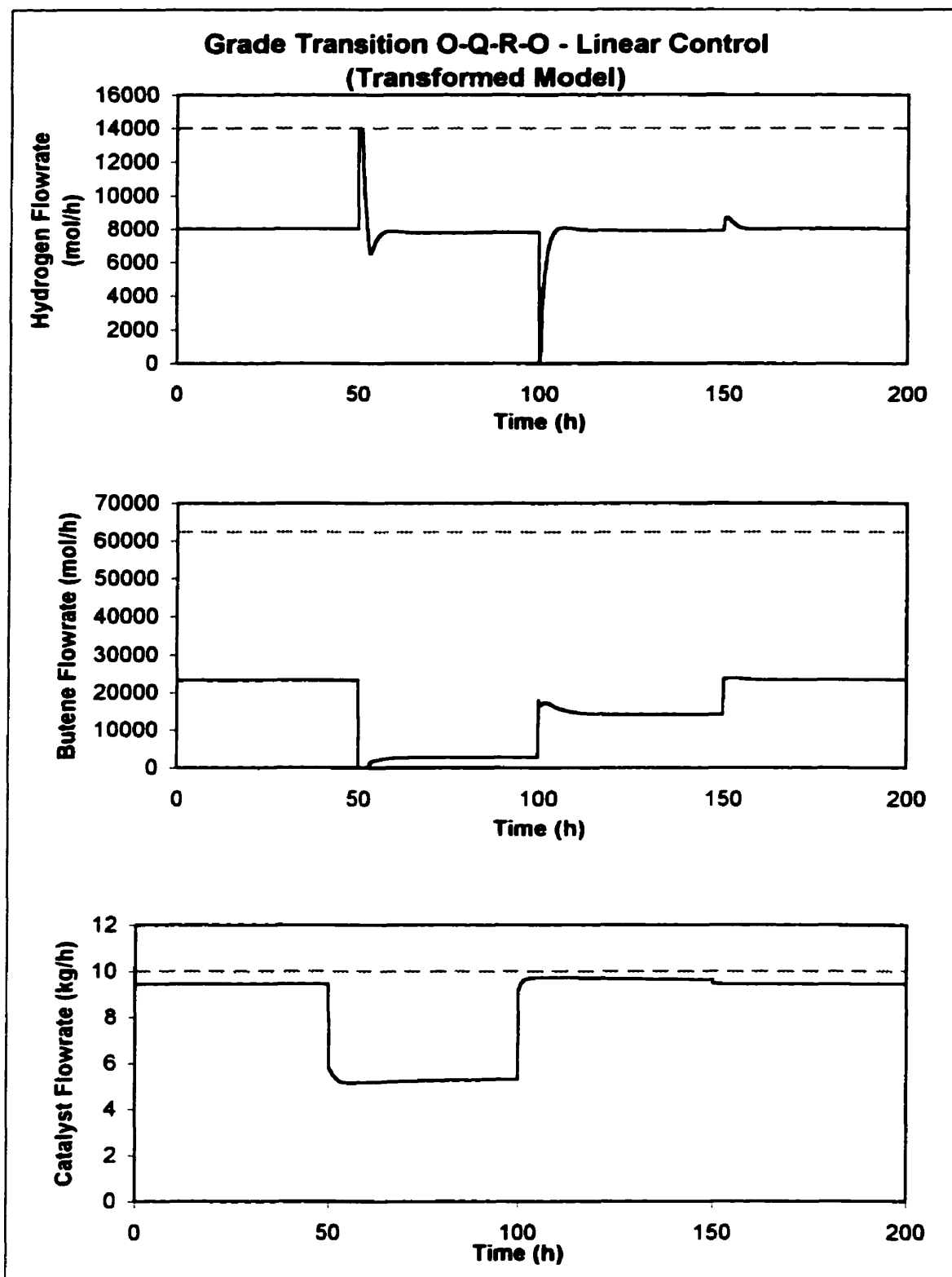
Figure A3.4.b. Simulation of the J-K-G-K grade transition, under nonlinear control of the transformed model. Solid line: manipulated variable. Dashed line: manipulated variable bound.
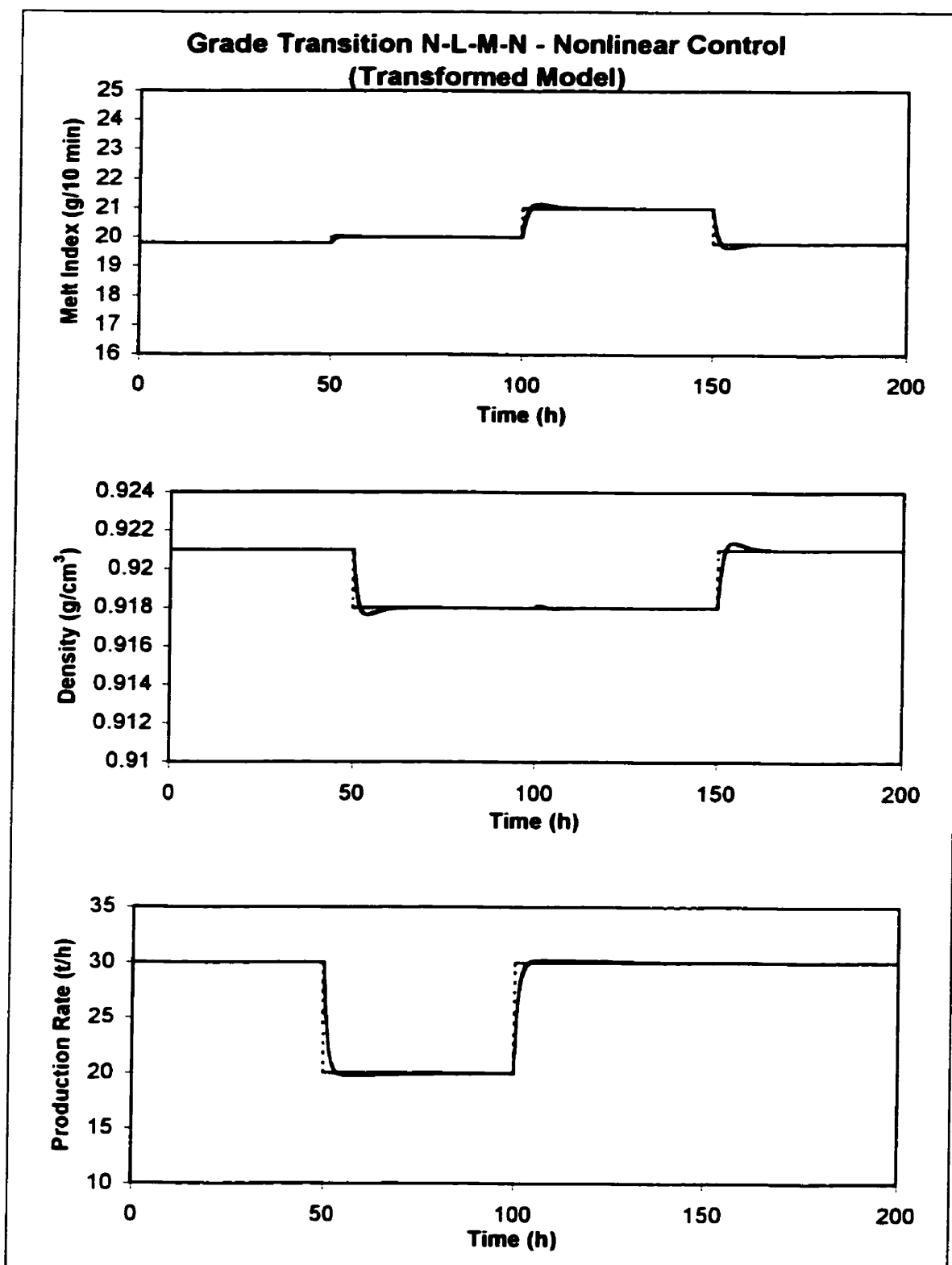
Figure A3.4.c. Simulation of the J-K-G-K grade transition, under linear control of the transformed model. Dashed line: set point. Thick line: output. Thin line: error-trajectory specification.

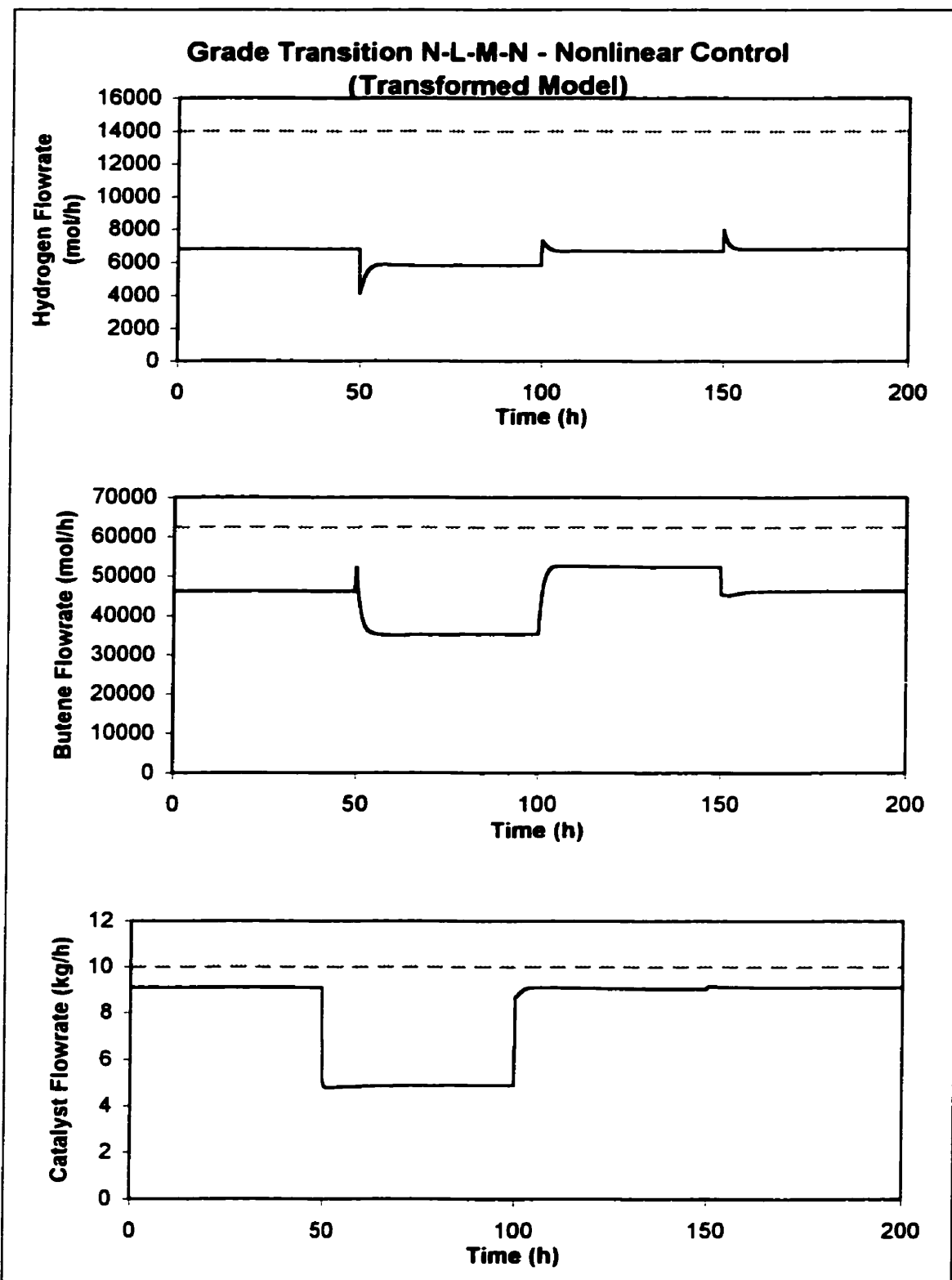**Figure A3.4.d.** Simulation of the J-K-G-K grade transition, under linear control of the transformed model. Solid line: manipulated variable. Dashed line: manipulated variable bound.

Figure A3.5.a. Simulation of the O-Q-R-O grade transition, under nonlinear control of the transformed model. Dashed line: set point. Thick line: output. Thin line: error-trajectory specification.

Figure A3.5.b. Simulation of the O-Q-R-O grade transition, under nonlinear control of the transformed model. Solid line: manipulated variable. Dashed line: manipulated variable bound.
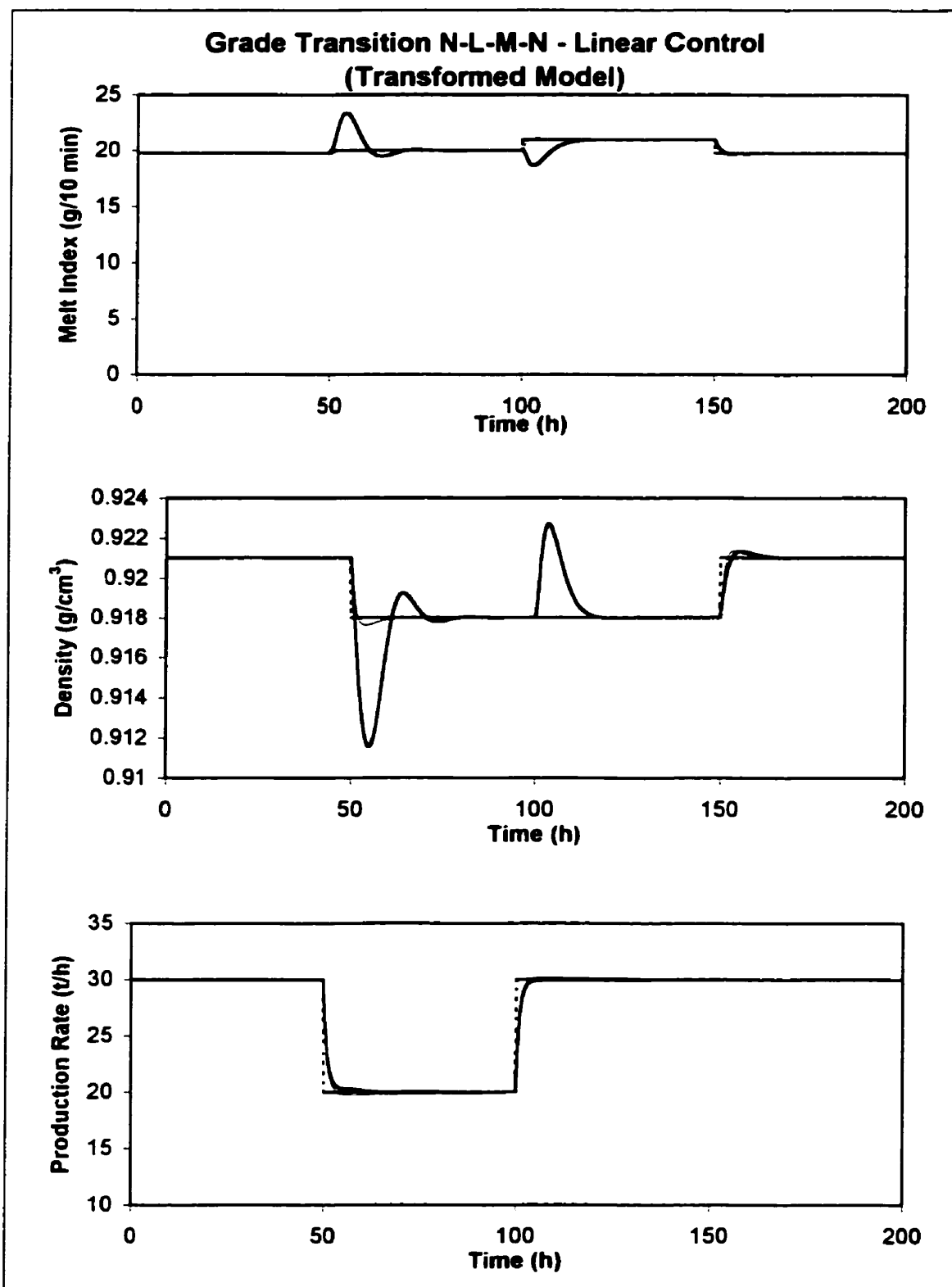
Figure A3.5.c. Simulation of the O-Q-R-O grade transition, under linear control of the transformed model. Dashed line: set point. Thick line: output. Thin line: error-trajectory specification.
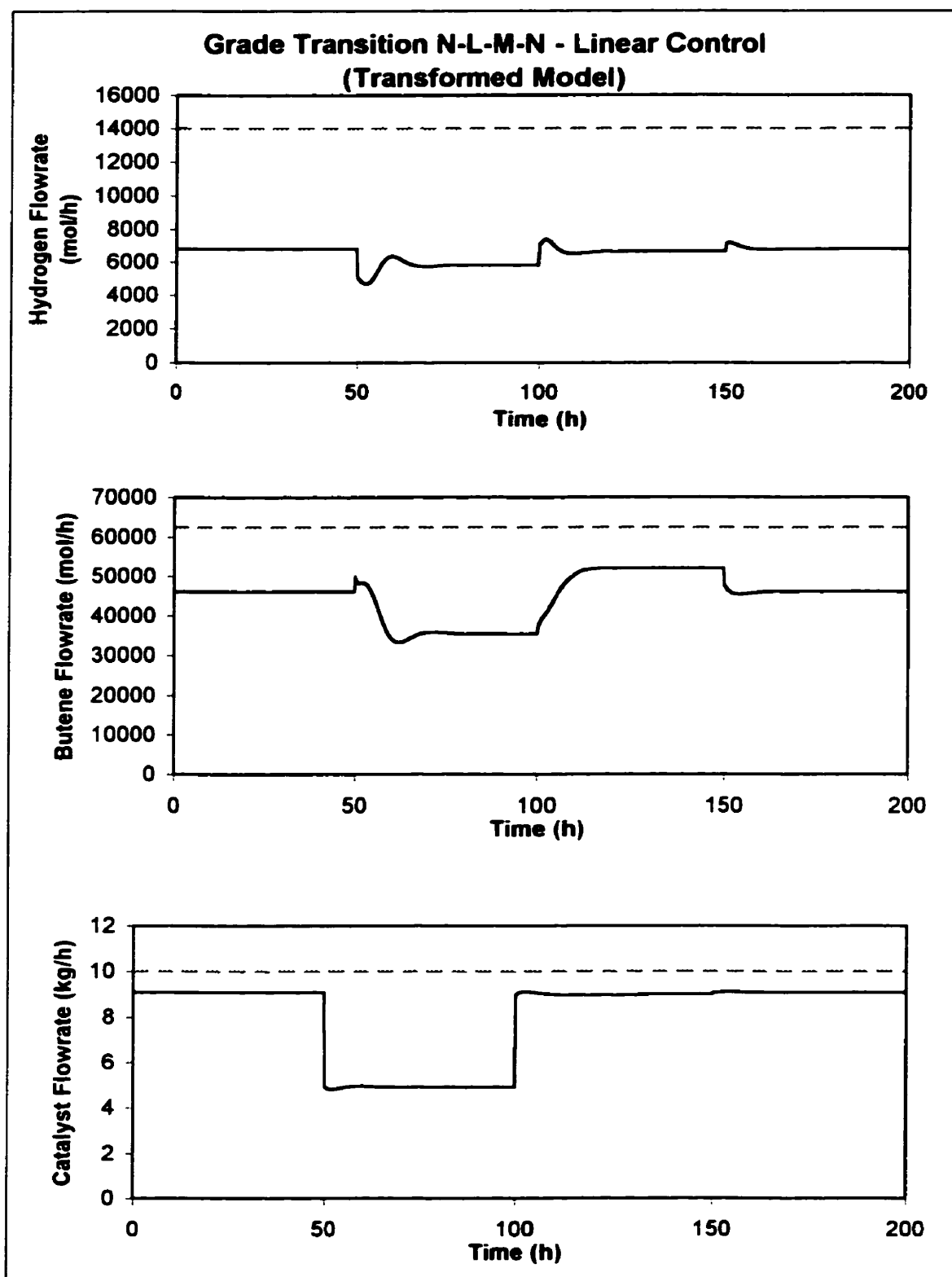
Figure A3.5.d. Simulation of the O-Q-R-O grade transition, under linear control of the transformed model. Solid line: manipulated variable. Dashed line: manipulated variable bound.

Figure A3.6.a. Simulation of the N-L-M-N grade transition, under nonlinear control of the transformed model. Dashed line: set point. Thick line: output. Thin line: error-trajectory specification.

Figure A3.6.b. Simulation of the N-L-M-N grade transition, under nonlinear control of the transformed model. Solid line: manipulated variable. Dashed line: manipulated variable bound.

Figure A3.6.c. Simulation of the N-L-M-N grade transition, under linear control of the transformed model. Dashed line: set point. Thick line: output. Thin line: error-trajectory specification.

167

Figure A3.6.d. Simulation of the N-L-M-N grade transition, under linear control of the transformed model. Solid line: manipulated variable. Dashed line: manipulated variable bound.
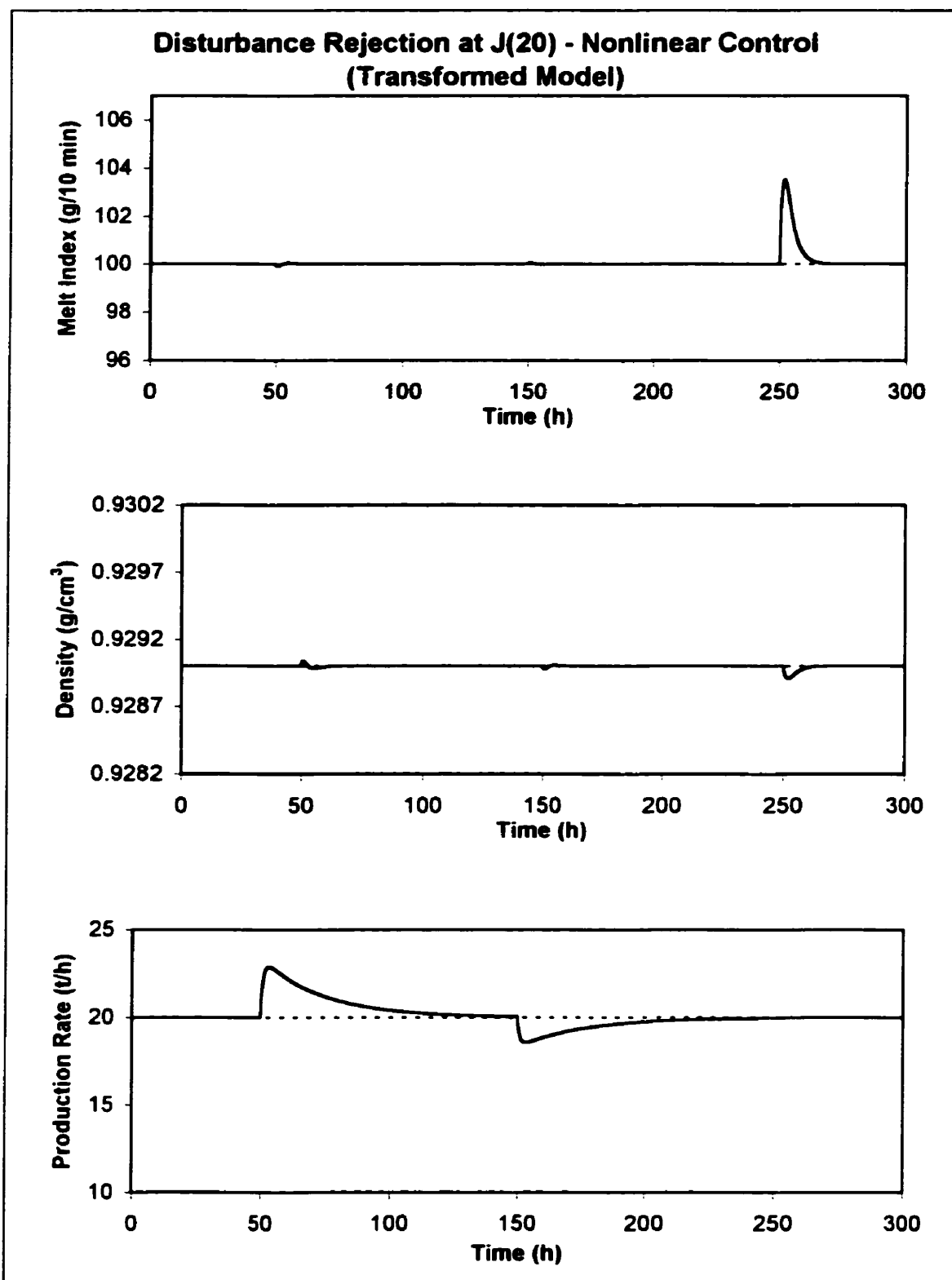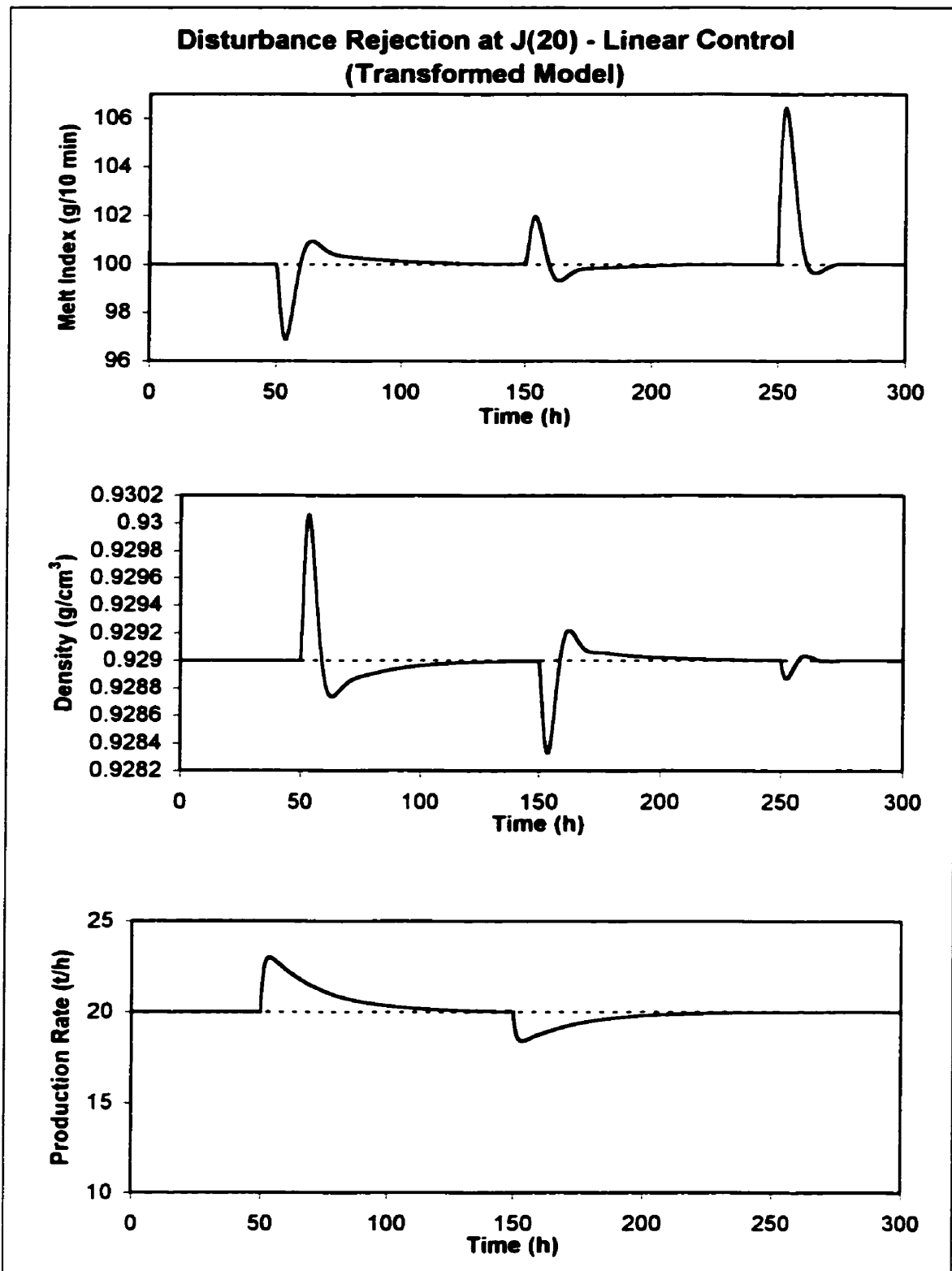
Figure A3.7.a. Simulation of disturbance rejection at point J(20), under nonlinear control of the transformed model. Solid line: controlled variable. Dashed line: set point
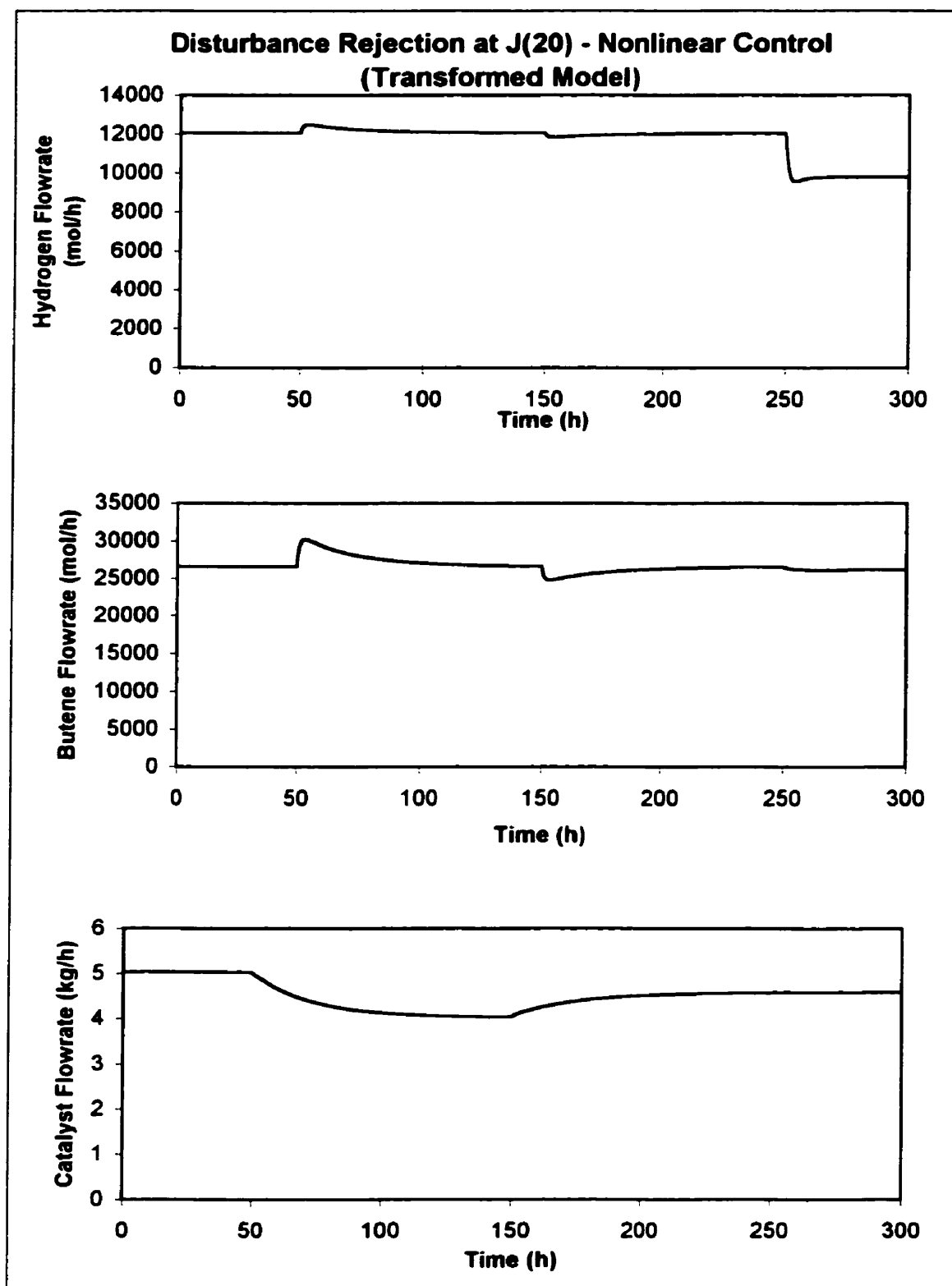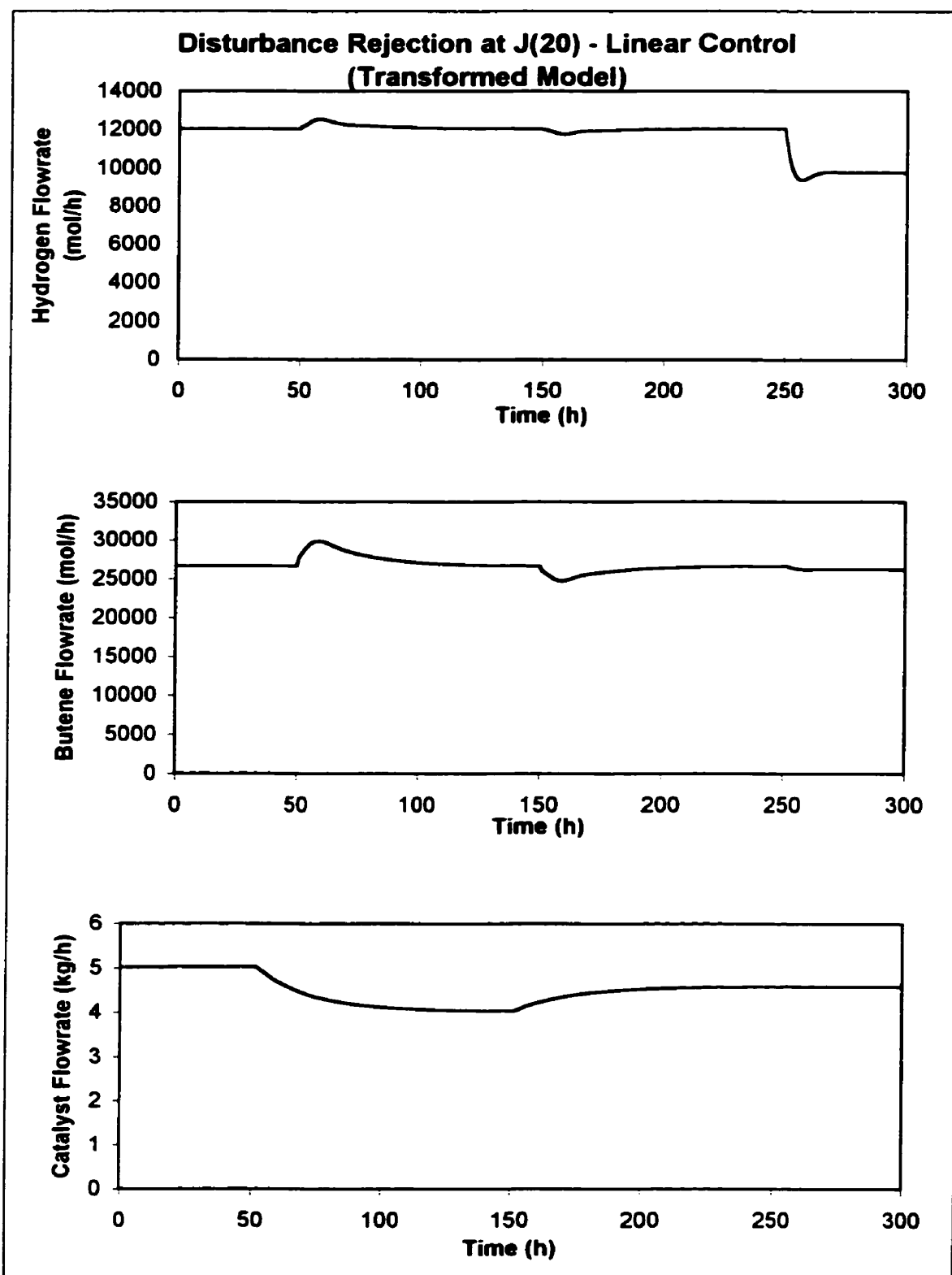
Figure A3.7.b. Simulation of disturbance rejection at point J(20), under nonlinear control of the transformed model. Solid line: manipulated variable.

Figure A3.7.c. Simulation of disturbance rejection at point J(20), under linear control of the transformed model. Solid line: controlled variable. Dashed line: set point.

171

Figure A3.7.d. Simulation of disturbance rejection at point J(20), under linear control of the transformed model. Solid line: manipulated variable.
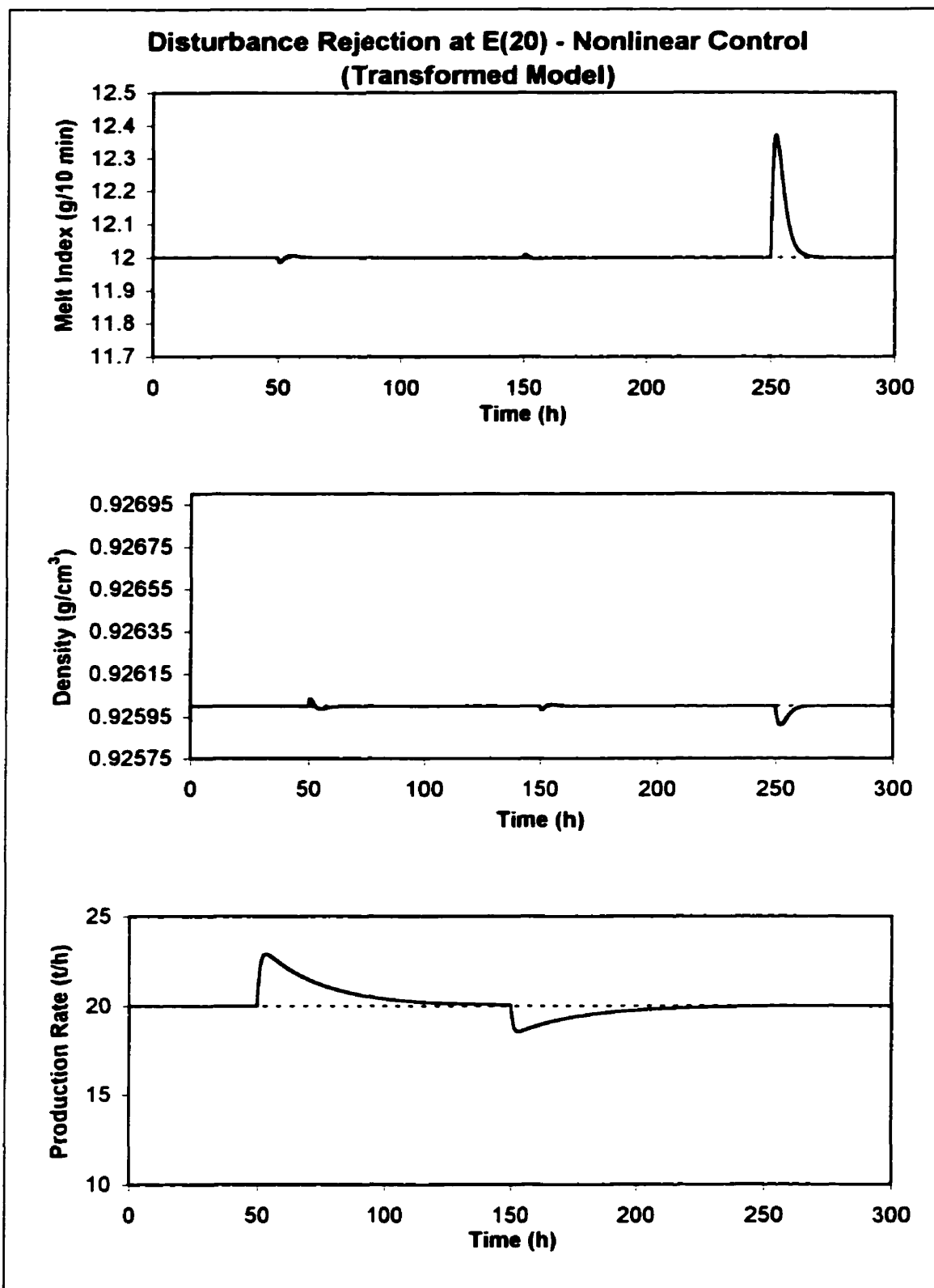
Figure A3.8.a. Simulation of disturbance rejection at point E(20), under nonlinear control of the transformed model. Solid line: controlled variable. Dashed line: set point.
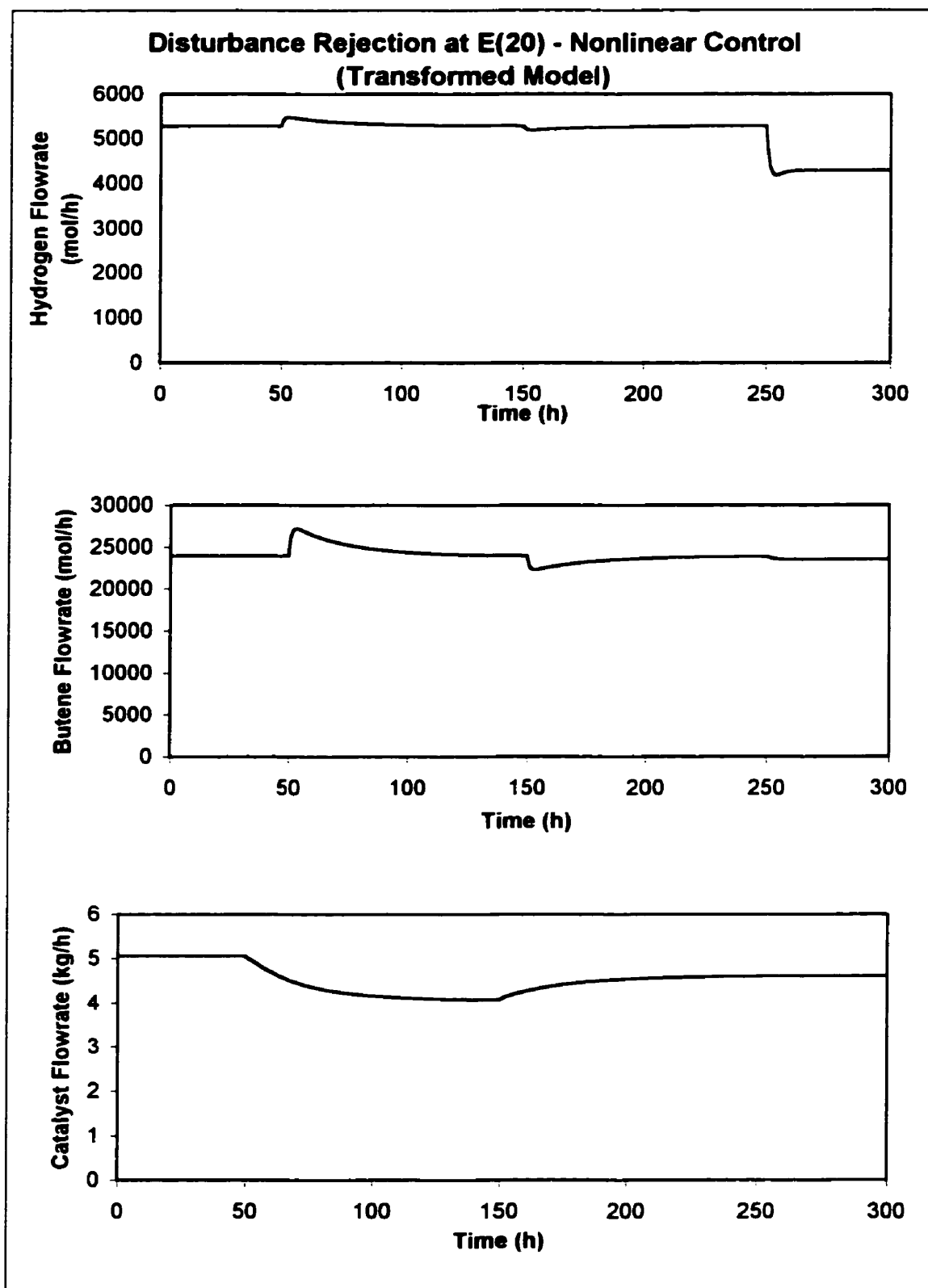
Figure A3.8.b. Simulation of disturbance rejection at point E(20), under nonlinear control of the transformed model. Solid line: manipulated variable.
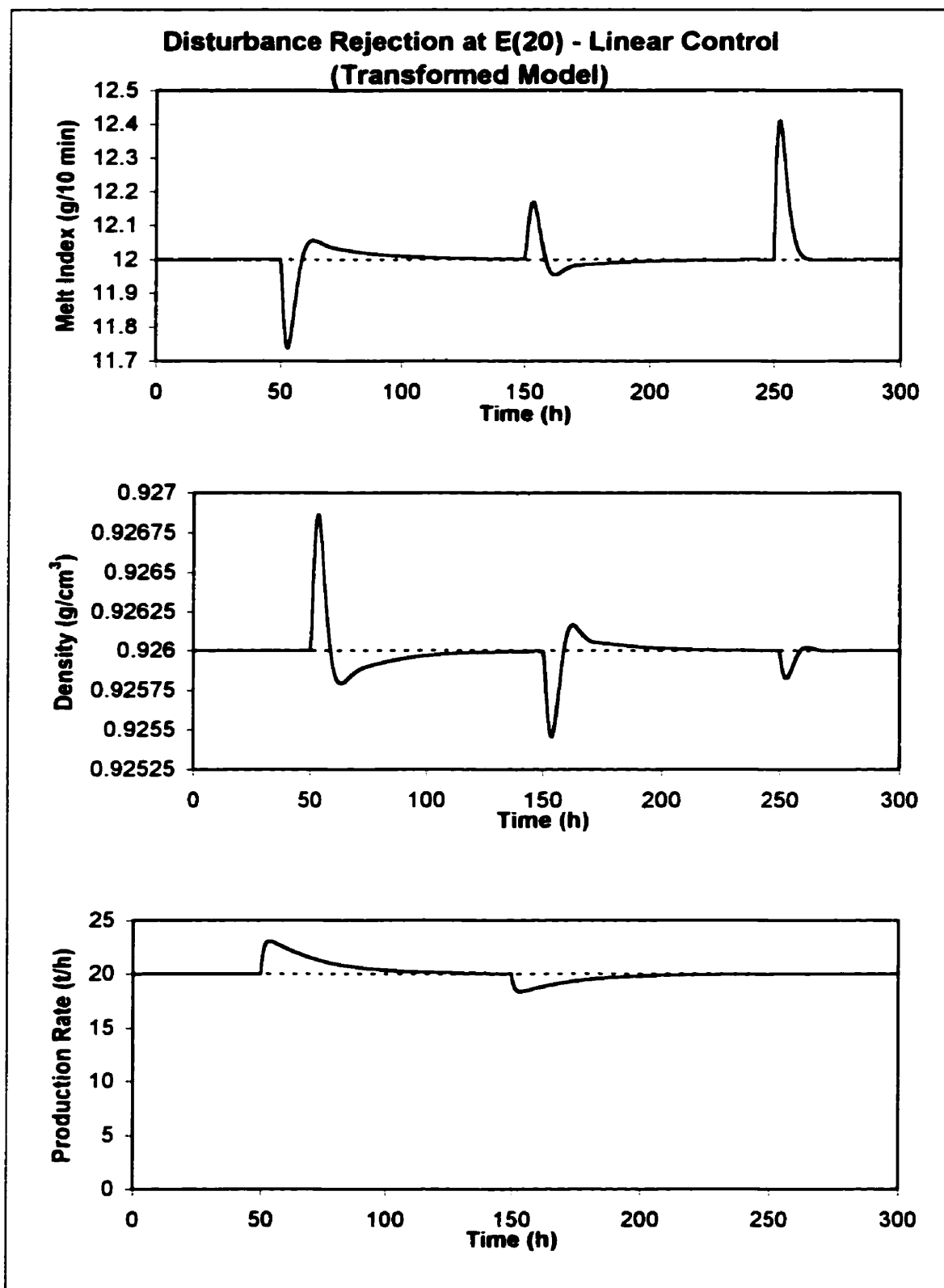
Figure A3.8.c. Simulation of disturbance rejection at point E(20), under linear control of the transformed model. Solid line: controlled variable. Dashed line: set point.
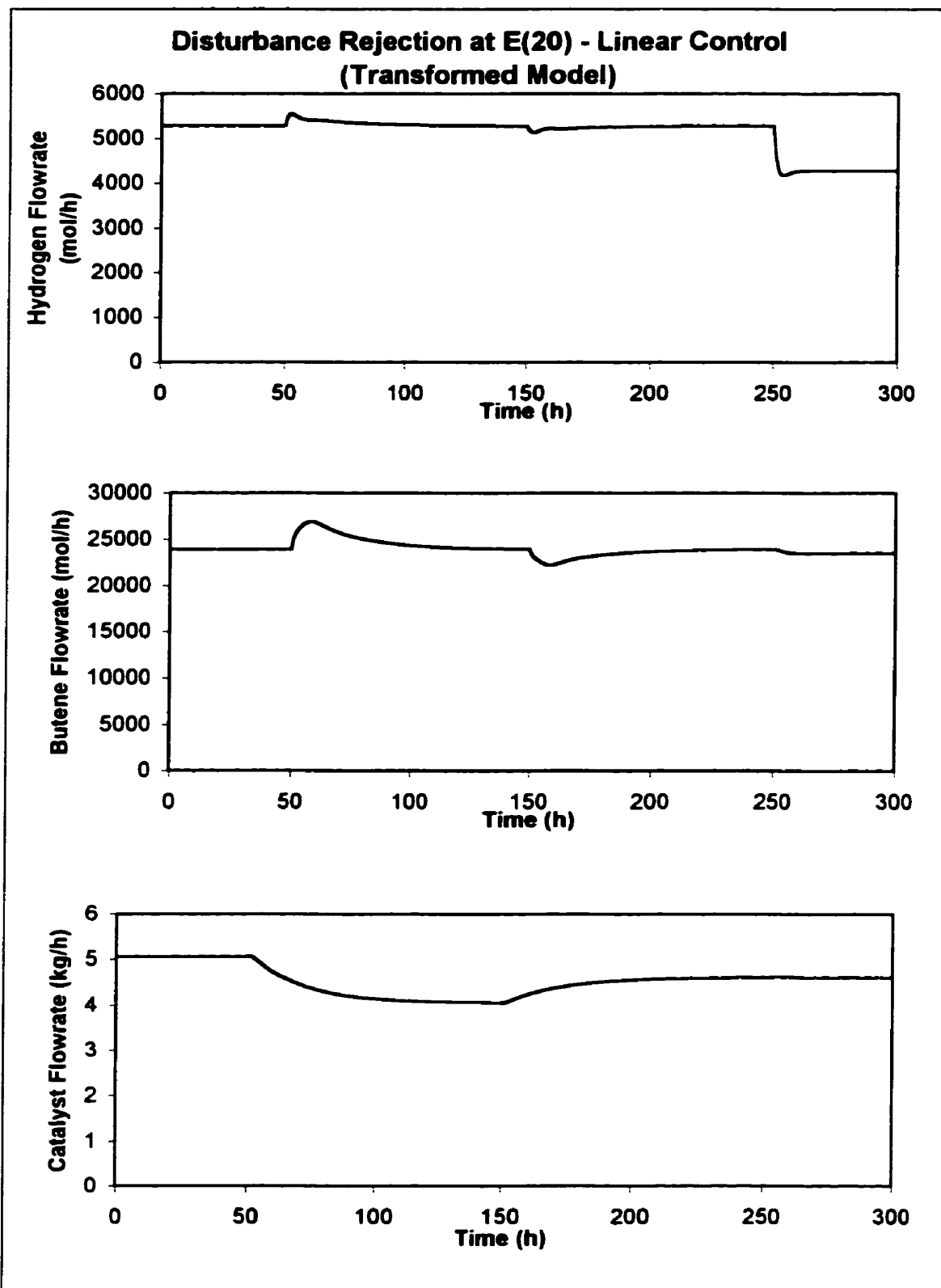
Figure A3.8.d. Simulation of disturbance rejection at point E(20), under linear control of the transformed model. Solid line: manipulated variable.

Figure A3.9.a. Simulation of disturbance rejection at point I(30), under nonlinear control of the transformed model. Solid line: controlled variable. Dashed line: set point.

Figure A3.9.b. Simulation of disturbance rejection at point I(30), under nonlinear control of the transformed model. Solid line: manipulated variable.
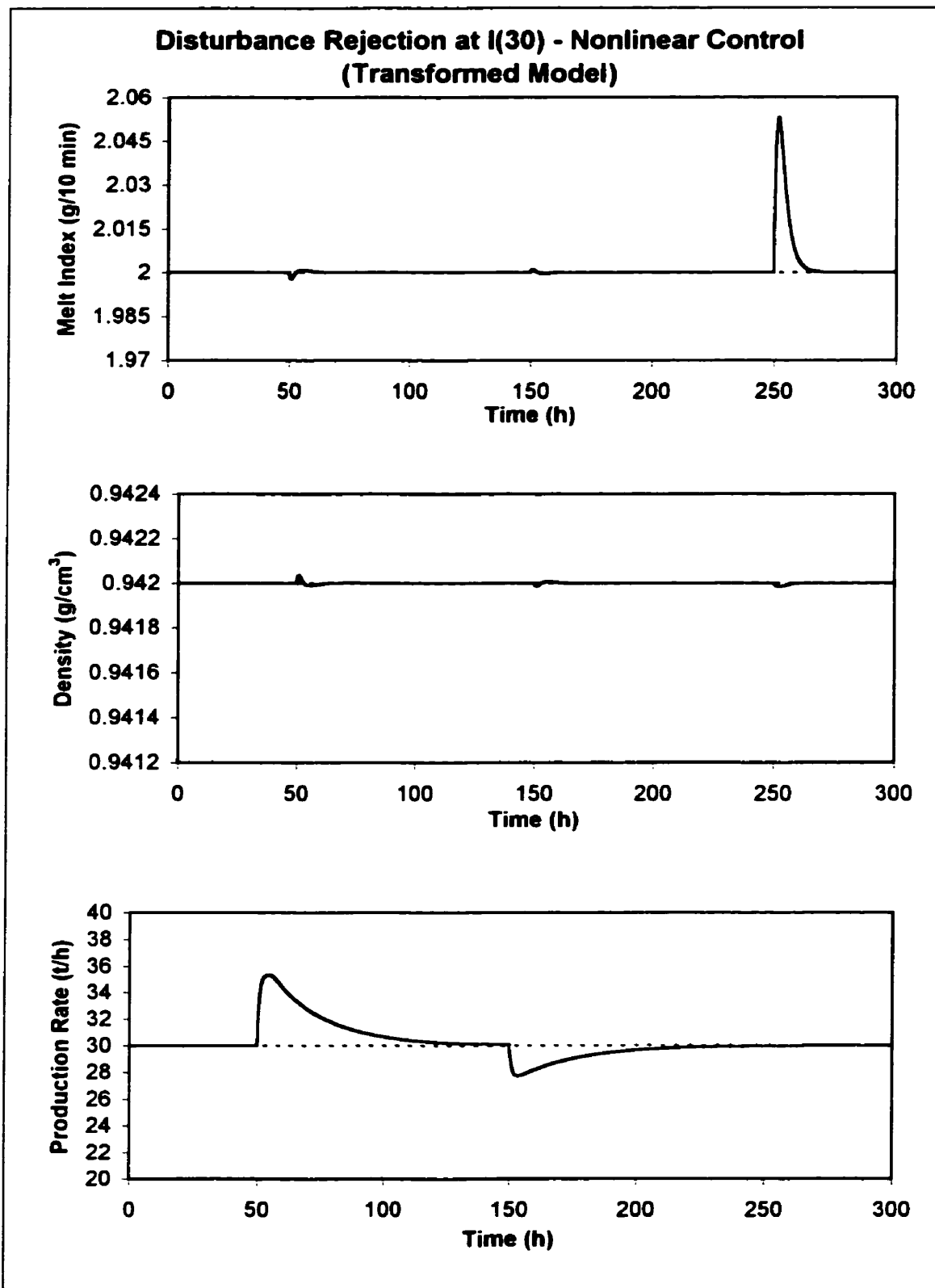
Figure A3.9.c. Simulation of disturbance rejection at point I(30), under linear control of the transformed model. Solid line: controlled variable. Dashed line: set point.
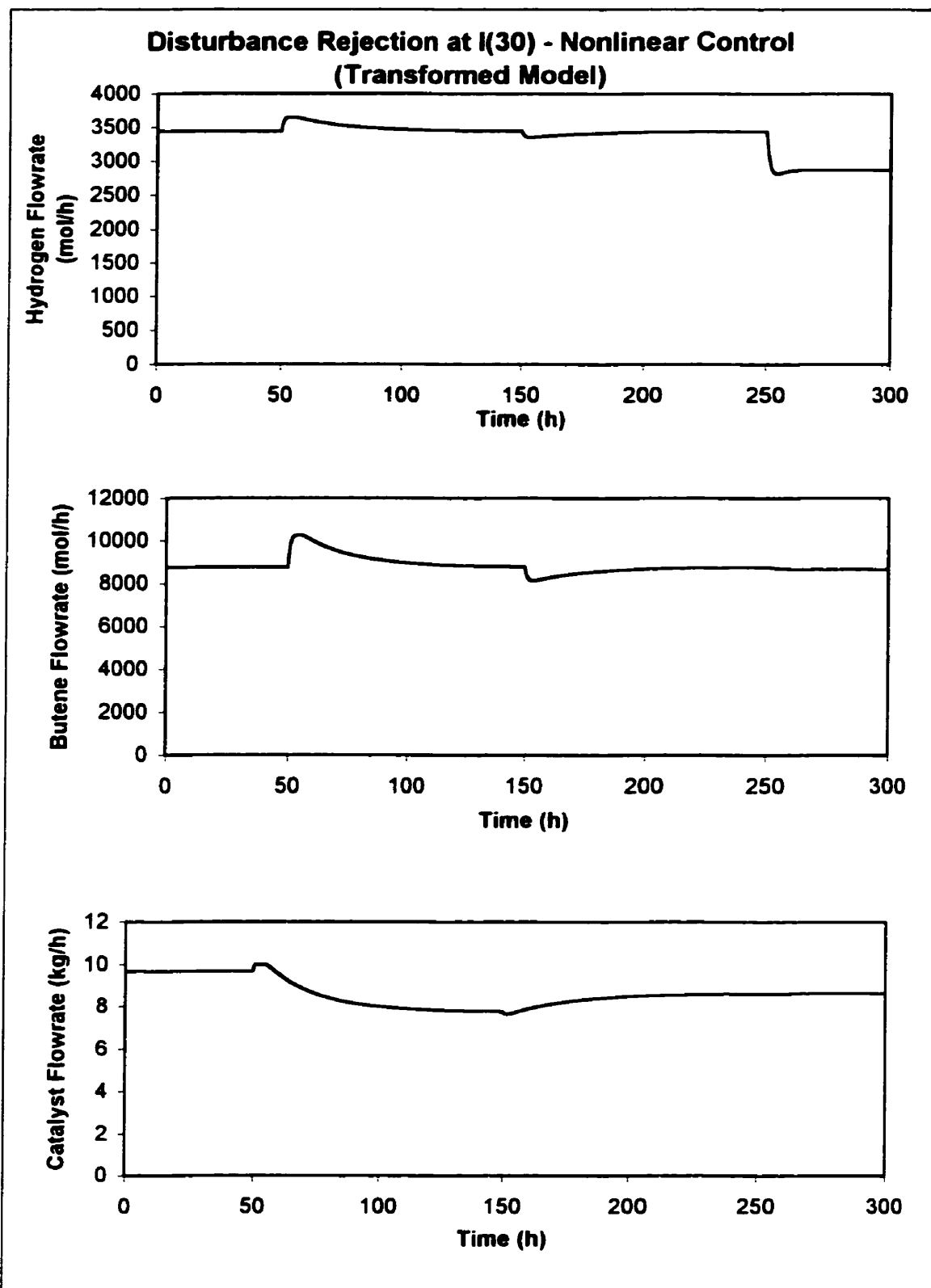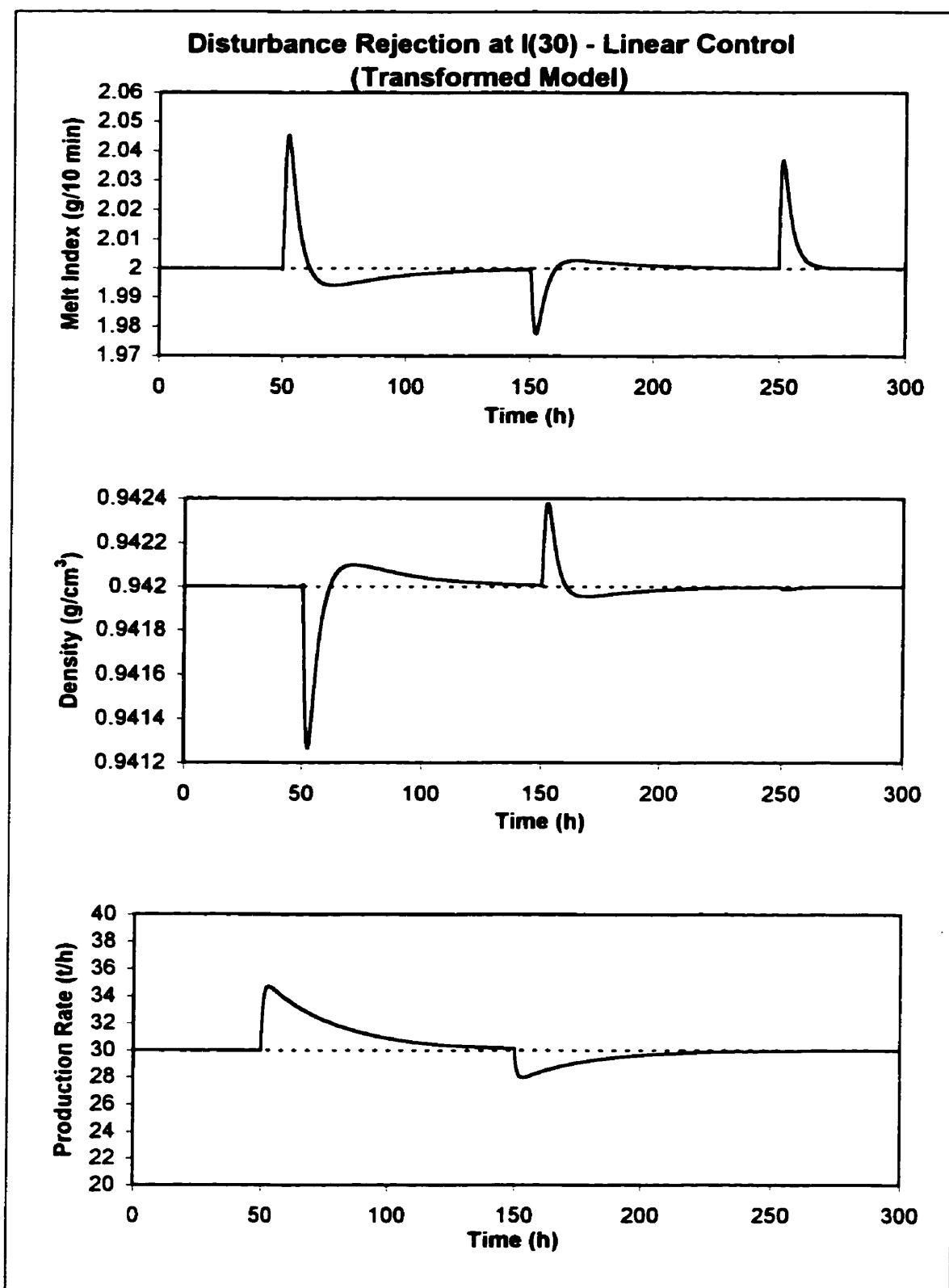
Figure A3.9.d. Simulation of disturbance rejection at point I(30), under linear control of the transformed model. Solid line: manipulated variable.
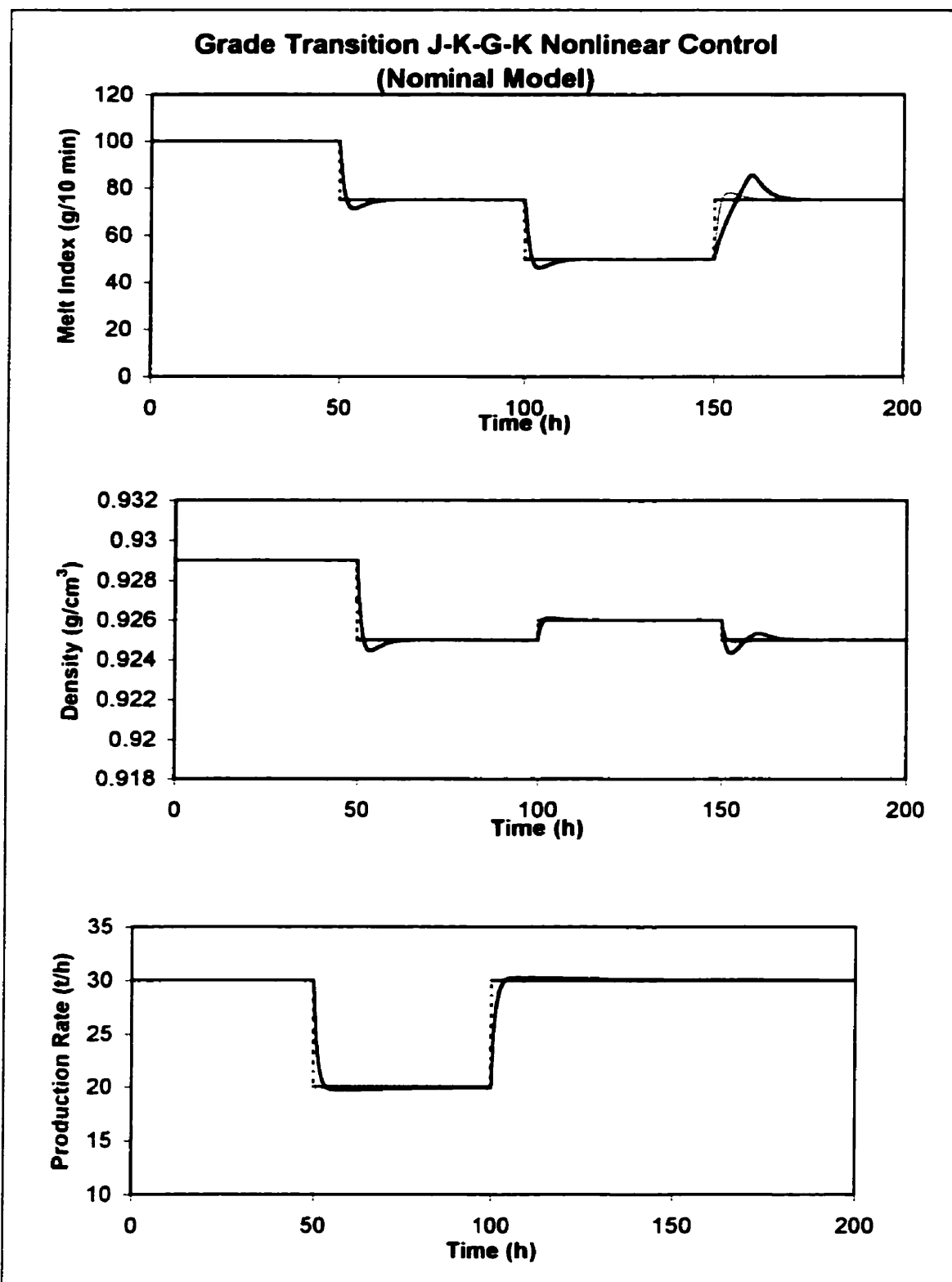
Figure A3.10.a. Simulation of the J-K-G-K grade transition, under nonlinear control of the nominal model. Dashed line: set point. Thick line: output. Thin line: error-trajectory specification.
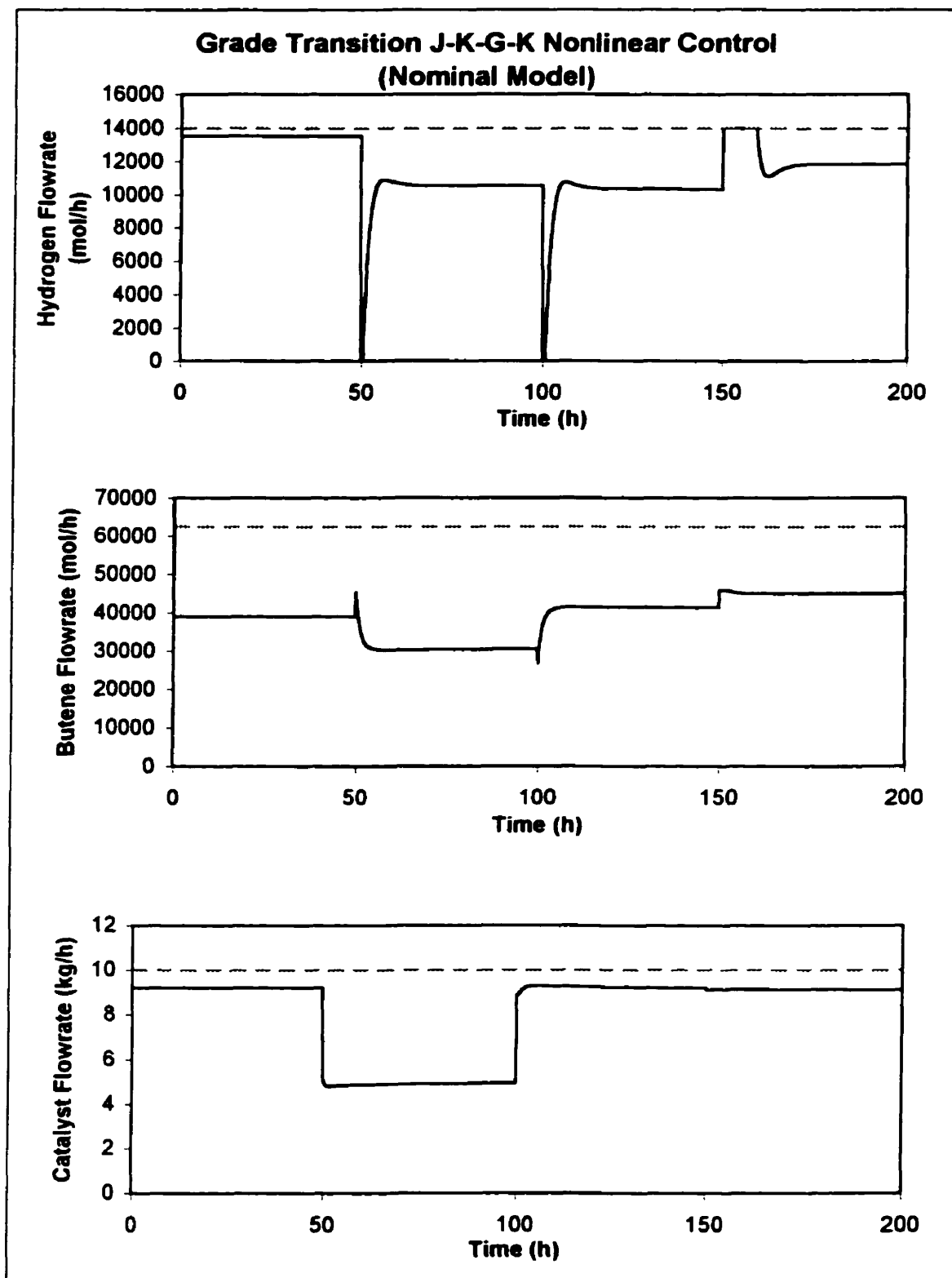
Figure A3.10.b. Simulation of the J-K-G-K grade transition, under nonlinear control of the nominal model. Solid line: manipulated variable. Dashed line: manipulated variable bound.
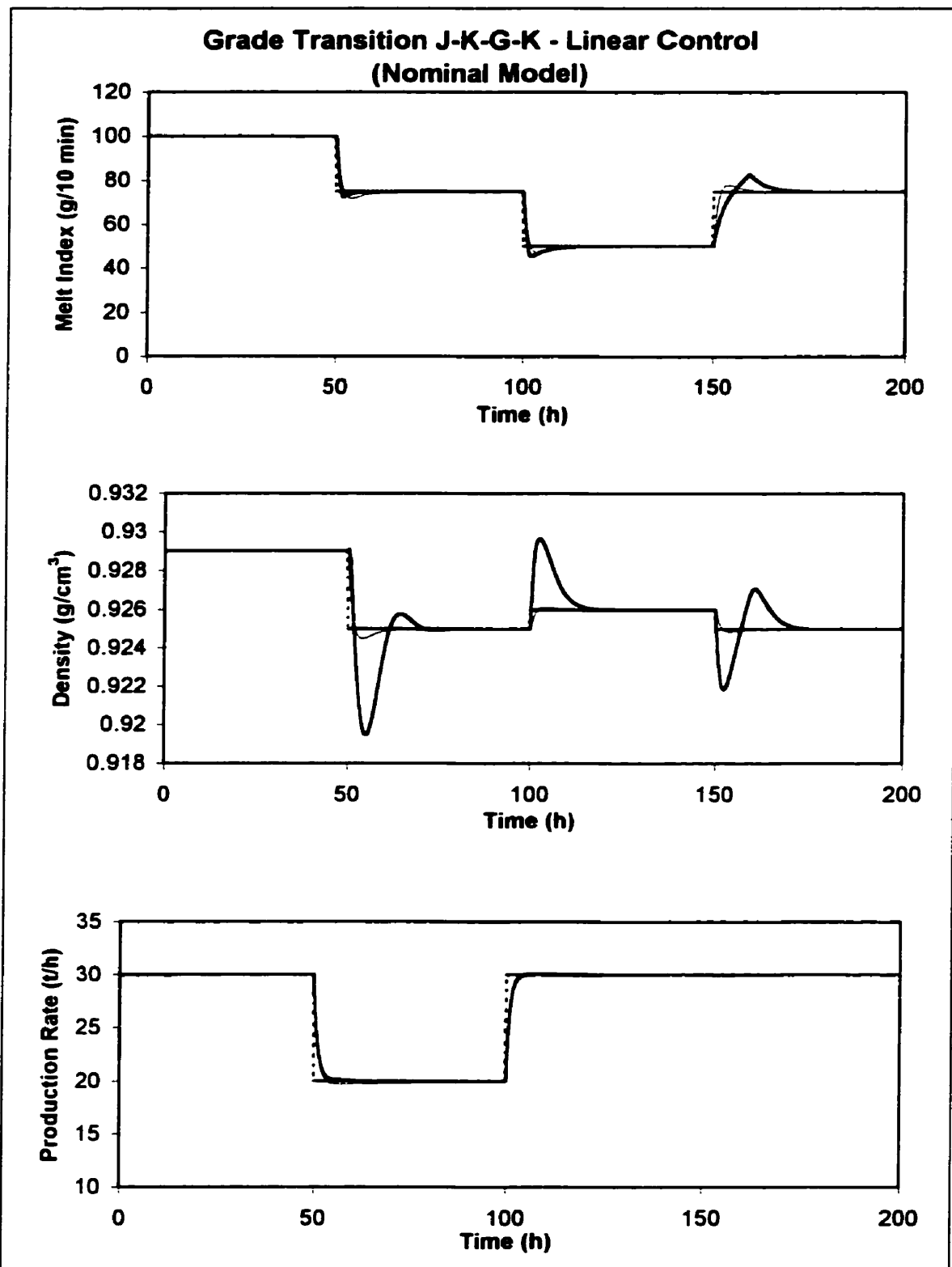
Figure A3.10.c. Simulation of the J-K-G-K grade transition, under linear control of the nominal model. Dashed line: set point. Thick line: output. Thin line: error-trajectory specification.
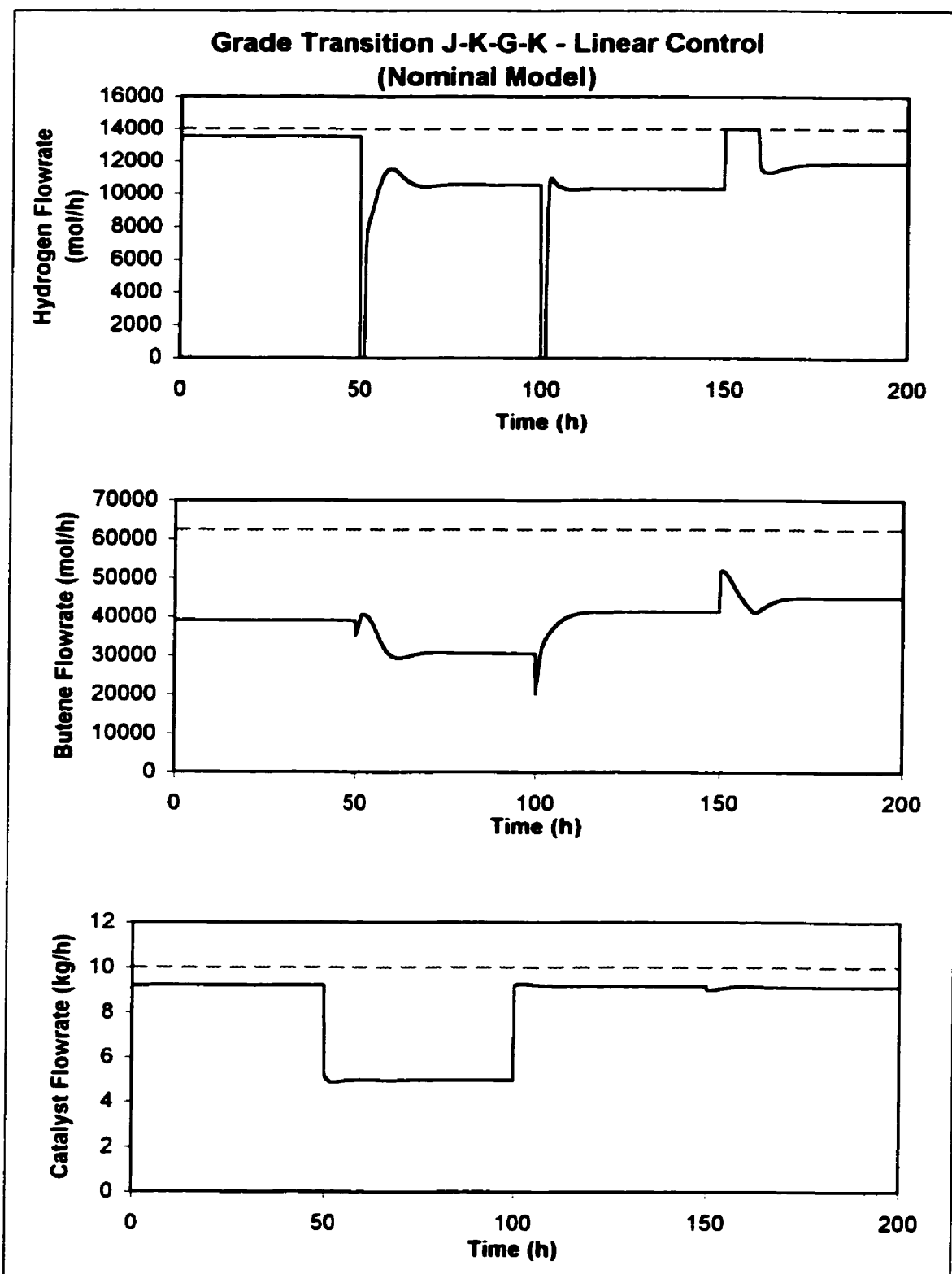
Figure A3.10.d. Simulation of the J-K-G-K grade transition, under linear control of the nominal model. Solid line: manipulated variable. Dashed line: manipulated variable bound.
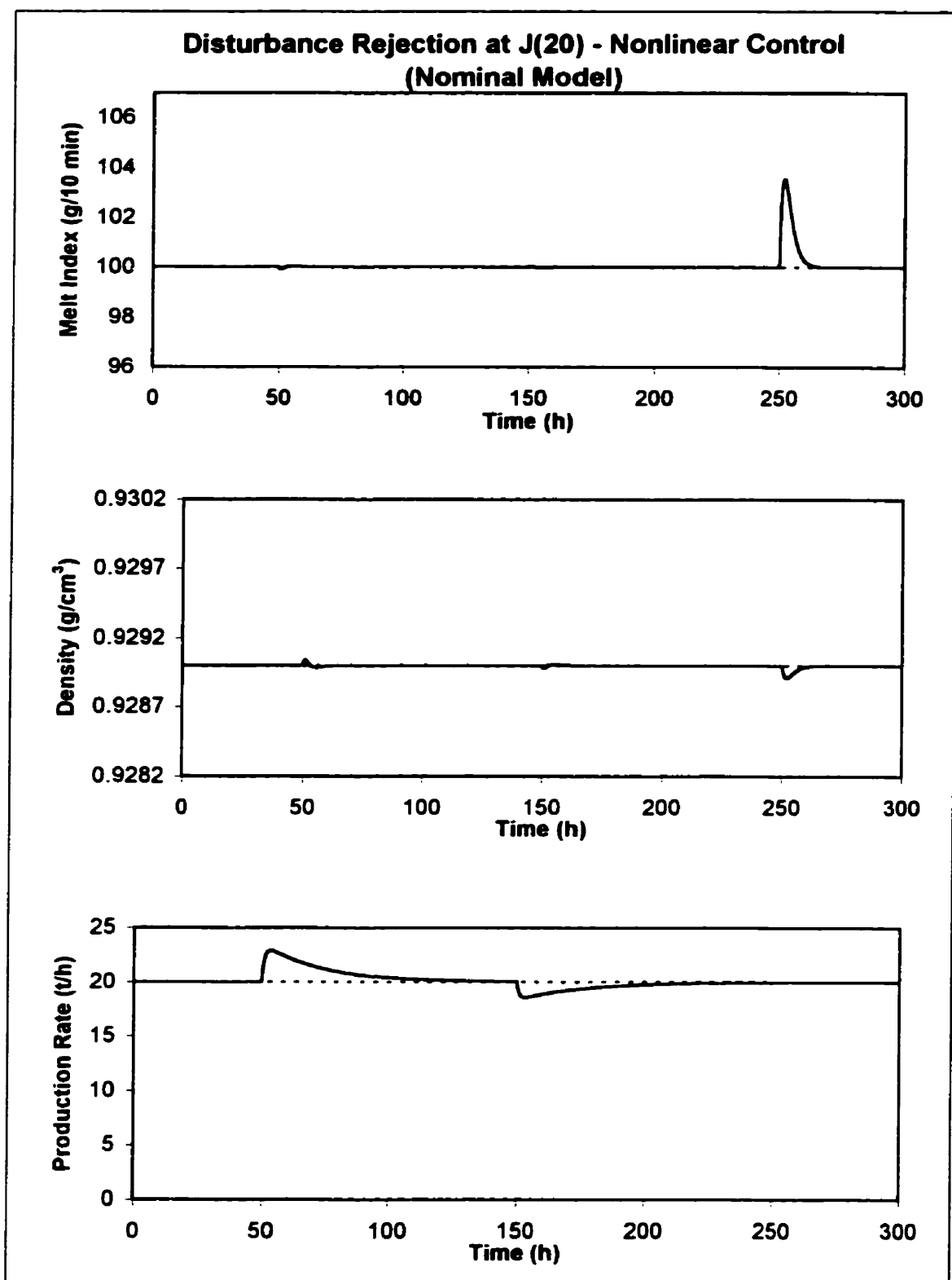
Figure A3.11a. Simulation of disturbance rejection at point J(20), under nonlinear control of the nominal model. Solid line: controlled variable. Dashed line: set point.
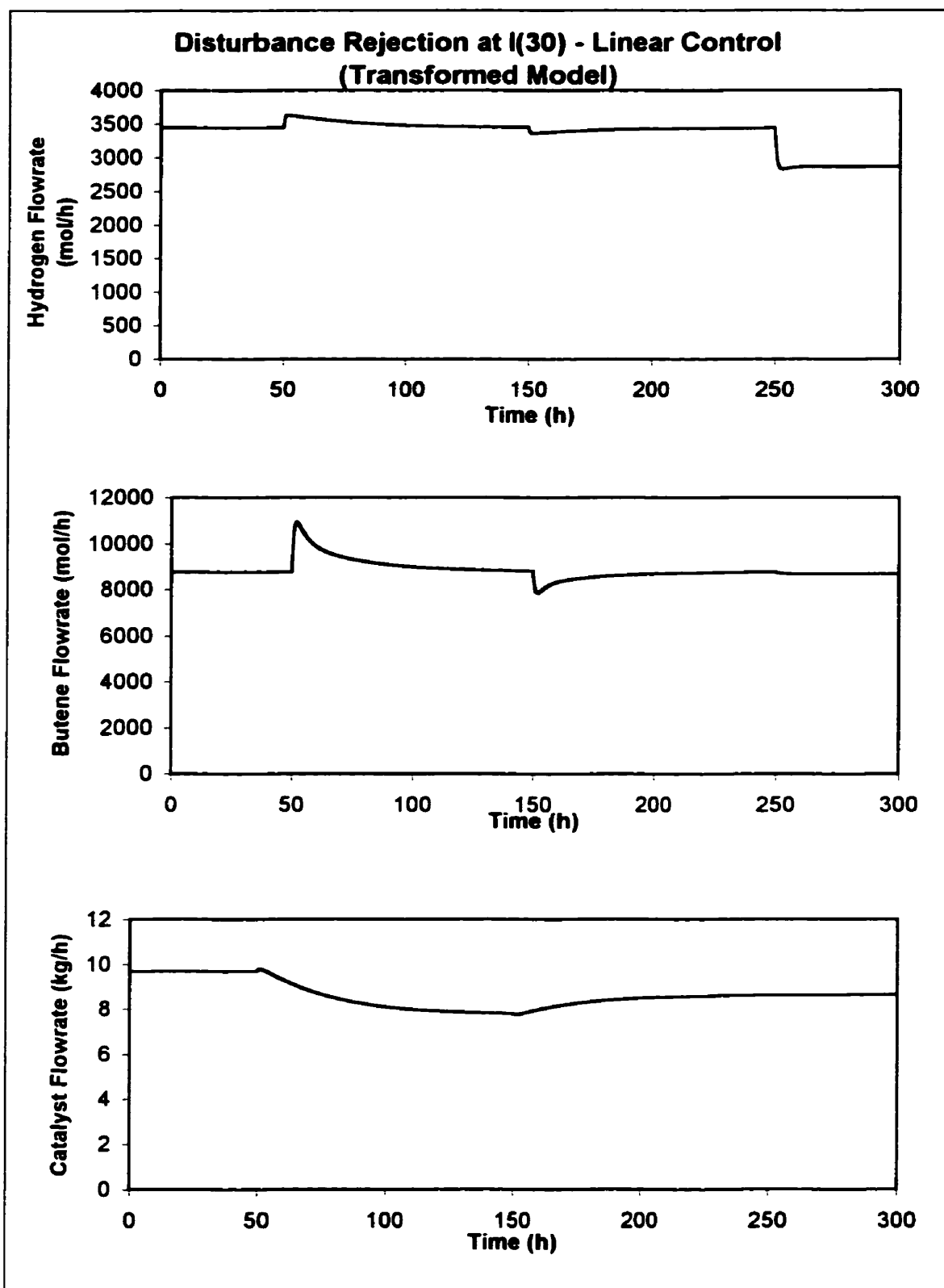
Figure A3.11.b. Simulation of disturbance rejection at point J(20), under nonlinear control of the nominal model. Solid line: manipulated variable.

Figure A3.11c. Simulation of disturbance rejection at point J(20), under linear control of the nominal model. Solid line: controlled variable. Dashed line: set point.
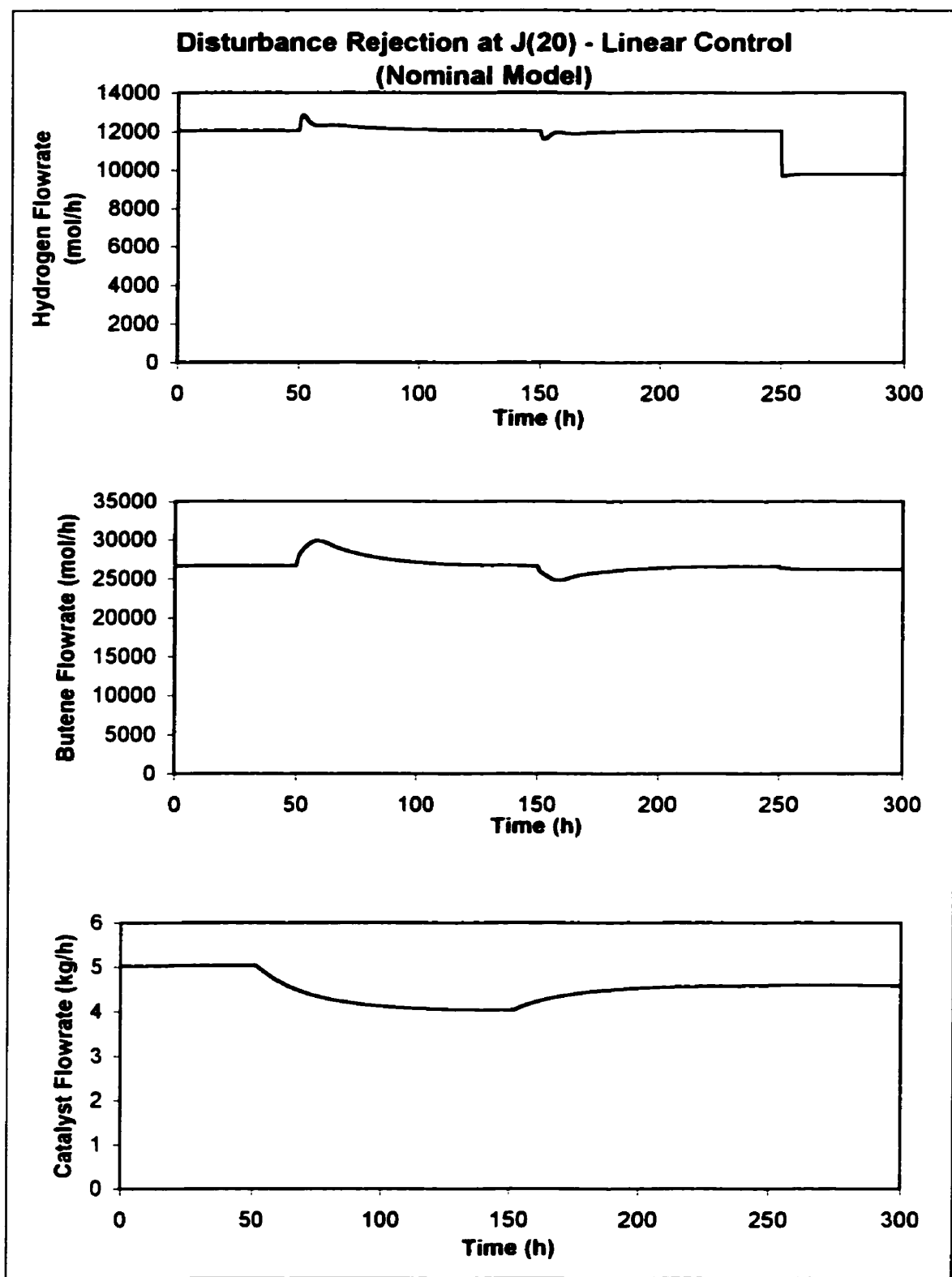
Figure A3.11d. Simulation of disturbance rejection at point J(20), under linear control of the nominal model. Solid line: manipulated variable.

Appendix B

Program Code

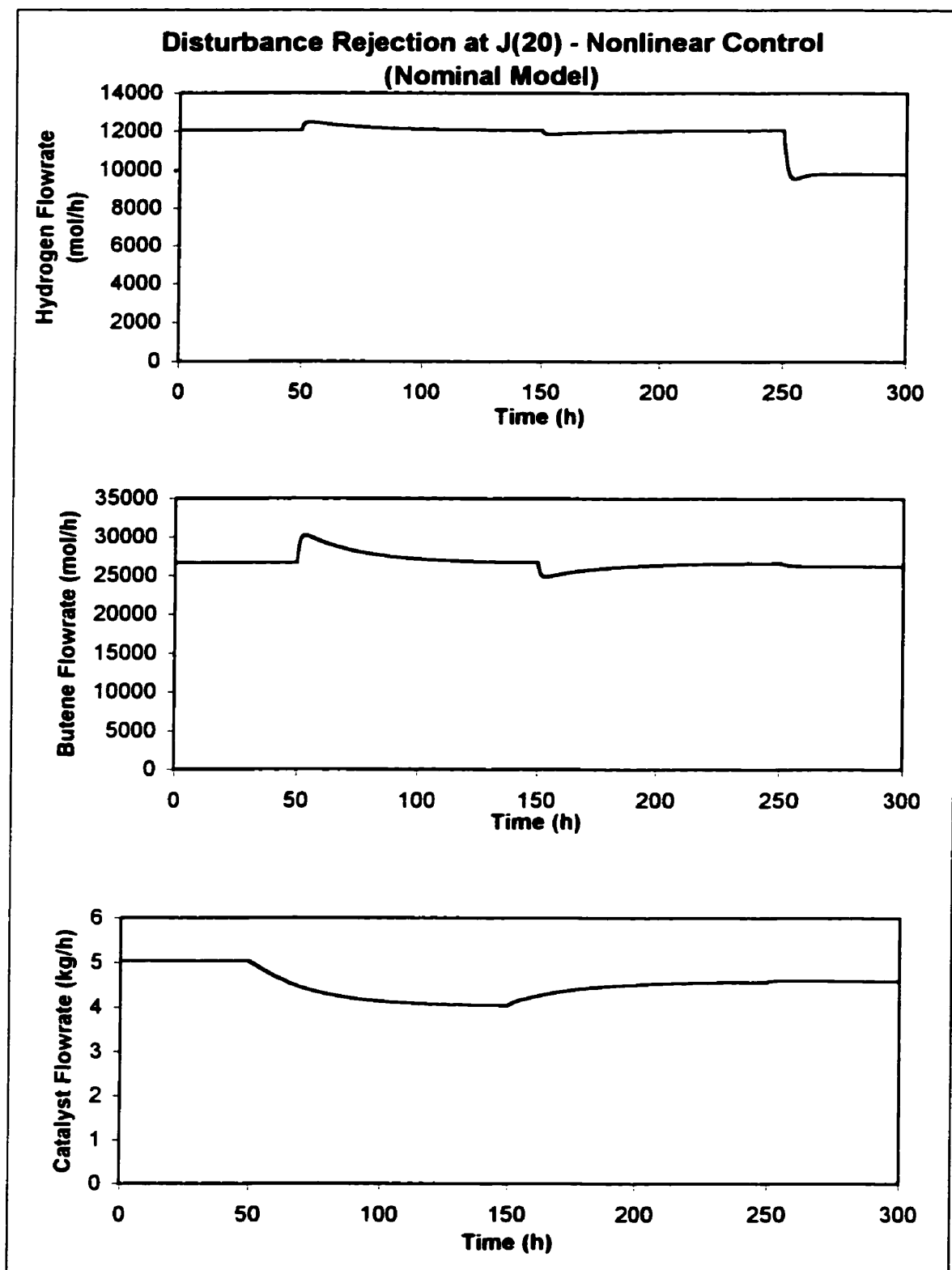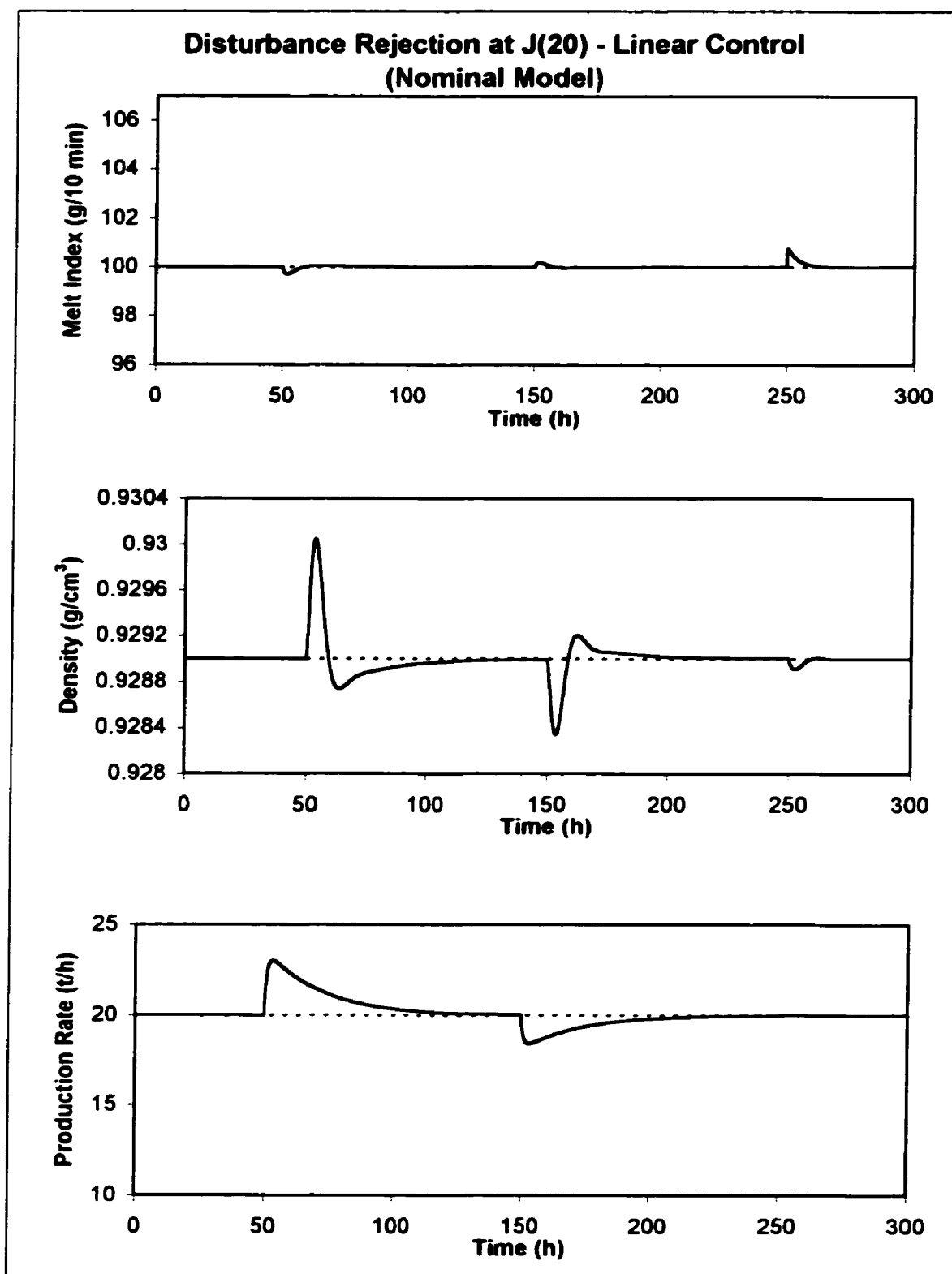This appendix contains the Maple™ and Matlab™ code used for computations in this thesis. Additional information considering these routines can be obtained from Jim McLellan (mclellnj@chee.queensu.ca).

B.1   Maple™ Code

The Maple™ (Maple V Release 5) code (filename GRADE_SPECcurvlnMI.mws) shown below was employed to calculated the RMS curvature of the product properties of the polyethylene reactor model. In addition, this worksheet calculates directional curvature and RGA information.

GRADE_SPECcurvlnMI.mws

This worksheet calculates the curvature of the ln(Melt Index) and Density model..
[H2] (=) mol/L, [M2] (=) mol/L, Y(=) mol, Bw (=) Tonnes, MI(=)g/10 min,
Density(=)g/mL, PR (=) Tonnes/h
> restart;
> with(linalg):
Warning, new definition for norm
Warning, new definition for trace
ENTER THE GRADE AND PRODUCTION RATE AT WHICH RMS IS TO BE
CALCULATED.
> lnMI:= ln(100):
> rho:=0.929:
> PR:=20:
Specify half-ranges of outputs:
> halfrangelnMI:=0.0620:
> halfrangerho:=0.001:
> halfrangePR:=3:

For the directional curvatures, must enter the input direction of interest (in original input coordinates):
> e_original:=vector(3,[2876,8677,8.626]):
MODEL EQUATIONS
These are the governing equations for [H2], [M2], and Y, respectively. This form of the model assumes perfect bed weight control, constant ethylene inflow. 'f',the time derivative of state x, equals zero.

```
> f1:=(1/Vg)*(FH2-kh*Y(FH2,FM2,Fcat)*H2(FH2,FM2,Fcat)-H2(FH2,FM2,Fcat)*b/Ct-
gl*H2(FH2,FM2,Fcat)):
> f2:=1/(Vg+Vs)*(FM2-kp2*Y(FH2,FM2,Fcat)*M2(FH2,FM2,Fcat)-
M2(FH2,FM2,Fcat)*b/Ct-
S*M2(FH2,FM2,Fcat)*Y(FH2,FM2,Fcat)*(kp1*M1*mw1+kp2*M2(FH2,FM2,Fcat)*m
w2)):
> f3:=Fcat*acat-
(Y(FH2,FM2,Fcat))^2*(kp1*M1*mw1+kp2*M2(FH2,FM2,Fcat)*mw2)/1000000/Bw-
kd*Y(FH2,FM2,Fcat):
```
These next equations are going to be used to calculate the steady state values, given a set of inputs.
```
> f1o:=(1/Vg)*(FH2o-kh*Yo*H2o-H2o*b/Ct-gl*H2o):
> f2o:=1/(Vg+Vs)*(FM2o-kp2*Yo*M2o-M2o*b/Ct-
S*M2o*Yo*(kp1*M1*mw1+kp2*M2o*mw2)):
> f3o:=Fcato*acat-Yo^2*(kp1*M1*mw1+kp2*M2o*mw2)/1000000/Bw-kd*Yo:
```
Enter the nonlinear mapping of states to outputs. Keep these states separate from those above because here we are only differentiating with respect to x, not u, so the states don't have to be in the form X(FH2, FM2, Fcat);
y1 = lnMI,   y2 = density,   y3 = production rate,
```
> y1:=3.5*ln(k0+k1*M2/M1+k3*H2/M1):
> y2:=p0+p1*y1-(p2*M2/M1)^p4:
> y3:=Y*(kp1*M1*mw1+kp2*M2*mw2)/10^6:
```
PARAMETERS AND CONSTANTS
```
> kh:=0.28*3600: b:=18571: acat:=0.000304*3600: kp1:=84*3600: M1:=0.259634:
mw1:=28.05: mw2:=56.12: kp2:=10.68*3600:gl:=3600*10^(-12): kd:=3600*0.0001:
Vg:=423747.3: Vs:=151121.9: S:=0.0021589: Ct:=0.711: Bw:=70:
> k0:=0.40: k1:=1.50: k3:=2.20: p0:=0.96: p1:=0.0025: p2:=0.007: p4:=0.5:
```
GIVEN THE SPECIFIC GRADE AT THE BEGINNING, CALCULATE
CORRESPONDING INPUTS
```
> Y1:=3.5*ln(k0+k1*M2_/M1+k3*H2_/M1)-lnMI:
> Y2:=p0+p1*lnMI-(p2*M2_/M1)^p4-rho:
> Y3:=Y_*(kp1*M1*mw1+kp2*M2_*mw2)/1000000-PR:
> states:=solve({Y1,Y2,Y3},{H2_,M2_,Y_}):
> assign(states):
> dx1dt:=(1/Vg)*(FH2_-kh*Y_*H2_-H2_*b/Ct-gl*H2_):
> dx2dt:=1/(Vg+Vs)*(FM2_-kp2*Y_*M2_-M2_*b/Ct-
S*M2_*Y_*(kp1*M1*mw1+kp2*M2_*mw2)):
> dx3dt:=Fcat_*acat-(Y_^2*(kp1*M1*mw1+kp2*M2_*mw2)/Bw/1000000)-kd*Y_:
> inputs:=solve({dx1dt,dx2dt,dx3dt},{FH2_,FM2_,Fcat_}):
> assign(inputs);
```
SOLVE THE STEADY STATE EQUATIONS
Enter the values of the inputs here:
```
> FH2o:=FH2_; FM2o:=FM2_; Fcato:= Fcat_;
```

$$FH2o := 12044.22857$$

FM2o := 26609.17812

Fcato := 5.027962624

> #FM2o := 40869.72025; Fcato := 6.869317124; FH2o := 4511.316867;
> ss:=solve({f1o,f2o,f3o},{H2o,M2o,Yo}):
> assign(ss):
> H2o;M2o;Yo;

.3470013941

.06703560091

8.521729219

FIRST DERIVATIVE INFORMATION
We have a model of the form y=h(x) where x=F(u). So y=h(F(u)). Solve for
dy/du=dh/dx*dx/du.
Differentiate h(x)
> x:=vector(3,[H2,M2,Y]):
> y:=vector(3,[y1,y2,y3]):
> dhdx:=jacobian(y,x):
Now change the above matrix so that the states appear as a function of inputs. We will
need it in this form so that we can use the relation dy/du=dh/dx*dx/du
>
dhdx:=matrix([[29.65713273*1/(.40+5.777363519*M2(FH2,FM2,Fcat)+8.473466495*H
2(FH2,FM2,Fcat)),20.22077232*1/(.40+5.777363519*M2(FH2,FM2,Fcat)+8.473466495
*H2(FH2,FM2,Fcat)),0],[.7414283183e-
1*1/(.40+5.777363519*M2(FH2,FM2,Fcat)+8.473466495*H2(FH2,FM2,Fcat)),.505519
3079e-1*1/(.40+5.777363519*M2(FH2,FM2,Fcat)+8.473466495*H2(FH2,FM2,Fcat))-
.8209907090e-
1*1/((M2(FH2,FM2,Fcat))^.5),0],[0,2.157701760*Y(FH2,FM2,Fcat),2.202298671+2.15
7701760*M2(FH2,FM2,Fcat)]]):
Now find the derivatives dx/du:
> u:=vector(3,[FH2, FM2, Fcat]):
> f:=vector(3,[f1,f2, f3]):
> alias(AdH2dFH2=diff(H2(FH2, FM2, Fcat), FH2), AdH2dFM2=diff(H2(FH2, FM2,
Fcat), FM2),AdH2dFcat=diff(H2(FH2, FM2, Fcat), Fcat),AdM2dFH2=diff(M2(FH2,
FM2, Fcat), FH2),AdM2dFM2=diff(M2(FH2, FM2, Fcat),
FM2),AdM2dFcat=diff(M2(FH2, FM2, Fcat),Fcat), AdYdFH2=diff(Y(FH2, FM2, Fcat),
FH2),AdYdFM2=diff(Y(FH2, FM2, Fcat), FM2),AdYdFcat=diff(Y(FH2, FM2, Fcat),
Fcat));

I, AdH2dFH2, AdH2dFM2, AdH2dFcat, AdM2dFH2, AdM2dFM2, AdM2dFcat,

AdYdFH2, AdYdFM2, AdYdFcat

> dfdu:=jacobian(f,u):
The following command was executed in order that I might copy the output and place it in my command line. I then change the aliased variables into ones that haven't been aliased, and used the assign command. Note that because the governing equations don't change, I executed the solve command once, and then copied the output. To speed up calculation during worksheet execution, I have made the following a comment line.
> #sol1:=solve({dfdu[1,1], dfdu[1,2], dfdu[1,3], dfdu[2,1], dfdu[2,2], dfdu[2,3], dfdu[3,1], dfdu[3,2], dfdu[3,3]}, {AdH2dFH2, AdH2dFM2, AdH2dFcat, AdM2dFH2, AdM2dFM2, AdM2dFcat, AdYdFH2, AdYdFM2, AdYdFcat});
Now I copy the output from the above calculation so that I can assign new names to the solution.
> sol1 := {dH2dFM2 =
.22321111945e35*H2(FH2,FM2,Fcat)*Y(FH2,FM2,Fcat)^2/(.1968521104e40*Y(FH2,F
M2,Fcat)^3+.1388835967e40*Y(FH2,FM2,Fcat)^3*M2(FH2,FM2,Fcat)+.63461440001e4
1*Y(FH2,FM2,Fcat)^2+.3958263150e41*M2(FH2,FM2,Fcat)*Y(FH2,FM2,Fcat)^2+.32
94846793e42*Y(FH2,FM2,Fcat)+.3119328896e39*Y(FH2,FM2,Fcat)^3*M2(FH2,FM2,
Fcat)^2+.9314843171e41*Y(FH2,FM2,Fcat)*M2(FH2,FM2,Fcat)+.1764395506e42+.80
82883617e40*M2(FH2,FM2,Fcat)^2*Y(FH2,FM2,Fcat)^2), dH2dFcat = -
.4555832213e21*H2(FH2,FM2,Fcat)*(.7515195212e20*Y(FH2,FM2,Fcat)+.454356398
4e20+.1620633817e20*Y(FH2,FM2,Fcat)*M2(FH2,FM2,Fcat))/(.1968521104e40*Y(F
H2,FM2,Fcat)^3+.1388835967e40*Y(FH2,FM2,Fcat)^3*M2(FH2,FM2,Fcat)+.6346144
001e41*Y(FH2,FM2,Fcat)^2+.3958263150e41*M2(FH2,FM2,Fcat)*Y(FH2,FM2,Fcat)^
2+.3294846793e42*Y(FH2,FM2,Fcat)+.3119328896e39*Y(FH2,FM2,Fcat)^3*M2(FH2,
FM2,Fcat)^2+.9314843171e41*Y(FH2,FM2,Fcat)*M2(FH2,FM2,Fcat)+.1764395506e4
2+.8082883617e40*M2(FH2,FM2,Fcat)^2*Y(FH2,FM2,Fcat)^2), dM2dFH2 = 0,
dM2dFM2 =
.5218578417e17*(734099557.*Y(FH2,FM2,Fcat)+719233920.*Y(FH2,FM2,Fcat)*M2(
FH2,FM2,Fcat)+4200000000.)/(.1655070443e31*Y(FH2,FM2,Fcat)^2+.1167689467e31
*M2(FH2,FM2,Fcat)*Y(FH2,FM2,Fcat)^2+.1046977446e32*Y(FH2,FM2,Fcat)+.30223
64210e31*Y(FH2,FM2,Fcat)*M2(FH2,FM2,Fcat)+.5724890620e31+.2622633329e30*
M2(FH2,FM2,Fcat)^2*Y(FH2,FM2,Fcat)^2), dM2dFcat = -
.3830400000e12*M2(FH2,FM2,Fcat)*(.7515195212e20+.8103169084e19*M2(FH2,FM
2,Fcat))/(.1655070443e31*Y(FH2,FM2,Fcat)^2+.1167689467e31*M2(FH2,FM2,Fcat)*
Y(FH2,FM2,Fcat)^2+.1046977446e32*Y(FH2,FM2,Fcat)+.3022364210e31*Y(FH2,FM
2,Fcat)*M2(FH2,FM2,Fcat)+.5724890620e31+.2622633329e30*M2(FH2,FM2,Fcat)^2*
Y(FH2,FM2,Fcat)^2), dYdFM2 = -
.1876689306e26*Y(FH2,FM2,Fcat)^2/(.1655070443e31*Y(FH2,FM2,Fcat)^2+.1167689
467e31*M2(FH2,FM2,Fcat)*Y(FH2,FM2,Fcat)^2+.1046977446e32*Y(FH2,FM2,Fcat)+
.3022364210e31*Y(FH2,FM2,Fcat)*M2(FH2,FM2,Fcat)+.5724890620e31+.262263332
9e30*M2(FH2,FM2,Fcat)^2*Y(FH2,FM2,Fcat)^2), dYdFcat =
.3830400000e12*(.7515195212e20*Y(FH2,FM2,Fcat)+.4543563984e20+.1620633817e

20*Y(FH2,FM2,Fcat)*M2(FH2,FM2,Fcat))/(.1655070443e31*Y(FH2,FM2,Fcat)^2+.11
67689467e31*M2(FH2,FM2,Fcat)*Y(FH2,FM2,Fcat)^2+.1046977446e32*Y(FH2,FM2,
Fcat)+.3022364210e31*Y(FH2,FM2,Fcat)*M2(FH2,FM2,Fcat)+.5724890620e31+.2622
633329e30*M2(FH2,FM2,Fcat)^2*Y(FH2,FM2,Fcat)^2), dYdFH2 = 0, dH2dFH2 =
1179948.521*1/(1189388109.*Y(FH2,FM2,Fcat)+.3081972431e11)}:
> assign(sol1);
Now form matrix dx/du:
> dxdu:=matrix(3,3,[dH2dFH2, dH2dFM2, dH2dFcat, dM2dFH2, dM2dFM2, dM2dFcat,
dYdFH2, dYdFM2, dYdFcat]):
Now perform dy/du=dh/dx*dx/du
> dydu:=evalm(dhdx&*dxdu):
SECOND DERIVATIVE INFORMATION
Now calculate the accelerations. Here dy1dFH2du represents d^2 y1 / dFH2du. I.e. I am
calculating the gradient.
> dy1dFH2du:=grad(dydu[1,1], u): dy1dFM2du:=grad(dydu[1,2], u):
dy1dFcatdu:=grad(dydu[1,3], u): dy2dFH2du:=grad(dydu[2,1], u):
dy2dFM2du:=grad(dydu[2,2], u): dy2dFcatdu:=grad(dydu[2,3], u):
dy3dFH2du:=grad(dydu[3,1], u): dy3dFM2du:=grad(dydu[3,2], u):
dy3dFcatdu:=grad(dydu[3,3], u):
By grouping the gradients by the states that they have differentiated, we are left with
three Hessians.
> accface1:=matrix(3,3,[dy1dFH2du, dy1dFM2du, dy1dFcatdu]):
> accface2:=matrix(3,3,[dy2dFH2du,dy2dFM2du,dy2dFcatdu]):
> accface3:=matrix(3,3,[dy3dFH2du,dy3dFM2du,dy3dFcatdu]):
NOW CALCULATE THE VELOCITY AND ACCELERATION VALUES.
> vel1:=subs({FM2=FM2o, FH2=FH2o, Fcat=Fcato, H2(FH2,FM2,Fcat)=H2o, M2(FH2,
FM2, Fcat)=M2o, Y(FH2,FM2,Fcat)=Yo}, evalm(dydu)):
> acc1:=subs({
AdH2dFH2=vel1[1,1],AdH2dFM2=vel1[1,2],AdH2dFcat=vel1[1,3],AdM2dFH2=vel1[2,
1],AdM2dFM2=vel1[2,2],AdM2dFcat=vel1[2,3],AdYdFH2=vel1[3,1],AdYdFM2=vel1[
3,2],AdYdFcat=vel1[3,3],FM2=FM2o, FH2=FH2o, Fcat=Fcato,
H2(FH2,FM2,Fcat)=H2o, M2(FH2, FM2, Fcat)=M2o, Y(FH2,FM2,Fcat)=Yo},
evalm(accface1)):
> acc2:=subs({
AdH2dFH2=vel1[1,1],AdH2dFM2=vel1[1,2],AdH2dFcat=vel1[1,3],AdM2dFH2=vel1[2,
1],AdM2dFM2=vel1[2,2],AdM2dFcat=vel1[2,3],AdYdFH2=vel1[3,1],AdYdFM2=vel1[
3,2],AdYdFcat=vel1[3,3],FM2=FM2o, FH2=FH2o, Fcat=Fcato,
H2(FH2,FM2,Fcat)=H2o, M2(FH2, FM2, Fcat)=M2o, Y(FH2,FM2,Fcat)=Yo},
evalm(accface2)):
> acc3:=subs({
AdH2dFH2=vel1[1,1],AdH2dFM2=vel1[1,2],AdH2dFcat=vel1[1,3],AdM2dFH2=vel1[2,
1],AdM2dFM2=vel1[2,2],AdM2dFcat=vel1[2,3],AdYdFH2=vel1[3,1],AdYdFM2=vel1[
3,2],AdYdFcat=vel1[3,3],FM2=FM2o, FH2=FH2o, Fcat=Fcato,
H2(FH2,FM2,Fcat)=H2o, M2(FH2, FM2, Fcat)=M2o, Y(FH2,FM2,Fcat)=Yo},
evalm(accface3)):
SCALING

Define the output scaling matrix. ###Smatrix=(Sin)*(gain matrix)^-1
> #Smatrix:=evalm(Sin&*(inverse(vel1)));

> Smatrix:=matrix(3,3,[1/halfrangeInMI,0,0,0,1/halfrangerho,0,0,0,1/halfrangePR]):
Now must find the nonredundant acceleration array.
> W:=matrix(3,6,[acc1[1,1], acc1[1,2], acc1[1,3], acc1[2,2], acc1[2,3], acc1[3,3],
acc2[1,1], acc2[1,2], acc2[1,3], acc2[2,2], acc2[2,3], acc2[3,3],acc3[1,1], acc3[1,2],
acc3[1,3], acc3[2,2], acc3[2,3], acc3[3,3]]):
> VW:=augment(vel1,W):
Now scale matrix
> VWscaled:=evalm(Smatrix&*VW):
ORTHOGONALIZATION OF THE TANGENT AND ACCELERATION VECTORS
Now perform QR decomposition uning Householder Transformations as described in
Bates and Watts, pp. 286.
> e1:=matrix(3,1,[1,0,0]):
> x1:=matrix(3,1,[VWscaled[1,1], VWscaled[2,1], VWscaled[3,1]]):
> magn_x1:=sqrt((x1[1,1])^2+(x1[2,1])^2 + (x1[3,1])^2):
> u_num:=evalm(x1+magn_x1*e1):
> u_den:=sqrt((u_num[1,1])^2 + (u_num[2,1])^2+(u_num[3,1])^2):
> u1:=evalm(u_num/u_den):
> Hu1:=evalm(&*()-2*u1&*transpose(u1)):
> X1:=evalm(Hu1&*VWscaled):
> e2:=matrix(3,1,[0,1,0]):
> x2:=matrix(3,1,[0, X1[2,2], X1[3,2]]):
> magn_x2:=sqrt(x2[1,1]^2 + x2[2,1]^2 + x2[3,1]^2):
> u2_num:=evalm(x2+magn_x2*e2):
> u2_den:=sqrt(u2_num[1,1]^2+u2_num[2,1]^2 + u2_num[3,1]^2):
> u2:=evalm(u2_num/u2_den):
> Hu2:=evalm(&*()-2*u2&*transpose(u2)):
> X2:=evalm(Hu2&*Hu1&*VWscaled):
> X2:=evalm(Hu2&*X1):
> R:=X2:
Since R=Q'X and R=Hu2Hu1X, therefore Q'=Hu2Hu1:
> Qinv:=evalm(Hu2&*Hu1):
> Q:=inverse(Qinv);

$$Q := \begin{bmatrix} -.9881997046 & -.1531568743 & .002076802599 \\ -.1531709544 & .9881088667 & -.01339872645 \\ .9999999980\ 10^{-12} & -.01355872338 & -.9999080755 \end{bmatrix}$$

> X:=evalm(Q&*R):
> evalm(VWscaled):
NOW IN NEW ORTHOGONAL BASIS:

194

Now for the curvature array. First extract the submatrix R1 from R. These are the velocities.
> R1:=submatrix(R, 1..3,1..3);

$$
R1 := \begin{bmatrix}
-.003741247250 & -.0001098194917 & 1.913968372 \\
-12 & & \\
-.3999632305\ 10 & -.0007982318198 & 2.723424064 \\
-14 & -11 & \\
.5423489356\ 10 & .505\ 10 & -.9191102806
\end{bmatrix}
$$

Now we can form the redundant acceleration array.
> Arface1:= matrix(3,3,[R[1,4], R[1,5], R[1,6], R[1,5],R[1,7], R[1,8], R[1,6],R[1,8], R[1,9]]);

$$
Arface1 := \begin{bmatrix}
-5 & -6 & \\
.1952726502\ 10 & .1207363501\ 10 & -.00091673l8556 \\
-6 & -8 & \\
.1207363501\ 10 & .8052505115\ 10 & -.00004532706206 \\
-.00091673l8556 & -.00004532706206 & -.4562158536
\end{bmatrix}
$$

> Arface2:=matrix(3,3,[R[2,4], R[2,5], R[2,6], R[2,5],R[2,7], R[2,8], R[2,6],R[2,8], R[2,9]]);

$$
Arface2 := \begin{bmatrix}
-16 & -17 & \\
.9999080763\ 10 & .9999080763\ 10 & 0 \\
-17 & -8 & \\
.9999080763\ 10 & -.1742940708\ 10 & .0002438785036 \\
0 & .0002438785036 & -1.259382234
\end{bmatrix}
$$

> Arface3:=matrix(3,3,[R[3,4], R[3,5], R[3,6], R[3,5],R[3,7], R[3,8], R[3,6],R[3,8], R[3,9]]);

Arface3 :=

$$
\begin{bmatrix}
-17 & -18 & \\
-.1355872339\ 10 & -.1355872339\ 10 & 0 \\
-18 & -10 & -5 \\
-.1355872339\ 10 & .2681288255\ 10 & -.2976333591\ 10
\end{bmatrix}
$$

```
                   [              -5              ]
                   [0 , -.2976333591 10   , .1845160632]

> K:=inverse(R1):
> Cr1:=evalm((transpose(K))&*Arface1&*K);


              [.1395110474    .02123525022    .0868433008 ]
              [                                            ]
       Cr1 := [.02123525021   .004154176515   .03142626530]
              [                                            ]
              [.08684330096   .03142626528    -.8956422355]


> Cr2:=evalm((transpose(K))&*Arface2&*K);

  Cr2 :=

         [          -11              -11              -10]
         [.7143766569 10   , .3127961079 10   , -.1212549294 10   ]


         [          -11                                  ]
         [.3127961078 10   , -.002735419193 , .3243067800]


         [          -10                                  ]
         [-.1212549294 10   , .3243067799 , .4551197253]


> Cr3:=evalm((transpose(K))&*Arface3&*K);

  Cr3 :=

         [          -13              -13              -12]
         [-.9686925943 10   , -.4227361450 10   , .4059266410 10   ]


         [          -13                                  ]
         [-.4227361451 10   , .00004208089038 , -.003932121018]


         [          -12                                  ]
         [.4059266408 10   , -.003932121018 , .1947512054]
```

ROOT MEAN SQUARE CURVATURE
Calculate RMS curvature.
> P:=3;

$$P := 3$$

```
>
c2:=1/(P*(P+2))*(2*(Cr1[1,1]^2+Cr1[1,2]^2+Cr1[1,3]^2+Cr1[2,1]^2+Cr1[2,2]^2+Cr1[2
```

,3]^2 + Cr1[3,1]^2 + Cr1[3,2]^2 + Cr1[3,3]^2
+Cr2[1,1]^2+Cr2[1,2]^2+Cr2[1,3]^2+Cr2[2,1]^2+Cr2[2,2]^2+Cr2[2,3]^2 + Cr2[3,1]^2 +
Cr2[3,2]^2 + Cr2[3,3]^2 +
Cr3[1,1]^2+Cr3[1,2]^2+Cr3[1,3]^2+Cr3[2,1]^2+Cr3[2,2]^2+Cr3[2,3]^2 + Cr3[3,1]^2 +
Cr3[3,2]^2 + Cr3[3,3]^2)+(Cr1[1,1] +Cr1[2,2]+Cr1[3,3])^2
+(Cr2[1,1]+Cr2[2,2]+Cr2[3,3])^2+(Cr3[1,1]+Cr3[2,2]+Cr3[3,3])^2);

$$c2 := .2265465463$$

> RMS:=sqrt(c2);

$$RMS := .4759690602$$

Now check to see if this method of calculating RMS is correct. Compare to Jim's
calculation below.
>
c2Jim:=eval(1/P/(P+2)*sum('2*sum(sum(Cr.ii[jj,k]^2,k=1..P),jj=1..P)+sum(Cr.ii[jj,jj],jj=
1..P)^2','ii'=1..P));

$$c2Jim := .2265465463$$

> RMSJim:=sqrt(c2Jim);

$$RMSJim := .4759690602$$

TWO-WAY INTERACTION MEASURE:
Calculate the RGA:
> evalm(vel1):
> gain:=vel1:
> gaininv:=inverse(gain):
> gaininvT:=transpose(gaininv):
> RGA:=matrix(3,3,[gain[1,1]*gaininvT[1,1], gain[1,2]*gaininvT[1,2] ,
gain[1,3]*gaininvT[1,3], gain[2,1]*gaininvT[2,1],gain[2,2]*gaininvT[2,2],
gain[2,3]*gaininvT[2,3], gain[3,1]*gaininvT[3,1], gain[3,2]*gaininvT[3,2],
gain[3,3]*gaininvT[3,3]]):
CURVATURE IN A GIVEN DIRECTION, e.
> e:=evalm(e_original/norm(e_original,2)):
> ce_num1:=evalm(transpose(e)&*Arface1&*e):
> ce_num2:=evalm(transpose(e)&*Arface2&*e):
> ce_num3:=evalm(transpose(e)&*Arface3&*e):
> ce_numerator:=sqrt(ce_num1^2+ce_num2^2+ce_num3^2):
> ce_den:=evalm(R1&*e):
> ce_denominator:=ce_den[1]^2+ce_den[2]^2+ce_den[3]^2:
> ce:=ce_numerator/ce_denominator:
RESULTS
So here are our final results for the 3x3 output system:

> RMS;

.4759690602

> evalm(RGA);

$$
\begin{bmatrix}
.9522791298 & .04250033397 & .005220536340 \\
.04772087031 & .9171435616 & .03513556852 \\
0 & .04035610486 & .9596438953
\end{bmatrix}
$$

> ce;

.2401545339

>

B.2 Matlab™ Code

This Matlab™ code (filename InMIgradetrans1.m) was used to run grade transitions of the transformed model, under nonlinear control. Minor adjustments are made to run the nominal model and linear controllers.

InMIgradetrans1.m

```
%This is the main program for simulating the control of the
%polyethylene grade
%changeovers, where the outputs are [ln(MI), density, production rate].

clear

%PARAMETERS

k0=0.4;
k1=1.5;
k3=2.2;
p0=.96;
p1=.0025;
p2=.007;
p4=.5;
M1=0.259634;
kp1=302400;
kp2=38448;
mw1=28.05;
mw2=56.12;
timestep=0.1;

%CHOOSE INITIAL STEADY STATES
%For initial grade D(30) :       choose SSscheme=1
%For initial grade J(30) :       choose SSscheme=2
%For initial grade [80, .935 30] : choose SSscheme=3
%For initial grade C(30) :       choose SSscheme=4
%For initial grade N(30) :       choose SSscheme=5
%For initial grade O(30) :       choose SSscheme=6
%For initial grade S(30) :       choose SSscheme=7

SSscheme=4;

%CHOOSE SET POINT SCHEME:

SPscheme=5;

%INITIAL CONDITIONS

initlnMIgrtrans1
tfholder=[];
time=[];
t0=0;
tf=timestep;
state=[];
output=[];
```

```
input=[];
SPholder=[];
tfholder=[tfholder;tf];
ITAE=[0;0;0];
ITAEMI=[0;0;0];
e=[0;0;0];

%START AT STEADY STATE AND RUN FOR 50 HOURS
[t,x] = model5s(1,'polstates',[t0 tf], x0, [], u);
state=[state;x];
time = [time ; t];
sizet=size(t);
for k=1:sizet
    input=[input; u'];
end
sizex= size(x);
numrow=sizex(1);
for j=1:numrow
    lnMI=3.5*log(k0+k1*x(j,2)/M1+k3*x(j,1)/M1);
    rho=p0+p1*lnMI-(p2*x(j,2)/M1)^p4;
    PR=x(j,3)*(kp1*M1*mw1+kp2*x(j,2)*mw2)/1000000;
    output=[output ; [lnMI rho PR]];
    SPholder=[SPholder;y0];
end
Ysp=y0;

%IMPLEMENT SET POINT CHANGES

simlength=200;
t0=t0+timestep;
tf=tf+timestep;
tfholder=[tfholder;tf];
while tf < simlength
    if (tf >= 50 & tf < 100)
    Ysp=SP(1,:);
        if (tf>=50 & tf< 51)
            disp(' time is 50')
    end
    elseif (tf >= 100 & tf<150)
    Ysp=SP(2,:);
    if (tf>=100 & tf< 101)
            disp(' time is 100')
    end
    elseif (tf >= 150 & tf <200)
    Ysp=SP(3,:);
    if (tf>=150 & tf< 151)
            disp(' time is 150')
    end

    elseif (tf >= 200 & tf <250)
    Ysp=SP(4,:);
    if (tf>=200 & tf< 201)
            disp(' time is 200')
    end

    elseif (tf >= 250 & tf <300)
    Ysp=SP(5,:);
```

```
if (tf>=250 & tf< 251)
        disp(' time is 250')
end

elseif (tf >= 300 & tf <350)
Ysp=SP(6,:);
if (tf>=300 & tf< 301)
        disp(' time is 300')
end

end

X=x(numrow, :);
sizeout=size(output);
lastout=sizeout(1);
Y=output(lastout, :);

% CHOOSE CONTROLLER
% 1 - nonlinear multivariable controller with integral mode.
% 2 - linear multivariable controller with integral mode.
% 3 - nonlinear multi-loop controller with integral mode.
% 4 - linear multi-loop controller with integral mode.

controller=1;
if controller == 1
    lnMInlmv
elseif controller == 2
    lnMIlmv
elseif controller == 3
    lnMInlml
elseif controller == 4
    lnMIlml
end

%BOUNDS ON THE MANIPULATED VARIABLES
bounds=1;   %0=off, 1=on.
if bounds==1
    if FH2 < 0
    FH2=0;
    end
    if FM2 < 0
    FM2=0;
    end
    if Fcat < 0
    Fcat=0;
    end
    if FH2 > 14000
    FH2=14000;
    end
    if FM2>62400
    FM2=62400;
    end
    if Fcat>10
    Fcat=10;
    end
end
u=[FH2; FM2; Fcat];
```

```
    [t,x]=model5s(1,'polstates',[t0 tf], X, [], u);
    state=[state; x];
    time=[time;t];
    sizex=size(x);
    numrow=sizex(1);
    for i=1:numrow
    lnMI=3.5*log(k0+k1*x(i,2)/M1+k3*x(i,1)/M1);
    rho=p0+p1*lnMI-(p2*x(i,2)/M1)^p4;
    PR=x(i,3)*(kp1*M1*mw1+kp2*x(i,2)*mw2)/1000000;
    output=[output ; [lnMI rho PR]];
    SPholder=[SPholder;Ysp];
    end
    t0=t0+timestep;
    tf=tf+timestep;
    tfholder=[tfholder;tf];
    sizet=size(t);
    for l=1:sizet
    input=[input;[FH2 FM2 Fcat]];
    end
end

sizetime=size(time);
halftime=0.5*sizetime
halftime=round(halftime)
timea=time(1:halftime,1);
timeb=time(halftime:sizetime,1);

output=[exp(output(:,1)) output(:,2) output(:,3)];
SPholder=[exp(SPholder(:,1)) SPholder(:,2) SPholder(:,3)];

errortraj

figure(1)
    subplot(3,1,1)
    plot(time, state(:,1));
    ylabel('[Hydrogen] (mol/L)')
    xlabel('time (h)')

    subplot(3,1,2)
    plot(time, state(:,2));
    ylabel('[Butene] (mol/L)')
    xlabel('time (h)')

    subplot(3,1,3)
    plot(time, state(:,3));
    ylabel('Active sites (mol)')
    xlabel('time (h)')

    figure(2)
    subplot(3,1,1)
    plot(time,SPholder(:,1),'r--', time_e,exp(e_traj(:,1)),'r.', ...
    time, output(:,1));
    ylabel('MI')
    xlabel('time (h)')
```

```
        subplot(3,1,2)
        plot(time,SPholder(:,2),'r--', time_e,e_traj(:,2),'r.', ...
        time, output(:,2));
        ylabel('density')
        xlabel('time (h)')

        subplot(3,1,3)
        plot(time,SPholder(:,3),'r--', time_e,e_traj(:,3),'r.', ...
        time, output(:,3));
        ylabel('Production Rate')
        xlabel('time (h)')

        figure(3)
        subplot(3,1,1)
        plot(time, input(:,1));
        ylabel ('FH2 (mol/h)')
        xlabel ('time (h)')

        subplot(3,1,2)
        plot(time, input(:,2));
        ylabel ('FM2 (mol/h)')
        xlabel ('time (h)')

        subplot(3,1,3)
        plot(time, input(:,3));
        ylabel('Fcat (kg/h)')
        xlabel ('time (h)')

end

endnotice=bleep;
```

The following Matlab files are called by InMIgradetrans1.m. The file polstates.m integrates the dynamic model equations. The nonlinear control law is coded in InMInlmv.m.

polstates.m

```
function xdot = polstates(t,x,uin)

% This file contains the differential equations for the state model
% and integrates them over a given time interval.


FH2 = uin(1);
FM2 = uin(2);
Fcat = uin(3);

% THE PARAMETERS
Vg=423747.3;
Vs=151121.9;
```

```
kh=1008;
kp1=302400;
kp2=38448;
kd=0.36;
gl=9/2500000000;
mw1=28.05;
mw2=56.12;
b=18571;
S=0.0021589;
Ct=0.711;
acat=1.0944;
M1=0.259634;
Bw=70;

xdot=[1/Vg*(FH2-kh*x(3)*x(1)-x(1)*b/Ct-gl*x(1)); ...
    1/(Vg+Vs)*(FM2-kp2*x(3)*x(2)-x(2)*b/Ct-S*x(2)* ...
    x(3)*(kp1*M1*mw1+kp2*x(2)*mw2)); ...
    Fcat*acat-x(3)^2/1000000*(kp1*M1*mw1+kp2*x(2)*mw2)/Bw-kd*x(3)];
```

lnMInlmv.m

```
% This is the nonlinear multivariable controller
% with INTEGRAL MODE for PE for (ln(MI), rho, PR)

%PARAMETERS
Vg=423747.3;
Vs=151121.9;
kh=1008;
kd=0.36;
gl=9/2500000000;
b=18571;
S=0.0021589;
Ct=0.711;
acat=1.0944;
Bw=70;
B1=1;
B2=1;
B3=1;
gamma1=1/4;
gamma2=1/4;
gamma3=1/30;

enow=[(Ysp(1)-Y(1))*timestep;(Ysp(2)-Y(2))*timestep ;(Ysp(3)-
Y(3))*timestep];

e=enow+e;

dh1dx1=3.5*k3/M1/(k0+k1*X(2)/M1+k3*X(1)/M1);
dh1dx2=3.5*k1/M1/(k0+k1*X(2)/M1+k3*X(1)/M1);
dh2dx1=p1*dh1dx1;
dh2dx2=p1*dh1dx2-p4*p2/M1*(p2*X(2)/M1)^(p4-1);
dh3dx2=(kp2*mw2*X(3))/1000000;
dh3dx3=(kp1*mw1*M1+kp2*X(2)*mw2)/1000000;
```

```
eq1=1/Vg*(-kh*X(3)*X(1)-X(1)*b/Ct-g1*X(1));
eq2=1/(Vg+Vs)*(-kp2*X(3)*X(2)-X(2)*b/Ct-S*X(2)*X(3)*(kp1*M1*mw1+...
    kp2*X(2)*mw2));
eq3=-X(3)^2*(kp1*M1*mw1+kp2*X(2)*mw2)/Bw/1000000-kd*X(3);


FH2=Vg*(-B2*Ysp(2)*dh1dx2+B2*Y(2)*dh1dx2-gamma2*e(2)*dh1dx2-
eq1*dh1dx1*dh2dx2+...
    dh2dx1*eq1*dh1dx2+dh2dx2*B1*Ysp(1)-
dh2dx2*B1*Y(1)+dh2dx2*gamma1*e(1))/...
    (dh1dx1*dh2dx2-dh1dx2*dh2dx1);


FM2 =-(Vg+Vs)*(-dh1dx1*B2*Ysp(2)+dh1dx1*B2*Y(2)-dh1dx1*gamma2*e(2)+...
    dh1dx1*dh2dx2*eq2+B1*Ysp(1)*dh2dx1-
B1*Y(1)*dh2dx1+gamma1*e(1)*dh2dx1-...
    dh1dx2*eq2*dh2dx1)/(dh1dx1*dh2dx2-dh1dx2*dh2dx1);


Fcat=1/acat*(B3*Ysp(3)*dh1dx1*dh2dx2-B3*Ysp(3)*dh1dx2*dh2dx1-...

B3*Y(3)*dh1dx1*dh2dx2+B3*Y(3)*dh1dx2*dh2dx1+gamma3*e(3)*dh1dx1*dh2dx2-
...
    gamma3*e(3)*dh1dx2*dh2dx1-
dh3dx2*dh1dx1*B2*Ysp(2)+dh3dx2*dh1dx1*B2*Y(2)-...
    dh3dx2*dh1dx1*gamma2*e(2)+dh3dx2*B1*Ysp(1)*dh2dx1-
dh3dx2*B1*Y(1)*dh2dx1+...
    dh3dx2*gamma1*e(1)*dh2dx1-dh3dx3*eq3*dh1dx1*dh2dx2+...
    dh3dx3*eq3*dh1dx2*dh2dx1)/((dh1dx1*dh2dx2-dh1dx2*dh2dx1)*dh3dx3);
```